Application of ensemble approaches to the assimilation of remotely sensed data into spatialized numerical simulations of seasonal snow cover

Bertrand Cluzet

THÈSE

En vue de l'obtention du

DOCTORAT DE L'UNIVERSITÉ DE TOULOUSE

Délivré par : *l'Université Toulouse 3 Paul Sabatier (UT3 Paul Sabatier)*

Présentée et soutenue le *11/12/2020* **par :**

Bertrand Cluzet

Application des approches d'ensemble à l'assimilation de données télédétectées dans des simulations numériques spatialisées du manteau neigeux saisonnier

---

JURY

Tobias Jonas	Dr.	Rapporteur
Michael Durand	Prof.	Rapporteur
Marie Dumont	Dr.	Directrice thèse
Matthieu Lafaysse	Dr.	Co-directeur de thèse

École doctorale et spécialité :
SDU2E : Surfaces et interfaces continentales, Hydrologie
Unité de Recherche :
Centre National de Recherches Météorologiques (UMR 3589)
Directeur(s) de Thèse :
Marie Dumont et *Matthieu Lafaysse*
Rapporteurs :
Tobias Jonas et *Michael Durand*

Résumé

La connaissance de la variabilité du manteau neigeux est indispensable pour la prévision du risque d'avalanche ainsi que pour le suivi de la ressource en eau. D'une part, la couverture spatio-temporelle des observations in-situ et télédétectées de la neige est limitée. Les réflectances satellites dans le visible et le proche infra-rouge fournissent de précieuses informations sur les propriétés de surface du manteau neigeux mais ont une couverture parcellaire, notamment à cause des nuages. De la même manière, les observations in-situ de hauteur de neige (HN) ont une représentativité et une couverture spatiale limitées. D'autre part, les modèles détaillés du manteau neigeux offrent la possibilité de simuler la stratigraphie complète du manteau neigeux en tout point. Cependant ceux-ci souffrent d'importantes erreurs provenant de leurs forçages météorologiques ainsi que de leur propre représentation de la physique de la neige. Dans ce contexte, l'assimilation de données, qui permet d'intégrer l'information provenant des observations dans les simulations de ces modèles, semble prometteuse. L'objectif de cette thèse est d'évaluer la capacité de l'assimilation de réflectances satellites et d'observations in-situ de HN à améliorer la simulation du manteau neigeux en montagne. Les problématiques suivantes seront donc abordées :

- **Les observations de réflectances satellites de la neige permettent-elles de mieux contraindre la modélisation du manteau neigeux en montagne ?**
- **Peut-on propager de l'information sur l'état du manteau neigeux depuis des zones observées vers des zones non-observées ?**
- **Dans quelle mesure peut-on utiliser les observations in-situ de HN pour améliorer les simulations du manteau neigeux dans leur voisinage ?**

Nous avons choisi d'utiliser une approche d'assimilation de données ensembliste séquentielle, untilisant le Filtre Particulaire (FP) qui est adapté aux modèles détaillés du manteau neigeux. Le système de modélisation d'ensemble est basé sur ESCROC, un ensemble de modèles multi-physiques du manteau neigeux, forcé par un ensemble de perturbations stochastiques des analyses météorologiques SAFRAN. Cette conception permet à la chaîne de modélisation de tenir compte de ses principales sources d'incertitude. Plusieurs versions innovantes du FP ont été développées afin d'assimiler un grand nombre d'observations simultanément, tout en évitant la dégénérescence du FP, un problème apparaîssant lorsque le nombre d'observations augmente.(Palchetti et al., 2021)

Le potentiel de l'assimilation de réflectances satellites a été estimé en comparant des observations du capteur satellite MODIS avec des sorties de simulations. Des expériences jumelles assimilant des observations partielles nous ont permis d'analyser la capacité du FP à propager de l'information vers des zones non-observées. Enfin, nous avons évalué l'apport de l'assimilation d'un réseau d'observations de HN couvrant les Alpes et les Pyrénées par une approche de validation croisée de type "un contre tous".

Nos résultats montrent que l'approche proposée permet d'éviter la dégénérescence du FP tout en réussissant à propager de l'information entre différentes conditions topographiques. Un biais a été mis en evidence dans les observations standard MODIS, qui empêche leur assimilation directe. En revanche, nous avons mis en valeur le bénéfice de l'assimilation de HN dans les zones où les erreurs de modélisation sont systématiques et dépassent la variabilité naturelle. Ce travail ouvre la voie à l'assimilation d'autres produits satellitaires ainsi que d'observations in-situ de HS dans un contexte spatialisé, représentant un saut qualitatif important pour la prévision du risque d'avalanche et l'hydrologie de montagne.

Mots-clefs : Manteau neigeux, modélisation, assimilation, télédétection

Abstract

Understanding mountain snowpack variability is key to anticipate avalanche hazards and monitor water resources. On the one hand, remotely-sensed and in-situ observations of snow have a limited spatial and temporal coverage. For instance, visible and near infrared satellite reflectances provide useful information on snowpack surface properties, but are affected by important gaps of coverage e.g. due to clouds. Likewise, in-situ observations of the height of snow (HS) are reliable but with a limited representativeness and spatial coverage. On the other hand, detailed snowpack models can simulate the complete snow stratigraphy virtually anywhere, but they suffer from large uncertainties in their meteorological inputs and their representation of snow physical processes. Thus, data assimilation offers an unique opportunity to merge information from observations and models into a better estimate of the snowpack state. The aim of this thesis is to investigate the potential for satellite reflectances and in-situ HS to improve snowpack simulations in mountainous areas via assimilation. In this work, we will try to address the following questions:

- **Can we use observations of snowpack reflectance from satellites to better constrain snowpack modelling over mountainous areas?**
- **Can we propagate information on the snowpack state from observed areas to unobserved areas with data assimilation?**
- **To what extent can we use in-situ observations of HS to improve snowpack simulations in their neighborhood?**

We opt for a sequential ensemble data assimilation strategy, using the Particle Filter algorithm (PF), which is well adapted to detailed snowpack models. An ensemble modelling system is built by forcing ESCROC, a multiphysics ensemble of snowpack models, with an ensemble of stochastic perturbations on SAFRAN meteorological analyses. This design enables the modelling system to account for its main sources of uncertainty. Several innovative versions of the PF are developed in order to assimilate large numbers of observations and propagate information to unobserved areas while avoiding PF degeneracy, an issue arising when the number of observations increases.

The potential for assimilation of satellite reflectance is assessed by comparing MODIS observations with simulated reflectances. We conduct twin experiments assimilating partial observations to analyse the ability of the PF to propagate information into unobserved areas. Finally, we assess the added value of the assimilation of HS observations from an observation network over the Alps and Pyrenees using a Leave-One-Out approach.

Results show that the proposed methodology is efficient to tackle PF degeneracy while managing to propagate information across topographic conditions. Though standard MODIS observations cannot be directly assimilated because they are biased, the assimilation of HS observations have some added value where modelling errors are systematic and larger than

natural variability. This work is a novel contribution to improve the assimilation of other satellite products and in-situ HS observations in a spatialised context, a significant qualitative leap for avalanche forecasting and hydrological studies.

Keywords : Snowpack, modelling, data assimilation, remote sensing

Contents

Pour toi,
Pour Simon,
Pour Jonas,
Chaque jour,
S'améliorer.

General introduction

Preamble

Just as matter is essentially made of vacuum, snow is often more made of air than of ice. Indeed, the ice matrix of snow hosts so many air cavities that snow density can be ten times lower than pure ice density. But snow is not only made of ice and air. Liquid water and water vapour can fill its matrix. Hitch-hiking dusts can find their way from Sahara into Alpine snow. Its myriad of prisms is a labyrinth for photons. They generally find their way out –snow is white– but sometimes get trapped: snow is bluish like water, and episodically brownish as dusts absorb the visible light besides red. Snow is an ever-evolving medium which transforms under the laws of diffusion, phase change, light scattering and gravity. In the mountains, the snow is highly variable. Transported by the wind, trapped by vegetation, shaded by peaks: snow can change in the blink of an eye, from one footstep to another. Grasping its diversity and variations with any sensor, any equation, any model alone, is an impossible task. But what comes up if we put all these sources of information together? This is our challenge. Before getting into this adventure, let's see why it is worth it.

Snow has a strong influence on the climate (Solomon et al., 2007). It is one of the Earth's most reflective natural surfaces (in the visible part of the spectrum). As a good thermal insulator, snow controls on the ground thermal regime (Domine et al., 2006b) and shrub growth spring offset (Pulliainen et al., 2017; Francon et al., 2020) In the montains snow is used by many animals to hunt, hide or protect from te cold (Storch, 1993; Zimova et al., 2018). Snowmelts contributes to river flow, irrigating downstreams ecosystems (Arnell and Reynard, 1996; Rolls et al., 2012, e.g.). As a matter of fact, snow is both a resource and a risk. In the mountains, snow is indeed a source of leisure activities which serve as a substrate for local economy, which in turns attracts humans into the mountains (Xiao et al., 2015). This situation exposes them to numerous snow-related natural hazards such

as avalanches, landslides and floods (Haeberli and Whiteman, 2015). Monitoring mountain snow conditions, and forecasting their evolution (from hourly to climatic timescales) is essential to understand, evaluate and anticipate the potential snow-related risks and opportunities (Morin et al., 2020).

Snow is an ice matrix filled with air and eventually a liquid phase. A snowpack builds up b the accumulation of solid and liquid precipitation. It can be macroscopically described by the height of snow (HS (m)) or its snow water equivalent (SWE (kg m^{-2})). The chronology of precipitation results in strong variations of its internal properties on the vertical scale. Close to the snowpack surface, strong energy exchanges (visible-near infrared (shortwave, SW) and thermal longwave (LW) radiative fluxes, as well as turbulent heat exchange with the atmosphere) determine an important share of the energy budget along with ground thermal fluxes. If a snow layer has a positive energy budget, it will heat up and potentially melt provided that it reaches 0^oC. If this liquid water doesn't refreeze, it will percolate through the underlying layers, and leave the snowpack by its bottom. Surface snow can also sublimate under dry wind conditions. In both situations, the snowpack looses some mass: these processes are referred as ablation. As snowpack energy interactions with its environment are confined to its bottom and its base, and since the snow is a good thermal insulator, a strong macroscopic thermal gradient often forms. This gradient is one of the drivers of modifications of the microstructural properties of snow.

Snow microstructural properties undergo perpetual modifications, from snowfall to ablation. Due to local thermodynamic imbalances, ice crystals forming the snowpack will change of shape due to sublimation, melt or recrystallisation. In the presence of liquid water, snow grains tend to grow and round.
These changes in microstructural properties have a decisive influence on the optical properties of snow, particularly in the SW, where ice is a partially absorbing material. Depending on the geometric properties of the myriad of prisms that make up the snowpack, photons will have more or less chance of "escaping" from it, or conversely, of being absorbed, thus contributing to "warming" the snow. These microstructural optical properties can be partly described by the SSA (Specific Surface Area (m^2 kg^{-1}), (Domine et al., 2006a)), which characterises the total air/ice interface area per unit mass of snow. From a macroscopic point of view, the albedo, defined as the ratio of the SW energy backscattered by the snowpack to the incident SW energy, is used to describe the ability of the snowpack to reflect incident SW radiation. Although snow is one of the most reflective materials in the visible range (hence its white colour), its albedo varies greatly with the wavelength: it is important to look at its spectral variation, or reflectance.

The reflectance of snow is higher in the visible than in the infrared. The SSA induces strong variations in the near infrared and to a lesser extent in the visible. High SSA values, typical of fresh snow, are associated with high reflectance. Low SSA values ("old snow") enhance the absorption of SW energy by the snowpack. For instance, this accelerates snow melting at the end of the season. Absorbing impurities, emanating from anthropogenic or natural combustion, as well as dust raised in particular by Saharan storms, can be deposited on the snowpack or during precipitation. They increase the energy absorption of the snowpack in the visible range, which can be noted by the orange colour of the snow in their presence, and also contribute to an earlier melting. Finally, it is important to note that reflectance depends on the illumination conditions (local incidence and presence or absence of direct radiation).
Net SW radiation is one of the most important terms in the energy balance. On a clear day, about 80% of this energy is received as direct radiation from the sun, the rest coming from SW radiation scattered by the atmosphere or adjacent slopes. In the mountains, the incident SW radiation is extremely variable in space and time. The more the radiation is normal to the surface, the grater the amount of SW energy per unit of surface will be received. Moreover, mountains can hide the incident direct radiation to the surrounding slopes. This is the main reason why, at the same altitude and in our latitudes, the snowpack melts faster on the southern slopes than on the northern slopes. Clouds can also temporarily intercept the direct part of the radiation. In addition, snow is a very "backscattering" material, so that two facing snow-covered slopes can re-illuminate each other. Snow cover properties can therefore be extremely variable depending on the topography.

In the same way, several factors induce a great spatial variability of snowpack surface properties as well as of its integrated quantities such as SWE or HS (Blöschl, 1999; Helbig et al., 2020), and a fortiori of its stratigraphy (e.g. Bellaire and Schweizer, 2011). In addition to SW fluxes, topography controls the air temperature and the precipitation phase via the altitude. In interaction with the topography, the wind also plays a major role through its ability to redistribute snow, from the centimetre scale to the mountain scale. In addition, partly owing to wind fields, precipitation is also variable on a mountain scale, or even between the two sides of a ridge. Avalanches redistribute the snow towards less steep slopes while modifying its properties. Finally, vegetation can intercept the snow, and forests trap the LW radiation emitted by the underlying snow, thus limiting its night-time cooling. In summary, snow is extremely variable spatially, from metric to mountain scales.

Due to its high spatial variability, snow is difficult to accurately observe over large areas. The relatively widespread in-situ observations of HS or SWE cannot capture this variability

beyond the local scale, i.e. they have a limited representativeness. Fortunately, things seem to be simpler when we take a step up: satellites regularly provide us with images of snow over the entire surface of the globe. To date, visible and near-infrared observations from sensors such as MODIS (MODerate resolution Imaging Spectroradiometer) or the Sentinel-2 satellite, seem to be the only ones with sufficient information content and spatial resolution to better constrain the variability of the snow cover. Indeed, these observations contain valuable information on the surface properties of the snow, such as its absorbing impurities content and its SSA, which both affect the radiative budget. Such observations could make it possible to verify the chronology and phase of precipitation events (Dozier et al., 2009). However, there is no evidence that their level of accuracy is sufficient to constrain the properties of the snowpack (e.g. Warren, 2013). Reflectances can also be used to determine the snow cover fraction (SCF) of each pixel, which is very useful to constrain ablation rates or reconstruct snow cover dynamics in a retrospective manner (Aalstad et al., 2018). However, these observations are generally patchy, as they are unavailable or too inaccurate under clouds, in the presence of shadows, and in forests and steep slopes (Sirguey et al., 2009).

Snowpack models are complementary to observations in the sense that they can evaluate virtually any snow variable. They make it possible to forecast snow conditions anywhere, at any time, including in the future. Snowpack models are used for avalanche risk and hydrological forecasting. In practice, snowpack models simulate the mass and energy balance as well as a number of physical processes (albedo, metamorphism, settlement, turbulent fluxes, liquid water percolation, etc.) with a more or less fine vertical resolution. A high spatial resolution is also important to represent the main causes of snowpack variability (e.g. topography, wind drift, vegetation, etc.), but comes with a numerical overhead preventing their use on large scales. At present, snowpack models used for avalanche risk forecasting such as Crocus, the operational model of Météo-France, represent a detailed stratigraphy with a variable number of layers, and take into account the influence of the topography (semi-distributed geometry). However, such models generally ignore gravity and wind redistribution processes, which are too costly in terms of calculation time. These models are forced by imprecise weather forecasts in the mountains (e.g. Nousu et al., 2019), and are themselves limited by numerous errors and uncertainties linked in particular to uncertain parametrisations of the physical processes (Krinner et al., 2018), and to the non-representation of wind drift. These two sources of error and uncertainty contribute significantly to the modelling errors. Moreover, these are bound to persist. Since the atmosphere is inherently chaotic, weather models are insufficiently resolved in the mountains, and due to a lack of sufficiently detailed observations, snow modelling errors cannot be targeted and reduced enough(Menard et al., 2020).

The probabilistic approach allows to account for modelling errors and uncertainties. In this formalism, instead of estimating a single value, the model provides a probability density function (pdf), i.e. a "range of possibilities" for the considered variable. A method has emerged to provide this probabilistic approach: ensemble forecasting. This consists of simultaneously launching a set of simulations (or members) from different initial conditions, propagated by different versions of the model. The probability density of the forecast is directly estimated from the density of the values predicted by the members of the simulation. In this way it is possible to estimate the modelling uncertainties, whether they are linked to a particularly chaotic situation or to weaknesses of the model. If the probability density function of a forecast is "narrow" (the members have almost all the same value), one can deduce that the forecast is sure, otherwise the simulation will be considered uncertain. Of course, the model providing these forecasts must be trusted. To do this, some of its properties must first be checked against a large number of "test" events. Reliability, its ability to issue the right probability to an event, regardless of its likelihood, and resolution, its ability to discriminate between two different events, are essential properties.
Ensemble forecasting first appeared in numerical weather prediction and is now emerging in snowpack modelling (e.g. Essery et al., 2013; Magnusson et al., 2014; Vernay et al., 2015; Lafaysse et al., 2017; Nousu et al., 2019; Dumont et al., 2020). In particular, although it is essential to take both sources of uncertainty into account, ensembles of meteorological forcings have rarely been combined with ensembles of snow models (Günther et al., 2019).

Data assimilation is a unique opportunity to combine observations and models in an optimal way. Known as "the art of making sense of observations", it allows to establish an "analysis" taking into account the values predicted by the model and the observations, as well as their respective errors. It thus takes excellent advantage of ensemble modelling which provides a dynamic estimate of the modelling errors. In an idealised framework, the analysis is both closer to reality and more accurate than the two sources of information from which it is derived. In a real-time sequential context, where observations are assimilated as they become available, this analysis can then be fed back into the model, bringing it closer to reality. The model is then used until another observation becomes available. This sequential approach lends itself well to the problem of weather forecasting, and in particular to avalanche risk forecasting and hydrological monitoring.

Data assimilation has made spectacular progress in numerical weather prediction over the last 40 years. It then appeared in snowpack modelling, through hydrological forecasting (Slater and Clark, 2006), and continental surface modelling (De Lannoy et al., 2012).

For snowpack modelling, ensemble assimilation methods such as the ensemble Kalman filter (EnKF) or the particle filter with sequential resampling (PF) are the most widely used for forecasting purposes (e. e.g. Magnusson et al., 2014; Larue et al., 2018), and have been successful in assimilating integrated variables such as the height of snow (Magnusson et al., 2017), or even multiple variables (Piazzi et al., 2018). On the other hand, reflectance assimilation has never gone beyond the idealised framework (Charrois et al., 2016). Smoothing algorithms, such as Particle Batch Smoother (PBS, Margulis et al., 2015) are more suitable for backward-looking modelling problems working with variables such as the CWS (e.g. Aalstad et al., 2018). A comprehensive review of assimilation methods for snow has recently been proposed by Largeron et al. (2020).
Assimilation can also be used to propagate information from observed into unobserved areas. This is essential in our case to respond to the patchy nature of the observations (in-situ as well as satellite) available to us. Indeed, a "point by point" assimilation (e.g. Kim et al., 2019; Deschamps-Berger et al., in review) cannot correct the model in the unobserved zones, which leads to too large differences in performance with the observed zones. While spatial interpolation methods (from observations as well as from point analyses) (Slater and Clark, 2006; Cantet et al., 2019) have been proposed to fill these "holes", they seem too approximate in complex terrain. The question of the propagation of information by assimilation for the modelling of the snowpack in complex terrain remains largely unexplored.
As far as the problem of avalanche risk forecasting is concerned, the PF seems best suited to Lagrangian models such as Crocus, which involve a variable number of numerical layers. Moreover, it is the only method that preserves the physical consistency between the variables in a certain way. This is important, as small local vertical gradients can have a significant impact on the modelled metamorphism. The analysis of the PF consists in rejecting the members (or particles) furthest from the observation (with respect to the observation error), and replacing them with the closest members(Gordon et al., 1993; Kitagawa, 1996).
One of the major difficulties encountered by the PF is the degeneracy problem: when the number of simultaneously assimilated observations increases, too few particles are duplicated to correctly represent the pdf of the system (Snyder et al., 2008). Solutions exist to solve it: inflation of the observation errors (Larue et al., 2018) or the localisation of the PF (Van Leeuwen, 2009).

The resolution of degeneracy by localisation methods is in fact linked to the question of the propagation (notably spatial) of information by the assimilation algorithm. When the degeneracy prevents the production of a global analysis on a whole domain, the localisation of the PF proposes to separate this problem into a set of local problems. An analysis is performed at each point, considering the observations in its neighbourhood. As a result, the

number of observations is reduced, and the degeneracy of the PF is avoided. On the other hand, each point receives a different analysis, causing spatial discontinuities in the analysis fields. This can cause problems when horizontal coupling requires a physical balance. Localization is therefore based on the notion of neighbourhood, which aims to define a set of positions that can contain relevant information on the considered point. It is necessary here to dwell on this notion of "relevance". Information on the state of a point can be used to improve the knowledge on the state of another point via assimilation if they are statistically linked (but not necessarily physically, this link can be caused by an external factor such as meteorological forcings). In most geophysical systems, points can be considered as statistically independent past a certain distance, and the classically accepted notion of neighbourhood is based on this principle, in the PF (e.g. Poterjoy, 2016) and the EnKF likewise. In the latter, this statistical independence is often inferred from the ensemble correlation structures (e.g. Hamill et al., 2001).
For the mountain snowpack, this link between distance and statistical independence remains to be verified. In the absence of snow transport by the wind, beyond a few metres, the points are to a large extent physically independent, for which most snow models are 1D, even the most physically detailed ones (e.g. Brun et al., 1989; Lehning et al., 1999). On the other hand, they can be subject to the same factors (meteorology, lighting conditions), resulting in statistical links, and thus, the possibility of propagating information. As mentioned for the EnKF, ensemble correlations can be used to estimate this statistical dependence, but at present, due to the still incipient use of ensembles for snowpack modelling, we know nothing about these spatial correlation structures. It is thus possible that the notion of neighbourhood, based on distance criteria, is not adapted to snow in complex terrain at the considered modelling scales (beyond a hundred metres). For a local analysis on a sunny south-facing slope, a distant observation, but in similar lighting conditions, could be better indicated than a closer observation, but coming from a shaded slope.

The objective of this thesis is to better characterise the spatial variability of the snowpack in the mountains. The method consists in trying to take advantage of in-situ snow height observations and satellite reflectances by including them in ensemble simulations of the snowpack with Crocus, using data assimilation. Our work will attempt to answer the following questions:

In this work, we will investigate the potential for assimilation of space-borne reflectance and in-situ snow depth observations into ensemble snowpack simulations in a spatialised context, with a particular focus on the question of the propagation of information from observed into unobserved areas. After an introduction to the problem in Chapter 1, Chapters 2-4 will respectively address the following questions:

- **Can we use observations of snowpack reflectance from satellites to better constrain snowpack modelling over mountainous areas?**

While their potential to constrain snowpack simulations has been proven with Crocus in an idealized setting, real snowpack spectral reflectance data have never been successfully assimilated before, let alone in a spatialized context. We will therefore investigate whether MODIS and Sentinel-2 reflectance data can be assimilated into ensemble simulations of the snowpack. To do so, the representation of uncertainties in the ensemble simulation system used will need to be improved to include snowpack modelling uncertainties. We will address this issue in Chapter 2.

- **Can we propagate information on the snowpack state from observed areas to unobserved areas with data assimilation?**

Satellite reflectances have a patchy spatial coverage (Sirguey et al., 2009). For example, they are rarely available on shaded slopes. We wonder if it is possible to improve snowpack simulations in unobserved areas using observations from observed areas through assimilation. The particle filter appears to be an appropriate assimilation method for modelling mountain snowpack, but suffers from degeneracy when too many observations are assimilated simultaneously. After having built a set assimilation system able to answer this problem, we will see if it is possible, in an idealized framework, to avoid this degeneration while managing to propagate information in the unobserved zones. This problem will be tackled in Chapter 3.

- **To what extent can we use in-situ observations of HS to improve snowpack simulations in their neighborhood?**

Several studies have successfully assimilated integrated snowpack (snow height or SWE) observations in a spatialized context in mountainous terrain (e.g. Magnusson et al., 2014; Winstral et al., 2019). These are based on an exceptionally dense network of observations. It is likely that the performance of such assimilation systems decreases with the density of available observations (Largeron et al., 2020), which would limit the scope of such an approach to a very limited number of mountain regions. We will apply our ensemble assimilation system to the case of a network of snow height observations covering the French Alps and Pyrenees, as well as Andorra. This network has very variable observation densities. We will thus be able to evaluate the contribution of assimilation in relation to the operational system of Météo-France in a wide variety of situations. This question will be treated in Chapter 4.

Dictes moy ou, n'en quel pays
Est Flora, la belle Rommaine,
Archipiades, ne Thaïs,
Qui fut sa cousine germaine,
Écho parlant quand bruyt on maine
Dessus riviere ou sus estan,
Qui beaulté ot trop plus qu'humaine.
Mais ou sont les neiges d'antan ?

Ou est la très sage Hellois
Pour qui chastré fut et puis moyne
Pierre Esbaillart a Saint Denis ?
Pour son amour ot ceste essoyne.
Semblablement, ou est la royne
Qui commanda que Buridan
Fust geté en ung sac en Saine ?
Mais ou sont les neiges d'antan ?

La royne Blanche comme lis
Qui chantoit a voix de seraine,
Berte au grant pié, Bietris, Alis,
Haremburgis qui tint le Maine,
Et Jehanne la bonne Lorraine,
Qu'Englois brulerent a Rouan,
Ou sont ilz, Vierge souveraine ?
Mais ou sont les neiges d'antan ?

Princes, n'enquerez de sepmaine
Ou elles sont, ne de cest an,
Qu'a ce reffrain ne vous remaine :
Mais ou sont les neiges d'antan ?

François Villon (XV$^{\text{ème}}$ siècle), *Ballade des dameuses du temps jadis*

Introduction Générale

Si on cherche de la neige, mieux vaut aller en montagne. En effet, les montagnes sont vastes, sublimes, inaccessibles, prétexte à de nombreuses rêveries et souvent couvertes de neige. Le poète du moyen-âge François Villon voit dans la neige saisonnière[1] une métaphore du cycle de vie (Frappier, 1971). Si chaque année, le destin de cette neige est de disparaitre, nous savons qu'elle resurgira un jour : cela n'a pas de sens de se demander si la neige reviendra. Cependant, par une étrange coïncidence, le glissement sémantique du mot "antan" de son sens originel (l'année passée) vers son sens actuel (passé lointain) a accompagné le bouleversement de notre climat : les neiges d'antan ne sont plus toujours au rendez-vous (Spandre et al., 2019). En sus de notre accès à quelques sensations fortes, c'est sans doute une part de notre identité qui est en jeu (Albrecht et al., 2007).

Ceci étant dit, il est entendu que la neige a une influence importante sur le climat (Solomon et al., 2007). En effet, c'est l'une des surfaces naturelles les plus réfléchissantes sur Terre (dans le spectre visible), et ses propriétés d'isolant thermique contrôlent le régime thermique des sols (Domine et al., 2006b) ainsi que la pousse printanière de la végétation arctique et alpine (Pulliainen et al., 2017; Francon et al., 2020). En montagne la neige est essentielle pour de nombreux animaux, qu'ils soient à l'affût, en cachette, ou encore à l'abri du froid (Storch, 1993; Zimova et al., 2018). Sa fonte nourrit le débit des rivières, ainsi précieuse à de nombreux écosystèmes en aval (e.g. Arnell and Reynard, 1996; Rolls et al., 2012). De manière plus pragmatique, les humains voient la neige à la fois comme une source d'opportunités, mais aussi de risques. Celle-ci est en effet prétexte à de nombreuses actitivés de loisir somme tout assez futiles mais servant de substrat à une économie locale, qui en retour incite les humains à s'installer en montagne (Xiao et al., 2015). Cette situation les expose à de nombreux risques naturels liés à la neige, tels que les avalanches, glissement de terrains et crues nivales (Haeberli and Whiteman, 2015). Il est indispensable de suivre les conditions d'enneigement en montagne, ainsi que de prédire leur évolution (à des échelles courtes comme climatiques) afin de comprendre, évaluer et anticiper les risques et opportunités liés à la neige (e.g. Morin et al., 2020).

[1] À l'époque, "antan" faisait référence à l'année passée, contrairement à son sens actuel (Frappier, 1971).

La neige est une matrice de glace remplie d'air et éventuellement d'une phase liquide. Le manteau neigeux se constitue par l'accumulation de précipitations solides et liquides, et peut être décrit macroscopiquement par sa hauteur de neige (height of snow, HS (m)) ou son équivalent en eau (snow water equivalent SWE, (kg m^{-2})). Il hérite de cette chronologie de précipitations d'importantes variations verticales de ses propriétés physiques. Près de sa surface, le manteau neigeux connait des échanges d'énergie (flux radiatifs dans le visible et le proche infrarouge (shortwave, SW) issus du rayonnement solaire, rayonnements thermique (longwave, LW) et échanges de chaleurs turbulents avec l'atmosphère) qui déterminent une grande part de son bilan d'énergie, l'autre part significative étant les échanges de chaleur avec le sol sous-jacent. Si une couche de neige a un bilan d'énergie positif, celle-ci va se réchauffer et éventuellement fondre, dès lors que sa température aura atteint 0°C. Si elle ne regèle pas, cette eau liquide pourra ensuite percoler à travers les couches inférieures du manteau neigeux et quitter celui-ci par sa base. La neige peut également se sublimer à la surface sous l'effet d'un vent sec. Dans les deux cas, le manteau neigeux perd de la masse : on parle d'ablation. Comme le manteau neigeux ne peut échanger de l'énergie avec l'extérieur que près de sa surface ou de sa base, et comme la neige est très bon isolant, le manteau neigeux est souvent soumis à un fort gradient thermique macroscopique, un des facteurs à l'origine de transformations dans les propriétés microstructurales de la neige.

Les propriétés microstructurales de la neige sont en perpétuelle évolution, depuis la chute des flocons de neige jusqu'à l'ablation. Sous l'effet de déséquilibres thermodynamiques locaux, induits par exemple par le gradient thermique macroscopique, les cristaux de glace composant la neige vont changer de forme, par sublimation ou recristallisation de glace. On retiendra qu'en présence d'eau liquide (par exemple lors de la fonte), les grains de neige ont tendance à s'arrondir et à grossir.
Ces changements de propriétés microstructurales ont une influence déterminante sur les propriétés optiques de la neige, notamment dans le SW, où la glace est un matériau partiellement absorbant. Selon les propriétés géométriques de la myriade de prismes qui compose neige. Ces propriétés optiques microstructurales peuvent être en partie décrites par la SSA (Specific Surface Area (m^2 kg^{-1}), (Domine et al., 2006a)), qui caractérise l'aire totale d'interface air/glace par unité de masse de neige. D'un point de vue macroscopique, l'albédo, défini comme le ratio entre l'énergie SW rétrodiffusée par le manteau neigeux et l'énergie SW incidente, permet de décrire la capacité du manteau neigeux à réfléchir le rayonnement shortwave incident. Si la neige est un des matériaux les plus réfléchissants dans le visible (d'où sa couleur blanche), son albédo varie fortement en fonction de la longueur d'onde : il est important de s'intéresser à sa variation spectrale, ou réflectance.
La réflectance de la neige est plus élevée dans le visible que dans l'infra-rouge. Celle-ci est

principalement affectée par la SSA, qui induit de fortes variations dans le proche infra-rouge et dans une moindre mesure, le visible. De fortes valeurs de SSA, typiques de neige fraîche, sont associées à une forte réflectance, tandis qu'à l'inverse des SSA faibles ("vieille neige") renforcent l'absorption d'énergie SW par le manteau neigeux, contribuant par exemple à accélérer sa fonte en fin de saison. Les impuretés absorbantes, émanant de la combustion anthropique ou naturelle, ainsi que les poussières soulevées notamment par les tempêtes sahariennes, peuvent se déposer sur le manteau neigeux ou au cours des précipitations. Celles-ci augmentent l'absorption d'énergie du manteau neigeux dans le visible, qui peut être notée par la couleur ocre prise par la neige en leur présence, et contribuent également à une fonte plus précoce. Enfin, il est important de noter que la réflectance dépend des conditions d'éclairement (incidence locale et présence ou non de rayonnement direct).
Le rayonnement net SW est l'un des termes prépondérants du bilan d'énergie, et provient du rayonnement solaire. Par ciel clair, 80% environ de cette énergie est reçue sous forme de rayonnement direct, le reste provenant du rayonnement SW diffusé par l'atmosphère ou les pentes adjacentes. En montagne, le rayonnement SW incident est extrêmement variable spatialement et temporellement. Plus le rayonnement direct sera orthogonal à la surface, plus celle-ci recevra d'énergie par unité de surface. C'est la raison principale pour laquelle à altitude égale et sous nos latitudes, le manteau neigeux fond plus vite en versant sud qu'en versant nord. Des montagnes peuvent cacher le rayonnement direct incident aux pentes environnantes. Des nuages peuvent également occulter la fraction directe du rayonnement de manière éphémere. En outre, la neige étant un matériau très "rétrodiffusant", des pentes enneigées se faisant face peuvent se rééclairer mutuellement. On comprend donc que les propriétés optiques du manteau neigeux peuvent être extrêmement variables en fonction de la topographie.

De la même manière, plusieurs facteurs induisent une grande variabilité spatiale des propriétés de surface du manteau neigeux ainsi que de ses grandeurs intégrées telles que le SWE ou HS (Blöschl, 1999; Helbig et al., 2020), et a fortiori de sa stratigraphie (e.g. Bellaire and Schweizer, 2011). En plus des flux SW, la topographie contrôle la température de l'air et la phase des précipitations via l'altitude. En interaction avec la topographie, le vent joue également un rôle prépondérant par sa capacité à redistribuer la neige, de l'échelle centimétrique à celle d'une montagne. En outre, en partie sous l'effet du vent, les précipitations sont également variables à l'échelle d'une montagne, ou même entre les deux versants d'une crête. Les avalanches contribuent a redistribuer la neige vers des pentes moins raides tout en modifiant ses propriétés. Enfin, la végétation peut intercepter la neige, et la forêt piège le rayonnement LW émis par la neige sous-jacente, limitant ainsi son refroidissement nocturne. En résumé, la neige est extrêmement variable spatialement, de l'échelle métrique à celle d'une montagne.

Du fait de sa grande variabilité spatiale, la neige est difficile à observer avec précision sur de grandes étendues. Les observations in-situ de HS ou de SWE, relativement répandues, ne peuvent pas suffire à capturer cette variabilité au delà de l'échelle locale, on dit alors que leur représentativité est limitée. Heureusement, les choses semblent plus simples quant on prend un peu de hauteur : les satellites nous fournissent régulièrement des images de la neige sur toute la surface du globe. À ce jour, les observations dans le visible et le proche infra-rouge, fournies par des capteurs comme MODIS (MODerate resolution Imaging Spectroradiometer) ou le satellite Sentinel-2 semblent les seules à avoir un contenu en information et une résolution spatiale suffisants pour mieux contraindre la variabilité du manteau neigeux (Dozier et al., 2016). En effet, ces observations contiennent de précieuses informations sur les propriétés de surface de la neige telles que son contenu en impuretés absorbantes et sa SSA, qui affectent son bilan radiatif, et pourraient permettre de vérifier la chronologie et la phase des événements de précipitation (Dozier et al., 2009). En revanche, rien ne dit que leur niveau de précision est suffisant pour contraindre les propriétés du manteau neigeux (e.g. Warren, 2013). Les réflectances permettent également de déterminer la fraction de couvert nival (snow cover fraction SCF) occupant chaque pixel, une grandeur très utile pour contraindre des taux d'ablation, ou reconstituer la dynamique de l'enneigement de manière rétrospective (e.g. Aalstad et al., 2018). Cependant, ces observations sont généralement parcellaires, car indisponibles ou trop peu précises sous les nuages, en présence d'ombres, et en forêts et pentes raides (Sirguey et al., 2009).

Les modèles de manteau neigeux peuvent permettre de compléter ces observations, en estimant les variables non-observées, et rendant possible la prévision de conditions d'enneigement où qu'on le souhaite, à n'importe quel moment, y compris dans le futur. Ceux-ci sont notamment utilisés pour la prévision du risque d'avalanche et la prévision hydrologique (Magnusson et al., 2014). En pratique, les modèles de manteau neigeux simulent le bilan de masse et d'énergie ainsi qu'un nombre plus ou moins élevé de processus physiques (albédo, métamorphisme, tassement, flux turbulents, percolation de l'eau liquide etc.) avec une résolution verticale plus ou moins fine. La résolution spatiale est également importante pour représenter les principales causes de variabilité du manteau neigeux (e.g. topographie, transport de neige par le vent, végétation, etc.), avec un surcoût numérique important empêchant leur application sur de grandes échelles. À l'heure actuelle, les modèles de manteau neigeux utilisés pour la prévision du risque d'avalanches tels que Crocus, le modèle opérationnel de Météo-France (Brun et al., 1989; Vionnet et al., 2012), représentent une stratigraphie détaillée avec un nombre variable de couches, et prennent en compte l'influence de la topographie (géométrie semi-distribuée). En revanche, ils ignorent

généralement les processus de redistribution de la neige par le vent et la gravité, notamment en raison de leur coût de calcul. Ces modèles sont forcés par des prévisions météorologiques particulièrement imprécises en montagne (e.g. Nousu et al., 2019), et sont eux mêmes entachés de nombreuses erreurs et incertitudes notamment liées à la paramétrisation incertaine des processus physiques (Krinner et al., 2018), et à la non-représentation du transport de neige par le vent. Ces deux sources d'erreurs et incertitudes contribuent significativement aux erreurs de modélisation (Raleigh et al., 2015). En outre, celles-ci sont vouées à perdurer, car l'atmosphère est intrinsèquement chaotique (Lorenz and Haman, 1996), les modèles météorologiques insuffisamment résolus en montagne, et à cause d'un manque d'observations suffisament détaillées permettant de cibler et réduire les erreurs de modélisation de la neige (Menard et al., 2020).

L'approche probabiliste permet de rendre compte des erreurs et incertitudes de modélisation. Dans ce formalisme, au lieu d'estimer une valeur unique, le modèle fournit une densité de probabilité (ou probability density function, pdf) une "étendue des possibles" pour la variable considérée. Une méthode s'est imposée pour fournir cette approche probabiliste : la prévision d'ensemble. Celle-ci consiste à lancer simultanément un ensemble de simulations (ou membres) à partir de conditions initiales différentes, propagées par des versions de modèles différentes. La densité de probabilité de la prévision est directement estimée à partir de la densité des valeurs prédites par les membres de la simulation.
On peut ainsi estimer les incertitudes de modélisation, qu'elles soient liées à une situation particulièrement chaotique, ou aux faiblesses du modèle. Si la densité de probabilité d'une prévision est "resserrée" (les membres ont quasiment tous tous la même valeur), on en déduira que la prévision est sûre, dans le cas contraire la précision sera considérée comme incertaine. Bien entendu, il faut que l'on puisse faire confiance au modèle fournissant ces prévisions. Pour cela, on doit avoir vérifié au préalable certaines de ses propriétés contre un grand nombre d'événements "tests". La fiabilité, sa capacité à donner la bonne probabilité à un événement, qu'il soit rare ou fréquent, et sa résolution, sa capacité à discriminer deux événements différents, sont des propriétés essentielles.
La prévision d'ensemble est apparue pour la prévision numérique du temps (Molteni et al., 1996), et est en cours d'émergence dans la modélisation du manteau neigeux (e.g. Essery et al., 2013; Magnusson et al., 2014; Vernay et al., 2015; Lafaysse et al., 2017; Nousu et al., 2019; Dumont et al., 2020). En particulier, bien qu'il soit indispensable de prendre en compte ces deux sources d'incertitudes, des ensembles de forçages météorologiques n'ont que rarement été combinés avec des ensembles de modèles de neige (Günther et al., 2019).

L'assimilation de données propose de combiner observations et modèles de manière

optimale, et est en cela une chance unique pour la modélisation. Connue comme "l'art de comprendre les observations" (Lahoz and Menard, 2010), elle permet d'établir une "analyse" tenant compte des valeurs prédites par le modèle, et les observations, ainsi que de leurs erreurs respectives. Elle tire donc un excellent parti des méthodes ensemblistes qui lui fournissent une estimation dynamique des erreurs de modélisation. En théorie, cette analyse est à la fois plus près de la réalité et plus précise que les deux sources d'information dont elle est issue. Dans un cadre séquentiel en temps réel, où les observations sont assimilées au fur et à mesure qu'elles sont disponibles, cette analyse peut ensuite être réinjectée dans le modèle, le rapprochant ainsi de la réalité. Celui-ci est alors utilisé jusqu'à ce qu'une autre observation soit disponible. Cette approche séquentielle se prête bien au problème de la prévision météorologique, et en particulier à la prévision du risque d'avalanche et au suivi hydrologique.

L'assimilation de données a permis des progrès spectaculaires en prévision numérique du temps ces quarantes dernières années. Elle est ensuite apparue dans la modélisation du manteau neigeux, où elle est encore balbutiante, par le biais de la prévision hydrologique (e.g. Slater and Clark, 2006), et de la modélisation des surfaces continentales (e.g. De Lannoy et al., 2012). En ce qui concerne la modélisation du manteau neigeux, les méthodes d'assimilation ensemblistes telles que le filtre de Kalman d'ensemble (EnKF) ou le filtre particulaire avec réechantillonnage séquentiel (PF) sont les plus répandues à des fins de prévision (e.g. Magnusson et al., 2014; Larue et al., 2018), et ont permis d'assimiler avec succès des variables intégrées telle que la hauteur de neige (e.g. Magnusson et al., 2017), voire même plusieurs variables (Piazzi et al., 2018). En revanche, l'assimilation de réflectances n'a jamais dépassé le cadre idéalisé (Charrois et al., 2016). Les algorithmes de lissage, tels que le Particle Batch Smoother (PBS, Margulis et al., 2015) sont eux plus adaptés aux problèmes de modélisation rétrospective travaillant avec des variables comme la SCF (e.g. Aalstad et al., 2018). Une revue complète des méthodes d'assimilation pour la neige a été récemment proposée par Largeron et al. (2020).
L'assimilation peut également être utilisée pour diffuser de l'information depuis les zones observées vers les zones non observées. Ceci est indispensable dans notre cas pour répondre à la parcellarité des observations (in-situ comme satellitaires) dont nous disposons. En effet, une assimilation "point par point" (e.g. Kim et al., 2019; Deschamps-Berger et al., in review) ne peut pas corriger le modèle dans les zones non-observées, ce qui induit de trop grandes différences de performance avec les zones observées. Si des méthodes d'interpolation spatiale (des observations comme des analyses ponctuelles) (e.g. Slater and Clark, 2006; Cantet et al., 2019) ont été proposées pour combler ces "trous", celles-ci semblent trop approximatives en terrain complexe. La question de la propagation de l'information par l'assimilation pour la modélisation du manteau neigeux en terrain complexe reste largement

inexplorée (Largeron et al., 2020), nous y reviendrons.
En ce qui concerne le problème de la prévision du risque d'avalanche, le PF semble le plus adapté aux modèles lagrangiens tels que Crocus, qui impliquent un nombre variables de couches numériques (Magnusson et al., 2017). En outre, c'est la seule méthode qui préserve la cohérence physique entre les variables de manière certaine. C'est important, car de petits gradients verticaux locaux peuvent avoir une incidence importante sur le métamorphisme modélisé. L'analyse du PF consiste en effet à rejeter les membres (ou particules) les plus loin de l'observation (par rapport à l'erreur d'observation), et de les remplacer par les membres les plus proches (Gordon et al., 1993; Kitagawa, 1996).
Une des grandes difficultés rencontrées par le PF est le problème de dégénérescence : lorsque le nombre d'observations simultanément assimilées augmente, un trop faible nombre de particules se trouve dupliqué pour correctement représenter la pdf du système (Snyder et al., 2008). Des solutions existent pour la résoudre: l'inflation des erreurs d'observations (Larue et al., 2018) ou la localisation du PF (Van Leeuwen, 2009).

La résolution de la dégénérescence par des méthodes de localisation est de fait liée à la question de la propagation (notamment spatiale) de l'information par l'algorithme d'assimilation. Lorsque la dégénérescence empêche de produire une analyse globale sur tout un domaine, la localisation du PF propose de séparer ce problème en un ensemble de problèmes locaux. Une analyse est effectuée en chaque point, en considérant les observations dans son voisinage. De ce fait, le nombre d'observations est réduit, et la dégénerescence du PF est évitée[2]. La localisation repose donc sur la notion de voisinage, qui vise à définir un ensemble de positions pouvant contenir des informations pertinentes sur le point considéré. Il est nécessaire ici de s'attarder sur cette notion de "pertinence". De l'information sur l'état d'un point peut servir à améliorer la connaissance sur l'état d'un autre point via l'assimilation si ceux si sont statistiquement liés (mais pas nécessairement physiquement, ce lien peut être causé par un facteur externe tel que des forçages météorologiques)[3]. Dans la plupart des systèmes géophysiques, des points peuvent être considérés comme statistiquement indépendants passée une certaine distance, et la notion de voisinage classiquement admise s'appuie sur ce principe, dans le PF (e.g. Poterjoy, 2016) comme l'EnKF. Dans ce dernier, ce sont souvent les structures de corrélations de l'ensemble qui sont utilisées pour estimer cette indépendance statistique (e.g. Hamill et al., 2001).
En ce qui concerne le manteau neigeux en montagne, ce lien entre distance et indépendance statistique reste à vérifier. En l'absence de transport de neige par le vent, au delà de quelques

[2]En revanche, on obtient des analyses discontinues, car différentes en chaque point, ce qui peut poser des problèmes lorsque ceux-ci sont couplés (Farchi and Bocquet, 2018)

[3]Reste à trouver le facteur externe reliant le changement sémantique du mot "antan" avec le changement climatique...

mètres, les points sont dans une grande mesure physiquement indépendants[4]. En revanche, ceux-ci peuvent être soumis à de mêmes facteurs (météorologie, conditions d'éclairement), apportant des liens statistiques, et donc, la possibilité de propager de l'information. Comme nous l'avons évoqué pour l'EnKF, les corrélations d'ensemble peuvent être utilisées pour estimer cette dépendance statistique, mais à l'heure actuelle, du fait de l'utilisation encore balbutiante des ensembles en modélisation du manteau neigeux, nous ne connaissons rien de ces structures spatiales de corrélation. Il est ainsi possible que la notion de voisinage, basée sur des critères de distance, ne soit pas adaptée à la neige en terrain complexe aux échelles de modélisation considérées (au delà de la centaine de mètres). Pour une analyse locale en pente sud ensoleillée, une observation distante, mais dans des conditions d'éclairement similaires, pourrait être mieux indiquée qu'une observation plus proche, mais venant d'un versant ombragé.

L'objectif de cette thèse est de mieux caractériser la variabilité spatiale du manteau neigeux en montagne. La méthode consiste à essayer de tirer parti des observations in-situ de hauteur de neige, et des réflectances satellitaires en les incluant dans des simulations d'ensemble du manteau neigeux avec Crocus, à l'aide de l'assimilation de données. Nos travaux tenteront de répondre aux questions suivantes:

- **Les observations de réflectances satellites de la neige permettent-elles de mieux contraindre la modélisation du manteau neigeux en montagne ?**

Si leur potentiel pour contraindre les simulations du manteau neigeux a été prouvé avec Crocus dans un cadre idéalisé (Charrois et al., 2016), des données réelles de réflectances spectrales du manteau neigeux n'ont encore jamais été assimilées avec succès, *a fortiori* dans un contexte spatialisé. Nous chercherons donc à voir si des données de réflectances MODIS et Sentinel-2 peuvent être assimilées dans des simulations d'ensemble du manteau neigeux. Pour ce faire, la représentation des incertitudes dans le système de simulation d'ensemble utilisé devra être améliorée afin d'inclure les incertitudes de modélisation du manteau neigeux. Nous traiterons de cette question dans le Chapitre 2.

- **Peut-on propager de l'information sur l'état du manteau neigeux depuis des zones observées vers des zones non-observées ?**

Les réflectances satellites ont une couverture spatiale parcellaire (Sirguey et al., 2009). Par exemple, elles sont rarement disponibles en versant Nord. On se demande s'il est possible d'améliorer les simulations du manteau neigeux dans les zones non observées à l'aide d'observations dans des zones observées grâce à l'assimilation. Le filtre particulaire semble une méthode d'assimilation appropriée à la modélisation du manteau neigeux en montagne, mais souffre de dégénérescence lorsque trop d'observations sont assimilées simultanément.

[4]Raison pour laquelle la plupart des modèles de neige sont 1D, même les plus détaillés physiquement (e.g. Brun et al., 1989; Lehning et al., 1999)

Après avoir construit un système d'assimilation ensembliste à même de répondre à ce problème, nous allons voir s'il est possible, dans un cadre idéalisé, d'éviter cette dégénérescence tout en parvenant à propager de l'information dans les zones non observées. Ce problème sera abordé en Chapitre 3.

- **Dans quelle mesure peut-on utiliser les observations in-situ de HN pour améliorer les simulations du manteau neigeux dans leur voisinage ?**

Plusieurs études sont parvenues à assimiler des observations intégrées du manteau neigeux (hauteur de neige ou SWE) dans un contexte spatialisé en terrain montagneux (e.g. Magnusson et al., 2014; Winstral et al., 2019). Celles-ci s'appuient sur un réseau exceptionnellement dense d'observations. Il est probable que la performance de tels systèmes d'assimilation décroisse avec la densité d'observations disponibles (Largeron et al., 2020), ce qui limiterait la portée d'une telle approche à un nombre très limités de régions montagneuses. Nous allons appliquer notre système d'assimilation ensembliste au cas d'un réseau d'observations de hauteur de neige couvrant les Alpes et Pyrénées françaises, ainsi que l'Andorre. Ce réseau a des densités d'observation très variables. On pourra ainsi évaluer l'apport de l'assimilation par rapport au système opérationnel de Météo-France dans une grande diversité de situations. Cette question sera traitée dans le Chapitre 4.

Acknowledgements - Remerciements

First of all, I'd like to thank the jury for their extensive review and the numerous comments that really helped improving the quality of my thesis. I really enjoyed the discussions after my defense. I wish I had the opportunity to meet you in person!

Marie, Matthieu, il y a six ans vous m'avez embarqué dans une aventure sans deviner l'importance qu'elle revêtrait pour moi. Disponibles, à la fois confiants et patients, vous avez été une grande source d'inspiration et de motivation. J'ai eu l'impression d'être à ma place au CEN, d'avoir trouvé mon biotope. Chacun sait à quel point c'est fragile. À quoi cela tient-il ? À un environnement administratif compréhensif et prévenant, en les personnes de Delphine et de Jean-Louis (puis de Laura), sachant aussi se venger avec une petite dose d'ironie bien sentie. À une équipe technique experte en plomberie informatique comme en dégât des œufs : Évelyne, Romain, François, Ulrick, chapeau. À une direction scientifique qui accorde beaucoup d'importance et d'intérêt à la faune des non-permanents. À Vincent, à la prévi, qui sait toujours ramener les doux réveurs-modélisateurs que nous sommes les pieds sur terre, et qui nous montre qu'une approche plus sensible, plus humaine a probablement plus de sens que la mécanique désincarnée de nos super-machins. Aux hommes et aux femmes du deuxième couloir, tout simplement, qui en font un lieu d'écoute et d'échanges humains: Jacques, Maurine, Yves, Anne, Cécile, Mathieu, Isa, Laure... : merci beaucoup.
Cet environnement fut un point d'eau où se nouèrent des amitiés de grande qualité. Rafife, Iheb, vous ne vous êtes jamais laissés décourager par mon aridité au bureau et m'avez toujours réservé de précieux moments d'échange et de complicité lors de vos pauses clopes. Carlo, qui tente sans relâche de nous faire croire qu'il est un gros macho nul en code alors que tout le monde a compris que c'est un geek-nounours et une personne aux qualités rares. Maxim, qui cultive sans relâche son image d'anglais excentrique. François qui a bien compris que les dreads c'est avant tout pratique (corde de secours, boule-quiès, casque, oreiller, épouvantail à fâcheux, détecteur de morilles et de peuf). César, dont l'initiative de la Cafète Masquée, qui nous a permis de nous amuser tout en maintenant un semblant d'ambiance de labo, fut magnifique. Cette thèse fut également le cadre de nombreuses collaborations et périgrinations jubilatoires. Manu, Jesus, Youness, travailler avec vous a donné beaucoup de sens à des mois de code rébarbatifs, et m'a donné le goût du travail en équipe. Merci enfin à Clément et Simon, jeunes sages aux précieux conseils.
Anne, petite plaque qui m'a toujours supporté, je te dois la vie en quelque sorte, et je sais combien tu auras besoin de légèreté et d'attention. Un message enfin pour mes parents, pour Cécile, Clément et Oma qui me composent, pour vous je veux toujours m'Améliorer.

List of Abbreviations

ALADIN	**A**ire **L**imitée **A**daptation dynamique **D**éveloppement **I**nter**N**ational
ANENA	**A**ssociation **N**ationale pour l'**É**tude de la **N**eige et des **A**valanches
BC	**B**lack **C**arbon
CEN	**C**entre d' **E**tude de la **N**eige
DEM	**D**igital **E**levation **M**odel
DUFISSS	**DU**al **F**requency **I**ntegrating **S**phere for **S**now **S**SA measurement
ESCROC	**E**nsemble **S**ystem **CROC**us
IGE	**I**nstitut des **G**éosciences de l'**E**nvironnement
IPCC	**I**ntergovernmental **P**anel on **C**limate **C**hange
LAP	**L**ight-**A**bsorbing **P**article
LIDAR	**LI**ght **D**etection **A**nd **R**anging
LW	**L**ong**W**ave radiation
MOCAGE	**M**odèle de **C**himie **A**tmosphérique **A** **G**rande **E**chelle
MODIS	**MOD**erate resolution **I**maging **S**pectroradiometer
NWP	**N**umerical **W**eather **P**rediction
SAJF	**S**tation **A**lpine **J**ospeh **F**ourier
SROCC	**S**pecial **R**eport on the **O**cean and **C**ryosphere in a **C**hanging **C**limate
SURFEX	**SUR**face **EX**ternalisée
SSA	**S**pecific **S**urface **A**rea
SW	**S**hort**W**ave radiation
TARTES	**T**wo-stre**A**m **R**adiative **T**ransf**E**r in **S**now
TOA	**T**op **O**f **A**tmosphere

Chapter 1

Snowpack observations, modelling and data assimilation

1.1 Snow in the mountains

1.1.1 Why is snow important?

Snow is an essential component of mountainous areas worldwide. Though mountains cover only about 12% of the Earth's continental surfaces (excluding Antarctica) (Körner et al., 2011), they host an above average biodiversity (Mutke and Barthlott, 2005). About 10% of the humanity live close to mountain cryosphere (i.e. snow, glaciers, permafrost, lake and river ice) (Hock et al., 2019), of which snow is a major component. Understanding its spatio-temporal variability is therefore key to anticipate the influence of climate change on these areas.

Climate

Snow plays an important role on the climate (Solomon et al., 2007) as it is one of the Earth's more reflective surfaces, and its cover extends up to about 14% of the Northern Hemisphere continental surfaces in March (Pielke et al., 2004). Snow also has an impact on the carbon balance, since low vegetation cannot grow until it melts (Pulliainen et al., 2017), and on the soil and permafrost thermal regime due to its low thermal conductivity (Domine et al., 2006b). Many other climatic feedbacks implying e.g. snow photochemistry and impact on sea-ice are summarized in Domine et al. (2006b).

Biodiversity

Snow is key to many live species including mammals, birds and plants. Its insulating properties are used by lemmings and grouse to save energy during the winter (Domine et al., 2018; Storch, 1993), and controls the thermal regime of the ground, with implications for the vegetation (Sturm et al., 2001). For example, the snow melt-out date is key for the onset of plant growth in the Alps (Jonas et al., 2008; Francon et al., 2020). Snow whiteness is exploited for camouflage by many species in a predator-prey relationship (Zimova et al., 2018).

Human activities

Snow and glaciers inspire respect, fear, and fascination to humans. It is an intrinsic cultural element of many communities in mountainous areas worldwide, including the Andes, Himalayas and the Alps (Gagné et al., 2014; Jurt et al., 2015; Frappier, 1971, pp. 320-331). It is also a crucial part of the mountainous economy, both as a resource for recreational activities (Xiao et al., 2015; Spandre et al., 2019) and because of its controls on pastoral

resources (Fuhrer et al., 2014). Snow accumulates during the winter and its spring melt supplies the river flow of downstream areas hosting about a sixth of the earth's population (Barnett et al., 2005). This water is key for irrigation of crops (Nüsser and Schmidt, 2017), fisheries (McNeeley, 2017) and hydropower energy (Gaudard et al., 2014). As interannual variability is high, anticipating the amount and timing of the melt is essential, especially in a changing climate (Lafaysse et al., 2014).

Snow related hazards

There are several snow-related hazards, causing many human fatalities, billions of damages worth every year (Haeberli and Whiteman, 2015), and shaping mountainous ecosystems (Bebi et al., 2009). During the winter, snowfall events pile-up into a snowpack formed by the successive precipitation events. The cohesion between the different layers can be poor, and an avalanche may be triggered if the local slope is sufficient enough (Schweizer et al., 2003). Snow-related floods are also an important threat, especially during rain-on-snow events. Depending on several physical properties of the snowpack such as its liquid water content, liquid water from the rain may flow faster on the snowpack than it would through bare ground, thus causing a shorter but more intense flood peak (Pomeroy et al., 2016). Such events can result in extreme infrastructural damage and fatalities as during the centennial flood of the Garona river in the Pyrenees in 2013 (Fig. 1.1).

FIGURE 1.1: Infrastructural damages caused by the Garona river flash flood of 2013, June 18th, in Les (Spain). (©AEAG P. Barthe)

1.1.2 Physical properties of the snowpack

A snowpack is a pile of snow, formed by accumulation of successive precipitation events, resulting in vertically varying properties. In mid-latitude mountains, due to seasonality, this snowpack grows under snowfall during the winter and cold season (accumulation

period). Its fate is to melt during the spring and summer (ablation period). At intermediate altitudes, melt can occur any time during the season (Morin et al., 2012). Sublimation is also often a significant ablation process (Strasser et al., 2008a). If the balance between accumulation and ablation is positive, the snowpack will survive and accumulate from year to year, eventually forming a glacier. The key point of the evolution of a mountainous snowpack is therefore its mass and energy budget.

Mass and energy budget

Snow is an ice matrix filled with air and potentially liquid water. The mass budget of the snowpack includes its mass of ice and liquid water. The primary income for the mass budget is solid precipitation. The snowpack can be soaked up by liquid precipitation, therefore increasing its total mass. Phase changes at the surface from or to the vapor state can be significant. Snow deposition or ablation by wind transport and gravitational processes are significant too, but will be excluded in the following.
Under this hypothesis, the snowpack can loose mass by the three following processes: basal runoff of liquid water, sublimation of surface ice and evaporation of surface liquid water. Following Essery (2015), the snowpack mass variation can be formulated as:

$$\frac{dM}{dt} = P + E + S + R \tag{1.1}$$

With the following terms, counted positive when they increment the mass budget:

- M: the mass of ice and liquid water in the snowpack.
- P: the precipitation rate (liquid or solid).
- S: ice-vapor phase change flux, positive in the case of deposition (e.g. formation of surface hoar (Hachikubo and Akitaya, 1997)), negative for sublimation.
- E: the liquid-valor phase change flux, positive in the case of condensation, negative in the case of evaporation of surface liquid water (Bengtsson, 1980), in general negligible compared to S.
- R: the basal runoff (negative). Liquid water percolates until the bottom of the snowpack where it infiltrates on the ground or flows on it. Water percolation depends on the liquid water holding capacity of the snowpack layers, as well as the formation of preferential flows or capillary barriers. For further details, the reader is referred to Wever et al. (2015) and Quéno et al. (2020a).

The total energy $\mathcal{E}$ in the liquid and solid phase is convenient to represent the energy budget of the snowpack as it accounts for phase change inside the snowpack. Its variation can be

formulated as (in W):

$$\frac{d\mathcal{E}}{dt} = SW\downarrow + SW\uparrow + LW\downarrow + LW\uparrow + H + L_vE + L_sS + H_p + H_r + G \tag{1.2}$$

With the following terms, (positive sign for entering fluxes):

- $SW\downarrow$: Incoming shortwave (SW) radiation. The shortwave domain corresponds to the wavelength range [300 nm, 4 μm]. $SW\downarrow$ radiation is parted into direct and diffuse radiation. Direct radiation $SW_{dir}\downarrow$ is proportional to the cosine angle between the surface normal vector and the direction of the sun. Diffuse radiation $SW_{dif}\downarrow$ includes contribution from the atmosphere and adjacent slopes, and accounts for approximately 20% of $SW\downarrow$ under clear-sky conditions. SW does not penetrate much more than about 10 cm into the snowpack (Tuzet et al., 2019).
- $SW\uparrow$: Outgoing shortwave radiation, $SW\uparrow = -\alpha SW\downarrow$, with α the snow albedo. Snow albedo is mostly affected by light absorbing impurities present in the snowpack and snow surface microstructure (Warren, 1982).
- $LW\downarrow$: Incoming longwave (LW) radiation from the thermal emission of the overlying atmosphere, clouds, vegetation and surrounding slopes. The longwave domain is defined as the domain of thermal emission [4 μm, 100 μm]. As this term increases with the temperature and emissivity of the emitting body, it is particularly prominent for low clouds and under the forest.
- $LW\uparrow$: Outgoing longwave radiation in the form of thermal emission from the snow surface. Snow is an almost perfect black body, i.e. its emissivity ε is close to 1[1]:

$$LW\uparrow = -\varepsilon\sigma T_s^4 \tag{1.3}$$

- Heat and mass energy fluxes due to turbulent fluxes. Turbulent fluxes increase with the temperature gradient between the snow surface and the atmosphere as well as surface wind speed (Martin and Lejeune, 1998). H is the sensible heat flux from the atmosphere. Latent heat fluxes (LE) are related to phase changes. They include L_vE (evaporation fluxes), with L_v the latent heat of vaporisation, L_sS (sublimation fluxes), with L_s the latent heat of sublimation. LE fluxes are proportional to the deviation between the atmospheric specific humidity and its saturation value. The melting/refreezing of snow doesn't appear as $\mathcal{E}$ accounts for the total energy of liquid and solid phases. However, the melting of snow reduces the amount of energy available to warm up the snowpack. Latent heats of evaporation and sublimation are about ten times higher than the latent heat of melt, so these phase changes result in a stronger

[1] In fact, snow emissivity slightly depends on snow density and microstructure though the relation is yet not well known (Hori et al., 2006)

cooling effect per unit of mass concerned than melt.

- H_p: The total energy advected by the precipitation.
- H_r: The energy flux lost through the runoff (total energy of the runoff), proportional to R.
- G: ground heat flux. This heat flux generally prevents snowpack basal temperature from decreasing below zero in alpine terrain. G is also important during early snowfall when the soil temperature is still high.

Fig. 1.2 shows an example of the evolution of the energy budget terms along a snow season. Net SW and LW terms are usually dominant and opposite at mid-latitudes. LW is the major contributor to the snowpack cooling, because in general, snowpack radiative cooling during clear sky nights takes over incoming LW radiation. The amplitude of SW also strongly increases during the melting season.

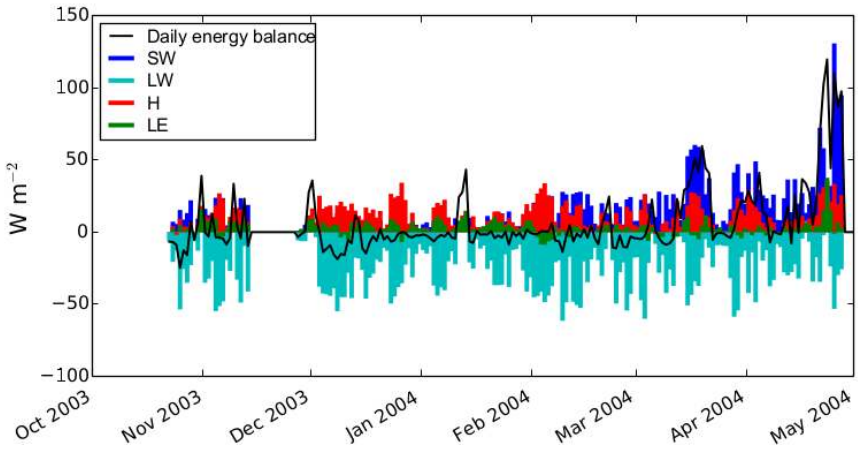

FIGURE 1.2: Example of daily simulated energy fluxes (excluding G) of an alpine seasonal snowpack (Col de Porte, 1325 m.a.s.l, French Alps), showing the order of magnitude of the different terms. Adapted from Lafaysse et al. (2017).

There is a high variability between the energy budgets of the different layers composing the snowpack, as most of the terms of the energy budget only affect the surface layers or the first upper layers. This often results in the formation of a temperature gradient, between the bottom of the snowpack, whose temperature is in general fixed to zero due to the ground flux G and the top, whose temperature is fixed by the energy exchanges with the atmosphere and can be much lower. This macroscopic temperature gradient induces a significant heat conduction through the snowpack, and increases for shallower snowpack and lower snow thermal conductivity. It is one of the drivers of snow metamorphism.

Snow metamorphism

A snowpack is an accumulation of snow grains deposited on the ground. Snow grains undergo perpetual transformations, the snow metamorphism, defined as the adjustment of local thermodynamic imbalance by sublimation or recrystallisation of ice. Snow mostly originates from snow crystals formed in the clouds below zero degrees Celsius[2]. Crystal shapes are very diverse, depending on the air temperature and vapor super-saturation (Fig. 1.3) during their growth. Super saturation quantifies the amount of water vapor above the vapor saturation pressure at the current pressure and temperature: it is the amount of water vapor potentially available for precipitation, in g m^{-3}. Snow crystals often aggregate, forming snowflakes. For a complete review of the formation of ice crystals the reader may refer to (Libbrecht, 2005).

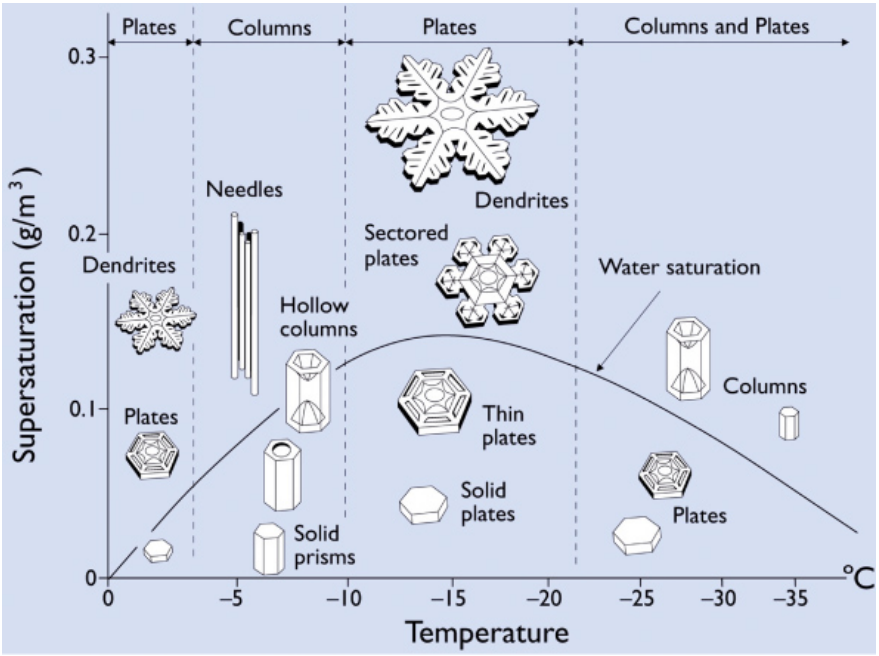

FIGURE 1.3: Morphology of the snow crystals as a function of super saturation and temperature, takem from (Libbrecht, 2005).

Once in the snowpack, snow particles are referred to as snow grains, as their shape and size is affected by metamorphism driven by phase changes, temperature and gravity. Metamorphism results in a diversity grain types described in Fierz et al. (2009). There are two types of metamorphism: wet snow metamorphism and dry snow metamorphism. Wet snow metamorphism occurs in the presence of liquid water, and leads to the rounding and coarsening of the snow grains. Dry snow metamorphism occurs below 0 ^{o}C under

[2]This classification excludes graupel, frozen precipitation particles formed by the successive accretion of cloud droplets on an ice particle. These particles can cause snowpack instability (Reinking, 1975; Abe, 2004).

temperature gradient. When the temperature gradient is small (about 5 K m^{-1} or less), dry metamorphism is driven by the grain curvature. Stronger temperature gradients lead to the formation of faceted crystals and depth hoar. For more details on snow metamorphism, the reader is referred to Colbeck (1982).

As it modifies the snow microstructure, snow metamorphism affects the albedo of snow and therefore has a significant impact on the SW radiative budget.

1.1.3 Shortwave radiative budget

In the mid-latitudes, and in a flat open terrain, the incoming shortwave radiation $SW\downarrow$ is generally the dominant term of the daily snowpack energy budget as seen in Fig. 1.2, and especially during the ablation period. Snowpack albedo, $\alpha = \frac{SW\uparrow}{SW\downarrow}$ can be seen as its capacity to reject this amount of energy, is therefore a key parameter. In the SW spectrum, snow albedo strongly varies with the wavelength. The reflectance is defined as the albedo for a given wavelength. The shortwave domain can be partitioned between the near-UV-visible range [300 nm , 4 μm] (VIS) and the Near Infra-Red (NIR). The amount of incoming energy, is equally parted between the VIS and NIR (Fig. 1.4). However, snow is more reflective in the VIS part of the spectrum (Fig. 1.5), therefore the amount of absorbed energy is higher in the IR. Note finally that SW radiation does not penetrate much into the snowpack. Penetration depth ranges from about a few tens cm (unpolluted snow) in the VIS to only a few millimeters in the IR (Warren, 1982; Tuzet et al., 2019). Therefore, the absorbed SW energy is concentrated at the top of the snowpack (Brun et al., 1992).

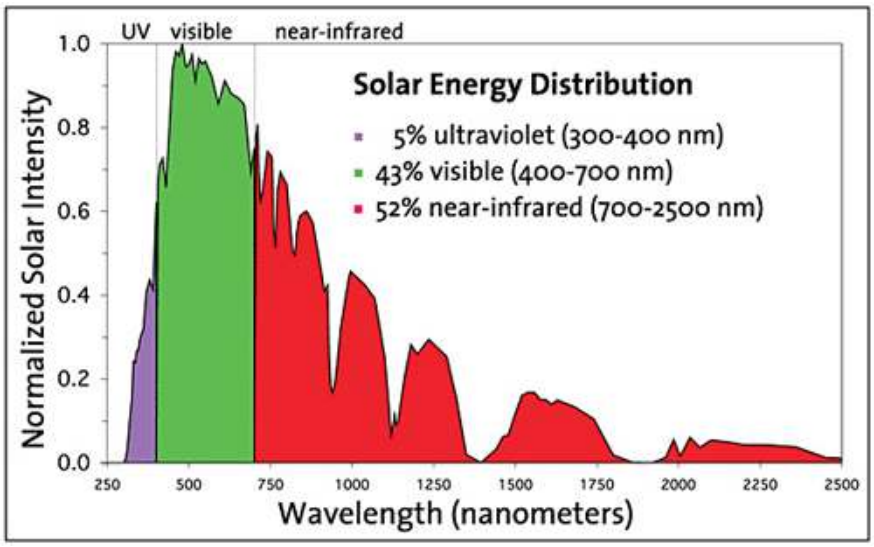

FIGURE 1.4: Example of normalized solar radiation intensity at the bottom of atmosphere (clear-sky conditions). Source: www.lmd.polytechnique.fr

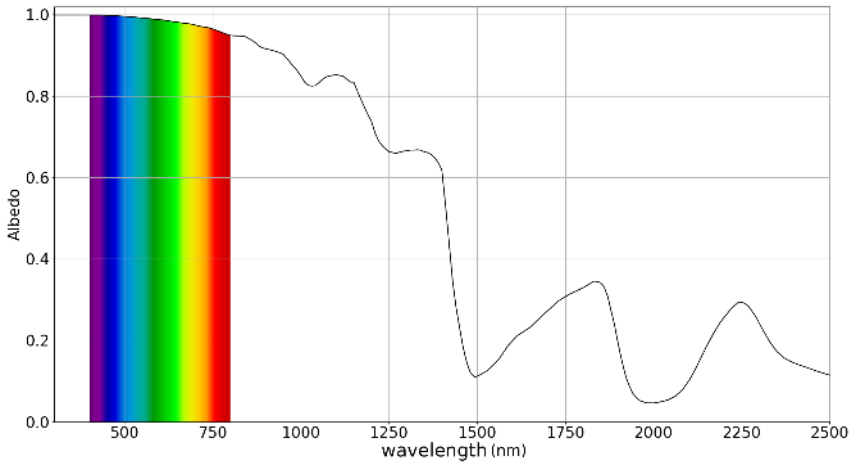

FIGURE 1.5: Snow reflectance as a function of the wavelength, taken from Tuzet (2019).

The impact of snow microstructure

Snow grain microstructure influences the scattering and absorption of light inside the snowpack (Warren, 1982). Snow specific surface area (SSA (m^2 kg^{-1})) quantifies the area of air-ice interface per kilogram of snow, in relation with its optical properties (Domine et al., 2006a). The coarser the grains, the lower the SSA. Fig. 1.6 shows that a coarsening of the snow grains (lower SSA) causes a marked drop in near-infrared (NIR) reflectance and affects VIS reflectance to a lesser extent. This optical phenomenon leads to the so-called "albedo feedback effect" which is crucial for the radiative budget. A positive energy budget cause surface melt which favours wet metamorphism on the snowpack surface. This form of metamorphism leads to a coarsening of the grains (see Sec. 1.1.2), which in turns reduces snowpack reflectance. Finally, this albedo reduction leads to an enhanced positive energy budget through the *SW* terms.

Light Absorbing Particles

As depicted on Fig. 1.7, the presence of light absorbing particles (LAP) leads to a decrease in the visible reflectance of snow evidenced by its brown color (e.g. Fig. 1.8). This impact can extend to the closer part of the NIR for significant LAP concentrations.
LAP include aerosols such as black carbon (BC) from anthropogenic or biomass burning, mineral dust (dust), originating from deserts such as the Sahara, volcanic ash, as well as microscopic algae blooming during spring (Skiles et al., 2018).
BC and dust are the main LAP types in the Alps (Di Mauro et al., 2015). These particles are present in suspension in the air and inside precipitation particles. They can deposit on the snow without precipitation (dry deposition) and during precipitation (wet deposition).

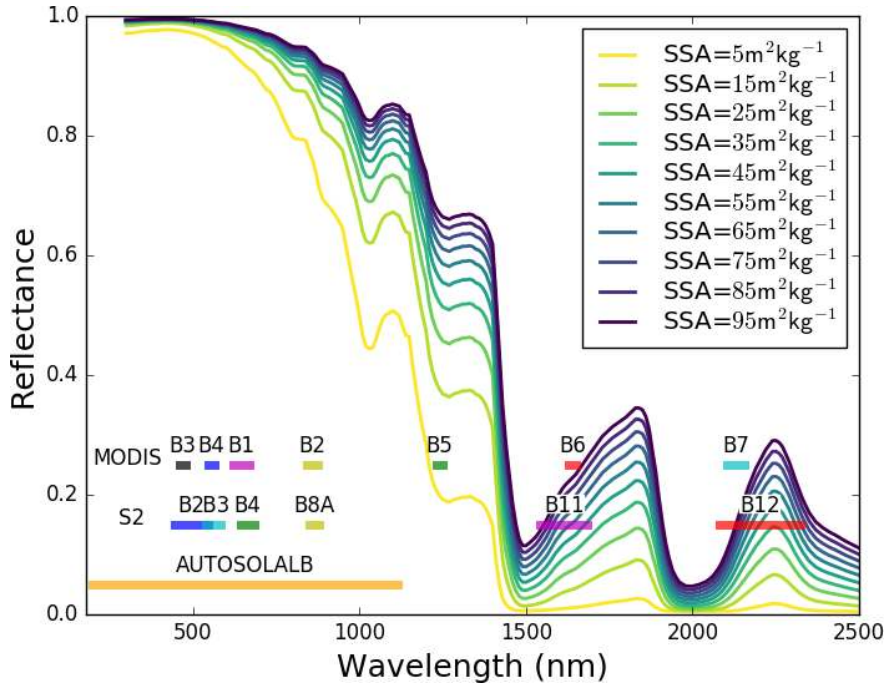

FIGURE 1.6: Influence of SSA on snow reflectance. Source : http://snowtartes.pythonanywhere.com

Black carbon fluxes are rather constant throughout the year, while dust deposition occurs only during specific events, when southern fluxes bring Saharan air masses over Europe, preferentially during the Spring (Di Mauro et al., 2019, e.g. Fig. 1.9). Only a small fraction of the BC and dust can scavenge to the bottom of the snowpack with percolating water (Flanner et al., 2007). As a result, most of the dust stratifies within the snowpack (Fig. 1.10) embedded with the layer it was deposited with (wet deposition) or onto (dry deposition), progressively becoming optically inactive due to the limited penetration depth of SW radiation. However, melt causes the "disappearance" of the snowpack superior layers through percolation or evaporation. This results in the re-emergence and accumulation of buried LAP on the snowpack surface which increases the radiative effect of LAP.

Geometrical properties

Snowpack spectral reflectance also varies with the properties of the incoming radiation such as the incidence angle Φ of $SW_{dir}\downarrow$ and the ratio between direct and diffuse incoming radiation. A detailed study of these geometric processes can be found in (Wiscombe and Warren, 1980; Dumont et al., 2017).

Without going much into details, we will note that the spectral reflectance increases with the incidence angle of the incoming light. As a consequence, since diffuse light is equally coming from all the hemisphere, diffuse reflectance is lower than direct reflectance for high

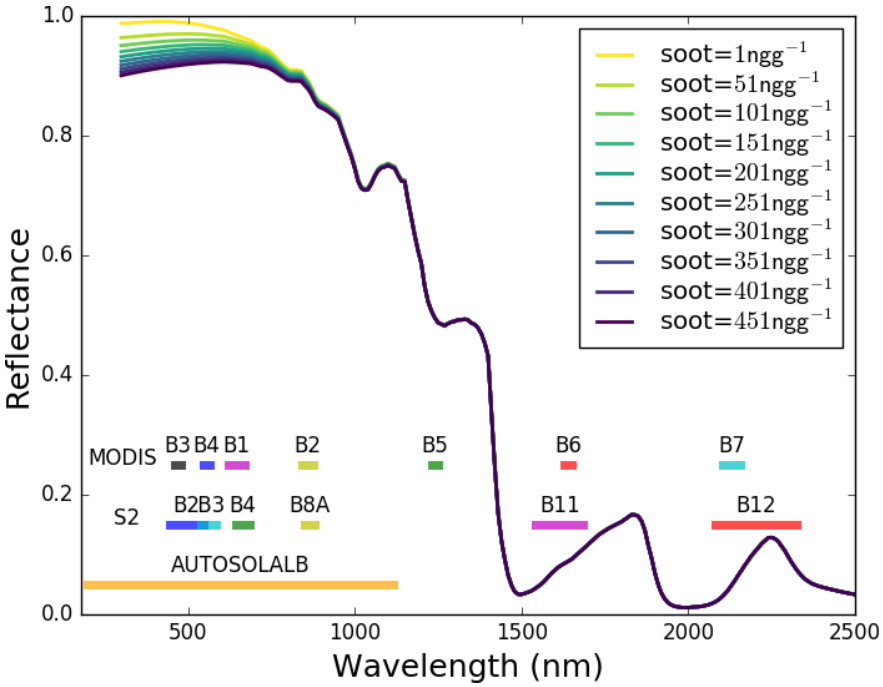

FIGURE 1.7: Influence of LAP concentration on snow reflectance. Source : http://snowtartes.pythonanywhere.com

FIGURE 1.8: Saharan dust on top of the snowpack in the Pyrenees (Pic du Midi D'Ossau, 2018 April 21th).

direct incidence angle Φ (the sun is close to the local horizon), and vice versa when Φ gets close to 0 (the sun direction gets close to the normal to the surface). Direct and diffuse reflectance equals at $\Phi \approx 53^{o}$ (Libois, 2014).

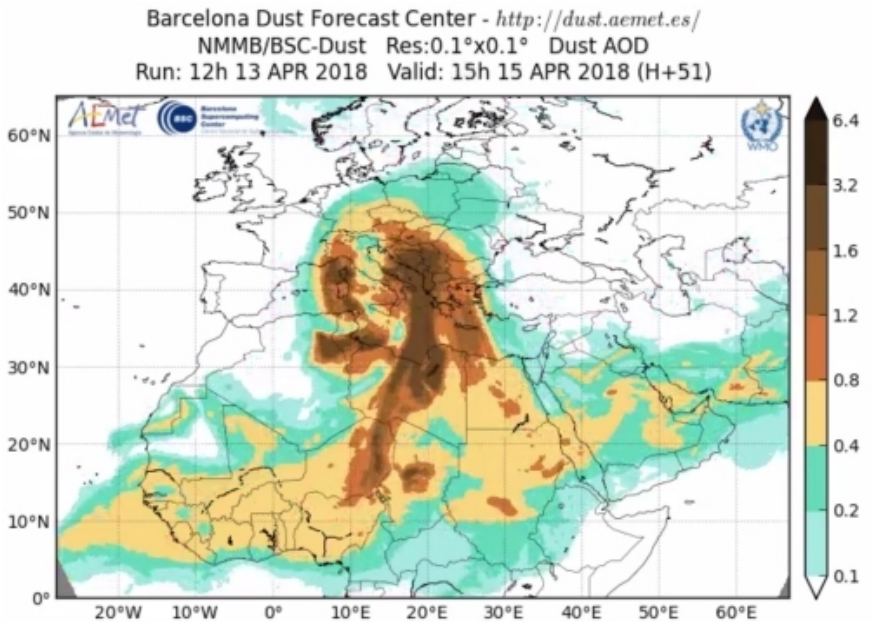

FIGURE 1.9: Dust aerosol optical depth (AOD) during a strong dust deposition event on April 15th, 2018. Source: Barcelona Dust Forecast Center, http://dust.aemet.es/.

FIGURE 1.10: Dust layer buried within the snowpack at col du Lautaret (2018, April 5th)

Since snow is highly reflective in the SW, it scatters a high amount of energy which can influence surrounding targets as shown on Fig. 1.11. However, it is also significantly non-isotropic (Dumont et al., 2010), requiring a complete knowledge of the illumination, surface properties and topographic geometry to account for any possible re-illumination. This phenomenon can be significant from small scales including snow surface roughness (Larue et al., 2020) to the kilometer scale (Sirguey, 2009; Lamare et al., 2020).

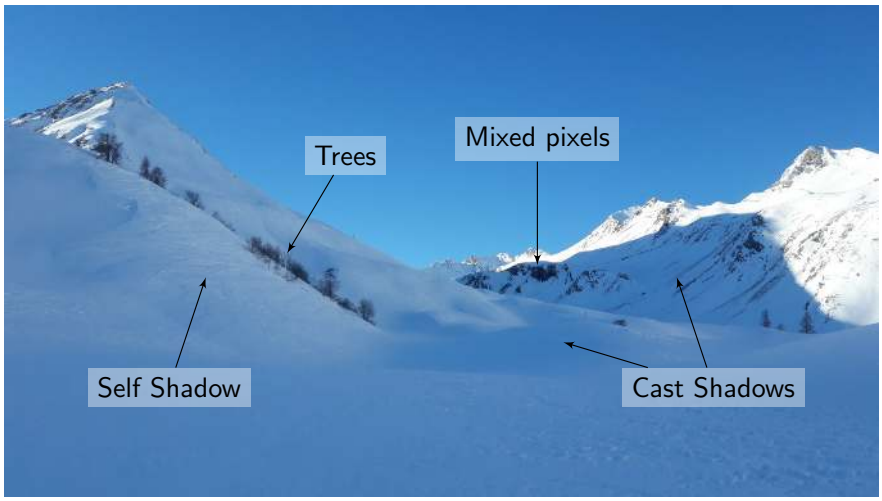

FIGURE 1.11: Example of reillumination in a valley. The slope on the left is reilluminated by the facing sunny slope. It seems brighter than the slopes in cast shadows, which, by essence, are facing self shadowed slopes (Sirguey, 2010). (col du Lautaret, 2017, December 20$^{\text{th}}$.)

1.1.4 Snow in a mountainous terrain

In the mountains, snowpack bulk properties, and a fortiori its stratigraphy, are highly variable. Mountain topography plays an important role on several terms of the energy and mass budgets such as SW radiation presented in previous Section 1.1.3. Indeed, the elevation, aspect and slope are fundamental local parameters. First of all, the air temperature decreases in the free atmosphere at a rate of approximately 0.0065 K m^{-1} in standard conditions (Minzner, 1977). As a consequence the elevation controls on the precipitation phase and energy fluxes such as the sensible heat flux H and indirectly the incoming $LW\downarrow$ which decrease with the elevation. Elevation has also indirect effects through other atmospheric parameters. A tendency to stronger winds at higher altitude also influence the heat fluxes. Lower vapor saturation pressure (through the temperature-elevation gradient), influences the latent heat fluxes and leads to enhanced precipitation. The orientation and slope affect the amount of incoming direct shortwave energy per surface unit, through the cosine effect (presented on Sec. 1.1.2).

To a lower extent, the topographic position relative to surrounding slopes exerts a control on shortwave atmospheric diffuse and longwave fluxes through the sky view factor, (the portion of visible sky), to which they are proportional. The complementary portion of the sky view factor controls the amount of longwave and shortwave radiations received from the surrounding slopes (see e.g. Fig.1.11 and Sec. 1.4).
Wind is also a direct cause of snowpack variability through its ability to transport snow. Wind drift is defined as the redistribution of snow from exposed to sheltered areas, as well as the preferential deposition of falling snow in sheltered area (Lehning et al., 2008). This phenomenon happens at every scale between a few centimetres to the scale of a mountain range. At small scales (below few meters) the snow surface interacts with the wind flow by forming surface patterns such as dunes and sastrugi (Kochanski et al., 2019). At the slope scale, (few meters-hundreds of meters), the wind drifts snow from wind-exposed edges into local thalwegs (Vionnet et al., 2014). At the mountain scale (hundreds of meters-kilometer), it occurs with preferential deposition of snow in the leeward slope, and the formation of precipitation eddies (Udina et al., 2020). At the scale of the mountain range (kilometers-hundreds of kilometers), orographic precipitation plays an important role, with often contrasted precipitation amounts between the wind exposed and leeward slopes of a mountain range, as exemplified by the usually strong contrast of precipitation between the French and Spanish sides of the Pyrenees. The reader is referred to Clark et al. (2011); Mott et al. (2018) for a complete review of wind-driven redistribution processes, including orographic precipitation and snow-vegetation interactions. Finally, the foehn effect (Richner and Hächler, 2013) is another example of strong contrasts in meteorological conditions with strong temperature and humidity gradients between two sides of a mountain range (e.g. Malardel, 2009).

To wrap things up, snowpack variability is caused by a multiplicity of factors. The topography is the primary factor, controlling the precipitation phase, temperature, and several energy fluxes. Snowpack variability is therefore primarily affected by the complexity of topography. Likewise, through its ability to transport snow, the wind is a key factor of variability in interaction with topography at every spatial scale, not to mention its influence on sensible and convective heat fluxes H and LE. This entanglement of spatial scales makes it a challenge to grasp snowpack variability with observations as any observation at any scale will be affected by some variability, which will limit its representativeness.

1.1.5 Summary

Snow is key to the Earth System and diverse human activities. Along with high shortwave albedo and thermal insulation properties, the snowpack has a complex and potentially unstable stratigraphy which can result in avalanches. Snow also controls on the hydrological regime of many watersheds worldwide. It is therefore essential to capture its spatial and temporal variations. They are considerable at various scales. Monitoring its evolution is therefore a challenge.

1.2 Snowpack observations

In-situ and satellite observations are useful to capture the spatial and temporal variability of the snowpack in the mountains. This section gives an overview of the observed variables and the techniques used to retrieve them. Our aim is to identify observations relevant to monitor the snowpack variability over large mountainous areas.

1.2.1 Snowpack internal variables and energy fluxes

For the most part, snowpack internal variables and energy fluxes are only measurable in-situ, which limits their potential to capture snowpack spatial variability at large scales.

Snowpack internal variables

Apart from a few exceptions, measurements of the snowpack internal variables require human operations and cannot be automated or remotely-sensed. Snowpack stratigraphy is traditionally performed by digging a snow pit in order to exhibit a vertical section of the snow layers. The layers can be sampled to measure parameters such as their density, snow grain type and size, hardness, SSA, temperature, liquid water content, and thermal conductivity (Lejeune et al., 2019). These measurements are routinely performed in ski resorts of many countries on a daily to weekly basis. Experts use them to evaluate the snowpack stability and monitor its thermal state, although their spatial representativeness is known to be very limited.

Snowpack energy fluxes

Snowpack energy flux measurements are mainly used to assess the ability of snowpack models to reliably represent snow physical processes (Morin et al., 2012). In most cases, they are only accessible in-situ in a very reduced number of sites around the world (Ménard et al., 2019). The radiative budget is measured by directly measuring broadband SW and LW incoming and upcoming fluxes (e.g. Lejeune et al., 2019). Convective fluxes H and LE

are much more difficult to assess, requiring a measurement of snow surface temperature, wind speed and turbulence close to the snow surface, along with classical meteorological variables such as air temperature, humidity and pressure (e.g. Martin and Lejeune, 1998). The basal heat flux G is measured by heat flux plates positioned on the soil surface.

1.2.2 Bulk variables

Bulk and surface observation are the only variables available at large spatial and temporal scales, since they are easily measurable and suited to remote sensing.

Height of snow

The height of snow (HS, m) defined as the vertical distance between the snow surface and its base, is probably the most commonly observed variable (Fierz et al., 2009). This bulk variable is of a primary interest to monitor the interactions of snow with topographic, wind and vegetation and any transport of snow, including avalanches. However, it only is a coarse estimate of the mass-energy budget because snow density is highly variable in time. HS can be measured with a wide diversity of techniques. In its simplest form, reliable points scale observations are obtained by manual measurements using a graduated snow probe or automated ultrasonic or laser HS gauges. Given the limited representativeness of point-scale measurements (Molotch and Bales, 2006; Grünewald and Lehning, 2015; Lejeune et al., 2019), a particular attention is in general paid to the location of these measurements, in order to increase their representativeness[3]. In general, such observations are located in areas where wind drift is limited. The power of these approaches stands in their reliability and simplicity. The deployment of operational manned or automated HS observation network over large areas is common in numerous countries (Morin et al., 2020).
Alternatively, remote measurements enabling to map the HS are the best way to capture snowpack variability. The use of LIDAR (LIght Detection And Ranging) technology emerged in the snow community about a decade ago (Prokop, 2008) producing HS maps of high resolution (metric or less). It was first used during measurement campaigns from ground sensor, thus with a limited spatial extent. In recent years, several airborne (i.e. from planes) Lidar campaigns (ALS for Airborne LaserScan) were conducted, providing meter-scale HS maps over large areas, which became operational in the western USA with a bi-weekly to monthly overpass (Painter et al., 2016). Finally, HS maps can also be derived from stereoscopic imagery from airplanes (Bühler et al., 2015), drones (e.g. Harder et al., 2020) , or agile optical satellites such as Pléiades (Marti et al., 2016). The latter method

[3]The representativeness of an observation is somewhat subjective (Molotch and Bales, 2006), e.g. a point scale observation cannot be representative for wind sheltered and wind-exposed areas at the same time...

covers areas of about 400 km^2 with a metric resolution (Deschamps-Berger et al., 2020). It requires the rotation of the satellite to acquire two or three successive along-track images of a target (with a different viewing angle), therefore only a few targets can be monitored per orbit). Though its pixel-accuracy ten times lower than of ALS, its spatial aggregates offer an accuracy suitable to monitor intermediate variability (Deschamps-Berger et al., 2020; Eberhard et al., 2020). Contrary to ALS, this technique virtually covers any location on the globe without any additional operating cost.

Snow water equivalent

Snow water equivalent (SWE, kg m^{-2}) is the mass of snow per unit area. SWE is the integrated mass budget and has many ranges of use in particular for hydrological studies. Its measurement is in general more complex than for HS. Manual measurements require to weight a vertical snow core of a given section. Several automated measurements are available. The so-called "snow pillows" are basically a buried scale (Serreze et al., 1999) weighting the overlying snow. This sensor is common in northern America but suffer from significant errors in the case of snow bridging over the scale. Other techniques using cosmic ray or gamma emission sensors are reliable but require yearly calibrations with snow cores (Paquet and Laval, 2006; Choquette et al., 2008; Gottardi et al., 2013). Networks of such sensors are generally sparser than HS networks and more oriented towards the monitoring of seasonal snow stock (i.e., higher altitudes) (e.g. Magnusson et al., 2014; Winstral et al., 2019). As for remote sensing, radar sensors aboard satellites such as Sentinel-1 shows some sensitivity to SWE though only for wet snow (Veyssière et al., 2019) or derived at a relatively coarse spatial resolution of about 1 km in our context (Lievens et al., 2019). Passive C and L band microwaves sensors such as AMSR-E are also sensitive to SWE (Durand et al., 2009), but their resolution is too coarse as well for mountain applications (Dozier et al., 2016).

Bulk density

Bulk density (kg m^{-3}) can be derived from co-located measurements of HS and SWE. Snow thermal conductivity increases with its density (Yen, 1981). Bulk density is therefore interesting to constrain its thermal state and in particular the snowpack ability to cool down during clear sky nights. The spatial variability of bulk density is generally lower than other bulk variables such as HS or SWE (e.g. Elder et al., 1998; López-Moreno et al., 2013).

1.2.3 Surface Reflectance

Surface reflectance is closely related to the SW radiative budget which is a key term of the energy budget (see Sec. 1.1.3). Surface information on SSA, characterizing snow microphysical properties can be derived from reflectance spectra (Fily et al., 1999; Durand and Margulis, 2007; Dozier et al., 2009; Painter et al., 2009; Mary et al., 2013) with interesting applications. For example, since fresh snow has a much higher reflectance than melt forms, the rain-snow line could be detected using reflectance observation following precipitation events, as well as binary information on the occurrence of solid precipitation. Snow surface metamorphism can be monitored via reflectance as well. However, because of the low penetration depth of the SW, deep and relatively thin fresh snow can have similar reflectance properties, making it difficult to discriminate using reflectance observations.
Reflectance is also sensitive to the presence of LAP on top of the snowpack. However, its sensitivity is lower than for SSA, and the required measurement accuracy might be out of reach to derive small BC concentrations (Warren, 2013). Recent studies demonstrated its potential to monitor large dust deposition events (Dumont et al., 2020).
Though only surface properties can be derived from snow reflectance, regular acquisitions of the reflectance along the season could yield information on the snowpack stratigraphy (Charrois et al., 2016) and detect the re-emergence of buried dust layers during the melting season which is critical for the timing of the melt (Tuzet et al., 2017; Dumont et al., 2020).
Reflectance can be monitored in-situ using bi-hemispherical spectrometers integrating the incoming and outgoing radiation (Dumont et al., 2017; Picard et al., 2020). However, there is only a handful of such sensors worldwide. Reflectance can also be retrieved from VIS/NIR top of atmosphere (TOA) radiances measured by satellite sensors such as MODIS, VIIRS or Sentinel-2 and 3. These sensors have various spatial resolution (10-300m) suitable to monitor snowpack variability in relation with the topography, and daily to weekly revisit times in the mid latitudes.

The retrieval of Reflectances from TOA radiances is not an easy task. Under clear-sky conditions, it requires to estimate the incoming and outgoing spectral illumination for each pixel. Incoming radiation primarily depends on the solar and atmospheric SW radiation (see Fig. 1.4 in Sec. 1.1.3), whose intensity and spectral signature depends on atmospheric conditions. The use of an appropriate atmospheric radiative transfer model is therefore needed to estimate this term. Then, because snow is highly reflective, direct and indirect (through the atmosphere) re-illumination occur, which are locally significant as depicted in Fig. 1.11. This coupling needs to be accounted for using a Digital Elevation Model (DEM) and terrain information (snow cover, land cover, vegetation properties...) of sufficient accuracy. As an example, neglecting re-illumination terms

would lead to consider that the same amount of incoming energy is received by pixels in self and cast shadows in Fig. 1.11, while the former receives more energy. Since the self-shadowed pixels appear more bright, it would lead to attribute them a higher reflectance, which is not necessarily the case. The anisotropy of reflectance, and several other geometrical phenomenon must be accounted for as well. Readers and authors are referred to Sirguey (2009); Lamare et al. (2020) for a thorough description of the methodology.

The retrieval of snow surface properties from SW sensors suffers from important spatio-temporal gaps (De Lannoy et al., 2012). Cloud coverage drastically limits their ability since they are opaque in this part of the spectrum. They also induce errors as they are sometimes difficult to distinguish from snow (Gascoin et al., 2019). However, cloud-free images are generally obtained on a weekly to bi-weekly frequency (Gascoin et al., 2015; Charrois et al., 2016). It is also difficult to retrieve snow properties from pixels with mixed cover (snow-vegetation or snow-rocks)(Sirguey et al., 2009; Masson et al., 2018) or illumination conditions (shadow/non-shadow) (Sirguey, 2009). This issue is even more important at coarser resolution (Lamare et al., 2020). It is finally impossible to retrieve snow properties under the forests which represent at least 19% of the snow-covered areas in the Northern Hemisphere (Rutter et al., 2009).
Thanks to its high contrast with other earth surfaces in the SW, the snow cover fraction (SCF) of each pixel can be retrieved from its SW reflectances (Sirguey et al., 2009; Masson et al., 2018). This variable is related to the HS or SWE via the snow depletion curve (e.g. De Lannoy et al., 2012), which strongly depends on the pixel size, topography, and land cover (Helbig et al., 2020). In the accumulation period, the SCF quickly reaches 1 for SWE above 20-40 kg m^{-2}. During the ablation period, an hysteresis phenomenon can be evidenced (e.g. Andreadis and Lettenmaier, 2006; Magand et al., 2014): same SWE values yield lower SCF values than during the accumulation period. The most important property here of the SCF is its saturation above 20-40 kg m^{-2}: for the most part, the information content of SCF is confined to snowfall on the ground events and during the ablation period. While it may be informative for intermittent snowpacks (Baba et al., 2018; Alonso-Gónzalez et al., 2020), or for reanalyses (Aalstad et al., 2018), it may be of least interest for seasonal snowpack modelling in alpine terrain. Furthermore, it is implicitly linked with snowpack reflectance since both are retrieved jointly by spectral unmixing methods (Masson et al., 2018).

1.2.4 Summary

Available observations of bulk and surface variables offer important information on the snowpack variability in mountainous areas. HS in-situ observations are widespread and operational but they have a limited spatial representativeness. Reflectance retrievals from satellite seem promising as they offer observations of the surface snow properties on a weekly to bi-weekly basis over whole mountain ranges. However, they suffer from important spatio temporal gaps.

1.3 Snowpack modelling and ensemble modelling

Snowpack modelling appears as a way to fill these gaps and more comprehensively assess the spatio-temporal variability of the snowpack without any restriction on spatial and temporal coverage.

1.3.1 On snowpack modelling and spatial discretization

Physically based snowpack models primarily aim at solving the energy and mass balance of the snowpack column (Anderson, 1976), as formulated in Sec. 1.1.2 (Eqs. 1.1& 1.2). As there are strong gradients between the bottom and the top of the snowpack, several numerical layers are necessary to properly solve the heat transfer (Essery et al., 2016). In particular, thermal gradients are higher close to the surface and the bottom, requiring a refined layering (Vionnet et al., 2012). Snowpack models used for stability assessment also require to account for the snow properties of the physical layers by an appropriate layering, leading to the use of more than 50 numerical layers in a lagrangian formulation, which implies a variable number of layers (Brun et al., 1992; Lehning et al., 1999). In addition, a large diversity of physical processes can be simulated or ignored: snowpack model complexity is therefore defined as the amount of processes, interactions and feedbacks that are accounted for in the model (Menard et al., 2020).

In the following, we will focus on Crocus (Brun et al., 1989; Vionnet et al., 2012) is the operational snowpack model for avalanche hazard forecasting at Météo-France (Morin et al., 2020), and was used in this work. It can be defined as a detailed snowpack model. Crocus is one-dimensional and includes up to 50 numerical layers. Each layer is represented by several several physical parameters such as the enthalpy (from which are derived the temperature and liquid water content), density, snow water equivalent, grain size and shape, etc. (see. Fig. 1.12). Crocus represents several physical processes such as heat conduction, liquid water percolation, snow metamorphism, phase change and snow compaction. Vertical

vapor fluxes are not explicitly represented. As a 1-D snow model, it can not account for horizontal fluxes (e.g. liquid water (Wever et al., 2016)) explicitly. Crocus is embedded within SURFEX surface platform (Masson et al., 2013) and therefore coupled with the land surface model ISBA (Noilhan and Planton, 1989). A detailed presentation of Crocus and its implementation in SURFEX can be found in (Vionnet et al., 2012). TARTES (Libois et al., 2013), a physically-based snowpack shortwave radiative transfer scheme was recently implemented within Crocus. Together with a realistic representation of the deposition and stratification of LAP within the snowpack (Tuzet et al., 2017, see Fig. 1.12), it allows for a better representation of the snowpack shortwave energy budget.

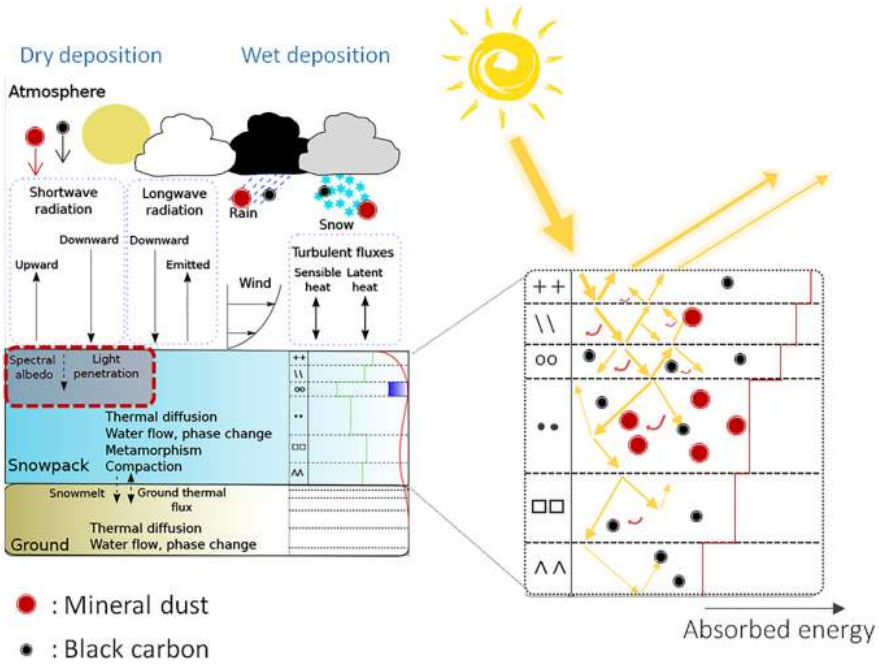

FIGURE 1.12: Main physical processes and variables model simulated by Crocus, including the shortwave radiative transfer (right part). Taken from Tuzet et al. (2017).

In parallel to model complexity (see above), snowpack models need to account for the complexity of the topography over large areas e.g. for avalanche forecasting or in order to monitor water resources. The semi-distributed approach is the simplest way to represent topographic-induced variability by running snowpack simulations in discrete topographic classes of given elevation, aspect and slope (Durand et al., 1999, see Fig. 1.13), which are the main drivers of energy balance and snowpack variability as described in Sec 1.1. This approach is operational for avalanche forecasting at Météo-France, and has been adopted for many hydrological applications ever since Beven and Kirkby (1979), (e.g. Lafaysse et al., 2011; Xie et al., 2012; Ajami et al., 2016). However this approach is purely conceptual, since it neglects local effects. Reasonably accounting for it requires to go down

to at least 250 m horizontal resolution (Fiddes and Gruber, 2012; Winstral et al., 2014; Vionnet et al., 2019; Baba et al., 2019)[4]. Other approaches use an irregular meshing which adapts to terrain ruggedness (Marsh et al., 2020) or statistical methods (Fiddes et al., 2019).

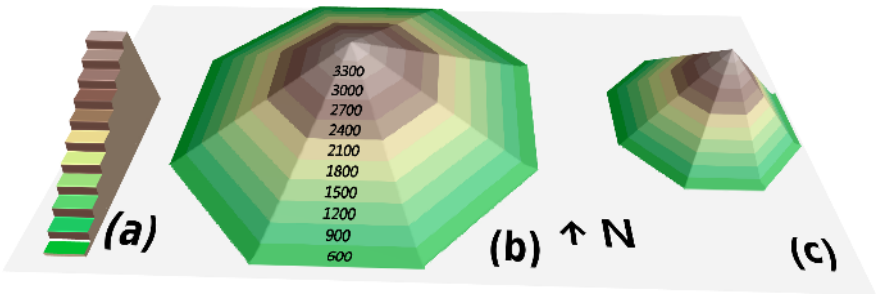

FIGURE 1.13: Representation of the semi-distributed geometry with the flat (a), 20° slope (b) and 40° slope (c) classes.

1.3.2 Modelling chains and uncertainties

Snowpack models require meteorological input, basal heat flux and topographic information in order to compute the different terms of the energy budget and mass transfer. Indeed, strong thermal and convective coupling occur between the snow surface and the atmospheric boundary layer (e.g. Arduini et al., 2019), and to a lower extent with the ground. To date explicit coupling between the snowpack and atmosphere models over large areas has mostly been done for NWP and climate applications (e.g. Dutra et al., 2012; Niwano et al., 2018). It is more unusual and generally localised when snow cover modelling is the main focus (e.g. Brun et al., 2011; Vionnet et al., 2014). Indeed, in such a situation (hydrology, avalanche hazard forecasting etc.), snow cover models are rather forced by pre-established estimates of meteorological conditions because (1) raw high-resolution NWP outputs are still less accurate than those estimates (e.g. Quéno et al., 2016) (2) it allows using more computationally expensive snow cover schemes. The snowpack models are sometimes coupled with a ground model (e.g. Decharme et al., 2016), and its outputs can be used for avalanche hazard assessment (Morin et al., 2020) or hydrological studies (e.g. Le Moigne et al., 2020).

In such modelling chains, snowpack models inherit from errors in the meteorological forcings which are particularly prominent in a mountainous terrain and account for about half of the modelling error (Raleigh et al., 2015; Günther et al., 2019). The downscaling of atmospheric models into resolutions suitable for snowpack modelling was also identified as

[4] A similar trend towards distributed modelling is observed in hydrology (e.g. Vincendon et al., 2010)

a key knowledge gap by the IPCC SROCC (Special Report on the Ocean and Cryophere in a Changing Climate by the Intergovenmental Panel on Climate Change, Hock et al., 2019). Snowpack models also suffer from uncertainties partly inherited from this uncoupled modelling structure. Indeed, snow-atmosphere interactions are parametrized in a wide variety of ways (e.g. for turbulent fluxes) with significant uncertainties, and without the capability to explicitly account for snow-atmosphere feedbacks. This is a major source of model error (Slater et al., 2001; Menard et al., 2020). According to these studies, *SW* albedo modelling is the other major source of modelling error. Other internal processes such as fresh snow density, compaction of snow, snow metamorphism, and the liquid water holding capacity are also important factors of uncertainty (Essery et al., 2013; Lafaysse et al., 2017). Reducing modelling errors requires to identify the best model parameterization and structure, which is not an easy task (and could even be a dead-end as more complex models do not necessarily yield better performance) as concluded by the recent model intercomparison projects (Krinner et al., 2018; Menard et al., 2020). An example of potential improvements is the recent implementation of fully-physical modelling of snow albedo (Tuzet et al., 2017; Skiles and Painter, 2019). However, the use of such formulations is not widespread as they require detailed and accurate LAP forcings from chemistry-transport models (Josse et al., 2004; Nabat et al., 2015; Horowitz et al., 2020), which are actually badly constrained in mountainous areas and over snow surfaces. Indeed, LAP forcing on snow radiative budget has been identified as a key knowledge gap in the SROCC (Hock et al., 2019).

Another aspect of snowpack modelling error and uncertainties lies in the difficult representation of gravitational redistribution of snow and wind drift. Gravitational redistribution is accounted for in a simplified manner in some models (Lehning et al., 2006; Strasser et al., 2008b). Pragmatically, it can be excluded by considering areas below 30^{o} of slope which are rarely affected by such processes (Schweizer et al., 2003). Wind drift is a more widespread phenomenon (see Sec. 1.1). Although a number of modelling strategies of various complexity have been proposed (e.g. Liston et al., 2007; Vionnet et al., 2017, 2020), large scale applications commonly ignore this process. Therefore, they are not representative for wind-exposed areas. This is mostly due to the prohibitive cost of downscaling atmospheric wind fields into the local topography and account for mass transfers between grid points, which is only an achievable goal at small scales (Lehning et al., 2006).

1.3.3 Ensemble modelling

As presented in previous Sec. 1.3.2, snowpack models suffer from uncertainties and errors which may be difficult to mitigate in the near future. These errors also vary with time and space: depending on the situation, simulations may be accurate, or not. A quantification of

uncertainties is necessary to provide model output users with an appropriate and objective level of confidence.

Principles of ensemble modelling

Ensemble modelling offers a way to issue probabilistic forecasts. The principle is to consider that since the available information (the initial state, the meteorological forecasts and the model) is approximate, it is impossible to determine the future state with certainty. Each slight modification of these conditions may, or may not result in significant variations of the future state. Ensemble modelling proposes to run different simulations, or members, each one with different settings and initial conditions exploring the likely ranges for the uncertain conditions. The members will then evolve on different trajectories. At a given forecast date, the distribution of the members can be analysed. This results in a probabilistic forecast: the most likely states are the ones where the density of members is the highest. The dispersion, or spread of the members, informs on the uncertainty of the simulation. The higher the dispersion, the higher the uncertainty of the simulation.

From an ensemble of predictions, one can derive the probability of an event to occur (e.g. for the snow depth to exceed a certain threshold) by calculating the proportion of members above this threshold. An ensemble is reliable if its issued probability are accurate regardless the probability level. As it is a statistical property, it needs to be verified over a large set of samples and a diversity of conditions (Atger, 1999; Bellier et al., 2017; Nousu et al., 2019). Reliability is equivalent to the verification data being statistically indistinguishable from the ensemble members. A necessary but insufficient condition for reliability is that the ensemble spread equals the average error of the ensemble (Fortin et al., 2015).
Another important property is ensemble resolution. Consider an ensemble issuing the climatology of a variable for a given day: this ensemble is reliable, since its distribution matches the distribution of the observations. However, its skill is limited: every year, it will issue the same forecast, regardless of the specific situation of the day. The resolution is the ability of a forecast to issue different forecasts for different situations (i.e. its ability to discriminate the different situations in different probability levels) (Atger, 1999). For a reliable ensemble, an ensemble resolution is equivalent to its spread: e.g. climatology has a poor resolution.

Brief history of ensemble modelling towards snow modelling

Ensemble forecasting first appeared in the NWP community as a way to account for the chaotic nature of the atmospheric system (Palmer, 1993; Tracton and Kalnay, 1993).

They are nowadays operationally used by national weather prediction centers worldwide (Bannister, 2017). Hydrologic and earth surface systems, including snow, generally exhibit "dampening" dynamics which make them less prone to chaotic error growth (Reichle and Koster, 2003; Reichle, 2008). Therefore, modelling uncertainties are inherited from uncertain meteorological conditions and model parametrization and structure.
Probably for this reason, ensemble modelling came a few years later into the hydrological modelling community (e.g. Clark and Hay, 2004; Schaake et al., 2007). This field is especially affected by meteorological errors (e.g. consider the impact that precipitation timing, localisation and intensity has on downstream river flow), and uncertainties in land surface initial conditions. Ensembles are now of standard use in hydrology (Cloke and Pappenberger, 2009), and usually combine meteorological ensembles with ensembles of hydrological models (e.g. Clark et al., 2008; Velázquez et al., 2011). Snow is also sensitive to meteorological uncertainty, justifying the use of meteorological ensembles as input (Slater and Clark, 2006). Ensembles of snowpack models emerged more recently from the acknowledgement that many uncertain physical parametrization lead to poor model behaviour (Slater et al., 2001; Rutter et al., 2009), and that quantifying it was necessary (Essery et al., 2013; Essery, 2015; Lafaysse et al., 2017; Günther et al., 2019). .

Generation of ensembles

In the NWP community, uncertainties in initial conditions probably exhibit the highest error growth rates, and originally, ensemble were generated by initializing deterministic models with an ensemble of initial conditions (Molteni et al., 1996). Later on, ensemble of models were generated by either stochastic perturbations (Leutbecher et al., 2017), or using multiphysics (Descamps et al., 2015). Stochastic perturbations have been first applied to state variables (e.g. Stochastically Perturbed Parametrisation Tendencies, SPPT Buizza et al., 1999) and to simulate unrepresented subgrid processes (Stochastic Kinetic Energy Backscatter, SKEB Palmer et al., 2009). These methods are easily tunable (i.e. amplitude, and spatio-temporal correlation of perturbations) and provide a convenient control on the ensemble spread, for example. One of the major limitations of SPPT is the introduction of physical imbalances, while SKEB might be less physically sound in the context of an increasing model resolution (Leutbecher et al., 2017).
Stochastic perturbations on uncertain parameters of the physical processes (SPP, Ollinaho et al., 2017) may be more consistent, and resolves imbalance issues. However, it only offers an indirect control on the ensemble behaviour therefore requiring more development effort to obtain the desired ensemble properties (e.g. spread). In a similar approach, multiphysics build ensembles by factorially combining different but fixed physical schemes

for several uncertain processes (e.g. Descamps et al., 2015). The different physical schemes are taken from the literature. This approach ensures an easy reproducibility of simulations (i.e. no stochastics), and can be used to explore some of the model structure errors (e.g. Clark et al., 2008; Günther et al., 2019). It is in general easy to implement (provided that several parametrisations exist in the literature), and ensemble properties can be calibrated by an adequate selection of ensemble configurations (e.g. Lafaysse et al., 2017). However, it may induce biases and violate the equiprobability property (i.e. in a proper ensemble, all ensemble members should be equiprobable, members should not exhibit systematic biases), as the several available parametrisations are not necessarily centred.

State of the art in the snowpack modelling community

Ensemble methods are much less advanced in the snowpack modelling community. Little is known about the sensitivity of seasonal snow modelling to errors in initial conditions, except that their influence is expected to diminish with the lead time (e.g. Gichamo and Tarboton, 2019). It likely depends on the initialisation date, and is probably more prominent at the beginning of the season (e.g. initial conditions of the soil thermal state). It seems most likely not to be the dominant source of snowpack modelling error (e.g. Rutter et al., 2009, see also Sec. 1.3.2). For this reason, so far, efforts have concentrated on using ensemble of meteorological forcings combined (or not) with ensembles of snowpack models.
Regarding meteorological input for snow models, many studies used perturbations of meteorological forcings (e.g. Magnusson et al., 2014; Raleigh et al., 2015; Charrois et al., 2016; Larue et al., 2018; Aalstad et al., 2018; Winstral et al., 2019; Smyth et al., 2019), Only a few studies used physically based meteorological ensembles such as the PEARP (Descamps et al., 2015) or the EFS (Molteni et al., 1996), which keep the consistency between the meteorological variables (e.g. Vernay et al., 2015; Nousu et al., 2019). However, meteorological ensembles seem to suffer from biases and under-dispersion in mountainous terrain (Nousu et al., 2019), which makes them impractical. As regards to snowpack models, perturbations have been used in several low complexity models with success (e.g. Aalstad et al., 2018; Smyth et al., 2019), probably because they offer an easy calibration of the meteorological uncertainty and systematic errors (see upper paragraph). The multiphysics approach, capitalising on a dense literature on the most uncertain snow processes (see e.g. Fig. 1.14), has been mostly used for detailed snowpack models (Essery et al., 2013; Lafaysse et al., 2017; Magnusson et al., 2017; Sandells et al., 2017; Pritchard et al., 2020; Dumont et al., 2020; Tuzet et al., 2020). Lastly, meteorological and snowpack models ensemble have rarely been combined, despite both equally contribute to snowpack modelling errors (Günther et al.,

2019).

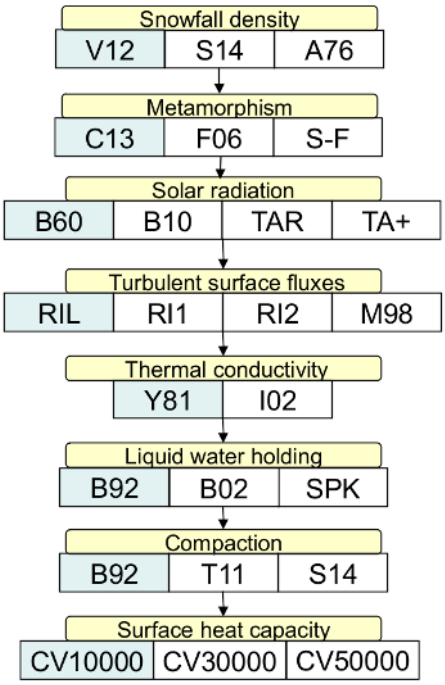

FIGURE 1.14: Physical options used in the multiphysics system ESCROC. Taken from Lafaysse et al. (2017).

1.3.4 Summary

Snowpack modelling potentially offers a comprehensive estimation of snowpack variability in the mountains, but suffers from important errors. Modelling chains use outputs from meteorological models to force snowpack models. Errors in such modelling chains are primarily inherited from uncertain meteorological forcings and snowpack modelling errors. Ensembles are used to account for these sources of uncertainties by using stochastic perturbations or multiphysics approaches. Meteorological and snowpack model ensembles have rarely been combined for snowpack modelling purposes yet it is essential in order to fully acknowledge for snowpack modelling errors.

1.4 Data assimilation of snowpack observations in the mountains

Previous sections showed a need for information on the spatial and temporal variability of the snowpack (Sec. 1.1.1), which cannot be fulfilled by observations alone given their spatio-temporal gaps (Sec. 1.2). Snowpack models can fill this gap and provide full stratigraphic informations, but suffer from large errors (Sec. 1.3), potentially estimated using ensemble methods. In this section, we consider data assimilation as a way to combine observations and models into a better estimate of the snowpack, at the light of the specificities of the mountain snowpack, snowpack observations and models.

1.4.1 Introduction to data assimilation

Data assimilation consists in updating the modelled state of a system based on observations. Models provide a physical and dynamical interpretation of the evolution of the system, often called "background" which is imperfect. Observations give insights on some variables of this system at given dates, with an associated uncertainty. Data assimilation consists in finding an "optimum estimate" of the system in the model space, based on the modelled and observed values and their associated uncertainties. The result, called an "analysis", inherits the comprehensiveness, physical consistency and dynamics from the model, but gets closer to the reality thanks to the observations. In general, data assimilation also provides an estimate of the uncertainty of such analysis.

Introductory example

A simple example from Lahoz and Menard (2010) is a nice introduction for two key concepts of data assimilation. Consider a background value x^b of uncertainty σ_b taken from a model, and an observation y^o of error σ_o. First, it can be shown in a Gaussian framework that the Best Linear Unbiased Estimate (BLUE Henderson, 1975) x^a is the barycentre of the two values weighted by the inverse of their respective uncertainties: the more we trust the model x^b respective to the observation, the closer the analysis will be to x^b. Second, the associated variance uncertainty of x^a (a for analysis) can be derived as:

$$ {\sigma_a}^2 = \frac{1}{\frac{1}{\sigma_b^2} + \frac{1}{\sigma_o^2}} \tag{1.4} $$

Therefore, σ_a is smaller than σ_b and σ_o, i.e. in general the analysis is more accurate than the background and the observations. In other words, even if the background is more accurate than observations, the analysis will benefit from both thanks to data assimilation:

data assimilation actually makes the best of models and observations.

Data assimilation strategies and goals

The primary aim of data assimilation is to reduce modelling errors by feeding models with external information on the system. As such, data assimilations strategies have been targeting the major sources of model uncertainty (see. Sec1.3.2): uncertain initial conditions and modelling errors. Consistently, data assimilation has first been used to better constrain initial conditions of the atmosphere for human experts or atmospherical models to predict its evolution, e.g. deriving a surface pressure-temperature field from spurious observations and a rough initial background (Cressman, 1959). In the 1980's, along with the progress of the modelling capacities and the emergence of satellite observations, state-of-the-art data assimilation turned into a dynamic problem, i.e. estimating the trajectory of a system along time, constrained by observation timeseries, by regularly updating the modelled state with the analyses.

Most applications of data assimilation are real-time: observations must be assimilated as time goes by. The filtering approaches such as the Kalman filter (Ghil et al., 1981), Ensemble Kalman Filter (EnKF) (Evensen, 2003) and the Particle Filter (Gordon et al., 1993; Van Leeuwen, 2009) assimilate new observations date-by-date, in a sequence of analyses. Other approaches such as the 4D-Variational approach (Talagrand and Courtier, 1987) and smoothers (e.g. Cosme et al., 2012; Evensen and Van Leeuwen, 2000) adjust the model trajectory over a temporal window of several observation dates, and are usually the most complex. In contrast with real time data assimilation, reanalyses are retrospective assimilations performed once all observations are available, either over a season (e.g. Margulis et al., 2015) or to reconstruct climate series (e.g. Hersbach et al., 2020).
As shown in the initial example, the relative importance of the observation and model errors is key for the data assimilation problem (e.g. Kalnay, 2003).These errors must be specified or dynamically estimated by any assimilation method. Determining observation errors is generally a challenge (e.g. Desroziers et al., 2005; Geer and Bauer, 2011), principally in the case of snow because of the representativeness errors (see Sec. 1.2). The most practical way of estimating modelling errors is to use ensembles (see Sec. 1.3.3). This is one of the main advantages of ensemble methods such as the EnKF or the PF. Furthermore, ensembles methods such as the EnKF have been used as companions to estimate background errors of 4D-Var methods in several NWP services (Bonavita et al., 2012; Clayton et al., 2013). For a complete overview of data assimilation strategies in the geosciences, the user is referred to the books of Lahoz and Menard (2010); Blayo et al. (2014) and the review Carrassi et al.

(2018).

Data assimilation serves several goals beyond the dynamical estimation of a sytem's state. Statistical analysis of the difference between the analysis x^a and the initial model state x^b, called the increment, enable modellers to identify systematic errors in the models and disentangle equifinality issues (Klinker and Sardeshmukh, 1992; Rodwell and Palmer, 2007; Durand and Margulis, 2008; Wong et al., 2020). Data assimilation can also contribute to a better estimation of model parameters (e.g. Ruiz et al., 2013; Kantas et al., 2015; Piazzi et al., 2018).

1.4.2 Data assimilation into snowpack models

In the last fifteen years, the trend towards snow cover data assimilation has been mostly driven by progresses in the retrieval of snow properties from satellite observations and the emergence of ensemble-based data assimilation (e.g. Andreadis and Lettenmaier, 2006; Durand and Margulis, 2007; Leisenring and Moradkhani, 2011; De Lannoy et al., 2012). Several reviews recently addressed this subject (Helmert et al., 2018; Largeron et al., 2020). Bayesian sequential methods (i.e. EnKF, PF) are suited to real-time applications such as avalanche hazard forecasting. The use of the EnKF is widespread within the snow hydrology community from points scale to large scale applications (e.g. Slater and Clark, 2006; De Lannoy et al., 2012; Piazzi et al., 2019). However, the EnKF is not well adapted to the lagrangian formulation (i.e. variable state vector dimension) used in detailed snowpack models, contrary to the Particle Filter with Sequential Importance Resampling (PF) (Magnusson et al., 2017). In addition, contrary to the EnKF, the PF preserves the physical consistency between the model state variables without effort (Charrois et al., 2016; Magnusson et al., 2017; Largeron et al., 2020). This last point is essential for avalanche hazard forecasting as even small, vertically-confined artificial gradients (e.g. temperature) could locally impact snow metamorphism (see. Sec. 1.1.2), leading to a change in the modelled stratigraphy and stability, not to mention direct changes in the stratigraphy due to the removal or addition of numerical layers.

For these reasons, the PF has been increasingly used for snow cover data assimilation in the last years. Charrois et al. (2016) demonstrated the potential of the assimilation of shortwave reflectance in point scale simulations with the PF, while Magnusson et al. (2017) assimilated in-situ observations of the height of snow (HS) thereby improving the modelled snow water equivalent (SWE). Larue et al. (2018) successfully assimilated passive microwave observation in the case of a network of snow stations, exhibiting a strong added

value on snow bulk properties. Piazzi et al. (2018) were the first to attempt to assimilate snowpack variables of different nature (e.g. surface temperature, albedo and bulk variables) at a site in the French Alps.
Spatialised applications include e.g. the assimilation of airborne microwave brightness temperatures (Kim et al., 2019). However, this application can be seen as a collection of in-situ problems as points were treated independently and the ensemble was not corrected where observations were not available. Several spatialised applications assimilating snow cover fraction included some corrections for unobserved areas by aggregating to the total snow cover area (e.g Thirel et al., 2013) or using a sophisticated score accounting for pixel-wise differences (Baba et al., 2018). However, Batch Smoothing techniques (Durand et al., 2008; Margulis et al., 2015; Aalstad et al., 2018; Alonso-Gónzalez et al., 2020) seem to make the best of snow cover fraction which is the most informative for reanalyses and during the ablation period (Dozier et al., 2016).

1.4.3 The Particle Filter

Notations

The following notations will be used for the formulation of the PF sequential data assimilation problem, adapted from Arulampalam et al. (2002). The studied system is represented within a model by the state vector x. Because the model is imperfect, x is only an approximation of the true state of the state vector x^t: the aim of data assimilation is to bring x closer to x^t. Before data assimilation, the model produces a first-guess, or prior, or background, denoted x^b. By comparing x^b to a vector of observations y, the data assimilation algorithm produces an analysis x^a, which hopefully will be closer to x^t than x^b.

The model $\mathcal{M}$ is used to propagate x between analysis dates t_k, which correspond to the dates when observations are available:

$$x_k = \mathcal{M}(x_{k-1}) + \varepsilon_k \tag{1.5}$$

Where ε_k is the modelling error.
Data assimilation algorithms are based on the comparison between modelled and observed values which must be expressed in the same units. Observed and modelled variables may be different, e.g. satellite TOA VIS/NIR radiances and modelled snowpack reflectance. To bridge such a gap, it is natural to bring the model into the observed space. This is a forward operation into a space of smaller or equal dimension. This operation is done by means of an observation operator, h, which comes with its own imperfections μ_k (i.e. operator errors and model representativeness errors) combined with sensor and retrieval errors from the

observation acquisition in itself η_k[5])[6]:

$$y_k = h(x_k^t) + \mu_k + \eta_k \tag{1.6}$$

Several additional quantities are useful for data assimilation algorithms or to evaluate them.

- R is the error covariance matrix of observations accounting for all the errors in the observation process (Eq. 1.6). On its diagonal lie the error variances of each variable and non diagonal terms are non-null when errors are not independent (i.e their errors are correlated). R is often badly constrained in geosciences, even its diagonal terms (Reichle and Koster, 2003), and in particular when it comes to snow in a mountainous terrain (e.g. Magnusson et al., 2014; Charrois et al., 2016). Therefore a common assumption is to consider R as constant along time and diagonal. Several approaches even consider its terms as a tuning parameter for the assimilation algorithm (e.g. Reichle and Koster, 2003; Larue et al., 2018).
- P^b is the background covariance matrix quantifying the error statistics of $x^b - x^t$, in other words, the model errors before assimilation. In ensemble methods such as the EnKF, P^b is approximated by the covariance matrix of the ensemble members, which is a convenient way to dynamically estimate this quantity. The ensemble covariance structures also allow to propagate information between variables or locations.
- $D = y - h(x^b)$ is the innovation (or departure) vector, quantifying the difference between the observations and the model before assimilation.
- $Res = y - h(x^a)$ is the residual.
- $Inc = x^a - x^b$ is the increment, assessing the impact of the analysis on all the modelled variables.

The PF equations

The Particle Filter is a sequential Bayesian ensemble data assimilation algorithm (Gordon et al., 1993). Its aim is to determine the probability density function of a system at time t_k given a sequence of observations $(y_1^o, ..., y_k)$. This quantity is the posterior distribution $p(x_k|y_{1:k}^o)$. The modelling process is assumed to be Markov: only present conditions are necessary to determine the future. As a result, observations can be assimilated sequentially. The assimilation sequence alternates propagation steps with analysis steps. The propagation

[5] representativeness errors can also be attributed to observations depending on the situation, without loss of generality.

[6] These errors would be much higher if the inverse operation was conducted into the model space, and would lead to a problem of higher dimension, explaining why this is not done in practice.

step uses the model to compute the transition density from t_{k-1} to t_k as $p(x_k|x_{k-1})$, producing the prior density $p(x_k|y^o_{1:k-1})$. Using the marginalisation rule, it can be formulated as:

$$p(x_k|y^o_{1:k-1}) = \int p(x_k|x_{k-1})p(x_{k-1}|y^o_{1:k-1})dx_{k-1} \tag{1.7}$$

Where $p(x_{k-1}|y^o_{1:k-1})$ is the analysis at t_{k-1}, i.e. the pdf of x at t_{k-1} given the observations until t_{k-1} and prior information. The following analysis expresses the posterior density $p(x_k|y^o_{1:k-1})$ using Bayes' rule and the independence of observations:

$$p(x_k|y^o_{1:k}) = \frac{p(y^o_k|x_k, y^o_{1:k-1})p(x_k|y^o_{1:k-1})}{p(y^o_k|y^o_{k-1})} \propto p(y^o_k|x_k)p(x_k|y^o_{1:k-1}) \tag{1.8}$$

In this term, the prior density is multiplied by the likelihood $p(y^o_k|x_k)$, and a normalisation factor. The likelihood can be derived from Eq. 1.6, provided that μ_k and η_k are known. In general, errors are assumed Gaussian, and the likelihood is expressed using the error covariance matrix R:

$$p(y^o_k|x_k) \propto \exp\left(-\frac{1}{2}[y^o_k - h(x_k)]^T R^{-1}[y^o_k - h(x_k)]\right) \tag{1.9}$$

The prior and posterior densities can not be fully known. Instead, in the Particle Filter, they are approximated by a set of N_e random states $x^1, ...x^{N_e}$, called particles. The prior is formulated as:

$$p(x_k|y^o_{1:k-1}) = \sum_{i=1}^{N_e} \omega^i_{k,prior}\delta(x_k - x^i_k), \qquad with \qquad \sum_{i=1}^{N_e} \omega^i_{k,prior} = 1 \tag{1.10}$$

And similarly the posterior writes:

$$p(x_k|y^o_{1:k}) = \sum_{i=1}^{N_e} \omega^i_{k,posterior}\delta(x_k - x^i_k), \qquad with \qquad \sum_{i=1}^{N_e} \omega^i_{k,posterior} = 1 \tag{1.11}$$

In these formulations, the particles x^i_k are attributed a weight w^i_k which quantifies their relative importance: the higher the weight of a particle, the higher the importance of the value x^i_k in the approximation of the true state pdf.
The idea of the Particle Filter is to update the weights at each analysis, thus integrating the information from the new observation y^o_k. Accounting for Eqs. 1.10 and 1.11, the analysis

Eq. 1.8 becomes:

$$\begin{aligned} p(x_k^i|y_{1:k}^o) &\propto p(y_k^o|x_k) \sum_{i=1}^{N_e} \omega_{k,prior}^i \delta(x_k - x_k^i) \\ &\propto \sum_{i=1}^{N_e} p(y_k^o|x_k^i) \omega_{k,prior}^i \delta(x_k - x_k^i) \end{aligned} \tag{1.12}$$

From which we derive by identification inside Eq. 1.11 that the analysis step simply consists in multiplying each particle x_k^i by the associated likelihood $p(y_k^o|x_k^i)$ and then normalizing:

$$\omega_{k,posterior}^i = \frac{\omega_{k,prior}^i p(y_k^o|x_k^i)}{\sum_{i=1}^{N_e} \omega_{k,prior}^i p(y_k^o|x_k^i)} \tag{1.13}$$

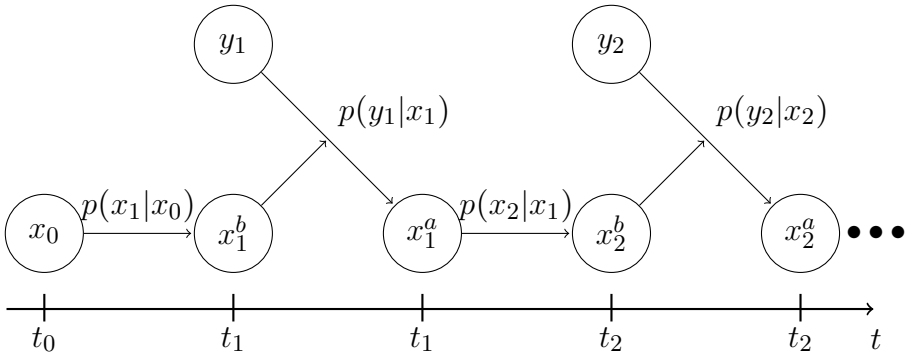

FIGURE 1.15: Schematic of the Particle Filter sequence whereby the pdf is propagated into time using the transition density $p(x_k|x_{k-1})$ and the analysis is done by computing the likelihoods for y_k^o.

Degeneracy of the PF

The PF suffers from a major issue, the phenomenon of degeneracy: usually, after several analyses, only a few particles have non-negligible weights. Indeed, Doucet (1998) demonstrated that the variance of the weights can only increase with time. As a result, most of the members do not significantly contribute to the estimation of the state pdf: they are useless. A solution to this issue is to perform a resampling of the particles after the analysis step, the so-called PF with Sequential Importance Resampling (PF-SIR). This method rejects the particles with the lower weights, and replicates the others based on their relative weights. Several resampling algorithm exists, the most common being from Kitagawa (1996).
Nevertheless, the degeneracy problem also appears with the PF-SIR when a too large number of observations is assimilated simultaneously, an issue called "the curse of dimensionality". Bengtsson et al. (2008); Snyder et al. (2008) showed that in order to avoid

degeneracy, the required number of particles increases exponentially with the number of independent observations. This issue is a severe drawback for the use of the PF-SIR in large scale geophysical problems (Snyder et al., 2015; Stigter et al., 2017).
Several solutions have been proposed to solve the curse of dimensionality. The proposal density (van Leeuwen, 2010) is one of the most sophisticated approaches yet it hasn't proved to be completely efficient to tackle this issue (Snyder et al., 2015). Larue et al. (2018) applied an inflation factor to observation errors, thus reducing the variance of the weights, obtaining good results. Inspired on the EnKF localisation (e.g. Houtekamer and Mitchell, 2001), localisation of the PF (Penny and Miyoshi, 2016; Poterjoy, 2016; Farchi and Bocquet, 2018) is a pragmatic solution aiming at reducing the number of simultaneously assimilated observations. It lies on the assumption that past a certain distance, locations can be considered as independent (Farchi and Bocquet, 2018). Independent analyses are performed on each point, only considering observations in their neighbourhood. One of the drawbacks of this approach is the lack of spatial consistency of the analyses, as each point receives a different analysis. These discontinuities can be minimized using optimal transport theory or other techniques (Farchi and Bocquet, 2018). For a complete review of the different implementations of the PF, the reader is referred to Van Leeuwen et al. (2019).

Propagation of information with the PF

As we presented in Sec. 1.2, snow observations suffer from spatial gaps. Spatial interpolation of observations (e.g. Brasnett, 1999; Slater and Clark, 2006) or particle filter weights (Cantet et al., 2019) have been used to fill these gaps but these methods might be too simplistic in a complex terrain (Dozier et al., 2016). In order to avoid discrepancies between the observed and the non-observed areas, we must find a way to propagate information from observations with the PF. In the EnKF (Evensen, 1994), information is propagated by the ensemble background covariance (e.g. Hamill et al., 2001; Reichle and Koster, 2003). Similarly, in the PF, information is implicitly propagated by the conditional pdf: information on one model state variable (i.e. variable or model point) can be used to constrain the marginal density for another model state variable.
Let's take an example with two points p_1 and p_2 where we want to predict he height of snow (HS) with a 160-member ensemble $\mathcal{E} = \{x^1, ..., x^{160}\} = \{(x_1^1, x_2^1), ..., (x_1^{160}, x_2^{160})\}$, (the components of the members correspond to the predicted values at p_1 and p_2, respectively). The left panel of Fig. 1.16 shows the HS values predicted by $\mathcal{E}$ over p_1 and p_2 at a given date t. Each dot corresponds to one member. From the density of ensemble members (black contours), we can deduce a statistical link between the predicted HS at p_1 and p_2, e.g. in general, the members predicting the lowest HS at p_1 also predict the lowest HS at p_2.

Now assume that we have one observation $y_1^o \pm \sigma_o$ available at p_1, and no observation at p_2. The ensemble seems to underestimate the HS at p_1, compared to this observation. The "information" conveyed by the observation is represented by the mauve rectangle: only the values at p_1 are constrained. As denoted by the spread of marginal densities of the prior (blue lines on the upper and right parts of this panel for p_1 and p_2, respectively), the prior uncertainties are much higher than the observation error (spread of the observation pdf in mauve on the upper part).
The PF analysis is based on the observation y_1^o and the predicted values at the same location: $p(x_1, x_2|y_1^o)$. This analysis consists in a resampling of the prior particles, represented on the central panel (green circles). The posterior marginal density of x_1 (green, upper panel) is narrower than the prior (blue) and closer to the observed values[7]. The analysis also impacts x_2 posterior marginal density. It is narrower than the prior and shifted towards higher HS values.
Assume now that an observation y_2 for p_2, taken at time t too, is available later on. It can be used to verify the PF analysis at x_2. The result is shown on the right panel. The observation, located at (y_1, y_2) is denoted by a star, and its pdf is plotted in dashed line on the right. The marginal density is closer to the observation than the prior on x_2 in this case. The PF analysis, using predicted values for x_1 and observations y_1, has brought the ensemble closer to the verification data y_2: information has been successfully transferred from x_1 to x_2, by implicitly exploiting the statistical relations between the predicted values in these locations. Finally, we see intuitively that the sharpness of the posterior pdf, depends of course on the observation error, but also on the original bivariate pdf $p(x_1, x_2)$. Indeed, if no relation had existed between the prior estimations for x_1 and x_2, the marginal posterior pdf for x_2 would be almost equal to the prior's: no information could be inferred. Conversely, if the prior bivariate pdf were wrong (imagine that x_2 decreases when x_1 increases, but that the observation is the same), then the analysis would be likely to degrade the ensemble performance at p_2.

What about snow in a complex terrain?

This example showed us how information is implicitly propagated by the PF (regardless of the quality of the outcome). No particular effort seems necessary to constrain unobserved areas. However, when trying to find a global PF analysis over a large domain, the PF degeneracy will sooner or later arise as the domain size increases (and concomitantly the number of observations). The problem of information propagation is indeed strongly connected to the curse of dimensionality.
Just as localisation is likely the best way to avoid PF degeneracy (Farchi and Bocquet,

[7] Similarly to the introductory example in Sec. 1.4.1.

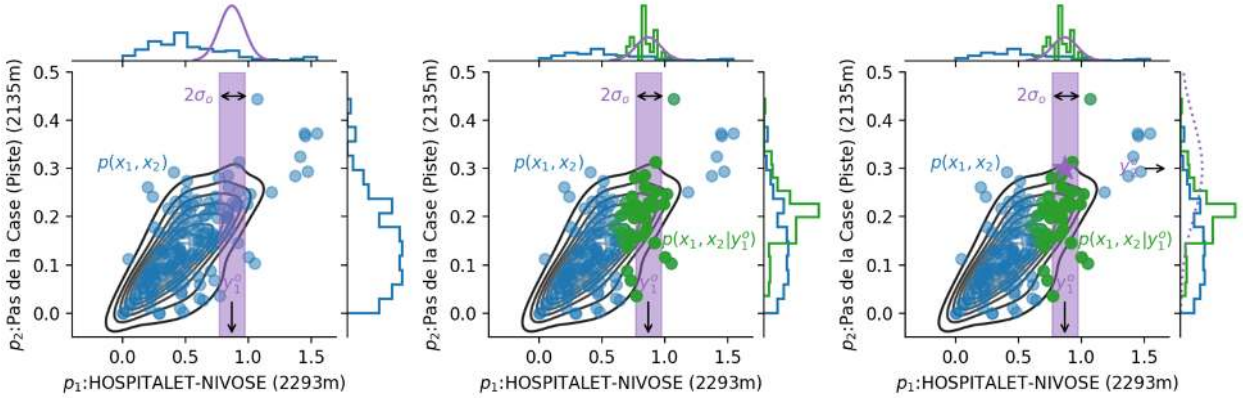

FIGURE 1.16: PF analysis on HS predicted by a 160-member ensemble on 2009, December 3rd, considering two neighbouring stations p_1 and p_2 in the Pyrenees. An observation $(y_1^o, y_2^o); \sigma_0 = 0.1$m is available. y_1^o value is assimilated and the analysis at p_2 is validated with y_2^o value. Left panel shows the prior state (blue, density contours in black), the assimilated observation (magenta rectangle for $y_1^o \pm \sigma_o$) and their marginal densities (same colours). The central panel shows the PF posterior $p(x_1, x_2|y_1^o)$, with its marginal densities (green). The right panel adds the verification data (magenta star at (y_1^o, y_2^o) and dashed marginal density on the right). Note that x-scale and y-scale are not equal. See text for more details. Adapted from Blayo et al. (2014, pp. 85-86).

2018), it has also strong links with the propagation of information. In the example of the EnKF, localisation is often based on covariance criteria (e.g. Houtekamer and Mitchell, 2001): meaningful observations come from correlated areas. Because no useful information can be inferred from observation coming from decorrelated areas, these areas must be excluded from the local analysis, thereby making the analysis more affordable[8]. Domain localisation, by excluding observation past a certain radius, can be seen as an implicit covariance localisation, because it assumes that points are uncorrelated past a certain distance. This hypothesis is reasonable in most NWP or land surface problems it has been used for.

It might not be the case for snow at the modelling scales we are considering (i.e. beyond a few hundreds of meters of resolution). As ensemble modelling is relatively new to the snowpack community, little is known about the spatial correlation of snowpack variables at such scales in a complex terrain. Though coupling processes exist (e.g. wind drift, re-illumination, gravitational redistribution, see Sec. 1.1.4), in many cases, they are not the dominant factor and locations can be reasonably well assumed independent (e.g Hanzer

[8]Another major reason for EnKF localisation is the presence of spurious correlations due to the finite ensemble size, which would induce information propagation where there shouldn't physically be (Houtekamer and Mitchell, 2001), but this "technical" consideration doesn't affect our reasoning.

et al., 2016). Under this hypothesis, spatial correlations are inherited from the external drivers of the snowpack. Precipitation fields exhibit spatial correlations, which should be transferred to snowpack variables. Similarly, the elevation smoothly controls on e.g. the precipitation phase and air temperature. On the contrary, several parameters of the topography which affect the energy budget, namely the orientation and slope, exhibit poor spatial correlation. As a result, we can not exclude that close points on the Northern and Southern sides of a ridge might be less correlated than two points of same orientation but separated by a large distance. Depending on the actual correlation fields, domain localisation could therefore be physically unsound, and lead to poor performance. The idea would therefore to base localisation on correlation criteria explicitly, rather than using a distance criteria. In other words, we could ask the ensemble what are the observed locations in which the snowpack looks similar to the local conditions, and base an analysis on these observations, rather than imposing the algorithm to take all the observations within a certain radius.

Whether such an approach is actually necessary (i.e. at the considered resolution, snowpack correlation fields are not primarily controlled by the distance), how should it be implemented, and what would be the result, are open questions.

1.4.4 Summary

Data assimilation offers a way to insert information content from observations into model simulations. Originating from the Numerical Weather Prediction community, it appeared only recently into the snowpack modelling community. Among a wealth of different approaches, the Particle Filter seems to fit detailed snowpack models such as Crocus well. However, it suffers from the issue of the degeneracy, when ingesting large numbers of observations. Localisation, whereby observations are only used in their vicinity is a convenient solution to this issue. In the mountains, the ability of the PF to implicitly exploit ensemble correlation patterns could be used to propagate information into unobserved areas.

1.5 Knowledge gaps

Snowpack variability is imperfectly captured by snowpack models, due to errors in the meteorological input, uncertain representation of physical processes and unresolved spatial scales. Satellite retrievals of snow reflectance provide a wealth of information on snow surface properties, with an intermediate to high resolution, and a daily to weekly revisit time. Information from such products could be leveraged by means of data assimilation into spatialised snowpack models. Similarly, information from in-situ observations of the height of snow could be used to correct snowpack simulations despite their limited representativeness. Since both type of observations suffer from spatial and temporal gaps, it is crucial to investigate whether information from such observations can be propagated from observed to unobserved areas. We therefore identified the following open questions:

- **Can we use observations of snowpack reflectance from satellites to better constrain snowpack modelling over mountainous areas?**
- **Can we propagate information on the snowpack state from observed areas to unobserved areas with data assimilation?**
- **To what extent can we use in-situ observations of HS to improve snowpack simulations in their neighborhood?**

1.6 Objectives

The aim of this thesis is to assimilate space-borne reflectance and in-situ HS observations in view of improving the representation of snowpack variability by snowpack models, and the associated errors and uncertainties. Capitalising on the operational snowpack modelling chain from Météo-France, which is applied in a semi-distributed geometry, we defined the following objectives:

- Build an ensemble version of the operational chain accounting for the major sources of snowpack modelling uncertainty.

- Evaluate the potential for assimilation of reflectance products retrieved from MODIS and Sentinel-2 observations by comparing the two entities with in situ observations and simulations over a semi-distributed domain.

- Develop a Particle Filter variant in this ensemble modelling framework able to assimilate a large number of observations simultaneously, and investigate ways of propagating information across topographic conditions.

- Evaluate the potential of such approach to leverage the information content of in-situ HS observations over large mountainous areas.

This manuscript is organised as follows:

In chapter 2, ensemble simulations are compared with reflectances retrieved from spaceborne MODIS and Sentinel-2 observations as well as in-situ observations over two contrasted snow seasons. Satellite products are aggregated into the modelling semi-distributed geometry. This comparison shows that despite a good agreement with the temporal variations of the ensemble, MODIS observations are negatively biased compared to in-situ observations, while the ensemble outputs are compatible with those in-situ observations of VIS/NIR reflectance. This bias is preventing from assimilating such observations. Band ratios seem less biased, and we subsequently try to assimilate it in an idealised setting, with limited success. We speculate that their information content is lower than the raw products. Furthermore, we show that observations of reflectance are not reliable in shadows, steep slopes, mixed terrain and forests.
In chapter 3, we address the issue of observation scarcity by developing CrocO, an ensemble data assimilation system suited to propagate information from snowpack observations in a mountainous terrain. Several innovative versions of the PF are implemented within CrocO. This system is tested in an idealised setting showing good potential for partial observations of HS and reflectance to correct simulations across a topographic conditions.
In Chapter 4, we finally evaluate the potential for in-situ HS observations across the Alps and Pyrenees to improve nearby simulations of the snowpack with CrocO. Results show that these observations yield precious improvements in areas where the pre-existing modelling error is the highest.
In the last Chapter 5, we summarize our main results, address the open questions we identified, and suggest avenues to further improve the modelling of snowpack variability in the mountains by means of data assimilation.

Chapter 2

Comparison of simulated and observed reflectances in a semi-distributed geometry

Contents

2.1 Extended abstract

Space-borne shortwave observations contain precious information on the snowpack variability over large mountainous areas (Dozier et al., 2016). Snowpack shortwave reflectances, retrieved from sensors such as MODIS or Sentinel-2, are sensitive to snowpack surface properties such as the specific Surface Area (SSA, (m^2 kg^{-1}) or the light absorbing particles content (LAP, (g g_{snow}^{-1})) (e.g. Durand and Margulis, 2006; Mary et al., 2013; Dumont et al., 2020, and Fig. 2 of the article). An observation operator for reflectances (Libois et al., 2013) has recently been implemented within Crocus, a detailed snowpack model. It makes it possible to directly compare observed and modelled reflectances. The potential for assimilation of reflectances within Crocus has been demonstrated (Charrois et al., 2016), yet in an idealised setting (synthetic observations), at the local scale, and without explicitly accounting for the LAP influence on the snowpack shortwave radiative transfer (Tuzet et al., 2017). Our aim is to address these limitations.

The study presented in Sec. 2.2 assesses the potential for assimilation of MODIS and Sentinel-2 reflectances into ensemble snowpack simulations performed in a semi-distributed geometry identical to the operational application of Crocus (based on topographic classes). This ensemble modelling system accounts for meteorological and snowpack modelling uncertainties (Fig. 4). It combines an ensemble of meteorological forcings (Charrois et al., 2016) including LAP deposition fluxes from MOCAGE chemistry-transport model (Josse et al., 2004), with a multiphysics ensemble snowpack model (Lafaysse et al., 2017) explicitly accounting for the presence of LAP in the snowpack (Tuzet et al., 2017).

The study takes place in the Grandes-Rousses an area of approximately 500 km^2 in the Central French Alps (Fig. 1), over snow seasons 2013-2014 and 2016-2017. Automated in-situ reflectance measurements were available at the Col du Lautaret (2058 m) for the last season (Tuzet et al., 2020). MODImLab algorithm (Sirguey, 2009) was used to retrieve snowpack surface reflectances and snow cover information from MODIS top of atmosphere radiances into a 250 m resolution. Sentinel-2 surface reflectances, retrieved with MAJA processor (Hagolle et al., 2017) were downloaded at 10 to 20 m resolution. In this Chapter, we will refer to these retrievals simply as *MODIS reflectances* and *Sentinel-2 reflectances* for the sake of brevity. Both were aggregated into the semi-distributed geometry (Figs. 5 and 6).

The significant level of spatial noise in the raw reflectance products (not shown), seemed successfully filtered by the topographic aggregation (Fig. 7). However, any valuable information on natural variability inside the topographic classes is lost in the process. Ensemble simulations seemed well compatible with in-situ observations (Fig. 9), although they do not account for intraclass variability either.

We showed that the variations of Sentinel-2 reflectance observations with the aspect did not

match those of MODIS and the ensemble (Fig. 7). Their amplitude seems too strong and opposite to expectations (i.e. lower reflectance for lower local zenith angle, e.g. Dumont et al., 2010). MAJA retrieval algorithm, which was not specifically designed for snow surfaces, is a likely cause of this issue.
Then, MODIS observations are strongly biased with respect to the ensemble and in-situ observations (Figs. 8, 9 and 10). However, strong temporal correlations between the ensemble and MODIS timeseries were evidenced in a wide diversity of classes (Fig. 11) showing that they might have compatible information contents.
The bias of MODIS observation make them impossible to directly assimilate. We evidenced that ratios of MODIS reflectances were not biased with respect to the ensemble (Figs 12-15). Moreover, these variables exhibited the same level of correlation with the ensemble than raw reflectances.

The potential for assimilation of band ratios was explored in Sec. 2.3 with a twin experiment setup (Charrois et al., 2016) at the col du Lautaret, on winter 2016-2017. An open-loop ensemble run (i.e. without assimilation) was performed, from which three members were extracted, corresponding to different quantiles of SWE in the open-loop (Fig. 2.1) . Investigations were performed on the optimal parameters for the ensemble setup and the value of band ratios observation errors (Fig. 2.2). Band ratios and raw reflectances from the selected members were assimilated with a Particle Filter. The performance of the runs assimilating band ratios was compared with the open-loop and the runs assimilating reflectances (Fig. 2.3).
Results show that the band ratios seem to convey less information than the raw reflectances, with only about 10-15% of CRPS improvement compared to the open-loop in the best case, against about 50% (best cases) for the raw reflectances. Assimilation performance seem rather unstable, potentially due to badly specified observation errors causing PF degeneracy. This issue will be further investiated in (Revuelto et al., 2021), and an avenue against PF degeneracy will be proposed in next Chap. 3).

To conclude, this study was the first one to perform ensemble snowpack simulations accounting for meteorological and snowpack modelling uncertainties in a spatialised setting. Simulation outputs seemed to well represent modelling errors of reflectance and snow depth at the Col du Lautaret. The aggregation of satellite reflectances into the modelling geometry reduces their level of noise. MODIS observations seem consistent with the ensemble in a wide diversity of topographic classes. However, they are not available in the shadows, steep slopes and forests. This stresses the need for a data assimilation algorithm able to propagate information from the observed classes into these locations. Moreover, MODIS

observations suffer from a significant bias which prevents from assimilating it without effort. Several ratios of reflectance are not biased but our attempt to assimilate these variables suggests that they do not provide as much information as the raw reflectances. Therefore, improving the topographic corrections of reflectance retrievals is a major prerequisite for their assimilation.

2.2 Towards the assimilation of satellite reflectance into semi-distributed ensemble snowpack simulations

Citation:

Cluzet, B., Revuelto, J., Lafaysse, M., Tuzet, F., Cosme, E., Picard, G., Arnaud, G. & Dumont, M. (2020). Towards the assimilation of satellite reflectance into semi-distributed ensemble snowpack simulations. Cold Regions Science and Technology, 170, 102918.

Author contribution:

- Merging the developments of Tuzet et al. (2017) into Crocus main code branch
- Several technical developments within Crocus
- Conception of the ensemble modelling system and embedding it in an High Performance Computing environment
- Launching the ensemble simulations and post-processing it
- Downloading Sentinel-2 data and aggregation of the reflectance products
- Results analysis and redaction of the article

Cold Regions Science and Technology 170 (2020) 102918

Contents lists available at ScienceDirect

Cold Regions Science and Technology

journal homepage: www.elsevier.com/locate/coldregions

Towards the assimilation of satellite reflectance into semi-distributed ensemble snowpack simulations

Bertrand Cluzet[a,*], Jesus Revuelto[a], Matthieu Lafaysse[a], François Tuzet[a,b], Emmanuel Cosme[b], Ghislain Picard[b], Laurent Arnaud[b], Marie Dumont[a]

[a] Univ. Grenoble Alpes, Université de Toulouse, Météo-France, CNRS, Centre d'Études de la Neige, Grenoble, France
[b] Institut des Géosciences de l'Environnement, IGE, UGA-CNRS, Grenoble, France

ARTICLE INFO

Keywords:
Snowpack modelling
Ensemble
Spatialization
MODIS
Sentinel-2
Assimilation

ABSTRACT

Uncertainties of snowpack models and of their meteorological forcings limit their use by avalanche hazard forecasters, or for glaciological and hydrological studies. The spatialized simulations currently available for avalanche hazard forecasting are only assimilating sparse meteorological observations. As suggested by recent studies, their forecasting skills could be significantly improved by assimilating satellite data such as snow reflectances from satellites in the visible and the near-infrared spectra. Indeed, these data can help constrain the microstructural properties of surface snow and light absorbing impurities content, which in turn affect the surface energy and mass budgets. This paper investigates the prerequisites of satellite data assimilation into a detailed snowpack model. An ensemble version of Météo-France operational snowpack forecasting system (named S2M) was built for this study. This operational system runs on topographic classes instead of grid points, so-called 'semi-distributed' approach. Each class corresponds to one of the 23 mountain massifs of the French Alps (about 1000 km^2 each), an altitudinal range (by step of 300 m) and aspect (by step of 45°). We assess the feasability of satellite data assimilation in such a semi-distributed geometry. Ensemble simulations are compared with satellite observations from MODIS and Sentinel-2, and with in-situ reflectance observations. The study focuses on the 2013–2014 and 2016–2017 winters in the Grandes-Rousses massif. Substantial Pearson R^2 correlations (0.75–0.90) of MODIS observations with simulations are found over the domain. This suggests that assimilating it could have an impact on the spatialized snowpack forecasting system. However, observations contain significant biases (0.1–0.2 in reflectance) which prevent their direct assimilation. MODIS spectral band ratios seem to be much less biased. This may open the way to an operational assimilation of MODIS reflectances into the Météo-France snowpack modelling system.

1. Introduction

The avalanche forecasting services of some countries use a chain composed of meteorological forcings, coming from either a Numerical Weather Prediction model (NWP) or observations, and a detailed multilayer snowpack model such as Crocus (Vionnet et al. 2012) or SNOWPACK (Lehning et al. 2002). Both meteorological forcings and snowpack modelling induce errors and uncertainties in the simulations (Essery et al. 2013; Vernay et al. 2015; Raleigh et al. 2015; Günther et al. 2019). These errors are considerably limiting the use of snowpack models by avalanche hazard forecasters (Morin et al., 2019). The representativeness of simulations is also limited in complex mountain terrain (Fiddes and Gruber 2012). In addition, most of these snowpack modelling chains do not operationally assimilate any available information on the snowpack properties (either in-situ or remotely-sensed) (Helmert et al. 2018). There are several reasons for that: (1) snowpack in-situ observations are sparse and lack representativeness (2) satellite observations retrieval is challenging (Nolin 2011; Helmert et al. 2018), (3) preserving state variable consistency within detailed snowpack models, which is a key point for avalanche forecasting, requires sophisticated assimilation algorithms (Magnusson et al. 2017). As a consequence, the errors often accumulate along the snow season leading to increasingly poor model performance and utility for avalanche hazard forecasting and other operational applications.

Data assimilation systems using ensemble approaches is the best way to reduce snowpack modelling errors (Charrois et al. 2016; Larue et al. 2018; Piazzi et al. 2018; Winstral et al. 2019). The Particle Filter (PF) ensemble assimilation algorithm seems to be especially well suited

* Corresponding author.
E-mail address: bertrand.cluzet@meteo.fr (B. Cluzet).

https://doi.org/10.1016/j.coldregions.2019.102918
Received 4 February 2019; Received in revised form 27 September 2019; Accepted 4 October 2019
Available online 30 October 2019

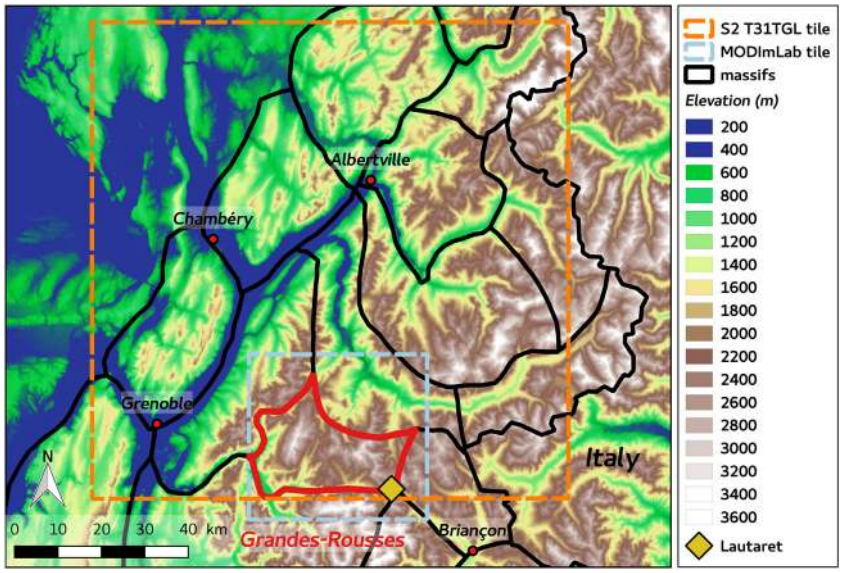

Fig. 1. Map of the study area of the Grandes-Rousses (red), located in the central French Alps. Lautaret field site (diamond) and satellite retrieval tiles (boxes) are also indicated, together with the limits of other SAFRAN massifs (black). Source: Shuttle Radar Topography Mission (SRTM), resolution: 90 m. (For interpretation of the references to colour in this figure legend, the reader is referred to the web version of this article.)

to reduce detailed snowpack modelling errors (Magnusson et al. 2017). Indeed, ensembles enable to quantify the uncertainties of (1) meteorological forcings, using physically based ensembles (Vernay et al. 2015) or statistical perturbations (Charrois et al. 2016; Winstral et al. 2019), and (2) snowpack modelling, using multiphysical systems (Essery 2015; Lafaysse et al. 2017). Charrois et al. (2016) did the first application of a PF within a detailed snowpack model, but only at one specific location and their ensemble only described the meteorological uncertainty, not model uncertainty. They were followed by Magnusson et al. (2017) and Larue et al. (2018). Recently, Piazzi et al. (2018) and Smyth et al. (2019) applied the PF to a combination of meteorological and model ensembles, but with a less complex model and at the local scale as well. In parallel, spatialized application of PF has been done in several studies (Thirel et al. 2013; Baba et al. 2018), but with deterministic and low complexity snow models, not suited for avalanche hazard forecasting. This paper fills a gap by implementing a combination of a meteorological ensemble and a multiphysical system of detailed snow models in a spatialized context.

Daily moderate-resolution observations (250 to 500 m) in the visible (VIS) and near infra-red (NIR) spectrum from the MODerate Resolution Imaging Spectroradiometer (MODIS) are suitable to monitor the snowpack properties (Hall et al. 2002). Sentinel-2 (S2) has a coarser revisit time (5 days) but captures much finer spatial scales (10–20 m). From MODIS and S2 spectral Top Of Atmosphere (TOA) radiance products, it is possible to retrieve the snowpack extent as a Snow Cover Fraction by pixel (SCF) and Bottom of Atmosphere (BOA) reflectances which requires to account for the complexity of the radiative transfer in mountainous area (Richter 1998; Sirguey 2009). Many studies focus on the assimilation of SCF, showing a strong impact of assimilation in hydrological models (De Lannoy et al. 2012; Thirel et al. 2013; Stigter et al. 2017; Aalstad et al. 2018; Baba et al. 2018). However, SCF is expected to be of less interest for detailed snowpack modelling in alpine terrain, because the information content is limited to the snow line (Andreadis and Lettenmaier 2006; Toure et al. 2018). Meanwhile, it is expected for the BOA reflectances to carry useful information on the temporal and spatial variability of the snowpack surface properties such as Light Absorbing Particles concentration (LAP, [kg kg_{snow}^{-1}]) and snow microstructure (quantified by the Specific Surface Area, SSA, [$m^2 kg^{-1}$]) (Dozier et al. 2009; Kokhanovsky et al. 2018). Indeed, these variables drive the shortwave (SW) radiation absorption of the snowpack, and thus carry crucial information on the snow surface energy budget (Skiles et al. 2018; Mauro et al. 2019). Moreover, monitoring the surface snow microstructure can help detect precipitation (solid and liquid) and melting events, while frequent observations of surface LAP contents can enable to constrain LAP vertical layering within the snowpack. In line with this, Charrois et al. (2016) showed that assimilating satellite reflectances could help reduce Snow Water Equivalent (SWE, [kg m^{-2}]) modelling uncertainties by up to 45%.

The most detailed snow models are also able to compute reflectances from the snowpack properties, through the use of a detailed radiative transfer (Libois et al. 2015; Skiles and Painter 2019) and the explicit evolution of SSA (Carmagnola et al. 2013) and LAP (Tuzet et al. 2017). Such radiative transfer models play the role of observation operators, computing observation-like variables from the model state variables. However, modelling geometries often differ from the distributed geometry of satellite retrievals (Mary et al. 2013). For instance, Météo-France multilayer snowpack model Crocus is operationally applied on several topographical classes (by 300 m elevation bands, for 8 different aspects and 3 different slopes, so-called "semi-distributed" geometry) inside so-called" massif" regions of about 1000 km^2 (Durand et al. 1999; Lafaysse et al. 2013). This semi-distributed framework, with around 200 topographical classes, was proven to be sufficient to represent the main features of snowpack variability with topography compared to fully distributed simulations at 25 to 250 m resolution (Fiddes and Gruber 2012; Revuelto et al. 2018). However, the feasibility of the assimilation of satellite reflectances in Crocus semi-distributed model using the PF ensemble data assimilation algorithm, still needs to be assessed.

The main objective of this paper is to assess the potential for semi-distributed assimilation of satellite observations of snowpack reflectances into ensemble snowpack simulations. For that purpose, we present extended comparisons of openloop simulations (e.g. without assimilation) with satellite observations from MODIS and S2 aggregated in this geometry. Section 2 presents the data and the modelling framework, while Section 3 introduces the aggregation method and defines the points of comparison from the assimilation perspective. Then Section 4 presents the comparison results, which are discussed in Section 5.

2. Data and model

2.1. Case study

This study focuses on two snow seasons (2013–2014 and 2016–2017) in the Grandes-Rousses (see Fig. 1). The area of about 500 km^2 is located in the Central French Alps, and is characterized by a

wide elevation range from the bottom of Romanche valley (about 700 m a.s.l.) to the top of Aiguilles d'Arve (3514 m a.s.l.). This specific massif was chosen because it encompasses the Col du Lautaret (2058 m a.s.l.), where field campaigns have been carried out since winter 2016–2017 close to an automatic weather station (Tuzet et al. 2019).

The two snow seasons have been selected because they show contrasted snow conditions. 2013–2014 is characterized by above average snow depths, with frequent snowfall events and two major dust deposition events (end of February, end of March) (Dumont et al. 2017; Di Mauro et al. 2015). 2016–2017 was a warm winter, without significant snowfall between late November and beginning of January, and early melting in spring. In addition, several minor dust deposition events occurred after the end of February according to MOCAGE outputs.

2.2. Digital Elevation Model (DEM) and landcover

2.2.1. DEM

Digital Elevation Models (DEM) of the study area are used here to retrieve satellite data and to perform a topographical aggregation of observations into the model semi-distributed geometry. For that purpose, DEM BD Alti®[1] (IGN25) from the French Geographical Institute (*Institut National de l'information Géographique et forestière*, IGN) with native 25 m resolution was used in this study at different scales: 125 m for the retrieval of MODIS images (IGN125) (see Section 2.3.1) and 250 m (IGN250) for the topographical aggregation. In addition, a different DEM from Shuttle Radar Topography Mission (SRTM, Farr et al. (2007)) with 90 m resolution (SRTM90) is employed in the retrieval of S2 data (see Section 2.3.2).

2.2.2. Land Cover

CORINE Land Cover database[2] was used to filter the land cover types of the region. Only land cover types 321 (grassland), 322 (moorland), 332 (bare rocks), 333 (sparse vegetation) and 335 (glaciers and perennial snow) were considered valid, hence excluding forests, urbanized area, and water bodies from this study since both modelling and satellite retrieval are difficult in such areas (Gascoin et al. 2019).

2.3. Snow observations

2.3.1. MODIS observations

MODIS top of atmosphere radiance in the first seven spectral bands are available at 250 to 500 m spatial resolution depending on the channel (see. Table 1). As depicted in Fig. 2 and Table 1, reflectance in visible bands (1,3,4) is mostly affected by the impurities content in snow (BC and dust) whereas it depends mostly on SSA in the near-infrared spectral bands (2,5,6,7) (Dozier et al. 2009).

We extracted and post-processed these data in a 36 × 41 km^2 region (23,616 pixels of 250 m resolution, see Fig. 1) including the Grandes-Rousses and Col du Lautaret field site during 2013–2014 and 2016–2017 snow seasons with MODImLab retrieval algorithm. In such context of complex terrain, MODImLab retrieval algorithm (Sirguey 2009) was shown to outperform other products in many studies (Dumont et al. 2012; Charrois et al. 2013). Indeed, MODImLab accounts for atmospherical radiative transfer, direct and diffuse contribution, multiple topographical reflection, terrain shading and snow reflectance anisotropy (see Fig. 3).

For mixed pixels, MODImLab's spectral unmixing algorithm computes the reflectance of the snow fraction of the pixel together with a Snow Cover Fraction (SCF). For all the pixels, resulting product is the bi-hemispherical reflectance (accounting in particular for snow Bidirectional Refletance Density Function (BRDF), (Dumont et al. 2011)), with 250 m resolution in all bands. MODImLab provides additional masks for shadows (self and cast, see Fig. 3) and clouds. For both snow seasons, dates with good geometrical acquisition properties (Sensor Zenithal Angle (SZA) ≤ 30°), and clear sky were selected (see Table A.1 in Appendix) in order to ensure a maximal accuracy, following Sirguey et al. (2016) and Charrois et al. (2016).

2.3.2. Sentinel-2 observations

S2 is an ESA-Copernicus satellite program operational since 2016, carrying a multi-spectral high resolution (10–20 m) VIS/NIR sensor with several bands coinciding with MODIS wavelengths (see Table 1 and Fig. 2). Sentinel-2 ground flat bi-hemispherical reflectance products (product FRE, assuming a Lambertian surface) are retrieved by the MAJA processor (Hagolle et al. 2017), which is similar to MODImLab. Snow masks are retrieved by Let It Snow algorithm[3] and distributed by Theia Land data center[4] (Gascoin et al. 2019). Acquisition is done close to nadir, with $SZA \leq 10°$. Seven clear sky dates were selected during the 2016–2017 snow season (see Table A.1 in Appendix).

2.3.3. In-situ observations

Autosolalb is a high accuracy instrument measuring snow bi-hemispherical reflectance in the VIS/NIR spectrum (200–1100 nm, 3 nm resolution) including MODIS bands 1–4 (Dumont et al. 2017). In-situ Autosolalb observations of snowpack bi-hemispherical reflectance were acquired at Col du Lautaret field site (see Fig. 1 for location) during 2016–2017 winter. The acquisition time step is 12 min and acquisition for 2016–2017 winter started on 2017, February 16th. For a given observation time (see Table A.1 in Appendix), observation was computed as the mean of all available measurements within +30/−30 min and corrected for local slope effects as in Dumont et al. (2017).

2.4. Model

In S2M (SAFRAN-SURFEX/ISBA/Crocus-MEPRA), the Meteo-France operational modelling system of the snowpack, meteorological forcings from SAFRAN analysis (Durand et al. 1993) are used as inputs to the coupled multilayer ground/snowpack model SURFEX/ISBA/Crocus (Vionnet et al. 2012). Ensemble versions for these two components were used here.

2.4.1. Ensemble of meteorological forcings

In SAFRAN, a meteorological guess from the NWP model ARPEGE is adjusted with weather observations within each massif on the semi-distributed geometry. Here, in order to represent the uncertainties of this analysis, an ensemble of 35 meteorological forcings was generated by stochastic perturbations on all the meteorological variables of the reference SAFRAN analysis for the Grandes-Rousses. Following Charrois et al. (2016), the magnitude of perturbations was adjusted by a local assessment of SAFRAN errors. SAFRAN does not provide impurities deposition fluxes. Therefore, LAP wet and dry deposition fluxes for BC and dust were extrapolated from MOCAGE chemistry-transport model (Josse et al. 2004) at Lautaret field site (see Fig. 1). For LAP fluxes, Tuzet et al. (2017) showed that the order of magnitude were badly captured by ALADIN-Climate chemistry-transport model (Nabat et al. 2015), while the timing of events was well captured. Similar behaviour was found with MOCAGE, with an over estimation of BC fluxes in particular. As a consequence, each of the 4 LAP fluxes variables, for each of the 35 members, was multiplied by a constant random factor along the forcing time period, following a lognormal law ($\mu = 0.01$,

[1] http://professionnels.ign.fr/bdalti

[2] https://www.data.gouv.fr/fr/datasets/corine-land-cover-occupation-des-sols-en-france/

[3] http://tully.ups-tlse.fr/grizonnet/let-it-snow/blob/master/doc/tex/ATBD_CES-Neige.pdf

[4] CNES.; Gascoin, S.; Grizonnet, M.; Hagolle, O.; Salgues, G. Theia Snow collection, 2017

Table 1
MODIS considered spectral band properties together with the closest matching Sentinel-2 band.

Modis ID /S2 ID	B3/B2	B4/B3	B1/B4	B2/B8A	B5	B6/B11	B7/B12
Central wavelength *(nm)*	469/497	555/560	645/665	858.5/865	1240	1640/1614	2130/2202
Bandwidth *(nm)*	20/100	20/45	50/40	35/33	20	24/143	50/242
Resol. at nadir *(m)*	500/10	500/10	250/10	250/20	500	500/20	500
Spectral domain	VIS	VIS	VIS	VIS/NIR	NIR	IR	IR
Sensitivity to LAP	+ +	+ +	+ +	+			
Sensitivity to SSA	+	+	+	+ +	+ + +	+ +	+ +
Penetration depth *(m)*	Up to 10-20 cm	A few cm	A few cm	A few cm	mm	mm	mm

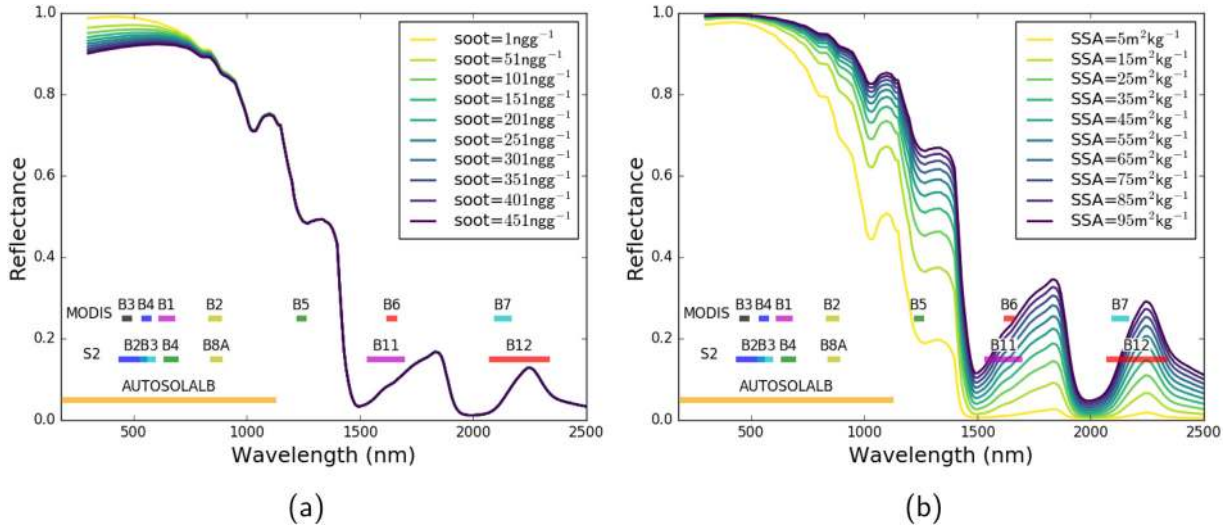

Fig. 2. Computation of snow diffuse reflectances using TARTES for varying soot concentrations (SSA = 40 m^2kg^{-1}) (1) and varying SSA (1), for 1 m of 300 $kg\,m^{-3}$300.^-3 density uniform snowpack, together with MODIS and S2 spectral bands.
Source: http://snowtartes.pythonanywhere.com

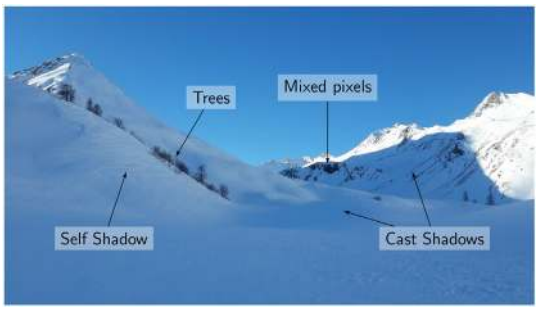

Fig. 3. Example of the complexity of the retrieval of reflectance affected by shadows, trees, and mixed snow covers in a complex terrain. (Bertrand Cluzet, Col du Lautaret, December 20th 2017).

$\sigma = 10$) for BC, and ($\mu = 1$, $\sigma = 10$) for dust.

2.4.2. Ensemble of snow models

ESCROC (Lafaysse et al. 2017) is the multiphysical ensemble version of SURFEX/ISBA/Crocus handling 7774 different model configurations. For this study, the last developments of the radiative transfer model TARTES and LAP handling in Crocus were mandatory to properly model the snowpack reflectance (T17 option of radiative transfer, Tuzet et al. (2017)), which were not included in Lafaysse et al. (2017). An ensemble of 1944 members using T17 option, so-called "E1tartes" was built for this study, including all the physical options described by Lafaysse et al. (2017) except for options of solar radiation absorption scheme.

2.4.3. Model chain

The ensemble modelling chain setup is summarized in Fig. 4. At the beginning of a simulation, 35 model configurations are randomly drawn from E1tartes. Each one is associated with a perturbed forcing file to perform the simulation for the whole year, totalling 35 different

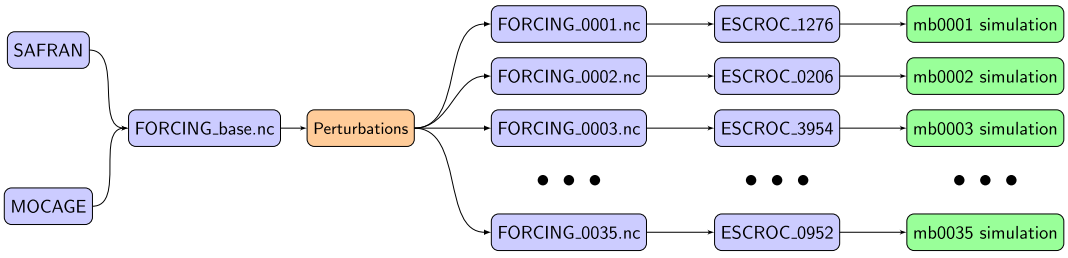

Fig. 4. Setup of the ensemble modelling chain.

snowpack simulations.

3. Methods

3.1. Topographic aggregation

An aggregation process is used to adapt the observations to the model semi-distributed geometry with the aim of assimilation. Another added value of the aggregation is to reduce random observation errors and average out features that are not accounted for in the model (Hyer et al. 2011).

3.1.1. DEM and topographical classification

In our modelling framework, a topographical class C_i is described by a triplet (e_i, a_i, s_i) where the elevation $e_i \in [600, 900, \ldots, 3600]$, the aspect $a_i \in [0, 45, 90, \ldots 315]$ (in degrees, clockwise from North), and the slope $s_i \in [20, 40]$ (in degrees). Flat classes are described by a triplet $(e_i, -, 0)$. In our case, there is a total of 187 different topographical classes. For each pixel p, a triplet (e,a,s) is computed from the IGN250 DEM (see Section 2.2.1) and thus is attributed to a topographical class. The classification rule is described as follows for tilted classes (Eq. (1)) and for flat classes (Eq. (2)):

$$p(e,a,s) \in C_i(e_i,a_i,s_i) \Leftarrow \begin{cases} e \in [e_i - 150,\ e_i + 150[\\ s \in [s_i - 10,\ s_i + 10[\\ a \in [a_i - 22.5,\ a_i + 22.5[\end{cases} \quad (1)$$

$$p(e,a,s) \in C_i(e_i,-,0) \Leftarrow \begin{cases} e \in [e_i - 150,\ e_i + 150[\\ s < 10 \end{cases} \quad (2)$$

Note that this classification process excludes pixels steeper than 50° were both modelling and remote sensing are unsound.

3.1.2. MODIS aggregation

An algorithm is used to aggregate MODIS distributed observations into semi-distributed observations in order to compare it with model outputs. In this process, a particular attention is paid to the validity and spatial representativeness of the observations, as described in Fig. 5. Regarding the validity, pixels with clouds, self/cast shadows, invalid CORINE land covers (see Section 2.2.2) as well as pixel lying outside the Grandes-Rousses are filtered out (A label in Fig. 5). Then for reflectance only, pixels with Snow Cover Fraction SCF_{pix} inferior to 0.85, are discarded (B), since MODImLab reflectance product is less accurate for mixed pixels (Mary et al. 2013). The product (B) is referred to as" distributed reflectance".

Finally, reflectance and SCF are aggregated into semi-distributed products by taking the median value within each class. In order to ensure the spatial representativeness of the aggregated observations, classes where the number of valid pixels is below ten and having less than 10% of pixels with reflectance observations are filtered out in this process (C and D). For the same reason, classes where the average Snow Cover Fraction SCF_{class} is inferior to 0.85 are masked for reflectance in a final step (E).

3.1.3. Sentinel-2 aggregation

S2 images were aggregated to the semi-distributed geometry in a similar process as for MODIS (see Section 3.1.2), as described in Fig. 6. In a first step, a validity masking is performed on Theia L2B Snow Mask using Theia L2A Clouds and Geophysical masks (A). Then, we produce the distributed S2 product (B) by classifying using the IGN250 DEM and discarding non-snow pixels. The aggregated SCF value (D) was here computed as the ratio between snowy and valid populations, when the valid population was above 10 pixels and 10 % of the total population (as described in the previous paragraph). Finally, aggregated SCF was used to filter the semi-distributed reflectance (D) as in Section 3.1.2.

3.2. Assessing the feasibility of data assimilation

Data assimilation algorithms generally require that systematical bias between the ensemble and the observations is negligible for a proper functioning (Dee and Da Silva 1998). In addition, for ensemble data assimilation such as the PF, the observation should usually lie within the ensemble envelope, otherwise the algorithm is likely to collapse (Charrois et al. 2016). Rank diagrams are commonly used in the ensemble forecasting community to check for both issues by computing the histogram of the position of the observation within the ensemble for all available dates and places (Hamill 2001). Furthermore, apart from these considerations, correlations between ensemble and observations timeseries can help quantify the information content from observation and its potential for assimilation (Reichle et al. 2004). If timeseries are weakly correlated, this means that it is likely that observations carry substantial information valuable for the ensemble, but that data assimilation of such different datasets will be a difficult task.

In order to assess the potential of applying assimilation algorithms to our spatialized ensemble simulation, a thorough comparison of observed and openloop (i.e. whithout assimilation) simulated reflectances is carried out here: (1) We assess the consistency of the spatial and temporal variations of the ensemble and observations based on two

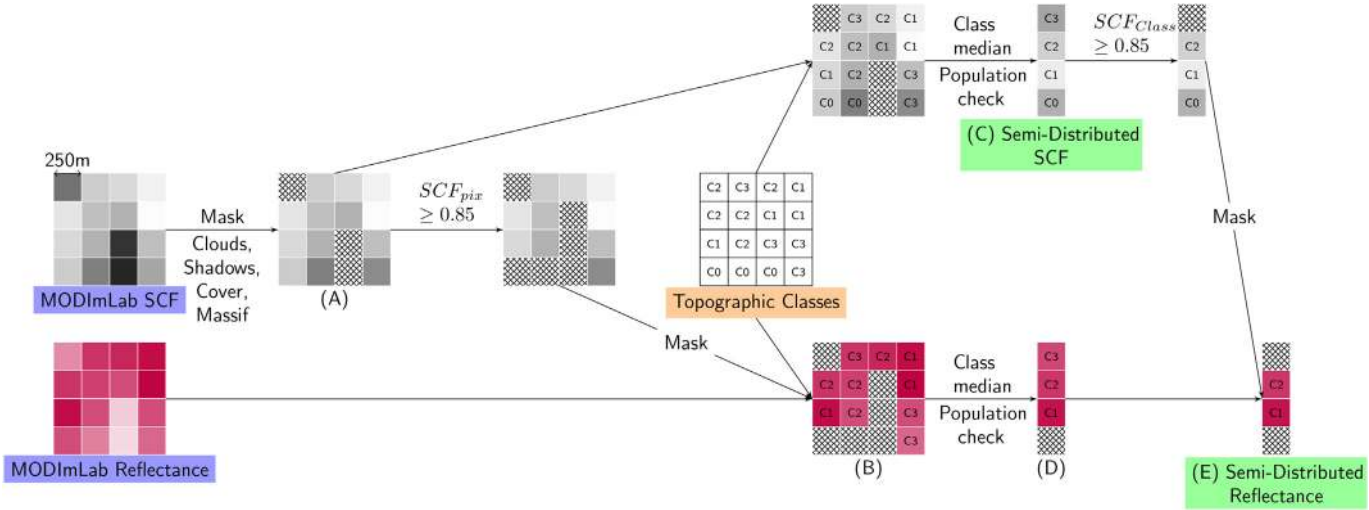

Fig. 5. Flowchart of the conversion of MODImLab products (purple) to semi-distributed data (green), using the Topographical Classification (orange) from Section 3.1.1. Masked data are hatched. (For interpretation of the references to colour in this figure legend, the reader is referred to the web version of this article.)

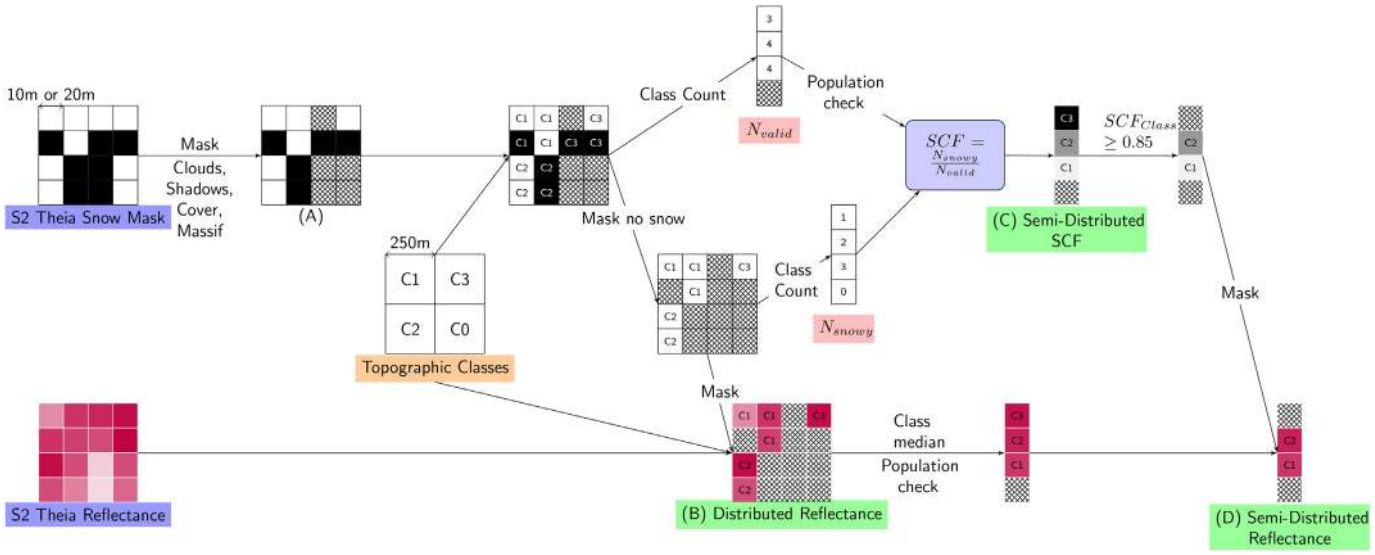

Fig. 6. Flowchart of the conversion of Sentinel-2 products (purple) to semi-distributed data (green), using the Topographical Classification (orange) from Section 3.1.1. (For interpretation of the references to colour in this figure legend, the reader is referred to the web version of this article.)

examples (one date and one topographic class). (2) We evaluate the products against in-situ observations, in order to detect systematic biases and errors. (3) We compute Pearson correlations (R) between the ensemble median and semi-distributed observations timeseries in a wide range of topographic classes, to have additional information on the potential of information. (4) We generalize the results by computing rank diagrams, looking for bias and observation position within the ensemble at the same time and over numerous topographic classes and dates.

4. Results

4.1. Comparison of observed and simulated variables

4.1.1. Spatial comparison on a specific date

Fig. 7 shows maps of NIR semi-distributed reflectance (MODIS band 2) for the two satellite products (MODIS and S2) and the ensemble mean on February 18–19th, 2017. All pixels within the same topographical class are attributed the same value, and in many classes, observations and model are masked out because of shadows.

MODIS and S2 remarkably agree on the snowpack extent, while the ensemble mean seems to overestimate it. Both satellite products show on average more contrasted and lower reflectance values than the model. However, MODIS and the model agree on the reflectance dependence on aspect (lower in South-Eastern slopes), contrary to S2.

4.1.2. Ensemble and satellite reflectance timeseries

Fig. 8 shows the timeseries of ensemble and observations in MODIS bands 4 (VIS) and 2 and 5 (NIR) for the two snow seasons, in 2400 m flat class. This specific class was chosen here because it is flat, above the tree line and with a long snow covered season, thus easing the comparison all along the snow season. Although there is a strong departure among observations and simulations (0.1–0.2 in bands 4 and 2, 0.1 in band 5), consistent time variations can be seen between semi-distributed observations (green stars) and the ensemble median (blue stars), for example in December and January of both snow seasons for band 5. For 2013–2014 winter (Fig. 8a,c,e), high values of reflectance in all bands during the mid-winter are consistent with the recent snowfall at observation dates during this period (fresh snow has a high SSA, thus a high reflectance as shown in Fig. 2. Decrease in reflectance in all bands from November 2013 to mid December and on January 12th is related with extended periods without snowfall as seen on the

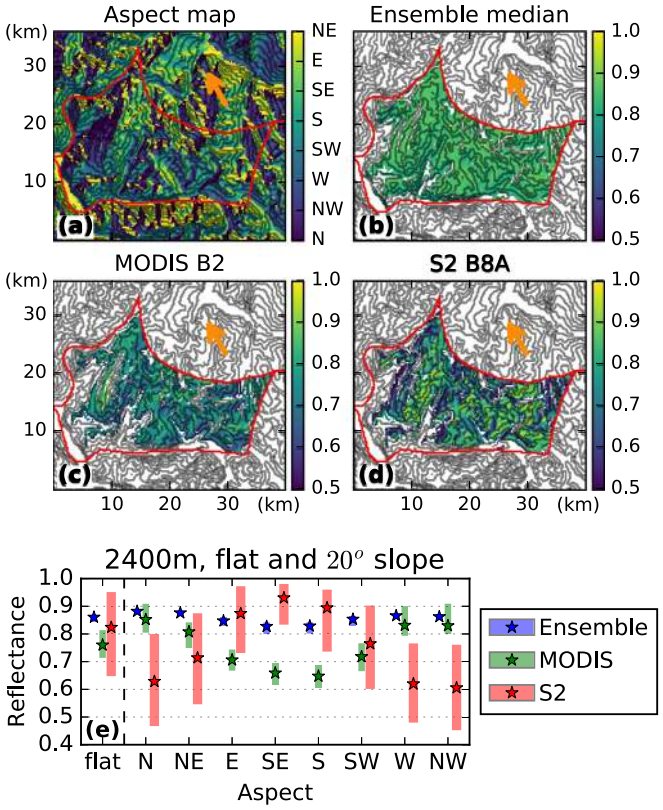

Fig. 7. Map of aspect in the Grandes-Rousses (a), and comparison of the 3 reflectance products in the NIR (860 nm) on 2017-02-18, 10:00 am: ensemble median (b), semi-distributed MODIS band 2 (c) and S2 Band 8A (2017-02-19, 11:00 am) (e). Boxplots (quartiles and medians) for the ensemble (blue), distributed MODIS (green) and S2 (red) in the 2400 m, flat and 20° slope classes. On the maps (a–d), the contours denote the model's 300 m elevation bands, orange arrows show the approximate sun direction and shadows are masked. (For interpretation of the references to colour in this figure legend, the reader is referred to the web version of this article.)

HS curve. At the end of the snow season, the snow melt causes a decrease in SSA (i.e. low reflectance in band 2 and 5) due to wet metamorphism (Carmagnola et al. 2014). Meanwhile, two dust deposition

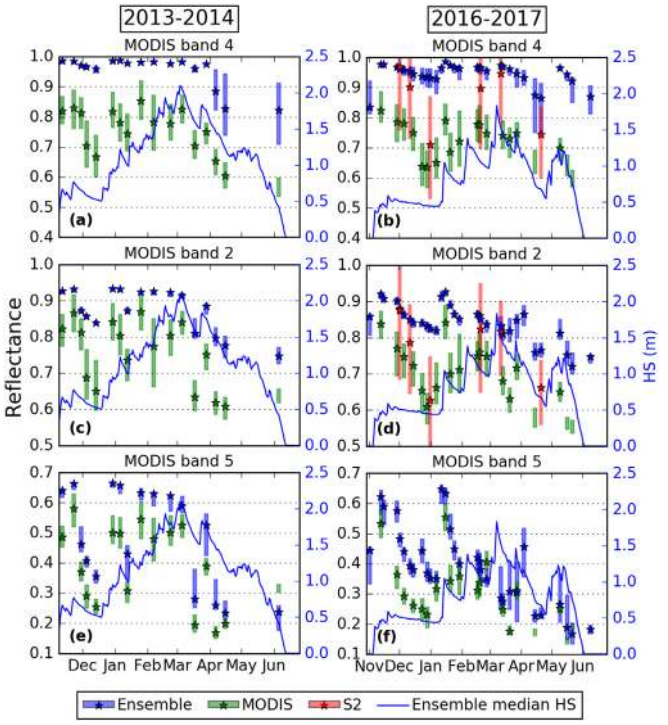

Fig. 8. 2013–2014 (a,c,e) and 2016–2017 (b,d,f) timeseries of reflectance in MODIS band 4 (a,b), 2 (c,d) and 5 (e,f) for the three different products (ensemble in blue, MODIS in green, S2 in red). The stars denote the median of the ensemble and the semi-distributed satellite products. The boxes shows the ensemble and distributed satellite products quartiles. See Table 1 for the wavelengths and S2 corresponding bands. The blue line denotes the ensemble median Height of Snow (HS). (For interpretation of the references to colour in this figure legend, the reader is referred to the web version of this article.)

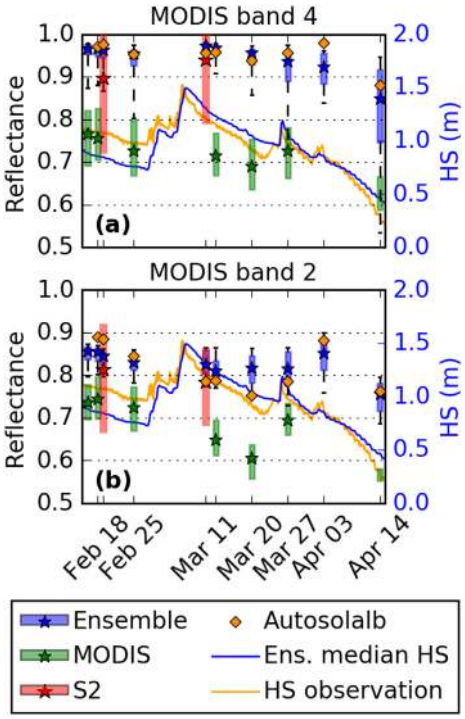

Fig. 9. Same as Fig. 8, in 2100 m.a.s.l flat class for 2016–2017 winter in MODIS band 4 (a) and 2 (b). In addition, Lautaret data from Autosolalb (orange diamonds), and observed HS (orange line) are displayed. Note that bars denote the ensemble 5–95th percentiles. (For interpretation of the references to colour in this figure legend, the reader is referred to the web version of this article.)

events (end of February 2014, end of March 2014 in MOCAGE model) can explain drops in band 4 reflectance through an increase in the snowpack surface LAP content. All those events appear in both ensemble and observation timeseries as well as in simulated surface impurities concentrations (not shown). Season 2016–2017 (Fig. 8b,d,f) had few, intense snowfall and extended dry periods with clear sky, allowing observe more pronounced reflectance variations.

Regarding the ensemble behaviour, in the visible bands, the ensemble Inter-Quartile Range (IQR) (blue boxes) seems generally lower during 2013–2014 winter than in 2016–2017. For all bands, the IQR is reduced after a snowfall (0.01–0.02 in bands 4 and 2, 0.02–0.03 in band 5), and increases with the time elapsed since the last snowfall and all along the melting season (up to 0.1 in bands 4 and 2 and 0.05 in band 5).

However, the main feature here is the strong departure between the ensemble and MODIS observations. For almost all dates of both winters, the semi-distributed observation is under all the members of the ensemble in bands 4 and 2. This deviation is smaller in band 5. Note also that the distributed observations IQR (green boxes) is considerable, and notably lower in band 5 (0.02–0.05) than in bands 2 and 4 (0.05–0.1). Regarding S2 observations, (Fig. 8b,d), agreement of semi-distributed observations (red stars) with the ensemble is good for fresh snow (2016, December 1st) but a strong departure (0.1–0.2) appears after extended periods without snowfall (2016, December 31th for exambple). Furthermore, the IQR of S2 distributed observations (red boxes) is 2–3 times larger than for MODIS.

4.1.3. Comparison with in-situ measurements

Comparison with field measurements at Col du Lautaret (Height of Snow (HS) and reflectance in bands 4 and 2) is possible for the 2100 m a.s.l flat class during 2016–2017 winter (see Fig. 9). First and foremost, there is a strong bias of MODIS observations with respect to in-situ Autosolalb observations (about 0.2 in band 4 and 0.1–0.15 in band 2). However, their time variations reproduce the temporal pattern obtained from in-situ observations for example between March 20th and 27th when an increase of reflectance is occurring in both products.

Meanwhile, the ensemble reflectance generally has the same magnitude as the in-situ observations in both bands. In band 4, the in-situ observations lie within the ensemble for fresh snow, for example on February 18th, March 27th and April 3rd. In band 2, reflectance is underestimated by the ensemble for those dates, except on March 27th. In addition, most of the members are overestimating reflectance in both bands during early melt (11th and 13th of March), while the comparison of the ensemble median and in-situ observed HS (blue and orange lines in Fig. 9) show that melt might be underestimated in the model. On March 20th, ensemble band 4 reflectance generally decreases while band 2 increases, together with a light snowfall in the model. Meanwhile, in-situ observations of HS show that there was no snowfall for this date.

4.1.4. Comparison over all reliable topographical classes

To investigate the distribution of this bias over time and space, MODIS observed semi-distributed values were plotted against the ensemble median. We restricted this study to topographical classes where the observation process is the most reliable, i.e. with low probability of being mixed/rocky (20° maximal slope) and with large enough pixel populations over the whole snow seasons (1800–3000 m.a.s.l.). In bands 4 and 2, Fig. 10a and b show a strong deviation from the 1:1 line. Moreover, the value range in band 4 is much lower in the model (about 0.05) than in the observations (about 0.3). In band 5 (Fig. 10c), observations and model better align with the 1:1 line.

In order to refine this analysis over space, linear regressions were systematically carried out between the ensemble median and the semi-distributed observations for each band inside each reliable topographical class (e.g. computing regressions between timeseries of blue

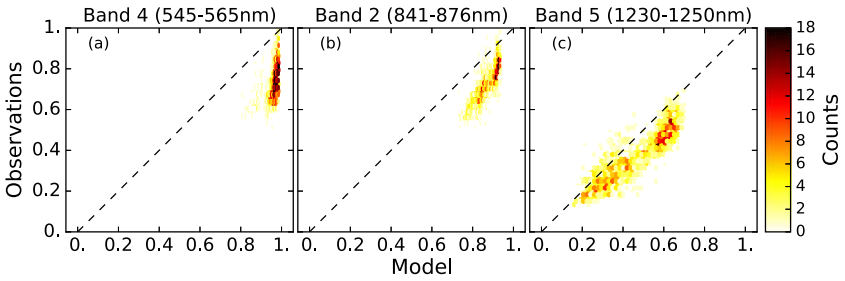

Fig. 10. Semi-distributed MODIS observations in band 4 (a), 2 (b) and 5 (c) against ensemble median (density in colour), for the 45 topographical classes within 1800–3000 m and 0–20 slope, for all the observation dates of 2013–2014 and 2016–2017 snow seasons. (For interpretation of the references to colour in this figure legend, the reader is referred to the web version of this article.)

stars and green stars in Fig. 8). The associated Pearson R^2, slope and intercept coefficients are shown in Fig. 11a and b for bands 2 and 5. In the absence of model or observational bias, Slope should be close to 1 and Intercept to 0.

In band 2, overall high and significant R^2 (0.75–0.85) are noted. Slope is generally > 1, and Intercept < -0.4. However, regression is close to identity in the sunny slopes (strong dependence on aspect) with higher correlations. Band 5 shows high and significant R^2 as well (about 0.8–0.9). Slope and Intercept moderately deviates from Identity (Slope < 1).

4.2. Spectral bands reflectance ratio

4.2.1. Timeseries comparison between the model and satellite products

The bias between observations and model described in Section 4.1 is likely to be problematic for data assimilation. Computing a ratio between the reflectances in two different bands (so-called “band ratio”) might reduce this issue.

To that aim, the ratios between bands 5 and 4 (r54) and bands 5 and 2 (r52) were computed for MODIS observations. To do so, each ratio was computed on every pixel of the distributed reflectance (label B in Fig. 5), and aggregated and masked with the same method as for raw reflectances.

Fig. 12 shows the temporal evolution of these variables in the 2400 m flat class. Time variations of the ensemble median and semi-distributed observations have compatible values (for example in r54 0.6–0.7 for fresh snow, and 0.25–0.4 in the late season). In about 50% of the cases, the semi-distributed observation falls within the ensemble IQR (blue boxes) for r54. In addition, note that r52 and r54 signals are very similar, be it in the model or the observations.

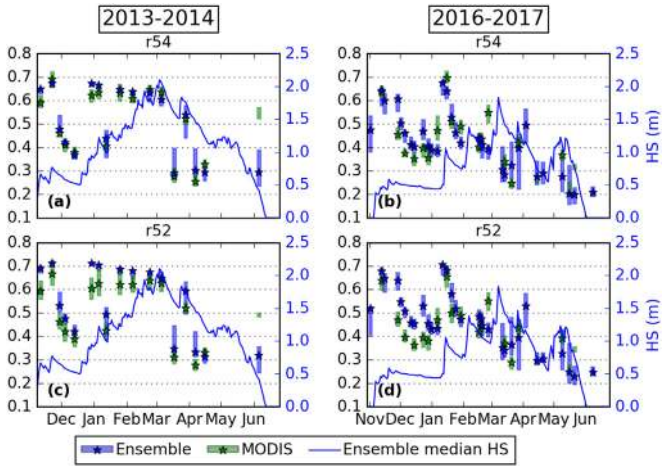

Fig. 12. Same as Fig. 8 for band ratios r54 (a,b) and r52 (c,d).

4.2.2. Comparison over all the reliable classes

Fig. 13 shows the semi-distributed observations against the ensemble medians for the ratios for all the reliable classes and the two snow seasons as in Section 4.1.4. There is no notable systematic bias between the observed ratios and the modelled ones.

Statistics of linear regression in Fig. 14a, and b show high R^2 values generally above 0.85, similar to those for band 5 in Fig. 11b. More interestingly, regression parameters are now around identity (Slope = 1, Intercept = 0) which illustrates the better agreement (no systematic bias) of observations and model for these ratios. While correlation patterns are almost identical for r54 and r52, Slope

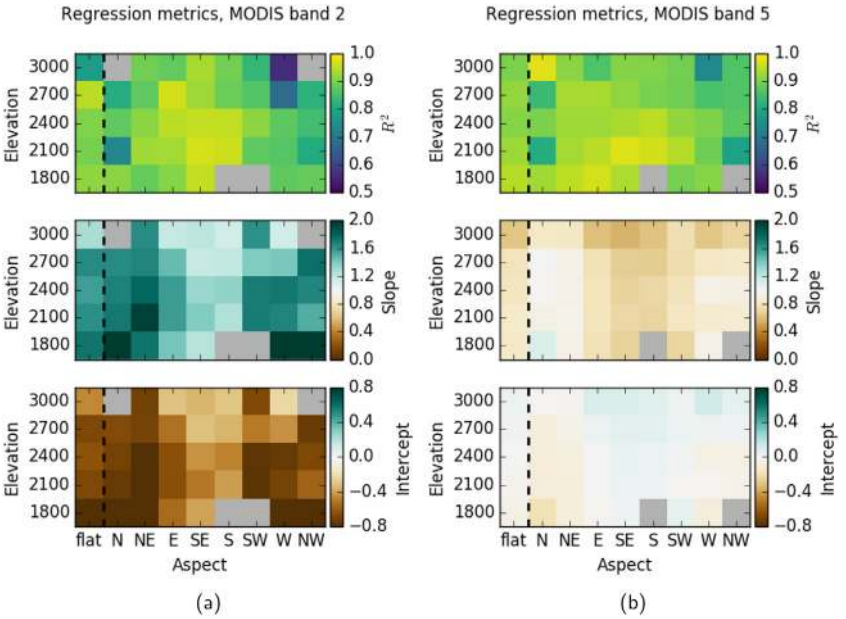

Fig. 11. Linear regression statistics (upper panel: squared Pearson correlations R2, center panel: regression slope, bottom panel: regression intercept) in band 2 (a) and 5 (b) between the time series of ensemble median and semi-distributed observations for the 45 classes within 1800–3000 m.a.s.l and 0–20 degrees of slope, during 2013–2014 and 2016–2017 snow seasons. Regressions with *p*-values > 0.01 and less than 6 dates overall are greyed out.

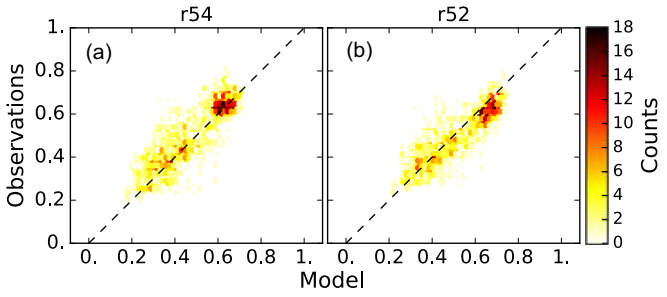

Fig. 13. Same as Fig. 10 for r54 (a) and r52 (b).

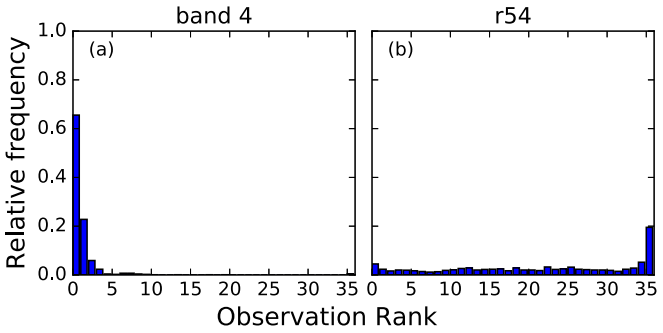

Fig. 15. Rank diagrams for the semi-distributed MODIS observations in band 4 (a) and r54 (b) within the ensemble for all classes between 1800 and 3000 m.a.s.l. and between 0 and 20° of slope, and all dates of 2013–2014 and 2016–2017 snow seasons (1009 occurrences).

parameter is generally more departing from identity for r52 than for r54, with a significant dependence on aspect (lower Slopes in sunny aspects).

4.3. Towards assimilation

Fig. 15a shows the rank diagram for the raw reflectance of band 4, over all considered dates and topographical classes of the two snow seasons. In this graph, the observations lie in rank 0 (under all members of the ensemble) about 60 % of the occurrences, consistently with the negative bias depicted in previous section. On the contrary, the rank diagram for band ratio r54 in Fig. 15b is highly improved with respect to band 4, the observation being in the ensemble 80 % of the occurrences. Result is similar for r52 (not shown). Though overestimation of frequency of ranks 0 (under the ensemble) and 36 (over the ensemble) denote that the ensemble dispersion is insufficient, the rank diagram is flat, all the ranks having similar frequencies.

5. Discussion

5.1. On the relevance of the comparison in the semi-distributed framework

The semi-distributed framework was chosen for the comparison between observed and simulated reflectances because it is the basis of the French operational snowpack modelling system, and considering that running this model on a 250 m-grid requires about 100 times more computer resources. Since it is quite specific, the different types of errors in observations and simulations in this semi-distributed geometry must be discussed for a correct interpretation of our results. Within a topographical class, observations are affected by (1) natural variability, (2) retrieval errors and (3) classification errors. In particular, DEM errors and resolution have a strong impact in satellite retrievals via shadows and subgrid topography (Baba et al. 2019; Davaze et al. 2018), leading to about ± 10% errors in broadband albedo for MODIS data (Dumont et al. 2012). Moreover, S2 data are particularly affected by the three sources, since the retrieval DEM (SRTM90) in the MAJA processor is too coarse to capture the topographic variability at the scale of the pixels (10–20 m) and because the classification is done to an even much coarser scale (IGN250). The resulting intraclass variability of S2 and MODIS is particularly visible in Figs. 7e, 8 and 9.

However, the resulting distributions of the observations within the classes are reasonably gaussian (see Fig. B.1), meaning that semi-distributed observations, aggregated by taking the median, should remove random unbiased noises and outliers.

From the model point of view, the ensemble approach in this study is expected to satisfactorily assess snowpack modelling errors by the combination of meteorological and multiphysical model ensembles. However the semi-distributed simulations can have a limited spatial representativeness due to the snowpack natural variability, for example when the snow line or rain-snow line lies within the topographic class. In the general case, though, we expect this issue to be of limited importance, in the line with other studies (Mary et al. 2013).

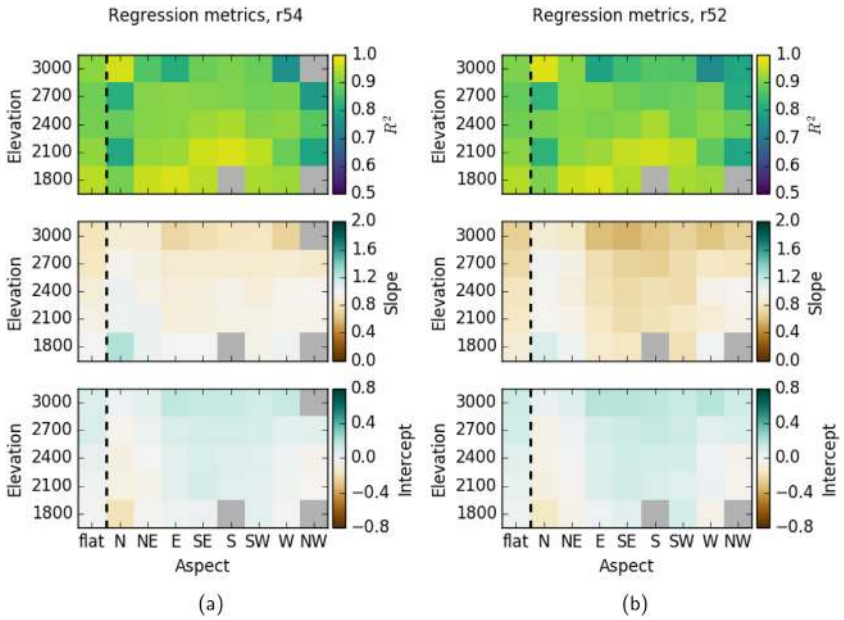

Fig. 14. Same as Fig. 11a for r54 (14a) and r52 (14b).

5.2. Assets and limits of the satellite products

Since we consider that the observation process is not reliable in shadowed area, we filter out many observations, thus reducing the amount of spatial information available for assimilation. This means that from November to February, North facing slopes will likely not be observed. Therefore, ensemble simulations would not be corrected there during this period, if the assimilation were to be carried out on each topographic class independently. This stresses the need for a spatially coherent data assimilation algorithm, e.g. assimilating all observed topographic classes at the same time, in order to spatially propagate the effect of assimilation and to avoid inconsistent spatial patterns. Furthermore, a spatially comprehensive assimilation of SCF would be needed beforehand to detect topographic classes where the ensemble and observations disagree on the presence of snow and assess where reflectance can be compared, similarly as in Baba et al. (2018).

Observations are also affected by significant errors and biases that are problematic for assimilation. S2 reflectance observations suffer from two significant inconsistencies. (1) The dependence of reflectance on aspect is too strong and unexpected. Higher band 2 reflectance are obtained in South-Eastern slopes where SSA should preferentially decrease owing to sun exposure (causing a decrease in reflectance through enhanced metamorphism) and lower SZA (Fig. 7) (Warren 1982). (2) Reflectance decrease with time in the absence of snowfall in the early 2016–2017 snow season is too pronounced (Fig. 8b and d). These two considerations can be explained by retrieval errors in the MAJA algorithm, probably owing to the representation of topography and atmosphere, which was not specifically designed for snow reflectance retrieval in complex terrain (Hagolle et al. 2017). In addition, the reflectance retrieval is also affected by the use in MAJA retrieval of a coarse DEM (SRTM90) compared to the native resolution of the data (10–20 m). For all those reasons, improvements in the retrieval of S2 absolute reflectance values is necessary before considering their future assimilation.

MODIS reflectance observations also have a strong bias with the model. This bias is unambiguously attributed to MODIS according to the comparison with in-situ observations (Fig. 9). It is much higher than the intraclass variability of the observations and the ensemble IQR. In addition, Figs. 10 and 11 show that this bias is well described by a linear function of reflectance which is rather invariant in space and well stable in time.

However, MODIS semi-distributed product (median) seems consistent, because: (1) we demonstrate that the median of the observations within the topographical classes is a representative value of the distribution in the general case, (2) reflectance dependence on aspect corresponds to the model one (Fig. 7) (3) date-to-date time variations notably match those of the ensemble, (4) these variations sometimes better matches in-situ observations than the ensemble, which proves that their information content is good (Fig. 9, in March). All these considerations give us good confidence in the intrinsic quality and information content of MODIS observations, but a solution to this bias is required for assimilation.

5.3. Assimilating band ratios

Biases are a common issue of snowpack remote sensing (Veyssière et al. 2019; Balsamo et al. 2018) and require a proper estimation or correction before assimilation. Many methods exist in the NWP community to correct for the bias or dynamically estimate it in a data assimilation system (Draper et al. 2015; Auligné et al. 2007). However, these methods would require either (1) to assume a non-biased model (2) a representative in-situ reflectance dataset to analyse and model the bias before correcting it on-line (3) extensive, representative, and continuous in-situ observations of snowpack variables to constrain satellite reflectance biases (4) additional data from other satellite sources (Balsamo et al. 2018). All of those suffer from limitations owing to the specificities of snowpack modelling and monitoring in a complex terrain, respectively: (1) snowpack reflectance modelling probably suffers from some biases (Tuzet et al. 2017) (2) absence of any operational network measuring in-situ snowpack reflectance (3) sparse in-situ snowpack measurements in general (4) lack of reliable reflectance retrieval from other satellite sources (as shown here for S2).

Therefore, computing reflectance ratios for assimilation could be an appropriate solution in the current state of the art, because it does not require any assumption on the bias attribution (observations and/or model) and nature. Results show that this method outstandingly allows to unbias the observations using r54 and r52 (Figs. 13 and 14). Furthermore, band ratios are at the core of snowpack surface properties retrieval from satellites (Lyapustin et al. 2009; Negi and Kokhanovsky 2011; Dumont et al. 2014; Kokhanovsky et al. 2018). It is not clear, however, whether all the precious information content of reflectance variables is preserved when computing band ratios. Firstly, the correlation of the two unbiased ratios is very high (≥ 0.9), as already noted by (Lyapustin et al. 2009), and these variables have similar temporal variations than MODIS band 5 (only sensitive to SSA) (see Figs. 8e,f and 12), suggesting that some information on the LAP content might be lost. Since it has been stated that reflectance assimilation requires at least two degrees of freedom, given the dependence of reflectance on LAP and SSA (Charrois et al. 2016), further work is required to infer whether these band ratios are varying sufficiently between polluted and pristine snowpacks. Other band combinations, with a higher sensitivity to LAP could also be used (if unbiased), as implemented in Di Mauro et al. (2015).

Nevertheless, rank diagrams are greatly improved compared to reflectance variables (Fig. 15). The obtained almost flat rank diagram for r54 shows that this variable is very likely to fall within the ensemble without any preferential position, for any topographical class and date. This is really encouraging towards spatialized assimilation of such variables.

5.4. Ensemble modelling

The remaining underdispersion of the ensemble evidenced by the over representation of the extremal positions in the rank diagrams, could be improved in the near future by a better characterization of the modelling chain uncertainties. (1) Increasing the amplitude of meteorological/impurities fluxes perturbations (Charrois et al. 2016) or using physical NWP ensemble such as PEARP (Descamps et al. 2015; Vernay et al. 2015) could allow to better account for NWP modelling uncertainties and intra-massif variability of weather conditions. (2) Including recent developments in Crocus such as blowing snow within the semi-distributed geometry (SYTRON, (Vionnet et al. 2018)) (3) Including different impurities scavenging parameter and optical properties configurations within the multiphysical ensemble (Tuzet et al. 2017).

Furthermore, adaptations to the presented ensemble modelling chain could make it more suitable for assimilation. First, the ensemble population ($N = 35$) is small compared to recent local ensemble assimilation attempts in snowpack modelling (e.g. Piazzi et al. (2018), Larue et al. (2018), Charrois et al. (2016)). However ensemble size must be kept to reasonable values for larger scale operational applications, and scores are not expected to highly depend on ensemble size for openloop simulations (Leutbecher 2018). In addition, though increasing the ensemble population would allow to run several combinations of the forcings with ESCROC members, note that combining each forcing member with only one physical configuration of the model, therefore limiting the combinations, is a current practice in NWP to sample uncertainties (Descamps et al. 2015). Secondly, the choice of randomly drawing “N” ESCROC configurations versus carefully building a given subset of “N” members can be discussed. Indeed, Lafaysse et al. (2017) showed that the ensemble error representativeness could be improved by an appropriate optimized sample of

members. However, this sample could not be tested here because it did not include T17 radiative transfer option (Tuzet et al. 2017), mandatory for reflectance modelling. Moreover, site-specific calibrations are expected to be suboptimal when applied over a wide diversity of sites (Krinner et al. 2018).

6. Conclusions

This study investigated the potential for assimilation of MODIS reflectance observations in ensemble snowpack simulations within a semi-distributed framework.

First, it is shown that MODIS observations of reflectance aggregated by topographic classes can be compared with semi-distributed ensemble simulation outputs, and that they convey substantial information content. However, it also clearly appears that MODIS observations are noisy and biased, due to the difficulty of retrieving surface reflectances in a complex terrain. In addition, it seems that S2 reflectance retrieval was affected by even bigger errors.

Meanwhile, it seems that the semi-distributed framework is particularly adapted to reflectance assimilation. First, it enables to efficiently remove observational noise thanks to aggregation within topographical classes. It is clear though, that monitoring the substantial intraclass natural variability of reflectance is then out of reach. Furthermore, state-of-the-art distributed snowpack modelling is currently not able to represent this spatial variability either. Reaching this goal would require the use of high resolution meteorological forcings (Quéno et al. 2016), and modelling of snow redistribution by wind and gravitation (Vionnet et al. 2014; Mott and Lehning 2010; Freudiger et al. 2017) in distributed simulations. However, such simulations would require intensive computational resources compared to the semi distributed framework, added to the increase in computational cost due to ensemble forecasting already present here.

This study was also the first attempt of spatialized ensemble detailed snowpack modelling using a combination of meteorological and model ensembles. Results showed that the semi-distributed setup is able to represent the associated errors and uncertainties in the modelling of reflectance well, and identified paths to make it more suitable to data assimilation.

Therefore, we are confident on the potential for assimilation to take full advantage of reflectance observations and detailed snowpack modelling in such a geometry. However, the remaining strong bias in MODIS semi-distributed reflectance observations prevents from directly assimilating them. A workaround was proposed for MODIS bias by computing ratios of reflectances, a simple method that should preserve the observations information content. We are confident that assimilating such variables is possible and could be beneficial for snowpack modelling in the near future. Furthermore, efforts to improve the retrieval of reflectances in complex terrain must be conducted, in order to reduce retrieval errors and bias, and implement retrieval of other medium-resolution satellite sources such as VIIRS and Sentinel3.

Data and code availability

The datasets analysed during this study and the code used to produce the figures are available from the corresponding author on request. ESCROC is developed inside the open source SURFEX project (http://www.umr-cnrm.fr/surfex). While it is not implemented in an official SURFEX release, the code can be downloaded from the specific branch of the git repository maintained by Centre d'Études de la Neige. The full procedure and documentation can be found at https://opensource.umr-cnrm.fr/projects/snowtools_git/wiki/Procedure_for_new_users and hhttps://opensource.umr-cnrm.fr/projects/snowtools_git/wiki/Data_assimilation_of_snow_observations. For reproducibility of results, the version used in this work is tagged as cluzetCRST. Processing of the albedo images has been performed using the open-source MODImLab algorithm, (version 1.2.5.d). This algorithm can be accessed by contacting its administrator, P. Sirguey.

Aknowledgements

CNRM/CEN is part of Labex OSUG@2020 (investissement d'avenir – ANR10 LABX56). This study was partly supported by the French ANR program ANR-16-CE01-0006 EBONI, LEFE ASSURANCE and APR CNES MIOSOTIS grants. The authors are grateful to Lautaret staff and Station Alpine Joseph Fourier (SAJF) for ensuring a proper working of the instruments and support for in-situ experiments, P. Sirguey for providing MODImLab code and helpful discussions on retrieval algorithm, and to S. Gascoin, for advice and comments on the handling of Sentinel-2 data. J. Revuelto is supported by a Post-doctoral Fellowship of the French AXA research fund (le Post-Doctorant Jesús Revuelto est. bénéficiaire d'une bourse postdoctorale du Fonds AXA pour la Recherche Ref: CNRM 3.2.01/17).

Declaration of Competing Interest

This manuscript has not been published and is not under consideration for publication elsewhere. We have no conflicts of interest to disclose.

Appendix A. Table of observation dates

Table A.1
Summary of observation dates for MODIS, S2 and Autosolalb sensors over 2013–14 and 2016–2017 winters. Time is given for the corresponding closest model output time step (hour).

Date	MODIS	S2	Autosolalb	Date	MODIS	S2	Autosolalb
2013-11-11 11:00	X			2016-12-14 10:00	X		
2013–11–22 10:00	X			2016-12-23 10:00	X		
2013–11–29 10:00	X			2016-12-28 11:00	X		
2013-12-04 11:00	X			2016-12-31 10:00		X	
2013-12-13 11:00	X			2017-01-06 11:00	X		
2013-12-29 11:00	X			2017-01-11 11:00	X		
2014-01-05 11:00	X			2017-01-15 11:00	X		
2014-01-12 11:00	X			2017–01–20 11:00	X		
2014–01–25 10:00	X			2017–01–24 10:00	X		
2014-02-06 11:00	X			2017–01–29 11:00	X		
2014-02-22 11:00	X			2017-02-16 11:00	X		X
2014-03-05 10:00	X			2017-02-18 10:00	X		X
2014-03-17 11:00	X			2017-02-19 11:00		X	X
2014-03-28 10:00	X			2017-02-25 10:00	X		X
2014-04-06 10:00	X			2017-03-11 11:00		X	X

(continued on next page)

Table A.1 (*continued*)

Date	MODIS	S2	Autosolalb	Date	MODIS	S2	Autosolalb
2014-04-15 10:00	X			2017-03-13 10:00	X		X
2014-06-05 11:00	X			2017-03-20 11:00	X		X
Winter 2016–2017				2017-03-27 11:00	X		X
2016-11-01 11:00		X		2017-04-03 11:00		X	X
2016-11-12 10:00	X			2017-04-14 10:00	X		X
2016-11-15 11:00	X			2017-04-20 10:00	X		X
2016-11-28 10:00	X			2017-05-09 10:00	X		
2016-12-01 11:00		X		2017-05-16 10:00	X		
2016-12-05 11:00	X			2017-05-21 11:00	X		
2016-12-11 11:00		X		2017-06-08 11:00	X		

Appendix B. Intraclass distribution of observations

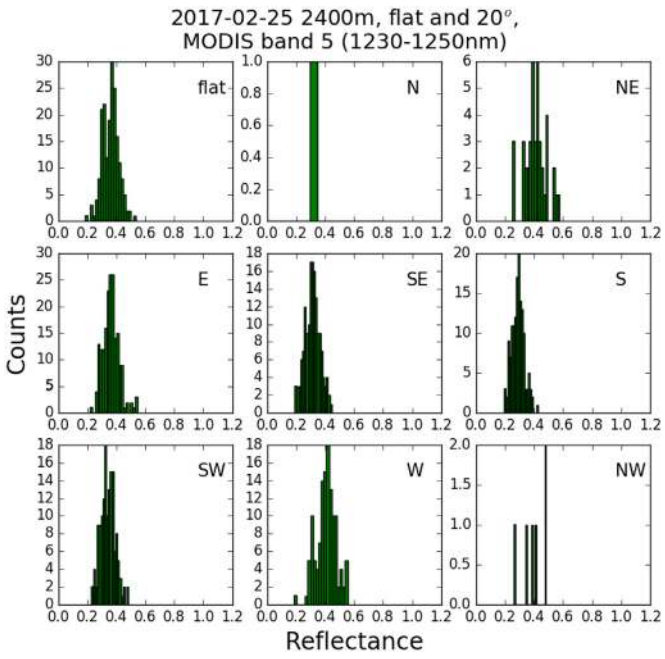

Fig. B.1. Histograms of MODIS band 5 reflectance in flat and 20° slope classes at 2400 m on 2017, February the 25th, 10:40 am.

References

Aalstad, K., Westermann, S., Schuler, T.V., Boike, J., Bertino, L., Jan 2018. Ensemble-based assimilation of fractional snow-covered area satellite retrievals to estimate the snow distribution at arctic sites. Cryosphere 12 (1) (doi:10.5194).

Andreadis, K.M., Lettenmaier, D.P., 2006. Assimilating remotely sensed snow observations into a macroscale hydrology model. Adv. Water Resour. 29 (6), 872–886.

Auligné, T., McNally, A., Dee, D., 2007. Adaptive bias correction for satellite data in a numerical weather prediction system. Q. J. R. Meteorol. Soc. 133 (624), 631–642.

Baba, M., Gascoin, S., Hanich, L., Dec 2018. Assimilation of sentinel-2 data into a snowpack model in the high atlas of morocco. Remote Sens. 10 (12), 1982 (doi:10.3390).

Baba, M.W., Gascoin, S., Kinnard, C., Marchane, A., Hanich, L., jul 2019. Effect of digital elevation model resolution on the simulation of the snow cover evolution in the high atlas. Water Resour. Res. 55 (7), 5360–5378 (doi:10.1029).

Balsamo, G., et al., 2018. Satellite and in situ observations for advancing global earth surface modelling: a review. Remote Sens. 10 (12). http://www.mdpi.com/2072-4292/10/12/2038.

Carmagnola, C.M., Domine, F., Dumont, M., Wright, P., Strellis, B., Bergin, M., Dibb, J., Picard, G., Libois, Q., Arnaud, L., Morin, S., 2013. Snow spectral albedo at summit, Greenland: measurements and numerical simulations based on physical and chemical properties of the snowpack. Cryosphere 7 (6), 1139–1160.

Carmagnola, C.M., Morin, S., Lafaysse, M., Domine, F., Lesaffre, B., Lejeune, Y., Picard, G., Arnaud, L., 2014. Implementation and evaluation of prognostic representations of the optical diameter of snow in the surfex/isba-crocus detailed snowpack model. Cryosphere 8 (2), 417–437.

Charrois, L., Dumont, M., Sirguey, P., Morin, S., Lafaysse, M., Karbou, F., 2013. Comparing different modis snow products with distributed simulation of the snowpack in the french alps. In: Proceedings of the International Snow Science Workshop, (Innsbruck, Austria).

Charrois, L., Cosme, E., Dumont, M., Lafaysse, M., Morin, S., Libois, Q., Picard, G., 2016. On the assimilation of optical reflectances and snow depth observations into a detailed snowpack model. Cryosphere 10 (3), 1021–1038.

Davaze, L., Rabatel, A., Arnaud, Y., Sirguey, P., Six, D., Letreguilly, A., Dumont, M., 2018. Monitoring glacier albedo as a proxy to derive summer and annual surface mass balances from optical remote-sensing data. Cryosphere 12 (1), 271–286. https://www.the-cryosphere.net/12/271/2018/.

De Lannoy, G.J., Reichle, R.H., Arsenault, K.R., Houser, P.R., Kumar, S., Verhoest, N.E., Pauwels, V.R., 2012. Multiscale assimilation of advanced microwave scanning radiometer–eos snow water equivalent and moderate resolution imaging spectro-radiometer snow cover fraction observations in northern Colorado. Water Resour. Res. 48 (1).

Dee, D.P., Da Silva, A.M., 1998. Data assimilation in the presence of forecast bias. Q. J. R. Meteorol. Soc. 124 (545), 269–295.

Descamps, L., Labadie, C., Joly, A., Bazile, E., Arbogast, P., Cébron, P., 2015. Pearp, the météo-France short-range ensemble prediction system. Q. J. R. Meteorol. Soc. 141 (690), 1671–1685.

Di Mauro, B., Fava, F., Ferrero, L., Garzonio, R., Baccolo, G., Delmonte, B., Colombo, R., 2015. Mineral dust impact on snow radiative properties in the european alps combining ground, uav, and satellite observations. J. Geophys. Res. 120 (12), 6080–6097.

Dozier, J., Green, R.O., Nolin, A.W., Painter, T.H., 2009. Interpretation of snow properties from imaging spectrometry. Remote Sens. Environ. 113, S25–S37.

Draper, C., Reichle, R., De Lannoy, G., Scarino, B., 2015. A dynamic approach to addressing observation-minus-forecast bias in a land surface skin temperature data assimilation system. J. Hydrometeorol. 16 (1), 449–464.

Dumont, M., Sirguey, P., Arnaud, Y., Six, D., 2011. Monitoring spatial and temporal variations of surface albedo on Saint Sorlin Glacier (French Alps) using terrestrial photography. Cryosphere 5 (3), 759–771. http://www.the-cryosphere.net/5/759/2011/.

Dumont, M., Gardelle, J., Sirguey, P., Guillot, A., Six, D., Arnaud, A.R.Y., 2012. Linking glacier annual mass balance and glacier albedo retrieved from modis data. Cryosphere 6, 1527–1539.

Dumont, M., Brun, E., Picard, G., Michou, M., Libois, Q., Petit, J., Geyer, M., Morin, S.,

Josse, B., 2014. Contribution of light-absorbing impurities in snow to greenland's darkening since 2009. Nat. Geosci. 7 (7), 509.
Dumont, M., Arnaud, L., Picard, G., Libois, Q., Lejeune, Y., Nabat, P., Voisin, D., Morin, S., 2017. In situ continuous visible and near-infrared spectroscopy of an alpine snowpack. Cryosphere 11 (3), 1091–1110.
Durand, Y., Brun, E., Mérindol, L., Guyomarc'h, G., Lesaffre, B., Martin, E., 1993. A meteorological estimation of relevant parameters for snow models. Ann. Glaciol. 18, 65–71.
Durand, Y., Giraud, G., Brun, E., Mérindol, L., Martin, E., 1999. A computer-based system simulating snowpack structures as a tool for regional avalanche forecasting. J. Glaciol. 45 (151), 469–484.
Essery, R., 2015. A factorial snowpack model (fsm 1.0). Geosci. Model Dev. 8, 3867–3876.
Essery, R., Morin, S., Lejeune, Y., Bauduin-Ménard, C., 2013. A comparison of 1701 snow models using observations from an alpine site. Adv. Water Resour. 55, 131–148.
Farr, T.G., Rosen, P.A., Caro, E., Crippen, R., Duren, R., Hensley, S., Kobrick, M., Paller, M., Rodriguez, E., Roth, L., et al., 2007. The shuttle radar topography mission. Rev. Geophys. 45 (2).
Fiddes, J., Gruber, S., 2012. Toposub: a tool for efficient large area numerical modelling in complex topography at sub-grid scales. Geosci. Model Dev. 5 (5), 1245–1257. http://www.geosci-model-dev.net/5/1245/2012/.
Freudiger, D., Kohn, I., Seibert, J., Stahl, K., Weiler, M., 2017. Snow redistribution for the hydrological modeling of alpine catchments. Wiley Interdiscip. Rev. Water 4 (5), e1232.
Gascoin, S., Grizonnet, M., Bouchet, M., Salgues, G., Hagolle, O., 2019. Theia snow collection: high-resolution operational snow cover maps from sentinel-2 and landsat-8 data. Earth Syst. Sci. Data 11 (2), 493–514.
Günther, D., Marke, T., Essery, R., Strasser, U., 2019. Uncertainties in snowpack simulations—assessing the impact of model structure, parameter choice, and forcing data error on point-scale energy balance snow model performance. Water Resour. Res. 55 (4), 2779–2800.
Hagolle, O., Huc, M., Descardins, C., Auer, S., Richter, R., 2017. Maja Algorithm Theoretical Baseline Document. (Tech. rep).
Hall, D.K., Riggs, G.A., Salomonson, V.V., DiGirolamo, N.E., Bayr, K.J., 2002. Modis snow-cover products. Remote Sens. Environ. 83 (1–2), 181–194.
Hamill, T., 2001. Interpretation of rank histograms for verifying ensemble forecasts. Mon. Weather Rev. 129 (3), 550–560.
Helmert, J., Şensoy Şorman, A., Alvarado Montero, R., De Michele, C., de Rosnay, P., Dumont, M., Finger, D., Lange, M., Picard, G., Potopová, V., et al., 2018. Review of snow data assimilation methods for hydrological, land surface, meteorological and climate models: results from a cost harmosnow survey. Geosciences 8 (12), 489.
Hyer, E., Reid, J., Zhang, J., 2011. An over-land aerosol optical depth data set for data assimilation by filtering, correction, and aggregation of modis collection 5 optical depth retrievals. Atmos. Meas. Techniq. 4 (3), 379–408.
Josse, B., Simon, P., Peuch, V.-H., 2004. Radon global simulations with the multiscale chemistry and transport model mocage. Tellus B 56 (4), 339–356.
Kokhanovsky, A., Lamare, M., Mauro, B.D., Picard, G., Arnaud, L., Dumont, M., Tuzet, F., Brockmann, C., Box, J.E., 2018. On the reflectance spectroscopy of snow. Cryosphere 12 (7), 2371–2382.
Krinner, G., Derksen, C., Essery, R., Flanner, M., Hagemann, S., Clark, M., Hall, A., Rott, H., Brutel-Vuilmet, C., Kim, H., et al., 2018. Esm-snowmip: assessing snow models and quantifying snow-related climate feedbacks. Geosci. Model Dev. 11, 5027–5049.
Lafaysse, M., Morin, S., Coléou, C., Vernay, M., Serça, D., Besson, F., Willemet, J.-M., Giraud, G., Durand, Y., 2013. Toward a new chain of models for avalanche hazard forecasting in french mountain ranges, including low altitude mountains. In: Proceedings of the International Snow Science Workshop - Grenoble and Chamonix, pp. 162–166.
Lafaysse, M., Cluzet, B., Dumont, M., Lejeune, Y., Vionnet, V., Morin, S., 2017. A multiphysical ensemble system of numerical snow modelling. Cryosphere 11 (3), 1173–1198. https://www.the-cryosphere.net/11/1173/2017/.
Larue, F., Royer, A., De Sève, D., Roy, A., Picard, G., Vionnet, V., Cosme, E., 2018. Simulation and assimilation of passive microwave data using a snowpack model coupled to a calibrated radiative transfer model over northeastern Canada. Water Resour. Res. 54 (7), 4823–4848.
Lehning, M., Bartelt, P., Brown, B., Fierz, C., Satyawali, P., 2002. A physical snowpack model for the Swiss avalanche warning. part II: snow microstructure. Cold Reg. Sci. Technol. 35 (3), 147–167.
Leutbecher, M., oct 2018. Ensemble size: how suboptimal is less than infinity? Quart. J. R. Meteorol. Soc. 145 (S1), 107–128 (doi:10.1002).
Libois, Q., Picard, G., Arnaud, L., Dumont, M., Lafaysse, M., Morin, S., Lefebvre, E., 2015. Summertime evolution of snow specific surface area close to the surface on the Antarctic Plateau. Cryosphere 9 (6), 2383–2398.
Lyapustin, A., Tedesco, M., Wang, Y., Aoki, T., Hori, M., Kokhanovsky, A., 2009. Retrieval of snow grain size over Greenland from modis. Remote Sens. Environ. 113 (9), 1976–1987.
Magnusson, J., Winstral, A., Stordal, A.S., Essery, R., Jonas, T., 2017. Improving physically based snow simulations by assimilating snow depths using the particle filter. Water Resour. Res. 53 (2), 1125–1143.
Mary, A., Dumont, M., Dedieu, J.-P., Durand, Y., Sirguey, P., Milhem, H., Mestre, O., Negi, H.S., Kokhanovsky, A.A., Lafaysse, M., Morin, S., 2013. Intercomparison of retrieval algorithms for the specific surface area of snow from near-infrared satellite data in mountainous terrain, and comparison with the output of a semi-distributed snowpack model. Cryosphere 7, 741–761.
Mauro, B.D., Garzonio, R., Rossini, M., Filippa, G., Pogliotti, P., Galvagno, M., Morra di Cella, U., Migliavacca, M., Baccolo, G., Clemenza, M., et al., 2019. Saharan dust events in the european alps: role in snowmelt and geochemical characterization. Cryosphere 13 (4), 1147–1165.
Morin, S., Horton, S., Techel, F., Bavay, M., Coléou, C., Fierz, C., Gobiet, A., Hagenmuller, P., Lafaysse, M., Lizar, M., Mitterer, C., Monti, F., Müller, K., Olefs, M., Snook, J.S., van Herwijnen, A., Vionnet, V., 2019. Application of physical snowpack models in support of operational avalanche hazard forecasting: A status report on current implementations and prospects for the future. Cold Regions Science and Technology. https://doi.org/10.1016/j.coldregions.2019.102910.
Mott, R., Lehning, M., 2010. Meteorological modeling of very high-resolution wind fields and snow deposition for mountains. J. Hydrometeorol. 11 (4), 934–949.
Nabat, P., Somot, S., Mallet, M., Michou, M., Sevault, F., Driouech, F., Meloni, D., di Sarra, A., Di Biagio, C., Formenti, P., et al., 2015. Dust aerosol radiative effects during summer 2012 simulated with a coupled regional aerosol–atmosphere–ocean model over the mediterranean. Atmos. Chem. Phys. 15 (6), 3303–3326.
Negi, H., Kokhanovsky, A., 2011. Retrieval of snow albedo and grain size using reflectance measurements in himalayan basin. Cryosphere 5 (1), 203–217.
Nolin, A.W., 2011. Recent advances in remote sensing of seasonal snow. J. Glaciol. 56 (200), 1141–1150.
Piazzi, G., Thirel, G., Campo, L., Gabellani, S., 2018. A particle filter scheme for multivariate data assimilation into a point-scale snowpack model in an alpine environment. Cryosphere 12 (7), 2287–2306.
Quéno, L., Vionnet, V., Dombrowski-Etchevers, I., Lafaysse, M., Dumont, M., Karbou, F., 2016. Snowpack modelling in the pyrenees driven by kilometric-resolution meteorological forecasts. Cryosphere 10 (4), 1571–1589. https://www.the-cryosphere.net/10/1571/2016/.
Raleigh, M.S., Lundquist, J.D., Clark, M.P., 2015. Exploring the impact of forcing error characteristics on physically based snow simulations within a global sensitivity analysis framework. Hydrol. Earth Syst. Sci. 19 (7), 3153–3179.
Reichle, R.H., Koster, R.D., Dong, J., Berg, A.A., 2004. Global soil moisture from satellite observations, land surface models, and ground data: Implications for data assimilation. J. Hydrometeorol. 5 (3), 430–442.
Revuelto, J., Lecourt, G., Lafaysse, M., Zin, I., Charrois, L., Vionnet, V., Dumont, M., Rabatel, A., Six, D., Condom, T., et al., 2018. Multi-criteria evaluation of snowpack simulations in complex alpine terrain using satellite and in situ observations. Remote Sens. 10 (8), 1171.
Richter, R., 1998. Correction of satellite imagery over mountainous terrain. Appl. Opt. 37 (18), 4004–4015.
Sirguey, P., 2009. Simple correction of multiple reflection effects in rugged terrain. Int. J. Remote Sens. 30, 1075–1081.
Sirguey, P., Still, H., Cullen, N.J., Dumont, M., Arnaud, Y., Conway, J.P., 2016. Reconstructing the mass balance of Brewster glacier, New Zealand, using modis-derived glacier-wide albedo. Cryosphere 10 (5), 2465–2484.
Skiles, S.M., Painter, T.H., 2019. Toward understanding direct absorption and grain size feedbacks by dust radiative forcing in snow with coupled snow physical and radiative transfer modeling. Water Resour. Res. 55, 7362–7378. https://doi.org/10.1029/2018wr024573.
Skiles, S.M., Flanner, M., Cook, J.M., Dumont, M., Painter, T.H., 2018. Radiative forcing by light-absorbing particles in snow. Nat. Clim. Chang. 1.
Smyth, E.J., Raleigh, M.S., Small, E.E., feb 2019. Particle filter data assimilation of monthly snow depth observations improves estimation of snow density and SWE. Water Resour. Res. 55 (2), 1296–1311 (doi:10.1029).
Stigter, E.E., Wanders, N., Saloranta, T.M., Shea, J.M., Bierkens, M.F., Immerzeel, W.W., 2017. Assimilation of snow cover and snow depth into a snow model to estimate snow water equivalent and snowmelt runoff in a himalayan catchment. Cryosphere 11 (4), 1647–1664.
Thirel, G., Salamon, P., Burek, P., Kalas, M., 2013. Assimilation of modis snow cover area data in a distributed hydrological model using the particle filter. Remote Sens. 5 (11), 5825–5850.
Toure, A.M., Reichle, R.H., Forman, B.A., Getirana, A., De Lannoy, G.J., 2018. Assimilation of modis snow cover fraction observations into the nasa catchment land surface model. Remote Sens. 10 (2), 316.
Tuzet, F., Dumont, M., Lafaysse, M., Picard, G., Laurent, A., Voisin, D., Lejeune, Y., Charrois, L., Nabat, P., Morin, S., 2017. A multilayer physically based snowpack model simulating direct and indirect radiative impacts of light-absorbing impurities in snow. Cryosphere 11 (6), 2633.
Tuzet, F., Dumont, M., Arnaud, L., Voisin, D., Lamare, M., Larue, F., Revuelto, J., Picard, G., 2019. Influence of light-absorbing particles on snow spectral irradiance profiles. Cryosphere 13 (8), 2169–2187.
Vernay, M., Lafaysse, M., Merindol, L., Giraud, G., Morin, S., 2015. Ensemble forecasting of snowpack conditions and avalanche hazard. Cold Reg. Sci. Technol. 120, 251–262.
Veyssière, G., Karbou, F., Morin, S., Lafaysse, M., Vionnet, V., 2019. Evaluation of sub-kilometric numerical simulations of c-band radar backscatter over the french alps against sentinel-1 observations. Remote Sens. 11 (1), 8.
Vionnet, V., Brun, E., Morin, S., Boone, A., Martin, E., Faroux, S., Le-Moigne, P., Willemet, J.-M., 2012. The detailed snowpack scheme crocus and its implementation in SURFEX v7.2. Geosci. Model Dev. 5, 773–791.
Vionnet, V., Martin, E., Masson, V., Guyomarc'h, G., Naaim-Bouvet, F., Prokop, A., Durand, Y., Lac, C., 2014. Simulation of wind-induced snow transport and sublimation in alpine terrain using a fully coupled snowpack/atmosphere model. Cryosphere 8 (2), 395–415.
Vionnet, V., Guyomarc'h, G., Lafaysse, M., Naaim-Bouvet, F., Giraud, G., Deliot, Y., 2018. Operational implementation and evaluation of a blowing snow scheme for avalanche hazard forecasting. Cold Reg. Sci. Technol. 147, 1–10.
Warren, S., 1982. Optical properties of snow. Rev. Geophys. 20 (1), 67–89.
Winstral, A., Magnusson, J., Schirmer, M., Jonas, T., 2019. The bias-detecting ensemble: a new and efficient technique for dynamically incorporating observations into physics-based, multilayer snow models. Water Resour. Res. 55 (1), 613–631.

2.3 Assimilation of MODIS-like reflectance ratios into ensemble simulations of the snowpack with a Particle Filter

Author contribution:

The materials in this section were produced by Youness El-Ouartassy, a 2nd year Masters student from the African Regional Center for Space Science and Technology in French Language (CRASTE-LF) in Rabat (Morocco)[1]. Here, I provide an overview of his method and results, which are available in his report (written in French).
I was the instigator of this internship, and his main supervisor.

- Definition of the research subject and supervision of the work
- Conception, development and maintenance of the ensemble data assimilation system
- Help with the analysis, writing and preparation for the Masters defense talk

2.3.1 Introduction

Snowpack modelling is key to better anticipate avalanche risks, but it badly captures snowpack variability in the mountains. Satellite reflectances from space-borne sensors like MODIS capture some of this variability and could be assimilated into snowpack models. Reflectances indeed provide useful informations on the surface properties of the snowpack, such as the Specific Surface Area, (SSA, m^2 kg^{-1}) informative on the snow microstructure and Light Absorbing Particles content (LAP, g g_{snow}^{-1}) (see Sec. 1.2.3 for more details). Both control on the snowpack shortwave (SW) net radiative shortwave, a key component of the snowpack energy budget in mid-latitude mountains. In a synthetic experiment assimilating reflectances, Charrois et al. (2016) reduced SWE modelling errors by up to a factor of two.
However, in recent work, Cluzet et al. (2020) showed that reflectance products retrieved from MODIS are biased and cannot be directly assimilated, an issue already faced by Charrois (2017) at the point scale. Cluzet et al. (2020) showed that ratios between MODIS spectral bands (so-called "band ratios") r52 (band 5 divided by band 2) and r54 (band 5 divided by band 4) are not biased and therefore could be assimilated. It is not sure whether the precious information content from the reflectances is preserved after this manipulation (Lyapustin et al., 2009). The aim of this Section is to investigate their potential for assimilation.

[1] Youness will start a PhD at CNRM-IRSN on Novermber 1st, 2020, under the supervision of Matthieu Plu.

This work capitalises on efforts from Cluzet et al. (2021) to build an ensemble data assimilation system of snowpack modelling accounting for modelling errors and uncertainties and including a Particle Filter. Charrois et al. (2016) evaluated the information content of MODIS reflectances at the point scale by means of twin experiments. In such a setup, an open-loop (i.e. without assimilation) ensemble run is performed beforehand. Several members are extracted from this open-loop, and its reflectance is used as synthetic truth for assimilation. The remaining state variables can be used for evaluation of the assimilation runs. One can then measure if the assimilation of the synthetic reflectances brings the simulation closer to the truth state than the open-loop.
Our aim is to evaluate the information content of band ratio respective t the raw reflectance products. We perform similar twin experiments over one year (winter 2016-2017) of simulations at Col du Lautaret, in the French Alps. Band ratios are assimilated an their impact on simulations is compared with the open-loop and results from raw reflectance assimilation to assess their information content.
Following Sec.2.3.2 briefly introduces the methods and the ensemble setup, Sec. 2.3.3 presents and discusses the results, and final Sec. 2.3.4 concludes and open perspectives.

2.3.2 Methods

Ensemble modelling setup

The ensemble modelling setup is the same as in Cluzet et al. (2020). It uses stochastic perturbations on SAFRAN forcings (Durand et al., 1993; Charrois et al., 2016) as input to an ensemble of different ESCROC configurations (Lafaysse et al., 2017).

Study site and synthetic observations

The col du Lautaret (2058 m.a.s.l) is located in the Central French Alps (see Fig. 1 of Cluzet et al. (2020) for a precise locations), in the Grandes-Rousses massif. Observation dates for the year 2016-2017 correspond to clear-sky and good acquisition conditions as described in Cluzet et al. (2020). Three synthetic truths were taken from different members of a 120-member open-loop simulation. They correspond to different percentiles of yearly average Snow Water Equivalent (SWE, kg m^{-2}) in the open-loop, (85, 55 and 13 respectively, see Fig. 2.1), in order to investigate the behaviour of data assimilation facing contrasted snow conditions and biases compared with the true state.

Evaluation

The assimilation runs are evaluated by comparing their ability to reproduce the SWE of the synthetic truth. We use the CRPS score, (see Hersbach (2000) for a definition of the

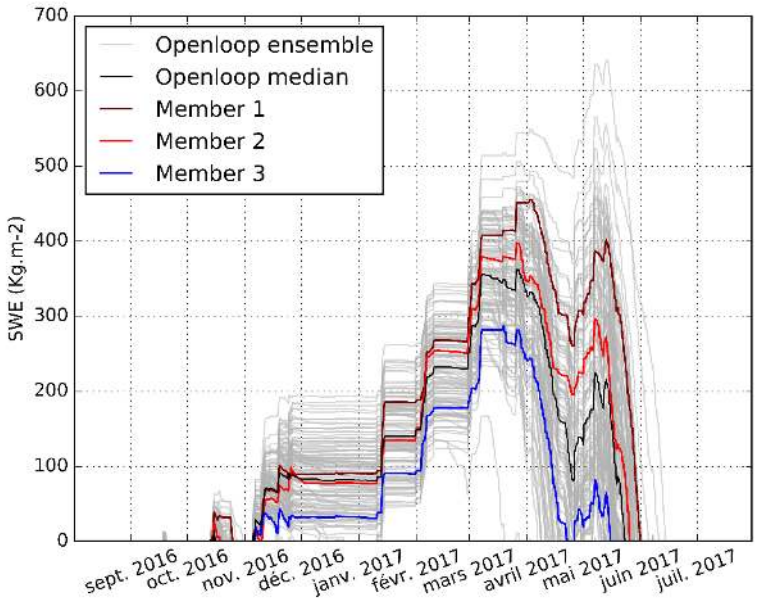

FIGURE 2.1: SWE of the open-loop simulation along the considered year at Col du Lautaret. The elected members are displayed in color, and the ensemble median in black.

CRPS score, or Cluzet et al. (2021) in Chapter 3 later on) wich is a metric accounting for the distribution of the ensemble respective to the verification data.

Data assimilation setup

The data assimilation strategy is identical to Charrois et al. (2016), i.e., we use a Particle Filter with Sequential Importance Resampling (PF)(Gordon et al., 1993; Arulampalam et al., 2002). Whenever an observation is available, the simulation is stopped, and the modelled reflectance (or band ratio) values are compared with the observations. Each ensemble member simulation (or "particle") is propagated in time by a single configuration formed by a perturbated forcing and an ESCROC model configuration. The particles are replicated or rejected proportionally to their gaussian distance to the observation (relative to the observation error), following Kitagawa (1996). The simulation restarts on the analysis date with the replicated particles, until next observation. Three setup questions emerge:

- what should be the value for band ratios observation error?
- how much should be the ensemble size?
- should we mix the particles at each assimilation, in order to break the forcing-model couples?

Setting the observation errors for band ratios

This choice of obseration errors controls the performance of the data assimilation. A too low observation error will likely reduce the ensemble spread until it causes PF degeneracy (Snyder et al., 2008), while the assimilation will not have any impact if they are too large. Charrois et al. (2016) used values from Wright et al. (2014) for the assimilation of reflectance. They lie in the range $10^{-3} - 10^{-4}$ and correspond to observation errors over the Greenland ice sheet. A wider range of observation errors was tested ($10^{-2} - 10^{-8}$), by assimilating band ratios individually. the values of 10^{-3} and 10^{-4} yielded the best results and their CRPS performance is shown on Fig. 2.2 for r54. Both values yield slightly lower (i.e. better performance) CRPS values than the open-loop. The value of 10^{-3} seems to yield lower and more stable value than 10^{-4}, whose performance is less stable, with analyses often degrading the performance (CRPS increasing). Similar results were obtained for r52. For this reason the value of 10^{-3} was selected for both band ratios in subsequent simulations.

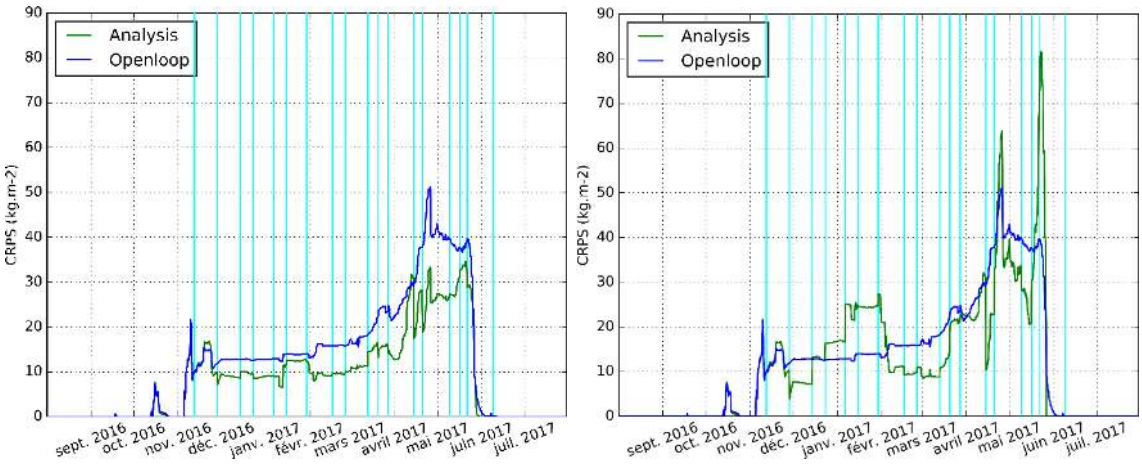

FIGURE 2.2: CRPS of the analysis (green) and the open-loop (blue) along the snow season for an observation error variance of 10^{-3} (left) and 10^{-4} (right) with a 120-member ensemble assimilating r54. Vertical cyan lines indicate the assimilation dates.

Choice of the ensemble size

The choice of the ensemble size is a compromise between the calculation cost (proportional to the ensemble members) and the risk of PF degeneracy, which decreases with the ensemble size (Bengtsson et al., 2008). (Charrois et al., 2016) used a 300-member ensemble in a similar setting, though with only one snow model. This setup likely favoured degeneracy. We performed assimilation runs with ensemble sizes of 120 and 320. The 320-ensemble run did not outperform the 120-member ensemble by much (not shown here). Therefore, the ensemble size was set to 120.

Mixing of the ensemble members configurations

The analysis only resamples the particle state vector, not the forcings and model used to subseqently propagate them in time. Therefore, the member in first position is always propagated by the same couple of forcing-model, while it could be beneficial to explore different combinations after every analysis, thus bringing more diversity in the ensemble. However, when evaluating on SWE, it seems that mixing the particles after every analysis is detrimental to the ensemble spread (not shown here). This under-dispersion did not seem desirable, and we deactivated ensemble mixing in the following.

2.3.3 Results and Discussion

Experiements assimilating the band ratios (either r52 and r54 individually or both assuming independent errors) of the three selected synthetic members were performed and compared with assimilation experiments assimilating several combinations of reflectances (assuming also independent errors). Results in terms of CRPS ratio ($CRPSS = CRPS_{assim}/CRPS_{open-loop}$) are depicted in Fig. 2.3. A value of 1 depicts a neutral performance, above 1 the assimilation degraded the performance compared with the open-loop, and below 1, the skill was improved. The performance depends a lot on the selected synthetic member, particularly for the reflectances. For member 1, strong improvements are obtained assimilating raw reflectances (CRPS ratio around 0.5, consistently with Charrois et al. (2016)), showing that raw reflectances have a strong potential to improve simulations. However, strong degradations (up to 1.9), probably due to PF degeneracy on specific dates, are observed for the other assimilation scenarios. This behavior was not seen by Charrois et al. (2016). Differences with their setup (i.e parameterised impurities forcings versus light-absorbing particle fluxes from chemistry-transport models and realistic LAP stratification (Tuzet et al., 2017), and deterministic version of Crocus ensemble of snow models from ESCROC) are likely to induce different optimal values for the observation error. It is probable that the reflectance observation errors were too low in these experiments causing PF degeneracy. Accommodation of observation error, when the PF sample population is too poor, might be an avenue to prevent that, as suggested by (Larue et al., 2018).

Meanwhile, the performance for the band ratios is more stable (degradation for only two out of 9 experiments) but are in the range 0.85-0.9, suggesting that their information content is much more reduced than for reflectances, at least for the first synthetic member. In particular, the joint assimilation of r52 and r54 does not significantly improve the simulations, while one would expect their information content to be complementary in terms of SSA

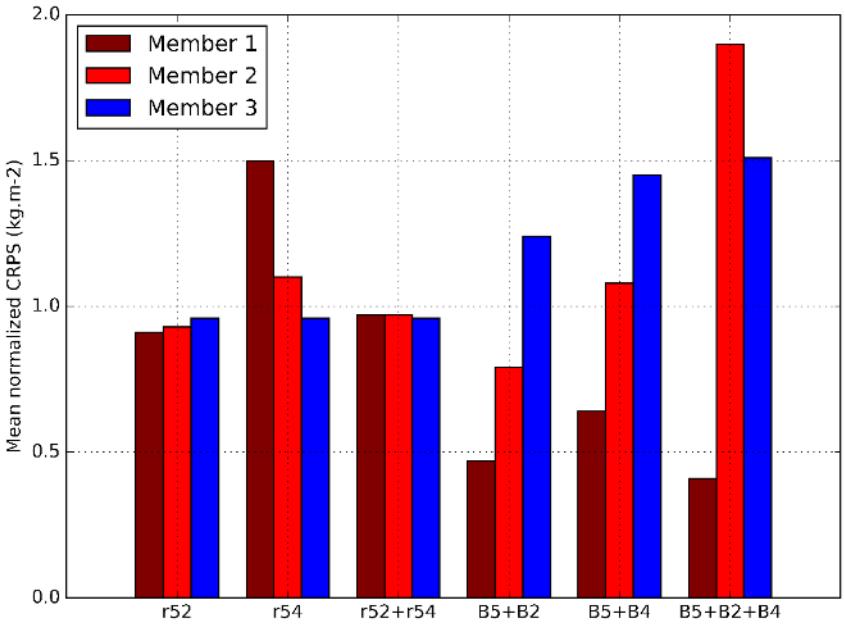

FIGURE 2.3: CRPS Skill of the different assimilation runs.

and LAP, with one variable being purely IR/NIR and the other IR/VIS. To investigate the relationship between those variables, the daily values of r54 and r52 simulated by the synthetic member 3 (i.e. the 13th percentile of open-loop SWE) are plotted in Fig. 2.4. The variables are almost perfectly aligned, a sign that they have a similar information content. A higher dispersion can only for the lowest ratio values (corresponding to coarse snow). This result is actually consistent with findings of Lyapustin et al. (2009).

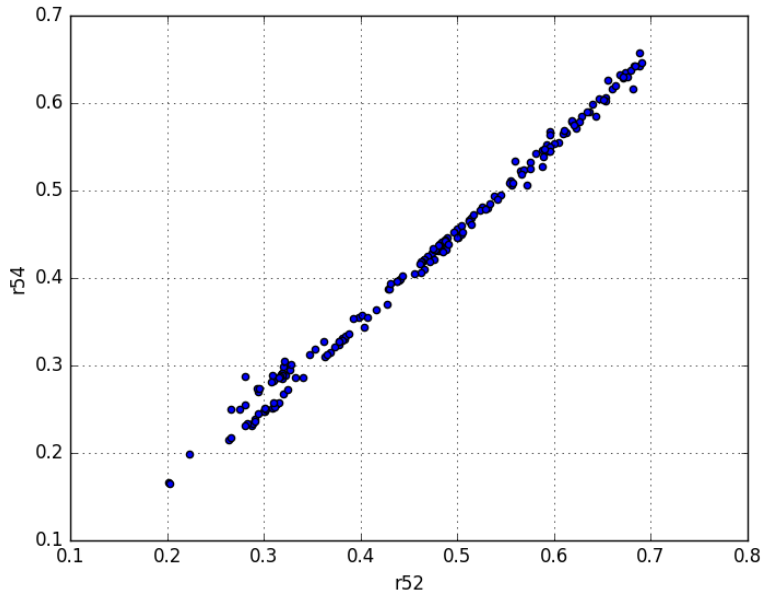

FIGURE 2.4: Daily values of r54 as a function of r52 for synthetic member 3.

2.3.4 Conclusion and outlook

This study was the first attempt to assimilate synthetic reflectances and ratios of reflectances in an ensemble accounting from meteorological and modelling uncertainties. This work provides insightful recommendations on the optimal setup of the ensemble and on the potential for assimilation of band ratios and reflectance. Regarding the ensemble setup, our results seem to indicate that an ensemble size of 120 members might be a good compromise, and that mixing the ensemble members after the analysis is not desired. Unstable performance of raw reflectance data assimilation for some synthetic members has been evidenced. This unstable behaviour, which was not evidenced by Charrois et al. (2016) might be due to mis-specified observation errors. Specific investigations will be conducted in Revuelto et al. (2021) to shed the light on this phenomenon and the potential link between the performance and the SWE percentile of the selected synthetic members.

Regarding the efficiency of data assimilation, band ratios do not seem to have such a high information content as reflectances as demonstrated in this idealised setting. Leveraging the information content from satellite reflectance products therefore stems from improvements of their retrieval in a rugged terrain (Lamare et al., 2020). Our results finally show that even in this idealised case, the performance is rather unstable likely due to PF degeneracy on specific dates. An adaptive observation error as proposed by Larue et al. (2018), might be required whenever reliable retrievals are available.

Chapter 3

Assimilation of synthetic observations in the semi-distributed geometry

Contents

3.1 Extended abstract

In the previous Chapter 2, we showed that satellite spectral reflectances provide precious information on the snowpack surface variability over large mountainous areas (Sec. 2). However reflectances suffer from a limitation which may last: they are not available under the clouds and the trees and in mixed terrain, and less accurate in the shadows, and steep slopes (e.g. Chap. 2, Sirguey, 2009; Lamare et al., 2020). Reducing modelling errors only in the observed locations would not be satisfactory. We need to assess whether non-observed areas can be succesfully constrained by distant observations of reflectance.

This issue is investigated in an idealised setting. We work in the same semi-distributed geometry as in Chap. 2 (see. Fig. 1 of the article), and assimilate synthetic observations (i.e. observations extracted from a prior model run and used as a true state for evaluation e.g. Durand and Margulis, 2006) of reflectance and height of snow (HS, (m)) over 4 years. Observations are masked in order to mimic the spatio-temporal coverage of actual reflectance observations: they are only available on clear-sky dates, above 1800 m, and in flat and 20^{o} South-West, South, South-East and East topographic classes (e.g. black dots on Fig. 5 of the article).

Our primary aim is to assess whether the representation of a bulk variable, the snow water equivalent (SWE (kg m^{-2})), can be improved by assimilating partial observations of reflectance. This is indeed a twofold question: whether reflectance information can be propagated in space and whether the assimilation algorithms successfully propagate information. To disentangle these questions, we assimilate HS, which is directly related to the SWE, contrary to reflectances. The assimilation of HS serves as a test for the assimilation algorithm, and then as a reference to evaluate the performance of reflectance assimilation.

The ensemble modelling setup is the same as in Sec. 2.2. An open-loop run is performed, and the members corresponding to the 20$^{\text{th}}$, 40$^{\text{th}}$, 60$^{\text{th}}$ and 80$^{\text{th}}$ percentiles of SWE are extracted for each year to serve as synthetic observations, thereby testing the assimilation against diverse accumulation conditions. Several ensemble sizes are also tested.

The choice of the particle filter (PF) assimilation algorithm has been justified in the introduction (see Sec. 1.4.3). It was included in the ensemble modelling framework (Fig. 2 of the paper). The most convenient way to propagate information is to do it implicitly, by looking for a global analysis over the domain, but in such a situation, the PF is likely to degenerate (see Sec. 1.4.3 and Sec. 2.3.1 of the paper). We developed two approaches to mitigate degeneracy. The first approach, called inflation, is either applied globally (so-called "global") or locally (considering only local observation, if any, so-called "rlocal") (see Sec. 2.3.1 of the paper). As we considered that the global approach might be suboptimal, and that distance localisation might be inappropriate for snow modelling at our modelling

scale (see Sec. 1.4.3 in the introduction), we implemented a localised strategy based on background correlation spatial patterns called k-localisation, or "klocal" (see Sec. 2.3.2 of the paper). This approach selects the observations coming from the locations exhibiting the strongest ensemble correlations with the considered location. The number of observations is iteratively decreased until degeneracy is mitigated.
We verified the ability of the inflation to prevent degeneracy by evaluating the behaviour of the global algorithm assimilating HS, in an unobserved class (Fig. 3). Results showed that without inflation, the global PF degenerated, while inflation managed to keep the ensemble close to the verification observation (lower spread, lower error than without inflation and than the open-loop run): information was successfully propagated, and degeneracy, mitigated.
The considered variables exhibit contrasted correlation patterns (Fig. 4), with "distant" locations sometimes more correlated than closer ones (e.g. in band 5 (infra-red)), suggesting that the klocal approach is more appropriate than a classical domain localisation.
Figs. 5 and 9 show that information from HS is successfully propagated by the klocal and the global approaches across aspects and slopes, contrary to the rlocal which is of course unable to correct the simulations in the unobserved areas. Propagation of information towards lower elevations is present, but more limited. Aggregated results over the assimilation experiments (all years and quantiles) in Fig. 6 show that the global and klocal approaches systematically improve the CRPS and Reli performance compared to the open-loop, both in the observed and unobserved classes.
Fig. 7 shows the same evaluation for the assimilation of reflectance. In general, information is succesfully transferred to the non-observed classes. The skill is lower than for HS but still positive on average. Increasing the ensemble size to 160 significantly improves the performance of the global and klocal. Results of spatial propagation for a given experiment (Fig. 8) shows that the spatial behaviour is the same than for HS (information is well transferred across aspects and slopes, and to a lower extent, across elevations).

To conclude, this paper proposes two different approaches to tackle PF degeneracy while propagating information into partially observed domains: inflation and k-localisation. Both algorithms successfully reach this twofold aim in an idealised setting, inside a domain which is only partly observed, showing their superiority over a purely local approach.
This study demonstrates that information from HS and reflectance can be propagated across topographic conditions, which had never been demonstrated for reflectances. This is really encouraging in the way of assimilating such information provided that their biases will one day be corrected (Lamare et al., 2020).
No significant skill difference could be found between the global and the klocal approach,

but this study proves that explicitly exploiting the correlation patterns from an ensemble is relevant from snowpack modelling. We suspect that the global approach might experience difficulties to obtain a satisfactory global analysis when dealing with real observations. Meanwhile, unrealistic ensemble background correlation patterns might be misleading for the klocal algorithm. Finally, as suggested by Fig. 9 and previous studies (e.g. Magnusson et al., 2014; Winstral et al., 2019), it seems that some point scale observations of HS could be used to reduce SWE modelling errors across a whole domain. Assimilation experiments with real observations are required to confirm this hypothesis, and will be conducted in the following Chapter 4.

3.2 CrocO_v1.0: a Particle Filter to assimilate snowpack observations in a spatialised framework

Citation:

Cluzet, B., Lafaysse, M., Cosme, E., Albergel, C., Meunier, L.-F., & Dumont, M. (2020). CrocO_v1.0: a Particle Filter to assimilate snowpack observations in a spatialised framework, *Geoscientific Model Development*, (in review)

Author contribution:

- Conception and implementation of the Particle Filter variants within SURFEX_v8.1
- Several technical developments within Crocus
- Embedding the data assimilation system and its pre/post-processing tasks in a High Performance Computing environment
- Analysis of results and redaction of the article

Geosci. Model Dev., 14, 1595–1614, 2021
https://doi.org/10.5194/gmd-14-1595-2021

Geoscientific Model Development
Open Access
EGU

CrocO_v1.0: a particle filter to assimilate snowpack observations in a spatialised framework

Bertrand Cluzet[1], Matthieu Lafaysse[1], Emmanuel Cosme[2], Clément Albergel[3,a], Louis-François Meunier[3], and Marie Dumont[1]

[1]Univ. Grenoble Alpes, Université de Toulouse, Météo-France, CNRS, CNRM, Centre d'Études de la Neige, Grenoble, France
[2]Institut des Géosciences de l'Environnement, IGE, UGA-CNRS, Grenoble, France
[3]CNRM, University of Toulouse, Météo-France, CNRS, 31057 Toulouse, France
[a]now at: European Space Agency Climate Office, ECSAT, Harwell Campus, Oxfordshire, Didcot OX11 0FD, UK

Correspondence: Bertrand Cluzet (bertrand.cluzet@meteo.fr) and Matthieu Lafaysse (matthieu.lafaysse@meteo.fr)

Received: 4 May 2020 – Discussion started: 10 July 2020
Revised: 16 November 2020 – Accepted: 4 December 2020 – Published: 19 March 2021

Abstract. Monitoring the evolution of snowpack properties in mountainous areas is crucial for avalanche hazard forecasting and water resources management. In situ and remotely sensed observations provide precious information on the state of the snowpack but usually offer limited spatio-temporal coverage of bulk or surface variables only. In particular, visible–near-infrared (Vis–NIR) reflectance observations can provide information about the snowpack surface properties but are limited by terrain shading and clouds. Snowpack modelling enables the estimation of any physical variable virtually anywhere, but it is affected by large errors and uncertainties. Data assimilation offers a way to combine both sources of information and to propagate information from observed areas to non-observed areas. Here, we present CrocO (Crocus-Observations), an ensemble data assimilation system able to ingest any snowpack observation (applied as a first step to the height of snow (HS) and Vis–NIR reflectances) in a spatialised geometry. CrocO uses an ensemble of snowpack simulations to represent modelling uncertainties and a particle filter (PF) to reduce them. The PF is prone to collapse when assimilating too many observations. Two variants of the PF were specifically implemented to ensure that observational information is propagated in space while tackling this issue. The global algorithm ingests all available observations with an iterative inflation of observation errors, while the *klocal* algorithm is a localised approach performing a selection of the observations to assimilate based on background correlation patterns. Feasibility testing experiments are carried out in an identical twin experiment setup, with synthetic observations of HS and Vis–NIR reflectances available in only one-sixth of the simulation domain. Results show that compared against runs without assimilation, analyses exhibit an average improvement of the snow water equivalent continuous rank probability score (CRPS) of 60 % when assimilating HS with a 40-member ensemble and an average 20 % CRPS improvement when assimilating reflectance with a 160-member ensemble. Significant improvements are also obtained outside the observation domain. These promising results open a possibility for the assimilation of real observations of reflectance or of any snowpack observations in a spatialised context.

1 Introduction

Seasonal snowpack is an essential element of mountainous areas. Monitoring the evolution of its physical properties is essential to forecasting avalanche hazard (Morin et al., 2020) and rain-on-snow-related floods (Pomeroy et al., 2016; Würzer et al., 2016) as well as monitoring water resources (Mankin et al., 2015). Observations alone are too scarce to monitor snowpack conditions. In situ observations provide precise observations of several key variables, but they lack spatial representativeness and have poor spatial coverage. Remote sensing of snowpack variables such as the height of snow (HS; m), snow water equivalent (SWE; $\mathrm{kg\,m^{-2}}$),

visible–near-infrared (Vis–NIR) reflectance and surface temperature provides comprehensive information over large areas but usually has a limited temporal resolution for a small set of variables. Furthermore, these observations are usually available in fractions of simulation domains only, even for spaceborne data (Davaze et al., 2018; Veyssière et al., 2019; Shaw et al., 2019). For instance, snowpack Vis–NIR reflectances from moderate-resolution (250–500 m) satellites such as MODIS and Sentinel-3 can help constrain snowpack surface properties such as microphysical properties (characterised by specific surface area – SSA; $m^2\,kg^{-1}$) and light-absorbing particle content (LAP; $g\,g_{snow}^{-1}$) (Durand and Margulis, 2006; Dozier et al., 2009). However, in areas covered by clouds or forests and/or affected by high sub-pixel variability (ridges, roughness, fractional snow cover) and shadows, satellite retrievals are less accurate (Masson et al., 2018; Lamare et al., 2020), and data should be filtered out (Cluzet et al., 2020a). The higher resolution offered by products from Landsat and Sentinel-2 might be an avenue to address this issue (e.g. Masson et al., 2018; Aalstad et al., 2020), but at these resolutions, reflectance retrievals are quite noisy due to e.g. digital elevation model errors (Cluzet et al., 2020a). Finally, note that pixel fractional snow cover (snow cover fraction, SCF) can be accurately retrieved even from noisy reflectances (Sirguey et al., 2009; Aalstad et al., 2020), but it inherits spatio-temporal limitations. SCF informativeness is also limited in deep snowpack conditions (De Lannoy et al., 2012).

Snowpack models of different complexity offer exhaustive spatial and temporal coverage (Krinner et al., 2018). They are applied within several spatial configurations, including the collection of points on regular or irregular grids (Morin et al., 2020). In this paper, "spatialised" indistinctly refers to any of these configurations. Detailed snowpack models are the only ones able to assess avalanche hazard and monitor water resources (Morin et al., 2020), but these applications are limited by their considerable errors and uncertainties (Essery et al., 2013; Lafaysse et al., 2017). In that context, combining remote sensing observations with models through data assimilation is an appealing solution (Largeron et al., 2020). Indeed, data assimilation combines the spatial and temporal coverage of snowpack models with the available information from observations in an optimal way. Assimilation of optical reflectance could reduce modelled SWE errors by up to a factor of 2 (Durand and Margulis, 2007; Charrois et al., 2016), and preliminary studies show its potential for spatialised assimilation (Cluzet et al., 2020a). Assimilation of HS is very efficient in reducing modelled SWE errors (Margulis et al., 2019). However, the limited spatial coverage of observations stresses the need for data assimilation algorithms able to propagate snowpack observational information into unobserved areas (Winstral et al., 2019; Cantet et al., 2019; Largeron et al., 2020).

A particle filter with sequential importance resampling (PF-SIR; Gordon et al., 1993; Van Leeuwen, 2009) is a Bayesian ensemble data assimilation technique well suited to snowpack modelling (Dechant and Moradkhani, 2011; Charrois et al., 2016; Magnusson et al., 2017; Piazzi et al., 2018; Larue et al., 2018). PF-SIR is a sequential algorithm relying on an ensemble of model runs (particles) which represents the forecast uncertainty. At each observation date, the prior (or background) composed of the particles is evaluated against the observations. The analysis of PF-SIR (later on PF) works in two steps. In a first step, so-called "importance sampling", the particles are weighted according to their distance to the observations (relative to the observation errors). Then, a resampling of the particles is performed in order to reduce the variance in the weights. The ensemble Kalman filter (EnKF Evensen, 2003) has also been widely used for snow cover data assimilation (e.g. Slater and Clark, 2006; De Lannoy et al., 2012; Magnusson et al., 2014). However, the PF is more adapted to models with a variable number of numerical layers such as detailed snowpack models (Charrois et al., 2016).

The PF could be used in a spatialised context to propagate information from observations as suggested by Largeron et al. (2020) and Winstral et al. (2019). Contrary to the EnKF, such applications are rare to date (e.g. Thirel et al., 2013; Baba et al., 2018; Cantet et al., 2019). Indeed, spatialised data assimilation with the PF is not straightforward because of the degeneracy issue, i.e. only a few particles are replicated in the analysis, often resulting in a poor representation of the forecast uncertainties. Degeneracy can be mitigated by increasing the number of particles, but the required population scales exponentially with the number of observations simultaneously assimilated (Snyder et al., 2008). Furthermore, an accurate representation of spatial error statistics by the ensemble is essential for the success of the assimilation system. To achieve that, the required ensemble size also scales exponentially with the system dimension, an issue known as the curse of dimensionality (Bengtsson et al., 2008). These issues are severe drawbacks when considering applications of the PF to large domains (i.e. implying a large number of observations and/or simulation points) with a reasonable number of particles (Stigter et al., 2017).

Several solutions exist to tackle PF degeneracy. A first approach is to inflate the observation errors in the PF. The tolerance of the PF is increased, leading to more particles being replicated. This approach is based on the fact that observation error statistics (including sensor, retrieval and representativeness errors) are usually poorly known and underestimated. It can also be used as a safeguard to prevent the PF from degenerating on specific dates when observations are not compatible with the ensemble. PF inflation was successfully implemented in point-scale simulations of the snowpack (Larue et al., 2018). When dealing with a large number of observations, inflation might lead to degeneracy or null analysis (posterior equal to the prior). In this work, we generalise over space the inflation of Larue et al. (2018), trying to ingest all

the observations into a single analysis over the domain in a so-called global approach.

PF localisation is a more widespread alternative, tackling degeneracy by reducing the number of observations that are simultaneously assimilated by the PF (Poterjoy, 2016; Poterjoy and Anderson, 2016; Penny and Miyoshi, 2016; Poterjoy et al., 2019; italic notations are taken from the review of Farchi and Bocquet, 2018). In this method, the simulation domain is divided into blocks whereby different PF analyses are performed considering a local subset of observations (domain) based on a localisation radius. This makes it possible to constrain the model in locations that are not directly observed but with nearby observations. Contrary to global approaches, localisation has the disadvantage of producing spatially discontinuous analyses (each point receives a different analysis). This issue can be mitigated in various ways (Poterjoy, 2016; Farchi and Bocquet, 2018; Van Leeuwen et al., 2019).

The underlying hypothesis of localisation is that model points are independent beyond a certain distance; i.e. constraining one point with the observation from a point that is too distant would be meaningless and likely degrade the analysis performance (Houtekamer and Mitchell, 1998). However, in the case of small simulation domains or modelled systems driven by large-scale coherent causalities, large-scale correlations (relative to the domain size) may be physically sound, and defining a localisation radius may be a difficult task. In order to address this issue, we developed a new localisation approach called *k* localisation, whereby localisation domains are based on background correlation patterns.

These developments were implemented into CrocO (Crocus-Observations), an ensemble data assimilation system able to sequentially assimilate snowpack observations with a PF in a spatialised context. CrocO can be implemented in any geometry (e.g. within a distributed (gridded) framework or any irregular spatial discretisation). Here, we apply CrocO in a semi-distributed framework, which is a conceptual spatialised geometry used operationally by Météo-France for avalanche hazard forecasting (Lafaysse et al., 2013; Morin et al., 2020). This framework is similar to many topographically based discretisations in hydrological models (e.g. Clark et al., 2015). This setup enables us to account for the snowpack variability induced by the topography at the scale of a mountain range through meteorological conditions (elevation controls the air temperature and precipitation phase) and the snowpack radiative budget (also dependent on the aspect and slope angle) (Durand et al., 1993).

CrocO uses an ensemble of stochastic perturbations from the SAFRAN meteorological analysis (Durand et al., 1993; Charrois et al., 2016) to force ESCROC (Ensemble System CROCus; Lafaysse et al., 2017), the multi-physical version of the Crocus snowpack model (Vionnet et al., 2012). The ensemble setup accounts for the major sources of uncertainties in snowpack modelling (Raleigh et al., 2015) and was formerly described and evaluated in semi-distributed geometry by Cluzet et al. (2020a).

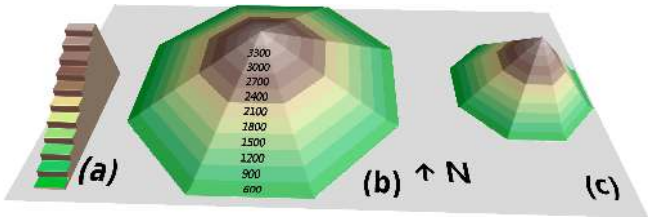

Figure 1. 3-D schematic view of the semi-distributed geometry, for which the numbers represent the altitudes of the elevation bands (m). From left to right, the three different mountains represent the flat, 20 and 40° slopes.

Inflation and *k* localisation were implemented into CrocO. Here, we present CrocO and evaluate how it addresses the issues of reflectance observation sparseness and PF degeneracy in the context of snowpack modelling. This problem is divided into two scientific questions. (1) Is CrocO PF able to efficiently spread the information from sparse observations in space without degenerating? (2) Is the spatial information content of reflectance observations valuable for snowpack models? We assess these questions by evaluating the performance of CrocO in modelling the SWE when assimilating synthetic observations of HS and reflectance covering only a portion of the domain.

Section 2 presents the CrocO system, i.e. the ensemble modelling system and the PF algorithms. Section 3 introduces the evaluation methodology. Subsequently, Sect. 4 assesses the performance of CrocO, and Sect. 5 discusses the results. Finally, Sect. 6 provides perspectives and research directions.

2 Material and methods

2.1 Modelling geometry

Simulations are performed in semi-distributed geometry. Mountain ranges such as the Alps are discretised into so-called massifs of about 1000 km^2 to account for regional variability of meteorological conditions. Within each massif, topographically induced variability is taken into account by running the model for a fixed set of topographic classes, e.g. by 300 m elevation bands, for 0, 20 and 40° slopes and eight aspects (see Fig. 1). This set enables us to reproduce the main features of snowpack variability (e.g. Mary et al., 2013).

In this study, we focus on the Grandes Rousses, a single massif in the central French Alps. This area of about 500 km^2 is represented by $N_{pts} = 187$ independent topographic classes (see Fig. 1). In the following, specific topographic classes are denoted as *elevation_aspect_slope*; e.g.

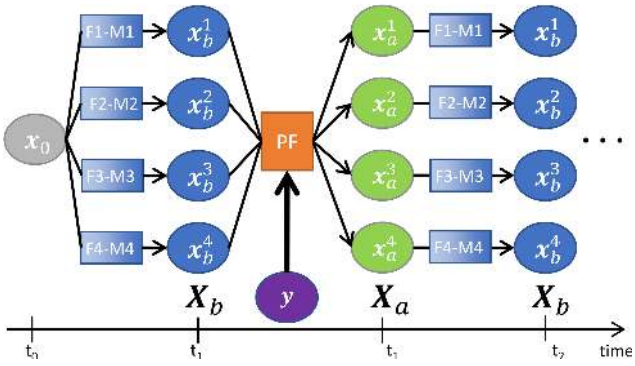

Figure 2. Workflow of CrocO ensemble data assimilation system with four members. $\widehat{x_0}$: initial state at time t_0, F_i: forcing, M_i: ESCROC member, X_b: background state, x_b^i: background particles, X_a: analysis, x_a^i: analysis particles, y: observation, t_1 and t_2: observation dates.

1800_N_40 stands for a 40° slope with a northern aspect at 1800 m a.s.l.

2.2 CrocO ensemble data assimilation setup

The ensemble data assimilation workflow of CrocO is represented in Fig. 2. In the following, only a short description of the system and its elements is provided. More details on the ensemble modelling setup are available in Cluzet et al. (2020a). Information about its implementation into the Météo-France high-performance computing (HPC) system can be found in Appendix B1.

2.2.1 Ensemble of snowpack models

Crocus is a detailed snowpack model coupled with the ground and atmosphere in the ISBA land surface model (Interaction Soil–Biosphere–Atmosphere). It is embedded within the SURFEX_v8.1 modelling platform (SURFace EXternalisée; Masson et al., 2013). The TARTES optical scheme (Libois et al., 2013, 2015) represents Vis–NIR spectral radiative transfer within the snowpack, driven by snow metamorphism (Carmagnola et al., 2014) and light-absorbing particle (LAP; $\mathrm{g\,g_{snow}^{-1}}$) deposition fluxes (Tuzet et al., 2017). Moreover, TARTES computes the snowpack reflectance with a high spectral resolution, making the model directly comparable to observations. As such, TARTES is both a physical component of Crocus and an observation operator.

ESCROC (Ensemble System CROCus; Lafaysse et al., 2017), the multi-physical ensemble version of Crocus, is used to account for snowpack modelling uncertainties. A random draw among 1944 ESCROC multi-physics configurations was performed and used in all the simulations and denoted $(M_i)_{0<i\leq N_\mathrm{e}}$, with N_e being the ensemble size (e.g. 40 or 160 members; see Fig. 2). These configurations are considered equiprobable before any data assimilation.

2.2.2 Ensemble of meteorological forcings

Meteorological forcings are taken from the SAFRAN (Durand et al., 1993) reanalysis, wherein forecasts from the ARPEGE numerical weather prediction (NWP) model are downscaled and adjusted with surface observations within the massif area. They are combined with MOCAGE LAP fluxes (Josse et al., 2004) interpolated at Col du Lautaret (2058 m a.s.l., inside the Grandes Rousses) to constitute the reference forcing dataset. Before the beginning of the simulation, spatially homogeneous stochastic perturbations (e.g. on a given date, the same perturbation parameter is applied across the whole domain) with temporal autocorrelations are applied to this forcing to generate an ensemble of forcings $(F_i)_{0<i\leq N_\mathrm{e}}$ with the same procedure as described in Cluzet et al. (2020a). More details on the perturbation procedure can be found in Appendix A. At the beginning of the simulation, each forcing F_i is associated with a random M_i ESCROC configuration, and this relation is fixed during the whole simulation.

2.2.3 The particle filter in CrocO

The PF is applied sequentially for each observation date to the background state vectors (soil and snowpack state variables, denoted BG in Fig. 2). Its analysis is an ensemble of initial conditions used to propagate the model forward. The algorithm is implemented into SODA (SURFEX Offline Data Assimilation; Albergel et al., 2017), the data assimilation module of SURFEX_v8.1, enabling a continuous execution sequence between ensemble propagation and analysis, as depicted in Fig. 2.

2.3 The particle filter equations

On a given observation date, we consider a set of observed variables available at several locations, totalling N_y different observations.

- Each member $\boldsymbol{x}_\mathrm{b}^i$ of the background state $\boldsymbol{X}_\mathrm{b}$ is projected into the observation space using the observation operator h. In our case, h is just an orthogonal projection of the N_y observations since HS and reflectance are diagnosed within Crocus (see Sect. 2.2.1). The projection $\hat{\boldsymbol{x}}_\mathrm{b}^i = h\boldsymbol{x}_\mathrm{b}^i = (\hat{\boldsymbol{x}}_k^i)_{0<k\leq N_y}$ corresponds to the modelled values at each observed variable and/or point.

- These N_y observations are collected in the vector $\boldsymbol{y} = (y_k)_{0<k\leq N_y}$. The associated observation error covariance matrix $\mathbf{R}$ (Eq. 1) is diagonal (e.g. observation errors are assumed independent):

$$\mathbf{R} = \mathrm{diag}(\sigma_k^2, 0 < k \leq N_y), \tag{1}$$

  where σ_k^2 stands for the observation error variance of observation k and depends only on the type of observation y_k (e.g. HS or reflectance).

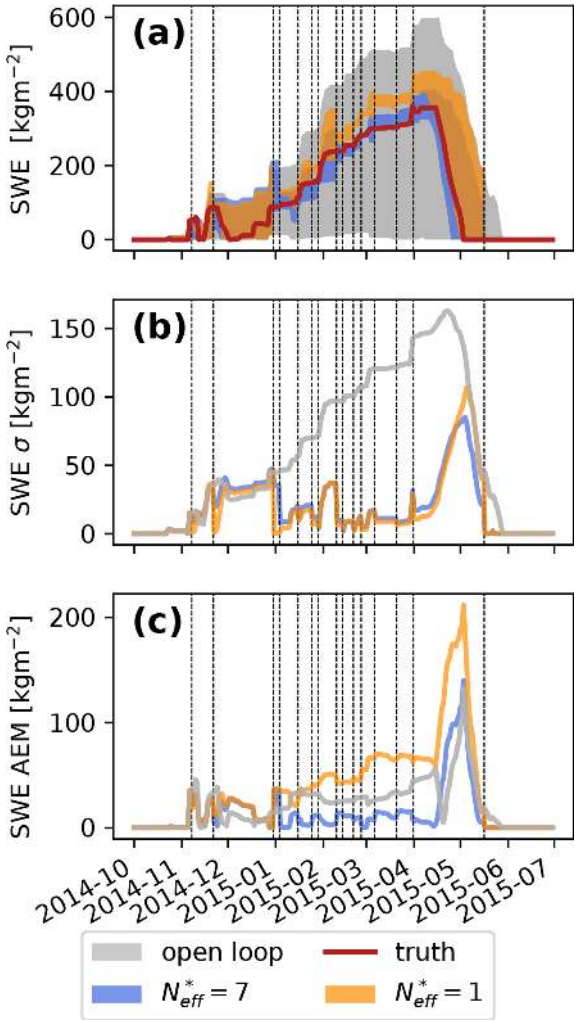

Figure 3. Impact of the inflation ($N^*_{\text{eff}} = 7$) vs. no inflation ($N^*_{\text{eff}} = 1$) in the 1800_N_40 topographic class (not observed) when assimilating HS of 2015_q80 with the global PF. **(a)** SWE minimum–maximum envelopes as a function of time, **(b)** spread and **(c)** AEM. Dashed lines represent the assimilation dates.

The PF analysis usually works in two steps.

1. Compute the particle weights w^i as the normalised observation likelihood for each particle (Eq. 2):

$$w^i = \frac{e^{-\frac{1}{2}(\boldsymbol{y}-\hat{\boldsymbol{x}}^i_{\text{b}})^T \mathbf{R}^{-1} (\boldsymbol{y}-\hat{\boldsymbol{x}}^i_{\text{b}})}}{\sum_{k=1}^{N_{\text{e}}} e^{-\frac{1}{2}(\boldsymbol{y}-\hat{\boldsymbol{x}}^k_{\text{b}})^T \mathbf{R}^{-1} (\boldsymbol{y}-\hat{\boldsymbol{x}}^k_{\text{b}})}}. \tag{2}$$

2. Resample the particles based on their weights to build the analysis vector $\boldsymbol{X}_{\text{a}}$. Here, we apply the PF resampling from Kitagawa (1996), which returns $\boldsymbol{s} = (s_i)_{0<i\leq N_{\text{e}}}$ ($s_i \in [1..N_{\text{e}}]$), a sorted vector with duplications representing the particles to replicate.

A sample reordering step was added for numerical optimisation with no expected influence on the PF behaviour (see Appendix B2 for more details).

Two simple variants of this algorithm can be identified in a spatialised context:

- for the global approach, perform one analysis over the domain, putting all the available observations in $\boldsymbol{y}$;
- for the *rlocal* approach, perform one analysis per model point, assimilating only local observations if any. This corresponds to a localised PF with a block and domain size of 1.

2.3.1 Particle filter degeneracy

Degeneracy occurs when only a small fraction of the particles have non-negligible weights, resulting in a sample $\boldsymbol{s}$ for which only a few different indices are present. It can be diagnosed from the weights using the effective sample size N_{eff} (Liu and Chen, 1995):

$$N_{\text{eff}} = \frac{1}{\sum_{i=1}^{N_{\text{e}}} (w^i)^2}. \tag{3}$$

With a degenerate sample, $N_{\text{eff}} \gtrsim 1$, and with innocuous analysis (all particles are replicated) $N_{\text{eff}} = N_{\text{e}}$.

A first approach to mitigate degeneracy is to use inflation. This heuristic method iteratively inflates $\mathbf{R}$ values until the effective sample size is large enough. Here, we develop a variant from the Larue et al. (2018) method, which does not explicitly rely on N_{eff} (Eq. 3). Consider applying an inflation factor $\frac{1}{\alpha}$ to $\mathbf{R}$ ($0 < \alpha \leq 1$, with $\alpha = 1$ being the value for no inflation) and update N_{eff} (Eqs. 2 and 3): N_{eff} is naturally a decreasing function of α (the more we inflate $\mathbf{R}$ the more different particles will be replicated). The idea of our method is to ensure that N_{eff} exceeds a target value, N^*_{eff}. If $N_{\text{eff}} < N^*_{\text{eff}}$ (degenerate case), we reduce α (inflate) until $N_{\text{eff}} = N^*_{\text{eff}}$ using Algorithm 1. In the following, inflation is used in the global and *rlocal* PF (see Sect. 2.2.3).

The core of Algorithm 1 is an hybrid bisection–secant method to find the zero of $f : \alpha \longmapsto N_{\text{eff}}(\alpha) - N^*_{\text{eff}}$ in $[0, 1]$. It is inspired by the **rtsafe** algorithm (Press et al., 1992). The **guess** function computes a new guess α_2 to minimise f. Note that in the unlikely case in which Algorithm 1 does not converge, all the particles are replicated.

Algorithm 1 Weighting algorithm with inflation.

Input: $\hat{\boldsymbol{x}}^i, \boldsymbol{y}, \mathbf{R}, N^*_{\text{eff}}$; **Output:** w^i

$\alpha \leftarrow 1$
$\mathbf{R} \leftarrow \frac{1}{\alpha}\mathbf{R}$
$w^i \leftarrow$ **weights**$(\hat{\boldsymbol{x}}^i, \boldsymbol{y}, \mathbf{R})$ (Eq. 2)
$N_{\text{eff}} \leftarrow$ **eff_weights**(w^i) (Eq. 3)
if $N_{\text{eff}} < N^*_{\text{eff}}$ **then**
  $\alpha_1 \leftarrow 0$
  $N_{\text{eff}_1} \leftarrow N_{\text{e}}$
  $cond \leftarrow$ **True**
  $i \leftarrow 0$
  while $cond$ **do**
    $\alpha_2 \leftarrow$ **guess**$(\alpha_1, \alpha, N_{\text{eff}_1}, N_{\text{eff}}, N^*_{\text{eff}})$
    $\mathbf{R} \leftarrow \frac{1}{\alpha_2}\mathbf{R}$
    $w^i_2 \leftarrow$ **weights**$(\hat{\boldsymbol{x}}^i, \boldsymbol{y}, \mathbf{R})$ (Eq. 2)
    $N_{\text{eff}_2} \leftarrow$ **eff_weights**(w^i_2) (Eq. 3)
    if $|N_{\text{eff}_2} - N^*_{\text{eff}}| < \epsilon$ **then**
      $cond \leftarrow$ **False**
      $\alpha \leftarrow \alpha_2$
      $w^i \leftarrow w^i_2$
    else
      $\alpha \leftarrow \alpha_1$
      $\alpha_1 \leftarrow \alpha_2$
      $N_{\text{eff}} \leftarrow N_{\text{eff}_1}$
      $N_{\text{eff}_1} \leftarrow N_{\text{eff}_2}$
    end if
    $i \leftarrow i + 1$
    if $i = maxiter$ **then**
      print "failed to converge, duplicating all particles"
      $w^i \leftarrow \frac{1}{N_{\text{e}}}$
    end if
  end while
end if

2.3.2 *k* localisation

In the *k*-localisation algorithm, degeneracy is mitigated by reducing the number of observations that are simultaneously assimilated. The PF analysis is applied to each simulation point sequentially. In order to build the analysis at point n, background correlations $\mathbf{B}_v$ are computed for each variable v (e.g. HS or reflectance) between n and all the observed points. In a first step, all observations from points exhibiting substantial background correlations (see below for the **select_k_biggest** function) are used. If the PF degenerates, the number of observations is progressively decreased until degeneracy is mitigated. As earlier, degeneracy is considered mitigated when $N_{\text{eff}} \geq N^*_{\text{eff}}$. This way, we ensure that a maximal number of observations has been ingested by the PF without degenerating.

In the case of degeneracy, the observation point displaying the lowest correlation is ruled out. The PF weights are computed (Eq. 2), and a new effective sample size is derived (Eq. 3). While the target sample size is not exceeded, this selection proceeds iteratively. The notation k in k localisation refers to the number, k, of retained observations for each variable. This approach is similar to the EnKF localisation algorithm whereby the localisation domain is based on background correlations (Hamill et al., 2001).

The detailed *k*-localisation algorithm is described in Algorithm 2, for which the following points apply.

- For each variable, the **select_k_biggest** method returns the domain $\boldsymbol{d}_v$ of up to k observed points (named p) that are the most correlated (in absolute value) with n and match the following criteria, which were adjusted in preliminary experiments.
  - In $\boldsymbol{x}^i_v$, at least 10 % of members are defined in both points. As reflectance is not defined when there is no snow, spuriously high correlation can be obtained when the computation of correlations is based on a very low number of pairs.
  - $|\mathbf{B}_v(n, p)| > 0.3$. If the absolute correlation is too low, it is likely that there is poor potential for the distant observation to constrain the ensemble locally. In such a situation, it is better to reject the observation from the local analysis. Negative ensemble correlations can be physically sound, e.g. after a rain-on-snow event between the HS of two points separated by the rain–snow line. In such a situation, an HS observation of either point can hold information on precipitation rates at both locations. At the observed location, the PF will probably select the members with the most appropriate precipitation rates. This sample is likely to perform well at both locations, so it can be used to constrain the unobserved location.
- The notation $\boldsymbol{d}$ represents the collection of domains $\boldsymbol{d}_v$.
- The **extract_points** function extracts $\boldsymbol{d}$ from $\boldsymbol{y}, \hat{\boldsymbol{x}}^i$ and $\mathbf{R}$.

Algorithm 2 k-localisation algorithm

Input: $\hat{\boldsymbol{x}}^i, \boldsymbol{y}, \mathbf{B}, \mathbf{R}, N^*_{\text{eff}}$; **Output:** $(w^i_n)_{0<n\leq N_{\text{pts}}}$

for $n = 1$ to N_{pts} **do**
  $k \leftarrow k_{\max}$ {try to ingest all available observations.}
  $cond \leftarrow$ **True**
  while $cond$ **and** $k > 0$ **do**
    for $v = 1$ to N_v **do**
      $\boldsymbol{d}_v \leftarrow$ **select_k_biggest**$(n, k, \mathbf{B}_v, \hat{\boldsymbol{x}}^i_v, \boldsymbol{y})$
    end for
    $\boldsymbol{y}_k, \hat{\boldsymbol{x}}^i_k, \mathbf{R}_k \leftarrow$ **extract_points**$(\boldsymbol{y}, \hat{\boldsymbol{x}}^i, \mathbf{R}, \boldsymbol{d})$
    $w^i_n \leftarrow$ **weights**$(\hat{\boldsymbol{x}}^i_k, \boldsymbol{y}_k, \mathbf{R}_k)$ (Eq. 2)
    $N_{\text{eff}} \leftarrow$ **eff_weights**(w^i_n) (Eq. 3)
    if $N_{\text{eff}} \geq N^*_{\text{eff}}$ **then**
      $cond \leftarrow$ **False**
    end if
    $k \leftarrow k - 1$
  end while
  if $k = 1$ **then**
    $w^i_n \leftarrow$ **inflation**$(\hat{\boldsymbol{x}}^i_k, \boldsymbol{y}_k, \mathbf{R}_k, N^*_{\text{eff}})$
  end if
end for

Table 1. Setup for the height of snow assimilation experiment.

PF algorithm	N_e	inflation	N^*_{eff}	HS σ_o^2 (m^2)
rlocal	40	on	7	1.0×10^{-2}
global	40	on	7	1.0×10^{-2}
klocal	40	on (if $k = 1$)	7	5.0×10^{-2}

2.3.3 Particle filter and reflectance observations

Assimilating reflectance with the PF requires some adaptations. In Crocus, the TARTES optical scheme (see Sect. 2.2.1) only provides snow reflectance, not all-surface reflectance: no value for the surface reflectance is issued in the absence of snow. Conversely, the weights of the particles are not defined in Eq. (2) if the members are snow-free. These issues were roughly accommodated by setting the reflectances of snow-free members and observations to 0.2 (the value of bare soil broadband albedo in the ISBA model) in the PF for Eq. (2) (Sect. 2.2.3).

3 Evaluation strategy

Our strategy is to assess the performance of the analysis by means of twin experiments, i.e. using synthetic observations (e.g. Reichle and Koster, 2003). The assimilation run is compared to an identical run without assimilation (open-loop run). Synthetic observations are extracted from a model run and assimilated without adding any noise. These observations mimic real observations with perfect knowledge of the true state. Analysis and open-loop experiments can therefore be compared with this true state anywhere for any variable. In a first step, this allows us to get rid of the error and bias issues inherent in real observations (Cluzet et al., 2020a), a reason why we did not add any noise to the synthetic observations as commonly done in twin experiments (Lahoz and Menard, 2010). This way, we can focus on the following two questions (see Sect. 1).

- Is CrocO PF able to efficiently spread the information from sparse observations into space without degenerating?
- Is the spatial information content of reflectance a valuable source of information for snowpack models?

In order to disentangle these questions, we run baseline experiments assimilating synthetic observations of HS, which is strongly linked to SWE (Margulis et al., 2019). These experiments are used to evaluate the PF algorithm efficiency and as a baseline for synthetic reflectance assimilation experiments evaluating the information content of reflectance.

Three different algorithms are evaluated: the global algorithm (with inflation), the *rlocal* algorithm (with inflation) and the k-localised algorithm *klocal*.

3.1 Experiments

3.1.1 Twin experiment setup

In our twin experiment setup, an open-loop ensemble is used as a reference and to generate synthetic observations. Open-loop simulations are carried out with CrocO for four consecutive winters (2013–2017) in the Grandes Rousses (see Sect. 2.1) with 160 members. For each year, the average of SWE over time and space is computed from each member, and members corresponding to the 20th, 40th, 60th and 80th percentiles of the ensemble are extracted to be used as synthetic observations (denoted *year*_p*percentile*, e.g. 2014_p80). This method enables us to evaluate the efficiency of data assimilation experiments under contrasting snow condition scenarios. Before any assimilation experiment, the open-loop member ($F_i - M_i$ couple in Fig. 2) used as the true state is withdrawn and replaced by a new random member.

The spatial coverage of synthetic observations was reduced, mimicking a typical reflectance mask. Synthetic observations were only available above an assumed constant treeline at 1800 m (see Fig. 1) and not available for steep slopes (over 20°) and northern aspects (shadows, considering a daily satellite pass around 10:00–11:00 UTC) for the whole snow season. As a result, in this case, only 35 (over 187) topographic classes are observed. Observation dates were chosen corresponding to clear-sky days with a MODIS overpass, resulting in an approximately weekly frequency (e.g. Revuelto et al., 2018; Cluzet et al., 2020a).

Reflectance is sensitive to the surface SSA and LAP (see Sect. 1). A minimal set of two different bands is used, corresponding to MODIS sensor bands 4 (555 nm, sensitive to SSA and LAP) and 5 (1240 nm, usually only sensitive to SSA) (e.g. Fig. 2 of Cluzet et al., 2020a). Observation error variances are set to 1.0×10^{-2} m^2 for HS and 5.6×10^{-4} and 2.0×10^{-3} for band 4 and band 5 reflectance, respectively (Wright et al., 2014). These values are only initial values for the inflation in the global and *rlocal* algorithms. Since the *klocal* algorithm only uses inflation if k drops to 1 (see Sect. 2.3.2), observation error variances are multiplied by a factor of 5 to enable the *klocal* algorithm to ingest observations from several points.

In order to study the ability of the global, *klocal* and *rlocal* algorithms to spread information in space, a first set of experiments is conducted assimilating HS with 40 members (see the setup in Table 1). In order to evaluate the algorithms' ability to assimilate reflectance (band 4 and band 5) a second set of experiments is conducted with other things being equal (Table 2). The ensemble size is increased from 40 to 160 in a third set of experiments assimilating reflectance in order to analyse the influence of a larger ensemble on the algorithm performance (Table 3). Note in Tables 1–3 that N^*_{eff} is adjusted to the ensemble size in order to preserve $N_e/N^*_{eff} \approx 5$–7 following Larue et al. (2018).

Table 2. Setup for the first reflectance assimilation experiment.

PF algorithm	N_e	Inflation	N^*_{eff}	B4 σ_o^2	B5 σ_o^2
rlocal	40	on	7	5.6×10^{-4}	2.0×10^{-3}
global	40	on	7	5.6×10^{-4}	2.0×10^{-3}
klocal	40	on (if $k = 1$)	7	2.8×10^{-3}	1.0×10^{-2}

Table 3. Setup for the second reflectance assimilation experiment.

PF algorithm	N_e	Inflation	N^*_{eff}	B4 σ_o^2	B5 σ_o^2
rlocal	160	on	25	5.6×10^{-4}	2.0×10^{-3}
global	160	on	25	5.6×10^{-4}	2.0×10^{-3}
klocal	160	on (if $k = 1$)	25	2.8×10^{-3}	1.0×10^{-2}

3.2 Evaluation scores

The performance of the assimilation and open-loop run is evaluated against the synthetic truth using several scores. The absolute error of the ensemble mean (AEM) and ensemble spread σ are two common metrics of ensemble modelling. Given an ensemble $E_{m,c,t}$ of N_e members m in topographic class c at time t and the corresponding truth $\tau_{c,t}$, the ensemble mean is described by Eq. (4):

$$\overline{E}_{c,t} = \frac{1}{N_e} \sum_{m=1}^{N_e} E_{m,c,t}, \tag{4}$$

from which we can compute the AEM (Eq. 5) and the spread (or dispersion) σ (Eq. 6):

$$\mathrm{AEM}_{c,t} = |\overline{E}_{c,t} - \tau_{c,t}| \quad \forall (c,t) \in [1, N_{\mathrm{pts}}] \times [1, N_t] \tag{5}$$

$$\sigma_{c,t} = \sqrt{\frac{1}{N_e} \sum_{m=1}^{N_e} (E_{m,c,t} - \overline{E}_{c,t})^2}, \quad \forall (c,t) \in [1, N_{\mathrm{pts}}] \times [1, N_t], \tag{6}$$

where N_t is the number of evaluation time steps.

The continuous ranked probability score (CRPS; Eq. 7; Matheson and Winkler, 1976) evaluates the reliability and resolution of an ensemble based on a verification dataset. An ensemble is reliable when events are forecast with the right probability and has a good resolution when it is able to discriminate distinct observed events. For a reliable system, the resolution is equivalent to the sharpness, which is the spread of the produced forecasts.

If we denote $F_{c,t}$ the cumulative distribution function (CDF) and $\mathcal{T}_{c,t}$ the corresponding truth CDF (Heaviside function centred on the truth value), the CRPS is computed at (c,t) following

$$\mathrm{CRPS}_{c,t} = \int_{\mathbb{R}} (F_{c,t}(x) - \mathcal{T}_{c,t}(x))^2 \mathrm{d}x \quad \forall (c,t) \in [1, N_{\mathrm{pts}}] \times [1, N_t]. \tag{7}$$

In this work, the $\mathrm{CRPS}_{c,t}$ value is averaged over time alone or time and space depending on the desired level of aggregation.

The CRPS can be decomposed into two terms following Candille et al. (2015):

$$\mathrm{CRPS} = \mathrm{Reli} + \mathrm{Resol}, \tag{8}$$

where Reli quantifies the reliability of the ensemble. The associated skill scores (CRPSS and ReliS) can be used to compare the performance of an ensemble E to a reference R, here the open-loop run:

$$\mathrm{CRPSS}(E) = 1 - \frac{\mathrm{CRPS}(E)}{\mathrm{CRPS}(R)}. \tag{9}$$

A skill score of 1 denotes a perfect score, 0 a neutral performance and $-\infty$ the worst achievable skill score.

4 Results

4.1 Preliminary results

4.1.1 Impact of the inflation

The inflation algorithm was introduced by Larue et al. (2018) in point-scale simulations, but to the best of our knowledge, it has never been applied in a spatialised context. Here we evaluate its impact on the global algorithm by switching it on and off. As an example, Fig. 3 shows the impact of inflation on SWE when assimilating the HS of 2015_p80 (as defined in Sect. 3.1.1) member with the global algorithm in a topographic class which is not observed (1800_N_40, as defined in Sect. 2.1). This choice of member and topographic class is representative of the impact of inflation on the global algorithm.

In this case, both inflation ($N^*_{eff} = 7$) and no inflation ($N^*_{eff} = 1$) lead to a significant reduction of the ensemble spread compared with the open loop (Fig. 3b). From January

2015 until the peak of SWE in mid-April 2015 (Fig. 3c), the simulation with inflation has significantly lower errors than without inflation and the open loop (10–20 vs. 60–80 and 30–50 $\mathrm{kg\,m^{-2}}$, respectively), leading to better agreement with the synthetic truth in the melting season (Fig. 3a). During the melting season (mid-April 2015 onwards), the AEM of the assimilation algorithms reaches a peak, coinciding with an absence of observations. In comparison, the open-loop AEM is smaller in the first part of the melting season, but the spread is 3 times larger, making it almost uninformative. For several analyses (21 November 2014 and 30 December 2014, for example) the ensemble spread without inflation drops to 0, while its AEM strongly increases compared to the open loop, suggesting that it is prone to degeneracy.

4.1.2 Correlation patterns

The *klocal* algorithm relies on background correlation patterns to define localisation domains. To illustrate the potential of using such information in the PF, Fig. 4 shows the correlation patterns of the 40-member open loop in an unobserved topographic class (1800_N_40, red dot) in the mid-winter (20 February 2015), several months after the snow season onset. The assimilation variables exhibit strong but contrasting correlation patterns. Band 4 (Fig. 4a) correlations are generally high (0.6–1) and uniform. Many of the observed classes (black dots) are strongly correlated with the considered class. Similar results are obtained for HS (Fig. 4c). Band 5 (Fig. 4b) exhibits substantial correlations, in particular across slopes. However, they are more restricted to the northern aspects, and only a few observed classes in the eastern aspects are substantially correlated with the considered class. Note that negative correlations are evidenced with some lower-altitude south-oriented topographic classes (e.g. 1500_S_40 in Fig. 4b). Finally, these patterns vary with time but remain substantial along the whole season (not shown), and increasing the ensemble size up to 160 leads to identical patterns (not shown).

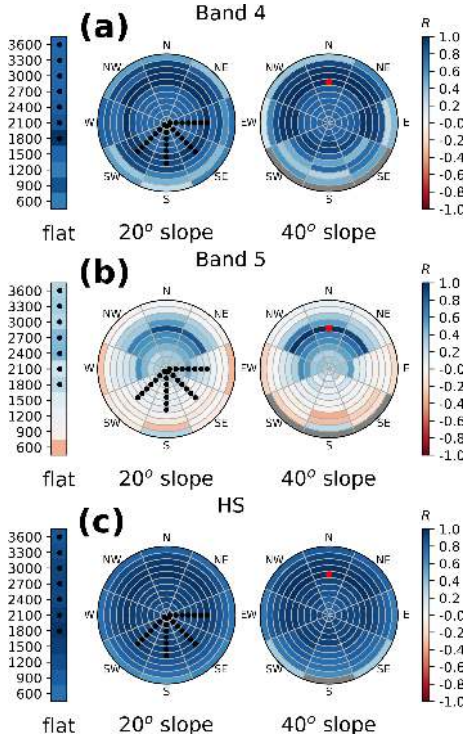

Figure 4. 20 February 2015 open-loop (40 members) Pearson correlations between the domain points and the 1800_N_40 topographic class (red dot) in band 4 **(a)**, band 5 **(b)** and HS **(c)**. Left bars show the flat topographic classes in the associated elevation bands, while pie plots show the 20 and 40° slope topographic classes, as depicted in Fig. 1. Black dots denote the observed classes.

4.2 Results of the experiments

4.2.1 Assimilation of the height of snow

In a first step, assimilation of HS from the different synthetic observation scenarios was conducted to serve as a reference for reflectance assimilation. Figure 5 shows the CRPSS (Eq. 9, aggregated over time only) of the HS assimilation with the three PF algorithms considering the synthetic member 2013_q20 as a reference. Results for this specific synthetic member were chosen here as a representative example of the algorithm performance.

The *rlocal* performance compared with the open loop is high (0.7–1) but limited to the observed classes (black dots) since there is no spatial propagation in this algorithm. The global and *klocal* algorithms have similar overall good performance, managing to strongly reduce modelling uncertainties except at very low altitudes (600–900 m) (skills of −0.2) where snow does not usually last for more than a few weeks.

This behaviour may vary with the snow conditions, i.e. between the different assimilated synthetic observation scenarios and from one year to another. In order to generalise this result, Fig. 6 shows the CRPS and Reli (aggregated over time and space) of the different algorithms for the 16 synthetic observation scenarios and differentiated between observed and unobserved classes. CRPS and reliability are considerably reduced compared with the open loop (by a factor of 2–3 and 4–5, respectively) for all the algorithms in the observed classes. This suggests that the PF manages to reduce the spread of the ensemble while reducing its errors. In the unobserved classes, the gain is almost as good (CRPSS of 0.6) except for the *rlocal* algorithm, which is identical to the open loop as expected. No significant difference in skill is obtained between the global and *klocal* algorithms.

4.2.2 Assimilation of reflectance

Optical reflectance is a promising assimilation variable due to its extended availability in satellite observations, but assimilation of raw reflectance products is not expected to con-

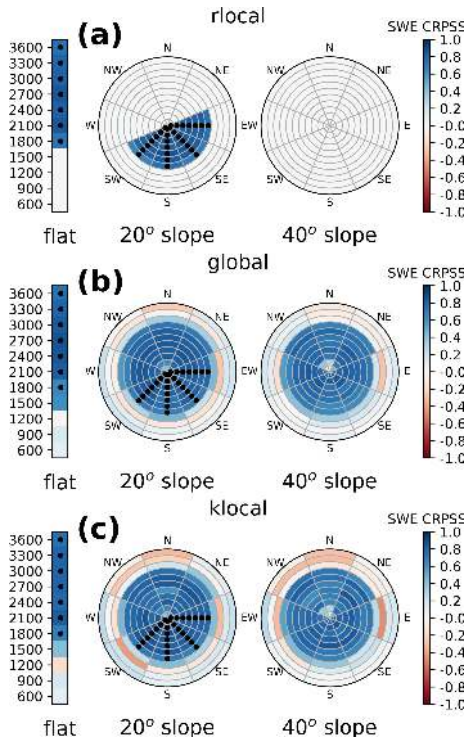

Figure 5. CRPSS of SWE for the *rlocal* **(a)**, global **(b)** and *klocal* **(c)** algorithms assimilating the HS of 2013_p20 synthetic observation scenario. The score is computed for the whole snow season for each topographic class. Black dots denote the observed classes.

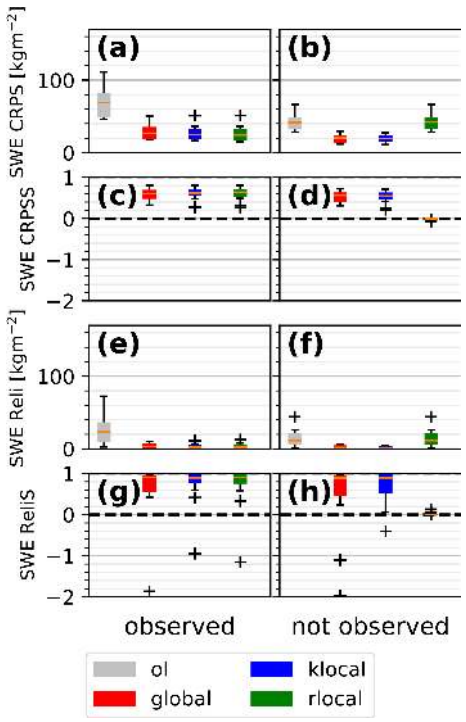

Figure 6. Box plots of SWE CRPS **(a, b)** and Reli **(e, f)** for the different algorithms for the 16 different synthetic observation scenarios, separated between observed **(a, c, e, g)** and not observed **(b, d, f, h)** classes. Panels **(c, d)** and **(g, h)** show the associated skill scores.

strain bulk variables like SWE or HS as much as HS assimilation. In order to assess this difference, we conduct assimilation of reflectance only in the same setup as in Sect. 4.2.1 with all other things being equal.

Figure 7 shows the performance of the reflectance assimilation for the 16 synthetic observation scenarios with 40 members (filled boxes). The different algorithms only lead to moderate improvements in CRPS (median CRPSS of 0–0.2, median ReliS of 0.2–0.4). Moreover, the global and *klocal* algorithms frequently degrade the performance, suggesting that this configuration is not robust.

Suspecting that 40 members are insufficient to properly represent the multivariate probability density function of reflectance and other model variables, the ensemble size was increased to 160 (hatched boxes), leading to marked improvements in the performance and robustness of the algorithms (median CRPSS of 0.2, median Reli of 0.4–0.6). The reliability of the global algorithm is significantly improved compared to the *klocal* algorithm.

Figure 8 shows the spatial performance of the different algorithms for member 2016_p60. Spatial patterns similar to the HS assimilation are found. The *rlocal* performance is limited to the observed classes, while global and *klocal* manage to improve the simulations across aspects and slopes. However, skill scores are lower than for HS (0.2–0.5), and the performance of all algorithms is poor in the classes that are farther away from the observations, i.e. at lower elevations (600–900 m) and in some of the high-altitude steep northern classes (e.g. 2100_N_40 in Fig. 8b and c). Finally, note that slight degradations of performance can sometimes be evidenced, even in the observed classes, for all the algorithms (e.g. in flat conditions at 3300 m in Fig. 8a for the *rlocal*, not evidenced by this example for the other algorithms).

5 Discussion

In this section, we discuss the performance of CrocO PF algorithms using the assimilation of HS and consider the potential of the assimilation of reflectance in view of assimilating real data.

5.1 Tackling particle filter degeneracy

Because they assimilate several observations at the same time, global and *klocal* approaches could be prone to PF degeneracy. However, they almost never degrade the performances when assimilating HS in a variety of years and synthetic observation scenario percentiles (Fig. 6). This suggests that inflating the observation errors (as demonstrated by Larue et al., 2018, a result we have generalised in space)

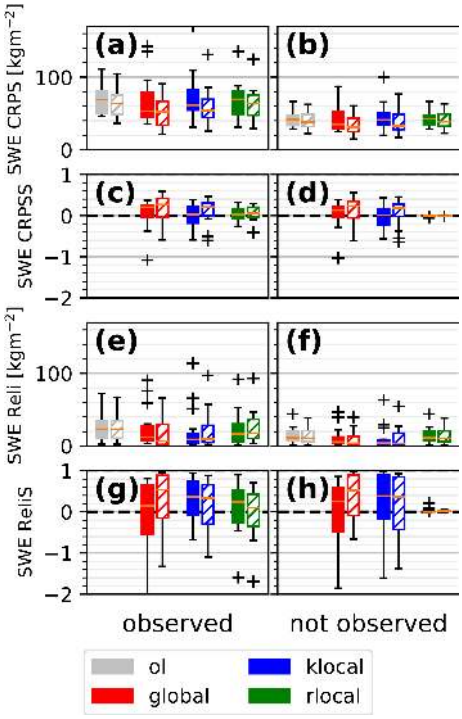

Figure 7. Same as Fig. 6 for reflectance with 40 members (filled) and 160 members (hatched).

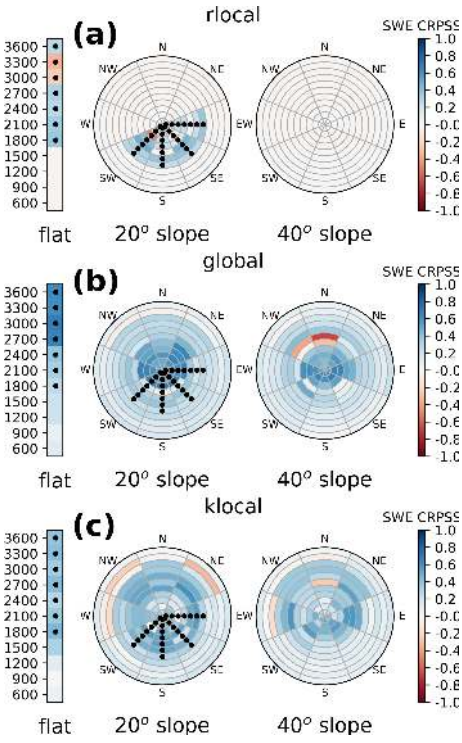

Figure 8. Same as Fig. 5 for the assimilation of the reflectance of the 2016_p60 synthetic observation scenario.

and exploiting background correlations to reduce the number of assimilated observations are two efficient approaches to tackle degeneracy.

In several cases though, strong degradation of the score occurs when assimilating reflectance (Fig. 7), which could either be attributed to an algorithmic failure in the PF or an intrinsic lack of informativeness of reflectance in some situations. Based on the good behaviour of the algorithm with HS, and because by construction, the global and *klocal* algorithms cannot lead to a degenerate PF sample, we consider this to come from the reflectance itself (this point will be further discussed in the following sections).

Beyond tackling degeneracy, the global and *klocal* algorithms also beat the *rlocal* approach on Reli and CRPSS (Figs. 7 and 8). This suggests that assimilating multiple observations increases the quality of the PF analysis, even locally. More precisely, most of the improvement is due to the Reli term of the CRPS. This property is crucial for ensemble modelling because it ensures that events are forecasted with the right frequency. However, this is not sufficient; e.g. the climatology has perfect reliability but is not informative at all. Successful assimilation manages to improve general metrics such as the CRPS while improving the reliability. For this aspect, the global and *klocal* algorithms have a satisfying performance.

5.2 Propagating the observation information

Having sparse observations is one of the most challenging issues for data assimilation systems of snowpack observations (Magnusson et al., 2014; Largeron et al., 2020). In our partially observed synthetic setup, the global and *klocal* PF variants developed here efficiently propagate the observational information to the unobserved classes with a generally better performance than the open-loop and *rlocal* approach in the unobserved classes when assimilating HS (Fig. 5).

The algorithms' performance is particularly good across aspects and slopes, with only a few steep northern aspect slopes exhibiting neutral to poor performances (Figs. 5 and 8). This suggests that southern aspect and flat classes are informative for the majority of the simulation domain. Conversely, considering that there are strong background correlations between the western and eastern sides of the domain, we can speculate that observing either side could yield overall good results.

In these figures, propagation of the information is limited towards lower elevation (600–1200 m). At such elevations, the snow cover is usually intermittent and a good discrimination of the precipitation phase is crucial. The PF does this indirectly through HS and reflectance observations because rain causes a decrease in HS through compaction and melting, while band 4 and band 5 reflectances also decrease because of quick isothermal metamorphism (i.e. the surface SSA decreases). However, in our setup, the lowest observed elevation is 1800 m; therefore, indirect observation

of the rain–snow line positioning under this level is not possible, potentially explaining the moderate performance of the PF there. In that case, assimilation of snow cover fraction might be the best solution; since the snowpack is intermittent there, the informativeness of this variable is maximal (Aalstad et al., 2018).

The global and *klocal* algorithms exhibit strong performances when assimilating HS (Fig. 5). HS is closely linked to the SWE (by the bulk density), and the interest of this variable for data assimilation is clear (Margulis et al., 2019). Here, it should be kept in mind that HS assimilation is used as a baseline experiment to evaluate the algorithms and put reflectance assimilation into perspective. The prescribed HS observation errors ($\sigma_0 = 0.1$ m) are not necessarily realistic. They should be adapted to the nature of the HS sensor. For example, spaceborne HS observation errors are typically larger (e.g. Eberhard et al., 2020; Deschamps-Berger et al., 2020). The assimilation of such observations would probably yield lower improvements.

Though the performance is lower for reflectance than in our HS experiments, it remains considerable and in line with previous results on point simulations (Charrois et al., 2016), with an average score improvement of 20 %–40 %. This study quite surprisingly suggests that reflectance information can be spread from southern slopes to the northern ones, although in many situations, the snowpack evolves in different ways for these two aspects. For example, in sunny conditions, melt and wet metamorphism will cause a drop in reflectance on southern slopes, while reflectance will not evolve much on northern slopes. Such a phenomenon could explain why low background correlations between southern and northern aspects are exhibited in band 5 (Fig. 4), which is the most sensitive to surface metamorphism through SSA. This example shows that band 5 reflectance observations on southern slopes are not necessarily informative for band 5 reflectance values in the northern aspect per se on every date. On average, however, the positive impact of reflectance observations suggests that they enable the PF to reject the ensemble members with inadequate meteorological forcings (snowfall or cloud cover would lead to wrong reflectance values) or multi-physical parameterisations (influencing e.g. the surface metamorphism), thus correcting the ensemble in the whole domain. These insights are consistent with the study of Winstral et al. (2019), wherein in situ observations are used to correct meteorological forcing parameters across large simulation domains.

Regarding the observations, our study has some methodological limits, however. Observation errors are very roughly prescribed, and the assimilated observations are not corrupted as usually done in synthetic experiments (e.g. Durand and Margulis, 2006). These choices were motivated by the fact that very little is known about the spatial correlation of reflectance observation errors in a semi-distributed setting (e.g. Cluzet et al., 2020a). In a recently submitted paper, the impact of random and systematic errors in reflectance observations on point-scale assimilation experiments is thoroughly investigated (Revuelto et al., 2021). Efforts to better characterise the spatial structure of these observation errors should be conducted in future work.

5.3 Towards the assimilation of real observations of reflectance

Reflectance is an appealing variable for snowpack modelling because of its sensitivity to snowpack surface properties (Dozier et al., 2009) and the abundance of moderate- to high-resolution spaceborne sensors (MODIS, Sentinel-2–3, VIIRS, Landsat) providing us with a handful of observations to assimilate, contrary to HS. The potential for assimilation of SCF, which is retrieved from reflectances, is clear (Margulis et al., 2016; Aalstad et al., 2018; Alonso-Gónzalez et al., 2020). This study demonstrates the potential of the PF to spread information and assimilate raw reflectances with a positive impact (Sect. 5.2). Yet, assimilating real observations of reflectance is another challenge for two reasons.

First, spaceborne reflectance observations are generally noisy and biased (e.g. Cluzet et al., 2020a). Satellite retrievals could be improved in the future (Kokhanovsky et al., 2019; Lamare et al., 2020), and Cluzet et al. (2020a) showed that assimilating ratios of reflectance could be a workaround to tackle this issue. In the near-infrared, the signal-to-noise ratio of reflectance observations might be sufficient to constrain the surface microphysical properties (Durand and Margulis, 2007; Mary et al., 2013), whereas the required accuracy for visible reflectance retrievals to remain informative on snowpack light-absorbing particles content is high (Warren, 2013), and it has yet to be proved whether either approach can achieve this requirement.

Second, in this twin experiment framework, spatial patterns of the synthetic observations are likely compatible with the ensemble since they come from the same modelling system. This may not be the case in reality, therefore making it more difficult to assimilate, and we refer to this issue as model or ensemble realism.

We must assess the strengths and weaknesses of the global and *klocal* approaches by addressing those two issues. The global algorithm assumes that a global optimum can be found across the whole domain; e.g. the information from the different observations is consistent and can be ingested in one block by the PF. With this strategy, the degeneracy due to the size of the observation vector is efficiently mitigated by the inflation algorithm as discussed in Sect. 5.1. The *klocal* approach considers only a fraction of the observation information to be relevant to constrain the model state at a given location. This algorithm tries to ingest as much information as possible while rejecting observations coming from snowpack conditions that are too statistically different. As a consequence, because we do not account for the real spatial patterns of observation errors and because we work in a twin experiment setup, a global optimum for the whole domain

can exist and can be found by the global algorithm. This might be a reason why it beats the *klocal* approach (Figs. 6 and 7). In the real world, from the model point of view, there might be contradictory information among the observations that would be difficult to disentangle with a global strategy. The *klocal* algorithm could be more suited to this situation because it looks for local optima based on the assumption that background correlations are a realistic representation of modelling errors.

These background correlation structures could be overestimated by the ensemble, and tests with real observations are necessary. Strong band 4 correlations (Fig. 4a) might be due to the spatially homogeneous perturbations of LAP fluxes used to force the simulations (see Sect. 2.2.2), a key driver of this variable, and because the same snow model configuration is applied for a given member across the simulation domain. Several studies suggest that LAP fluxes vary with elevation and other topographic parameters (de Magalhães et al., 2019; Sabatier et al., 2020), but to date no reliable model of such processes has been developed for complex terrain. In such a context, assuming uniform LAP forcing seems a reasonable compromise. Strong and almost uniform HS correlations (Fig. 4b) might be caused by the spatial homogeneity of precipitation perturbations and because we do not account for e.g. wind drift, intra-massif heterogeneity of meteorological conditions and gravitational redistribution of snow (Wayand et al., 2018). Despite this semi-distributed framework suffering from obvious limitations, the potential for high-resolution snowpack modelling (Vionnet et al., 2020; Fiddes et al., 2019; Marsh et al., 2020) is hampered by large errors of NWP models in mountainous areas (e.g. Nousu et al., 2019).

In the future, improving the ability of ensemble correlations to represent modelling errors could make the spreading of information an even more challenging task with the *klocal* algorithm. But significant potential should remain for information propagation, as suggested by results at larger scales (Magnusson et al., 2014; Cantet et al., 2019). The potential decorrelation of topographic classes would also impact the global algorithm. In an unobserved class, constraining the state of the snowpack with information from areas that are not linked to it would likely degrade the forecasting skill, as suggested by the poor performance of the algorithms at low altitudes (Figs. 5 and 8). In contrast, applying CrocO over larger domains (e.g. distributed simulations or a collection of semi-distributed massifs) would probably see the *klocal* algorithm outperform the global. The increased domain size would make it less plausible to find a global optimum over the domain, whereas spatial flexibility would be an asset of the *klocal* algorithm. Finally, in the case of modelled coupling between simulation points (e.g. snow drift), which was not the case here, the spatial discontinuities of the *klocal* analyses (see Sect. 1) might be a drawback compared to the global approach. Spatial discontinuities may also be revealed as impractical for the interpretation of individual simulation outputs by snow forecasters. The *klocal* approach is likely to reduce these discontinuities compared to the *rlocal* because similar locations will be treated with similar analyses (i.e. based on similar sets of observations). This issue could be partly mitigated by e.g. state–block–domain approaches (Farchi and Bocquet, 2018).

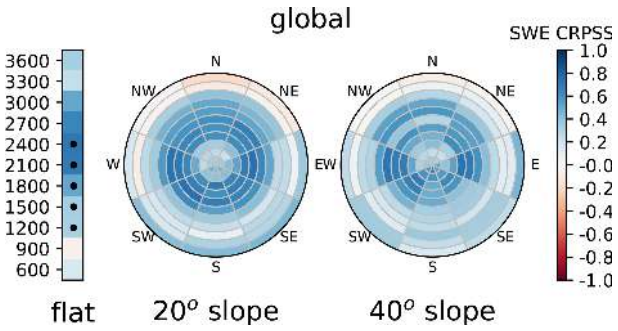

Figure 9. Same as Fig. 5 for the assimilation of HS of the 2016_p60 synthetic observation scenario in the 1200–2400 m flat classes.

5.4 Outlook for ensemble modelling and data assimilation

In the snowpack modelling community, ensemble modelling is a powerful tool to represent modelling uncertainties (Vernay et al., 2015; Richter et al., 2020) and for data assimilation (Essery et al., 2013; Lafaysse et al., 2017; Piazzi et al., 2018; Aalstad et al., 2018). This study offers a novel approach to extract valuable information on the snowpack spatial behaviour from spatial correlation patterns of the ensemble. These patterns could be used to diagnose links between locations, transfer information between areas or assess the representativeness of point simulations. More broadly, ensemble background correlations have long been exploited in the NWP and oceanographic communities to refine modelling error representation, which led to significant improvements in the data assimilation systems (Evensen, 2003; Buehner, 2005).

Ensembles might open a possibility for the assimilation of point-scale observations or sparse remotely sensed observations into spatialised simulations of the snowpack, as suggested by Winstral et al. (2019) and the present work. For instance, there are numerous snow gauges and snow pit observations at ski resorts in the French Alps. These data could be assimilated to correct the ensemble in spatialised simulations (Winstral et al., 2019). The spatial pattern of assimilated observations in the experiments of Sect. 4 does not correspond to the real-life spatial coverage of these kinds of observations. To give insight into their potential, we also applied our methodology to assimilate only five synthetic HS observations with the global PF in the 1200 to 2400 m flat classes. The results are shown in Fig. 9. The assimilation improves the performance in all aspects and slopes. Naturally, this suf-

fers from the same limitation as discussed in Sect. 5.3, not to mention the limited spatial representativeness of in situ observations, but it shows some potential for this idea.

In that way, a more rational use of the available observations could be implemented towards a new ensemble data assimilation system. In the present CrocO system, the SAFRAN reanalysis only assimilates weather station information (precipitation phase, temperature, wind) and makes no use of the numerous snow observations available. Here, snow observations are assimilated by the PF but are not used to correct meteorological forcings (only snow variables; see Fig. 2). In a new ensemble data assimilation system, within CrocO, the SAFRAN meteorological analysis could be bypassed, with the PF directly operating on both the meteorological and snowpack variables through a more comprehensive and coupled strategy.

6 Conclusions

In this study, we introduced CrocO, a new ensemble data assimilation system able to reduce the errors of a spatialised snowpack model in locations that are not observed. The ensemble is built by a combination of meteorological and multi-physical ensembles to represent modelling uncertainties. A particle filter assimilates observations of HS and reflectance. We developed two variants of the PF using inflation or k localisation in order to spread the information from partial observations of the system, without degeneracy of the PF. In the framework of synthetic experiments, we have shown in particular the following:

1. these variants are able to ingest numerous observations without degeneracy;
2. an efficient spreading of the observational information towards the unobserved areas is achieved with the global and *klocal* approaches; and
3. reflectance assimilation leads to an overall 20 % improvement in CRPS and 60 % in reliability.

We suggest that this approach could be used in any spatialised framework to assimilate sparse observations from e.g. networks of in situ snowpack observations. Beyond the snowpack modelling community, the inflation and k-localisation strategies could help address the problem of partially observed systems. This work is also a first step towards the operational assimilation of reflectance in a semi-distributed context. To reach that goal, biases of reflectance retrievals should be studied and observation error structures duly quantified. Snow cover fraction would be a good companion variable to jointly assimilate with reflectances, requiring the use of an appropriate observation operator. Extending the simulation domain to several massifs would allow the exchange of information between neighbouring massifs with the *klocal* algorithm.

Appendix A: Stochastic perturbations of the forcings

The stochastic perturbation procedure of the forcings is introduced in Sect. 2.2.2 and is identical to Charrois et al. (2016) for the meteorological parameters and Cluzet et al. (2020a) for the light-absorbing particle (LAP) fluxes. For a given date and forcing variable, perturbation values are the same for all the points in space (no spatial autocorrelation is considered), as SAFRAN semi-distributed massifs have a limited spatial extent (about 1000 km^2). Precipitation, incoming radiation, wind speed and air temperature from SAFRAN are perturbed with temporally autocorrelated stochastic parameters. The precipitation, incoming shortwave radiation, and wind speed are perturbed with multiplicative noise. Longwave radiation and air temperature are perturbed with additive noise.

For meteorological variables, the perturbation vector $\boldsymbol{V}$ is built as follows:

$$\boldsymbol{V}(t) = \phi \boldsymbol{V}(t-1) + \boldsymbol{\varepsilon}(t), \tag{A1}$$

where $\phi = e^{-\mathrm{d}t/\tau}$, with d$t$ the forcing time step, τ the decorrelation time (h) and $\boldsymbol{\varepsilon}$ a normal law of mean 0 and variance $\sigma^2(1-\phi^2)$. Parameter values for each variable are described in Table A1. The significantly high autocorrelation time of precipitation, 1500 h, was tuned to roughly adjust the ensemble spread to the observed intra-massif variability of yearly accumulated precipitation. Note that the precipitation phase is adjusted with the perturbed air temperature to ensure physical consistency. Further details on the procedure can be found in Charrois et al. (2016).

Regarding LAP fluxes, dry and wet black carbon and mineral dust deposition fluxes from MOCAGE are perturbed with a random factor which is constant throughout the year. Each member has a single multiplicative factor following a log-normal law of mean μ and variance σ (see Table A2). The mean of black carbon random perturbations was adjusted based on comparisons between simulations and field observations at Col du Lautaret, a mountain pass within the considered SAFRAN massif.

Table A1. Perturbation parameters for the meteorological variables.

Variable	Perturbation	σ	τ (h)
Precipitation ($kg\,m^{-2}\,h^{-1}$)	Multiplicative	0.7	1500
Shortwave radiation ($W\,m^{-2}$)	Multiplicative	0.7	3
Wind speed ($unitms^{-1}$)	Multiplicative	0.6	100
Longwave radiation ($W\,m^{-2}$)	Additive	24.5 $W\,m^{-2}$	30
Air temperature (K)	Additive	1.08 K	15

Table A2. Perturbation parameters for the LAP fluxes.

Variable	μ	σ
BC (wet and dry) ($kg\,m^{-2}\,h^{-1}$)	−2	1
Dust (wet and dry) ($kg\,m^{-2}\,h^{-1}$)	0	1

Appendix B: Complements on the implementation

B1 Technical implementation and code performance

CrocO is implemented within the Météo-France HPC (high-performance computing) environment, enabling us to fully parallelise the ensemble (one core per member) and bridge the gap with operational applications (Lafaysse et al., 2013; Morin et al., 2020). This implementation is strongly parallel. As an example, the execution time of a 1-year assimilation run of 187 model points with 160 members on four nodes of 40 cores each lasts only 2 h. The PF is a lightweight algorithm, and most of the computational burden is due to the propagation of the ensemble and input/output (I/O). Also note that no significant difference in execution time can be noted between the different PF algorithms.

B2 PF sample reordering

As mentioned in Sect. 2.3, a reordering step was implemented after the PF resampling from Kitagawa (1996) for practical reasons.

– (3) From $\boldsymbol{s}$, build $\tilde{\mathbf{s}}$ such that all elements of the unique values of $\boldsymbol{s}$ lie in the position given by their value. Example with 16 particles:

$$\boldsymbol{s} = [1,1,2,3,3,3,8,8,9,9,9,9,9,16,16,16]$$
$$\Rightarrow \tilde{\mathbf{s}} = [1,2,3,1,3,3,8,8,9,9,9,9,9,16,16,16].$$

Indeed, I/O represents a bottleneck in the PF. When building the analysis $\boldsymbol{X}_\mathrm{a}$, the background $\boldsymbol{X}_\mathrm{b}$ is already loaded in memory. Since $\boldsymbol{X}_\mathrm{a}$ is just a reordering of $\boldsymbol{X}_\mathrm{b}$ columns based on $\boldsymbol{s}$, a reordering of $\boldsymbol{s}$ avoids building a copy of $\boldsymbol{X}_\mathrm{b}$. This way, $\boldsymbol{X}_\mathrm{a}$ is built by an online modification of $\boldsymbol{X}_\mathrm{b}$ using two pointers. Reordering is a growing consideration in the PF community (Farchi and Bocquet, 2018).

Code availability. The Crocus snowpack model (including all physical options of the ESCROC system) and the particle filter algorithm are developed in the framework of the open-source SURFEX project. The source files of SURFEX code are provided at https://doi.org/10.5281/zenodo.3774861 (Cluzet et al., 2020b) to guarantee the permanent reproducibility of results. However, we recommend that potential future users and developers access the code from its Git repository (http://git.umr-cnrm.fr/git/Surfex_Git2.git, last access: 15 April 2020) to benefit from all tools of code management (history management, bug fixes, documentation, interface for technical support, etc.). This requires a quick registration, and the procedure is described at https://opensource.cnrm-game-meteo.fr/projects/snowtools/wiki/Procedure_for_new_users (last access: 4 January 2021). The version used in this work is tagged as CrocO_v1.0.

Python software called CrocO_toolbox was specifically developed in order to pre-process, post-process and launch CrocO experiments. It is available on GitHub (https://github.com/bertrandcz/CrocO, release v1.0 of the master branch, last access: 4 May 2020) along with documentation.

The article version of CrocO_toolbox is archived at https://doi.org/10.5281/zenodo.3784980 (Cluzet, 2020). This software strongly relies on two external Python projects ensuring file management between the different steps of a simulation and the interface with the Météo-France HPC system (including parallelisation and data storage): snowtools and vortex. Their sources are available at https://doi.org/10.5281/zenodo.3774861 (Cluzet et al., 2020b) (same archive as SURFEX) to guarantee the permanent reproducibility of results. However, as for the SURFEX project and for the same reasons, it is recommended to access snowtools code from its Git repository (https://git.umr-cnrm.fr/git/snowtools_git.git, last access: 4 May 2020). The version used in this work is also tagged as CrocO_v1.0. The vortex project gathers all environment-specific codes of Météo-France modelling systems relative to its HPC system. For this project, only the sources specific to this article's simulations are provided. Common object inheritance is based on vortex version 1.6.1. The version used in this work is also tagged as CrocO_v1.0 in the vortex Git repository.

Because these software programmes could not be applied outside the Météo-France HPC environment, CrocO Python software offers the possibility to run CrocO simulations locally. This functionality was not used here due to the high numerical cost of our simulations, which required the use of the Météo-France HPC environment.

Data availability. Input and output data necessary to reproduce the simulations and figures in this paper are provided at https://doi.org/10.5281/zenodo.3775007 (Cluzet et al., 2020c). This archive includes the SAFRAN reanalyses (also available at https://doi.org/10.25326/37, Vernay et al., 2021), MOCAGE forcings, namelists, configuration files and spin-up files necessary to reproduce the simulations. Raw model outputs can be provided on request, but since they can be up to 500+ GB, only post-processed simulation outputs are provided in this archive, along with scores and scripts to reproduce the figures in the paper.

Author contributions. BC wrote the paper. BC, ML and MD designed the study, and BC developed the code with help from ML, LFM and CA. BC, MD, ML and EC designed the PF variants. All authors contributed to results analysis and discussion.

Competing interests. The authors declare that they have no conflict of interest.

Acknowledgements. The authors are grateful to François Tuzet, Jesus Revuelto, Rafife Nheili, César Deschamps-Berger, Stéphanie Faroux (SODA) and Matthieu Vernay for their valuable help in collecting input data and code implementation. They would also like to thank Fanny Larue, Joseph Bellier, Pierre De Mey and Guilhem Candille for helpful discussions on the PF inflation and CRPS decomposition.

Review statement. This paper was edited by Richard Mills and reviewed by Kristoffer Aalstad and one anonymous referee.

References

Aalstad, K., Westermann, S., Schuler, T. V., Boike, J., and Bertino, L.: Ensemble-based assimilation of fractional snow-covered area satellite retrievals to estimate the snow distribution at Arctic sites, The Cryosphere, 12, 247–270, https://doi.org/10.5194/tc-12-247-2018, 2018.

Aalstad, K., Westermann, S., and Bertino, L.: Evaluating satellite retrieved fractional snow-covered area at a high-Arctic site using terrestrial photography, Remote Sens. Environ., 239, 111618, https://doi.org/10.1016/j.rse.2019.111618, 2020.

Albergel, C., Munier, S., Leroux, D. J., Dewaele, H., Fairbairn, D., Barbu, A. L., Gelati, E., Dorigo, W., Faroux, S., Meurey, C., Le Moigne, P., Decharme, B., Mahfouf, J.-F., and Calvet, J.-C.: Sequential assimilation of satellite-derived vegetation and soil moisture products using SURFEX_v8.0: LDAS-Monde assessment over the Euro-Mediterranean area, Geosci. Model Dev., 10, 3889–3912, https://doi.org/10.5194/gmd-10-3889-2017, 2017.

Alonso-González, E., Gutmann, E., Aalstad, K., Fayad, A., and Gascoin, S.: Snowpack dynamics in the Lebanese mountains from quasi-dynamically downscaled ERA5 reanalysis updated by assimilating remotely-sensed fractional snow-covered area, Hydrol. Earth Syst. Sci. Discuss., https://doi.org/10.5194/hess-2020-335, in review, 2020.

Baba, M., Gascoin, S., and Hanich, L.: Assimilation of Sentinel-2 Data into a Snowpack Model in the High Atlas of Morocco, Remote Sens.-Basel, 10, 1982, https://doi.org/10.3390/rs10121982, 2018.

Bengtsson, T., Bickel, P., and Li, B.: Curse-of-dimensionality revisited: Collapse of the particle filter in very large scale systems, in: Probability and statistics: Essays in honor of David A. Freedman, Institute of Mathematical Statistics, 2, 316–334, https://doi.org/10.1214/193940307000000518, 2008.

Buehner, M.: Ensemble-derived stationary and flow-dependent background-error covariances: Evaluation in a quasi-operational NWP setting, Q. J. Roy. Meteor. Soc., 131, 1013–1043, 2005.

Candille, G., Brankart, J.-M., and Brasseur, P.: Assessment of an ensemble system that assimilates Jason-1/Envisat altimeter data in a probabilistic model of the North Atlantic ocean circulation, Ocean Sci., 11, 425–438, https://doi.org/10.5194/os-11-425-2015, 2015.

Cantet, P., Boucher, M., Lachance-Coutier, S., Turcotte, R., and Fortin, V.: Using a particle filter to estimate the spatial distribution of the snowpack water equivalent, J. Hydrometeorol., 20, 577–594, 2019.

Carmagnola, C. M., Morin, S., Lafaysse, M., Domine, F., Lesaffre, B., Lejeune, Y., Picard, G., and Arnaud, L.: Implementation and evaluation of prognostic representations of the optical diameter of snow in the SURFEX/ISBA-Crocus detailed snowpack model, The Cryosphere, 8, 417–437, https://doi.org/10.5194/tc-8-417-2014, 2014.

Charrois, L., Cosme, E., Dumont, M., Lafaysse, M., Morin, S., Libois, Q., and Picard, G.: On the assimilation of optical reflectances and snow depth observations into a detailed snowpack model, The Cryosphere, 10, 1021–1038, https://doi.org/10.5194/tc-10-1021-2016, 2016.

Clark, M. P., Nijssen, B., Lundquist, J. D., Kavetski, D., Rupp, D. E., Woods, R. A., Freer, J. E., Gutmann, E. D., Wood, A. W., Brekke, L. D., Arnold, J. R., Gochis, D. J., and Rasmussen, R. M.: A unified approach for process-based hydrologic modeling: 1. Modeling concept, Water Resour. Res., 51, 2498–2514, 2015.

Cluzet, B.: bertrandcz/CrocO_toolbox: CrocO_toolbox: GMD mauscript version (Version 1.0), Zenodo, https://doi.org/10.5281/zenodo.3784980, 2020.

Cluzet, B., Revuelto, J., Lafaysse, M., Tuzet, F., Cosme, E., Picard, G., Arnaud, L., and Dumont, M.: Towards the assimilation of satellite reflectance into semi-distributed ensemble snowpack simulations, Cold Reg. Sci. Technol., 170, 102918, https://doi.org/10.1016/j.coldregions.2019.102918, 2020a.

Cluzet, B., Lafaysse, M., Cosme, E., Albergel, C., Meunier, L.-F., and Dumont, M.: CrocO: model source code and external librairies (Version v1.0), Zenodo, https://doi.org/10.5281/zenodo.3774861, 2020b.

Cluzet, B., Lafaysse, M., Cosme, E., Albergel, C., Meunier, L.-F., and Dumont, M.: CrocO: manuscript Dataset (Version v1.0) [Data set], Zenodo, https://doi.org/10.5281/zenodo.3775007, 2020c.

Davaze, L., Rabatel, A., Arnaud, Y., Sirguey, P., Six, D., Letreguilly, A., and Dumont, M.: Monitoring glacier albedo as a proxy to derive summer and annual surface mass balances from optical remote-sensing data, The Cryosphere, 12, 271–286, https://doi.org/10.5194/tc-12-271-2018, 2018.

De Lannoy, G. J., Reichle, R. H., Arsenault, K. R., Houser, P. R., Kumar, S., Verhoest, N. E., and Pauwels, V. R.: Multiscale assimilation of Advanced Microwave Scanning Radiometer–EOS snow water equivalent and Moderate Resolution Imaging Spectroradiometer snow cover fraction observations in northern Colorado, Water Resour. Res., 48, W01522, https://doi.org/10.1029/2011WR010588, 2012.

de Magalhães, N., Evangelista, H., Condom, T., Rabatel, A., and Ginot, P.: Amazonian Biomass Burning Enhances Tropical Andean Glaciers Melting, Sci. Rep.-UK, 9, 1–12, 2019.

Dechant, C. and Moradkhani, H.: Radiance data assimilation for operational snow and streamflow forecasting, Adv. Water Resour., 34, 351–364, https://doi.org/10.1016/j.advwatres.2010.12.009, 2011.

Deschamps-Berger, C., Gascoin, S., Berthier, E., Deems, J., Gutmann, E., Dehecq, A., Shean, D., and Dumont, M.: Snow depth mapping from stereo satellite imagery in mountainous terrain: evaluation using airborne laser-scanning data, The Cryosphere, 14, 2925–2940, https://doi.org/10.5194/tc-14-2925-2020, 2020.

Dozier, J., Green, R. O., Nolin, A. W., and Painter, T. H.: Interpretation of snow properties from imaging spectrometry, Remote Sens. Environ., 113, S25–S37, 2009.

Durand, M. and Margulis, S. A.: Feasibility test of multifrequency radiometric data assimilation to estimate snow water equivalent, J. Hydrometeorol., 7, 443–457, 2006.

Durand, M. and Margulis, S. A.: Correcting first-order errors in snow water equivalent estimates using a multifrequency, multiscale radiometric data assimilation scheme, J. Geophys. Res.-Atmos., 112, D13121, https://doi.org/10.1029/2006JD008067, 2007.

Durand, Y., Brun, E., Mérindol, L., Guyomarc'h, G., Lesaffre, B., and Martin, E.: A meteorological estimation of relevant parameters for snow models, Ann. Glaciol., 18, 65–71, 1993.

Eberhard, L. A., Sirguey, P., Miller, A., Marty, M., Schindler, K., Stoffel, A., and Bühler, Y.: Intercomparison of photogrammetric platforms for spatially continuous snow depth mapping, The Cryosphere Discuss., https://doi.org/10.5194/tc-2020-93, in review, 2020.

Essery, R., Morin, S., Lejeune, Y., and Bauduin-Ménard, C.: A comparison of 1701 snow models using observations from an alpine site, Adv. Water Res., 55, 131–148, https://doi.org/10.1016/j.advwatres.2012.07.013, 2013.

Evensen, G.: The ensemble Kalman filter: Theoretical formulation and practical implementation, Ocean Dynam., 53, 343–367, 2003.

Farchi, A. and Bocquet, M.: Review article: Comparison of local particle filters and new implementations, Nonlin. Processes Geophys., 25, 765–807, https://doi.org/10.5194/npg-25-765-2018, 2018.

Fiddes, J., Aalstad, K., and Westermann, S.: Hyper-resolution ensemble-based snow reanalysis in mountain regions using clustering, Hydrol. Earth Syst. Sci., 23, 4717–4736, https://doi.org/10.5194/hess-23-4717-2019, 2019.

Gordon, N. J., Salmond, D. J., and Smith, A. F.: Novel approach to nonlinear/non-Gaussian Bayesian state estimation, IEE Proc.-F, 140, 107–113, 1993.

Hamill, T. M., Whitaker, J. S., and Snyder, C.: Distance-dependent filtering of background error covariance estimates in an ensemble Kalman filter, Mon. Weather Rev., 129, 2776–2790, 2001.

Houtekamer, P. L. and Mitchell, H. L.: Data assimilation using an ensemble Kalman filter technique, Mon. Weather Rev., 126, 796–811, 1998.

Josse, B., Simon, P., and Peuch, V.-H.: Radon global simulations with the multiscale chemistry and transport model MOCAGE, Tellus B, 56, 339–356, 2004.

Kitagawa, G.: Monte Carlo filter and smoother for non-Gaussian nonlinear state space models, J. Comput. Graph. Stat., 5, 1–25, 1996.

Kokhanovsky, A., Lamare, M., Danne, O., Brockmann, C., Dumont, M., Picard, G., Arnaud, L., Favier, V., Jourdain, B., Le Meur, E., Di Mauro, B., Aoki, T., Niwano, M., Rozanov, V., Korkin, S.,

Kipfstuhl, S., Freitag, J., Hoerhold, M., Zuhr, A., Vladimirova, D., Faber, A.-K., Steen-Larsen, H. C., Wahl, S., Andersen, J. K., Vandecrux, B., van As, D., Mankoff, K. D., Kern, M., Zege, E., and Box, J. E.: Retrieval of snow properties from the Sentinel-3 Ocean and Land Colour Instrument, Remote Sens.-Basel, 11, 2280, https://doi.org/10.3390/rs11192280, 2019.

Krinner, G., Derksen, C., Essery, R., Flanner, M., Hagemann, S., Clark, M., Hall, A., Rott, H., Brutel-Vuilmet, C., Kim, H., Ménard, C. B., Mudryk, L., Thackeray, C., Wang, L., Arduini, G., Balsamo, G., Bartlett, P., Boike, J., Boone, A., Chéruy, F., Colin, J., Cuntz, M., Dai, Y., Decharme, B., Derry, J., Ducharne, A., Dutra, E., Fang, X., Fierz, C., Ghattas, J., Gusev, Y., Haverd, V., Kontu, A., Lafaysse, M., Law, R., Lawrence, D., Li, W., Marke, T., Marks, D., Ménégoz, M., Nasonova, O., Nitta, T., Niwano, M., Pomeroy, J., Raleigh, M. S., Schaedler, G., Semenov, V., Smirnova, T. G., Stacke, T., Strasser, U., Svenson, S., Turkov, D., Wang, T., Wever, N., Yuan, H., Zhou, W., and Zhu, D.: ESM-SnowMIP: assessing snow models and quantifying snow-related climate feedbacks, Geosci. Model Dev., 11, 5027–5049, https://doi.org/10.5194/gmd-11-5027-2018, 2018.

Lafaysse, M., Morin, S., Coléou, C., Vernay, M., Serça, D., Besson, F., Willemet, J.-M., Giraud, G., and Durand, Y.: Toward a new chain of models for avalanche hazard forecasting in French mountain ranges, including low altitude mountains, in: Proceedings of the International Snow Science Workshop – Grenoble and Chamonix, 162–166, 2013.

Lafaysse, M., Cluzet, B., Dumont, M., Lejeune, Y., Vionnet, V., and Morin, S.: A multiphysical ensemble system of numerical snow modelling, The Cryosphere, 11, 1173–1198, https://doi.org/10.5194/tc-11-1173-2017, 2017.

Lahoz, B. K. W. and Menard, R.: Data assimilation, Springer, Berlin, Heidelberg, https://doi.org/10.1007/978-3-540-74703-1, 2010.

Lamare, M., Dumont, M., Picard, G., Larue, F., Tuzet, F., Delcourt, C., and Arnaud, L.: Simulating optical top-of-atmosphere radiance satellite images over snow-covered rugged terrain, The Cryosphere, 14, 3995–4020, https://doi.org/10.5194/tc-14-3995-2020, 2020.

Largeron, C., Dumont, M., Morin, S., Boone, A., Lafaysse, M., Metref, S., Cosme, E., Jonas, T., Winstral, A., and Margulis, S. A.: Towards snow cover estimation in mountainous areas using modern data assimilation methods: A review, Front. Earth Sci., 8, 325, https://doi.org/10.3389/feart.2020.00325, 2020.

Larue, F., Royer, A., De Sève, D., Roy, A., and Cosme, E.: Assimilation of passive microwave AMSR-2 satellite observations in a snowpack evolution model over northeastern Canada, Hydrol. Earth Syst. Sci., 22, 5711–5734, https://doi.org/10.5194/hess-22-5711-2018, 2018.

Libois, Q., Picard, G., France, J. L., Arnaud, L., Dumont, M., Carmagnola, C. M., and King, M. D.: Influence of grain shape on light penetration in snow, The Cryosphere, 7, 1803–1818, https://doi.org/10.5194/tc-7-1803-2013, 2013.

Libois, Q., Picard, G., Arnaud, L., Dumont, M., Lafaysse, M., Morin, S., and Lefebvre, E.: Summertime evolution of snow specific surface area close to the surface on the Antarctic Plateau, The Cryosphere, 9, 2383–2398, https://doi.org/10.5194/tc-9-2383-2015, 2015.

Liu, J. S. and Chen, R.: Blind deconvolution via sequential imputations, J. Am. Stat. Assoc., 90, 567–576, 1995.

Magnusson, J., Gustafsson, D., Hüsler, F., and Jonas, T.: Assimilation of point SWE data into a distributed snow cover model comparing two contrasting methods, Water Resour. Res., 50, 7816–7835, 2014.

Magnusson, J., Winstral, A., Stordal, A. S., Essery, R., and Jonas, T.: Improving physically based snow simulations by assimilating snow depths using the particle filter, Water Resour. Res., 53, 1125–1143, 2017.

Mankin, J. S., Viviroli, D., Singh, D., Hoekstra, A. Y., and Diffenbaugh, N. S.: The potential for snow to supply human water demand in the present and future, Environ. Res. Lett., 10, 114016, https://doi.org/10.1088/1748-9326/10/11/114016, 2015.

Margulis, A., Cortés, G., Girotto, M., and Durand, M.: A Landsat-Era Sierra Nevada Snow Reanalysis (1985–2015), J. Hydrometeorol., 17, 1203–1221, https://doi.org/10.1175/JHM-D-15-0177.1, 2016.

Margulis, S. A., Fang, Y., Li, D., Lettenmaier, D. P., and Andreadis, K.: The Utility of Infrequent Snow Depth Images for Deriving Continuous Space-Time Estimates of Seasonal Snow Water Equivalent, Geophys. Res. Lett., 46, 5331–5340, 2019.

Marsh, C. B., Pomeroy, J. W., and Wheater, H. S.: The Canadian Hydrological Model (CHM) v1.0: a multi-scale, multi-extent, variable-complexity hydrological model – design and overview, Geosci. Model Dev., 13, 225–247, https://doi.org/10.5194/gmd-13-225-2020, 2020.

Mary, A., Dumont, M., Dedieu, J.-P., Durand, Y., Sirguey, P., Milhem, H., Mestre, O., Negi, H. S., Kokhanovsky, A. A., Lafaysse, M., and Morin, S.: Intercomparison of retrieval algorithms for the specific surface area of snow from near-infrared satellite data in mountainous terrain, and comparison with the output of a semi-distributed snowpack model, The Cryosphere, 7, 741–761, https://doi.org/10.5194/tc-7-741-2013, 2013.

Masson, T., Dumont, M., Mura, M. D., Sirguey, P., Gascoin, S., Dedieu, J.-P., and Chanussot, J.: An Assessment of Existing Methodologies to Retrieve Snow Cover Fraction from MODIS Data, Remote Sens.-Basel, 10, 619, https://doi.org/10.3390/rs10040619, 2018.

Masson, V., Le Moigne, P., Martin, E., Faroux, S., Alias, A., Alkama, R., Belamari, S., Barbu, A., Boone, A., Bouyssel, F., Brousseau, P., Brun, E., Calvet, J.-C., Carrer, D., Decharme, B., Delire, C., Donier, S., Essaouini, K., Gibelin, A.-L., Giordani, H., Habets, F., Jidane, M., Kerdraon, G., Kourzeneva, E., Lafaysse, M., Lafont, S., Lebeaupin Brossier, C., Lemonsu, A., Mahfouf, J.-F., Marguinaud, P., Mokhtari, M., Morin, S., Pigeon, G., Salgado, R., Seity, Y., Taillefer, F., Tanguy, G., Tulet, P., Vincendon, B., Vionnet, V., and Voldoire, A.: The SURFEXv7.2 land and ocean surface platform for coupled or offline simulation of earth surface variables and fluxes, Geosci. Model Dev., 6, 929–960, https://doi.org/10.5194/gmd-6-929-2013, 2013.

Matheson, J. E. and Winkler, R. L.: Scoring rules for continuous probability distributions, Manage. Sci., 22, 1087–1096, 1976.

Morin, S., Horton, S., Techel, F., Bavay, M., Coléou, C., Fierz, C., Gobiet, A., Hagenmuller, P., Lafaysse, M., Ližar, M., Mitterer, C., Monti, F., Müller, K., Olefs, M., Snook, J. S., van Herwijnen, A., and Vionnet, V.: Application of physical snowpack models in support of operational avalanche hazard forecasting: A status report on current implementations and prospects for the future, Cold Reg. Sci. Technol., 170, 102910, https://doi.org/10.1016/j.coldregions.2019.102910, 2020.

Nousu, J.-P., Lafaysse, M., Vernay, M., Bellier, J., Evin, G., and Joly, B.: Statistical post-processing of ensemble forecasts of the height of new snow, Nonlin. Processes Geophys., 26, 339–357, https://doi.org/10.5194/npg-26-339-2019, 2019.

Penny, S. G. and Miyoshi, T.: A local particle filter for high-dimensional geophysical systems, Nonlin. Processes Geophys., 23, 391–405, https://doi.org/10.5194/npg-23-391-2016, 2016.

Piazzi, G., Thirel, G., Campo, L., and Gabellani, S.: A particle filter scheme for multivariate data assimilation into a point-scale snowpack model in an Alpine environment, The Cryosphere, 12, 2287–2306, https://doi.org/10.5194/tc-12-2287-2018, 2018.

Pomeroy, J. W., Fang, X., and Marks, D. G.: The cold rain-on-snow event of June 2013 in the Canadian Rockies–Characteristics and diagnosis, Hydrol. Process., 30, 2899–2914, 2016.

Poterjoy, J.: A localized particle filter for high-dimensional nonlinear systems, Mon. Weather Rev., 144, 59–76, 2016.

Poterjoy, J. and Anderson, J. L.: Efficient assimilation of simulated observations in a high-dimensional geophysical system using a localized particle filter, Mon. Weather Rev., 144, 2007–2020, 2016.

Poterjoy, J., Wicker, L., and Buehner, M.: Progress toward the application of a localized particle filter for numerical weather prediction, Mon. Weather Rev., 147, 1107–1126, 2019.

Press, W. H., Flannery, B. P., Teukolsky, S. A., and Vetterling, W. T.: Numerical recipes in Fortran the art of scientific computing, 2nd Edn., Cambridge University Press, Cambridge, 1992.

Raleigh, M. S., Lundquist, J. D., and Clark, M. P.: Exploring the impact of forcing error characteristics on physically based snow simulations within a global sensitivity analysis framework, Hydrol. Earth Syst. Sci., 19, 3153–3179, https://doi.org/10.5194/hess-19-3153-2015, 2015.

Reichle, R. H. and Koster, R. D.: Assessing the impact of horizontal error correlations in background fields on soil moisture estimation, J. Hydrometeorol., 4, 1229–1242, 2003.

Revuelto, J., Lecourt, G., Lafaysse, M., Zin, I., Charrois, L., Vionnet, V., Dumont, M., Rabatel, A., Six, D., Condom, T., Morin, S., Viani, A., and Sirguey, P.: Multi-Criteria Evaluation of Snowpack Simulations in Complex Alpine Terrain Using Satellite and In Situ Observations, Remote Sens.-Basel, 10, 1171, https://doi.org/10.3390/rs10081171, 2018.

Revuelto, J., Cluzet, B., Duran, N., Fructus, M., Lafaysse, M., Cosme, E., and Dumont, M.: Assimilation of surface reflectance in snow simulations; impact on bulk snow variables, in preparation, 2021.

Richter, B., van Herwijnen, A., Rotach, M. W., and Schweizer, J.: Sensitivity of modeled snow stability data to meteorological input uncertainty, Nat. Hazards Earth Syst. Sci., 20, 2873–2888, https://doi.org/10.5194/nhess-20-2873-2020, 2020.

Sabatier, T., Largeron, Y., Paci, A., Lac, C., Rodier, Q., Canut, G., and Masson, V.: Semi-idealized simulations of wintertime flows and pollutant transport in an alpine valley: Passive tracer tracking (Part II), Q. J. Roy. Meteor. Soc., 146, 827–845, https://doi.org/10.1002/qj.3710, 2020.

Shaw, T. E., Gascoin, S., Mendoza, P. A., Pellicciotti, F., and McPhee, J.: Snow depth patterns in a high mountain Andean catchment from satellite optical tri-stereoscopic remote sensing, Water Resour. Res., 56, e2019WR024880, https://doi.org/10.1029/2019WR024880, 2019.

Sirguey, P., Mathieu, R., and Arnaud, Y.: Subpixel monitoring of the seasonal snow cover with MODIS at 250 m spatial resolution in the Southern Alps of New Zealand: methodology and accuracy assessment, Remote Sens. Environ., 113, 160–181, https://doi.org/10.1016/j.rse.2008.09.008, 2009.

Slater, A. G. and Clark, M. P.: Snow data assimilation via an ensemble Kalman filter, J. Hydrometeorol., 7, 478–493, 2006.

Snyder, C., Bengtsson, T., Bickel, P., and Anderson, J.: Obstacles to high-dimensional particle filtering, Mon. Weather Rev., 136, 4629–4640, 2008.

Stigter, E. E., Wanders, N., Saloranta, T. M., Shea, J. M., Bierkens, M. F. P., and Immerzeel, W. W.: Assimilation of snow cover and snow depth into a snow model to estimate snow water equivalent and snowmelt runoff in a Himalayan catchment, The Cryosphere, 11, 1647–1664, https://doi.org/10.5194/tc-11-1647-2017, 2017.

Thirel, G., Salamon, P., Burek, P., and Kalas, M.: Assimilation of MODIS snow cover area data in a distributed hydrological model using the particle filter, Remote Sens.-Basel, 5, 5825–5850, 2013.

Tuzet, F., Dumont, M., Lafaysse, M., Picard, G., Arnaud, L., Voisin, D., Lejeune, Y., Charrois, L., Nabat, P., and Morin, S.: A multilayer physically based snowpack model simulating direct and indirect radiative impacts of light-absorbing impurities in snow, The Cryosphere, 11, 2633–2653, https://doi.org/10.5194/tc-11-2633-2017, 2017.

Van Leeuwen, P. J.: Particle filtering in geophysical systems, Mon. Weather Rev., 137, 4089–4114, 2009.

Van Leeuwen, P. J., Künsch, H. R., Nerger, L., Potthast, R., and Reich, S.: Particle filters for high-dimensional geoscience applications: A review, Q. J. Roy. Meteor. Soc., 145, 2335–2365, 2019.

Vernay, M., Lafaysse, M., Merindol, L., Giraud, G., and Morin, S.: Ensemble Forecasting of snowpack conditions and avalanche hazard, Cold Reg. Sci. Technol., 120, 251–262, https://doi.org/10.1016/j.coldregions.2015.04.010, 2015.

Vernay, M., Lafaysse, M., Mérindol, L., Hagenmuller, P., Verfaillie, D., Morin., S., and Monteiro, D.: A 61-years meteorological and snow conditions re-analysis over the French mountainous areas (1958–2019) [Data set], AERIS, https://doi.org/10.25326/37, 2021.

Veyssière, G., Karbou, F., Morin, S., Lafaysse, M., and Vionnet, V.: Evaluation of Sub-Kilometric Numerical Simulations of C-Band Radar Backscatter over the French Alps against Sentinel-1 Observations, Remote Sens.-Basel, 11, 8, https://doi.org/10.3390/rs11010008, 2019.

Vionnet, V., Brun, E., Morin, S., Boone, A., Faroux, S., Le Moigne, P., Martin, E., and Willemet, J.-M.: The detailed snowpack scheme Crocus and its implementation in SURFEX v7.2, Geosci. Model Dev., 5, 773–791, https://doi.org/10.5194/gmd-5-773-2012, 2012.

Vionnet, V., Marsh, C. B., Menounos, B., Gascoin, S., Wayand, N. E., Shea, J., Mukherjee, K., and Pomeroy, J. W.: Multi-scale snowdrift-permitting modelling of mountain snowpack, The Cryosphere Discuss., https://doi.org/10.5194/tc-2020-187, in review, 2020.

Warren, S. G.: Can black carbon in snow be detected by remote sensing?, J. Geophys. Res., 118, 779–786, https://doi.org/10.1029/2012JD018476, 2013.

Wayand, N. E., Marsh, C. B., Shea, J. M., and Pomeroy, J. W.: Globally scalable alpine snow metrics, Remote Sens. Environ., 213, 61–72, 2018.

Winstral, A., Magnusson, J., Schirmer, M., and Jonas, T.: The Bias-Detecting Ensemble: A New and Efficient Technique for Dynamically Incorporating Observations Into Physics-Based, Multilayer Snow Models, Water Resour. Res., 55, 613–631, 2019.

Wright, P., Bergin, M., Dibb, J., Lefer, B., Domine, F., Carman, T., Carmagnola, C., Dumont, M., Courville, Z., Schaaf, C., and Wang, Z.: Comparing MODIS daily snow albedo to spectral albedo field measurements in Central Greenland, Remote Sens. Environ., 140, 118–129, 2014.

Würzer, S., Jonas, T., Wever, N., and Lehning, M.: Influence of initial snowpack properties on runoff formation during rain-on-snow events, J. Hydrometeorol., 17, 1801–1815, 2016.

Chapter 4

Assimilation of observations from an in-situ SD network over the Alps and the Pyrenees

Contents

4.1 Extended abstract

In the previous Chapter 3, we introduced two novel PF variants successfully propagating information from observations of the heigh of snow across topographic conditions, in an idealised setting. This study suggests (Fig. 9 of Sec. 3.2) that a handful of observations on flat conditions could be used to constrain ensemble simulations over a whole semi-distributed massif (representing an area of about 1000 km^2). A similar result has been obtained with real in-situ observations by Magnusson et al. (2014) and Winstral et al. (2019). However, their studies relied on an exceptionally dense observation network, and it is yet to prove that assimilation algorithms can take advantage of looser observational networks.

In this chapter, we applied the assimilation methodology proposed in previous Chap. 3 into a network of 295 in-situ stations covering the French Alps, French Pyrenees, and Andorra, from 2009 to 2019. This network exhibit strongly contrasted observation densities (Fig. 1 and 10 of the paper). Météo-France operational modelling chain and its open-loop ensemble counterpart –built for the purpose of this study–, serve as references. A localisation radius was introduced in the inflation (so-called "rlocal") and k-localisation algorithms (so-called "klocal") as a way to search for error structures of different spatial scales, ranging from 17 km (the approximate radius of a SAFRAN massif) to 300 km (maximal extent of the Alps and Pyrenees).

The operational deterministic (oper) and open-loop simulations exhibit contrasted inter-annual (Tab. 1 and Fig. 6) and spatial performance (Fig. 5). The open-loop is slightly negatively biased with respect to the oper, and exhibits higher RMSE. The different assimilation runs succesfully avoid degeneracy, and achieve lower errors (RMSE, biases) than the open-loop, but do not over-perform the oper run (Fig. 6). They are also under-dispersive, regardless the localisation radius (Fig. 6). The largest localisation radius, because it assimilates more observations, exhibit lower spread-skills, both for the rlocal and the klocal. Intermediate localisation radius of 35 and 50 km seem more appropriate (slightly lower RMSE).

Focusing on the klocal algorithm with a radius of 35 km, we show that this algorithm quite efficiently reduces the bias-elevation relation denoted for the reference runs (Fig. 7). Spatially, it seems to particularly over perform the open-loop in the Central-Eastern Pyrenees and Southern Alps (Fig. 8), while mitigated results are obtained in the Northern Alps. In Fig. 9 (right), we show that the improvement with respect to the open-loop is strongly linked to the open-loop bias, with significant improvements for negative open-loop bias (about 10-15%) and significant degradation for the positive biases. With respect to the stations elevation (Fig 9, left), results are significantly spread, (about 30% of the stations have degraded performance), the highest average performance being reached in the range 1500-2000 m.

The performance did not seem to increase with the density of available observations (Fig. 10). This is probably an artefact, explained in detail in Sec. 5.5.

To conclude with, this study showed that the PF variants we developed were successful in assimilating potentially large numbers of real in-situ snowpack observations without degenerating, which is a considerable advance with such an algorithm. Despite the different assimilation configuration do not yield significant RMSE improvements over the 10 years, they manage to reduce the open-loop bias, and yield on average, positive CRPSS of about 5-10%. Significant improvements are obtained in the most remote areas, suggesting that even scarce observations of the snowpack can be beneficial for snowpack modelling. Further improvements in the representation of snowpack variability factors such as wind drift processes may be necessary to take advantage of the information content from observations in the areas where simulation errors are presently the lowest.

4.2 Propagating information from snow observations with CrocO ensemble data assimilation system

Citation:

Cluzet, B., Lafaysse, M., Deschamps-Berger, C., Vernay, M., & Dumont, M., Propagating information from snow observations with CrocO ensemble data assimilation system: a 10-years case study over a snow depth observation network, (in prep)

Author contribution:

- Conception and implementation of the Particle Filter radius localisation within SURFEX_v8.1
- Data quality checks on the observations
- Analysis of results and redaction of the article

Propagating information from snow observations with CrocO ensemble data assimilation system: a 10-years case study over a snow depth observation network

Bertrand Cluzet[1, 2], Matthieu Lafaysse[1], César Deschamps-Berger[1, 3], Matthieu Vernay[1], and Marie Dumont[1]

[1]Univ. Grenoble Alpes, Université de Toulouse, Météo-France, CNRS, CNRM, Centre d'Études de la Neige, Grenoble, France
[2]WSL Institute for Snow and Avalanche Research SLF, Davos, Switzerland
[3]Centre d'Etudes Spatiales de la Biosphère, CESBIO, Univ. Toulouse, CNES/CNRS/INRA/IRD/UPS, 31401 Toulouse, France

Correspondence: Bertrand Cluzet (bertrand.cluzet@slf.ch)

Abstract. The mountainous snow cover is highly variable at all temporal and spatial scales. Snowpack models only imperfectly represent this variability, because of uncertain meteorological inputs, physical parameterisations, and unresolved terrain features. In-situ observations of the height of snow (HS), despite their limited representativeness, could help constrain intermediate and large scale modelling errors by means of data assimilation. In this work, we assimilate HS observations from an in-situ network of 295 stations covering the French Alps, Pyrenees and Andorra, over the period 2009-2019. In view of assimilating such observations into a spatialised snow cover modelling framework, we investigate whether such observations can be used to correct neighbouring snowpack simulations. We use CrocO, an ensemble data assimilation framework of snow cover modelling, based on a Particle Filter suited to the propagation of information from observed to unobserved areas. This ensemble system already benefits from meteorological observations, assimilated within SAFRAN analysis scheme. CrocO also proposes various localisation strategies to assimilate snow observations. These approaches are evaluated in a Leave-One-Out setup against the operational deterministic model and its ensemble open-loop counterpart, both running without HS assimilation. Results show that intermediate localisation radius of 35-50 km yield a slightly lower root mean square error (RMSE), and a better Spread-Skill than the strategy of assimilating all the observations from a whole mountain range. Significant continuous ranked probability score (CRPS) improvements of about 13% are obtained in the areas where the open-loop modelling errors are the largest, e.g. the Haute-Ariège, Andorra and the Extreme Southern Alps. Over these areas, weather station observations are generally sparser, resulting in more uncertain meteorological analyses, and therefore snow simulations. In-situ HS observations thus shows an interesting complementarity with meteorological observations to better constrain snow cover simulations over large areas.

1 Introduction

Better monitoring the spatio-temporal variability of the mountainous snow cover is paramount to improve the forecasting of snow-related hazards (Morin et al., 2020) and anticipate downstream river flow (Lettenmaier et al., 2015). In mountainous terrain, the snow cover inherits a high spatial variability from several factors. The topography controls on the precipitation phase, air temperature, wind exposition and radiation fluxes (Durand et al., 1993; Oliphant et al., 2003). Wind drift redistributes snow at every scale (Mott et al., 2018). Finally, vegetation traps the snow (Sturm et al., 2001) and also affects its net shortwave and longwave radiation (Qu and Hall, 2014; Malle et al., 2019).

Snowpack models are commonly used to derive snowpack properties in the mountains. Yet, their ability to represent snow cover variability over large areas is inherently limited by large errors in their meteorological forcings (Raleigh et al., 2015), and uncertain physical parameterisations (Essery et al., 2013; Krinner et al., 2018). In addition, explicitly accounting for processes such as wind drift and snow-vegetation interaction is not yet affordable at large scales.

In that context, additional sources of information are needed to mitigate snowpack modelling uncertainty in the mountains. Observations from weather stations located in the mountains can be used to correct Numerical Weather Prediction (NWP) model outputs. Dedicated downscaling and analysis schemes such as SAFRAN (Durand et al., 1993) or RhiresD interpolation in Switzerland (Frei and Schär, 1998) can be used to efficiently reduce the large errors of the NWP models in the mountains, in particular by the assimilation of local precipitation observations. Such approaches significantly improve snow cover simulations (Durand et al., 1999; Magnusson et al., 2014). These weather stations, however, are generally located below 1200m (Frei and Schär, 1998; Vernay et al., in review), and important errors in precipitations (for example) remain at higher elevations (Magnusson et al., 2014).

Data assimilation of snowpack observations may help address this issue in complement to these observations. Remotely-sensed retrieval of snow bulk properties (e.g. the height of snow (HS, m) and the snow water equivalent (SWE, $\mathrm{kg\ m^{-2}}$)) is a promising wealth of snowpack observations for data assimilation (e.g. Margulis et al., 2019) but it is inherently limited by spatio-temporal gaps (De Lannoy et al., 2012), or only available at coarse resolutions (Andreadis and Lettenmaier, 2006). In-situ observations of HS and SWE cover large mountainous areas and are operational on a daily basis in numerous countries (e.g. Serreze et al., 1999; Jonas et al., 2009; Durand et al., 2009b; Cantet et al., 2019). Their potential to improve local simulations is unambiguous as demonstrated by many studies (e.g. Magnusson et al., 2017; Piazzi et al., 2018; Smyth et al., 2019; Cantet et al., 2019). However, the representativeness of such observations is limited by the snow cover spatial variability (Grünewald and Lehning, 2015; Lejeune et al., 2019). The potential to transfer information into neighbouring areas is therefore a key question when considering their potential added value for snow cover modelling over large domains (e.g. Slater and Clark, 2006; Liston and Hiemstra, 2008; Gichamo and Tarboton, 2019). This question has long been debated. Cantet et al. (2019) successfully applied a spatialised Particle Filter (PF) over a very large domain (Southern Quebec), and with a loose observation network, though not in a rugged terrain, i.e. less spatial variability. In alpine terrain, Magnusson et al. (2014); Winstral et al. (2019) showed that enhancing snow cover simulations with in-situ snow observations from a dense network in Switzerland reduced modelling errors over unobserved locations. It is yet to demonstrate that this approach can be applied over mountainous areas with a

coarser in-situ observational coverage (Largeron et al., 2020).

Here, we investigate whether the assimilation of in-situ HS observations can improve simulations of the Météo-France operational modelling chain for snow cover monitoring and avalanche hazard forecasting in the vicinity of the measurement stations, and what is the most appropriate assimilation strategy for that purpose. We assess this in a network of in-situ HS observations over the French Alps, French Pyrenees, and Andorra, with contrasted observation densities. We use CrocO, an ensemble data assimilation system of snow cover modelling (Cluzet et al., 2021). CrocO is built around an ensemble version of the operational modelling system of Météo-France (Vionnet et al., 2012; Vernay et al., in review), accounting for modelling uncertainties from the meteorological forcings (Charrois et al., 2016; Deschamps-Berger et al., in review) and the snowpack model itself (Lafaysse et al., 2017; Dumont et al., 2020). CrocO includes several versions of the Particle Filter tailored for the propagation of information from observed into unobserved areas (Cluzet et al., 2021). These variants are used in a localised framework, in which only observations coming from a certain radius around the considered location are assimilated (Van Leeuwen, 2009; Penny and Miyoshi, 2016; Poterjoy, 2016; Farchi and Bocquet, 2018). Domain localisation is commonly used in the Ensemble Kalman Filter (EnKF, (Evensen, 1994)) and PF communities (Van Leeuwen, 2009; Poterjoy, 2016; Penny and Miyoshi, 2016; Farchi and Bocquet, 2018). It is used to remove far-range unrealistic correlations in the EnKF (Houtekamer and Mitchell, 2001) and to circumvent the curse of dimensionality, causing the PF to diverge when too many observations are assimilated simultaneously (so-called PF degeneracy) (Bengtsson et al., 2008). PF localisation proved to be efficient in several studies (e.g. Poterjoy and Anderson, 2016; Potthast et al., 2019).

To assess the potential transfer of information, we opt for a leave-one-out approach (e.g. Slater and Clark, 2006), whereby the assimilation is performed considering neighbouring observations, but discarding any local observation. The assimilation performance can be then evaluated using these independent local observations. If such potential transfer could be demonstrated, it would mean that the assimilation method is able to improve simulations at a sufficient distance of available observations to be efficient over the whole simulation domain. In other words, this network of observations could be used to constrain spatialised snowpack simulations over the French Alps, Pyrenees and Andorra. Furthermore, the methodology could be applied to other areas with similar densities of observations.

To summarize, the following questions will be addressed in this paper:

- What is the performance of data assimilation compared with the operational and ensemble models?
- Can data assimilation manage to propagate information in space?
- What is the best localisation strategy for assimilation?
- Could an increased observation density yield better results for assimilation?

The study area, observations, modelling chain and data assimilation scheme are described in Sec. 2. In Sec. 3, the evaluation strategy and scores are presented. The results are presented and discussed in Sec. 4 & 5. We finally conclude and open research perspectives in Sec. 6.

2 Material and methods

2.1 Study area and observations

The study area spans the French sides of the Alps and Pyrenees and Andorra. The French Alps culminate at the Mont-Blanc (4810 m) and are higher and about two times larger than the French Pyrenees (culminating at Vignemale, 3298 m). Andorra is a principality located at the center-East of the Pyrenees. In the following, for the sake of simplicity, we will refer to French Pyrenees and Andorra as "Pyrenees", and to French Alps as "Alps".

The winter climate of the Alps is contrasted between the North and the South. The Southern Alps are on average drier than the Northern Alps (Isotta et al., 2014). The Pyrenees are very elongated with a strong longitudinal gradient between the humid oceanic Western side to the drier Mediterranean Eastern side. The elevation of the winter snow line is around 1500 m in the Pyrenees (Durand et al., 2012), and about 1200 m in the Northern Alps (Durand et al., 2009a). Finally, the inter-annual variability of the snow cover is marked in both massifs (Durand et al., 2009a; Gascoin et al., 2015).

In this work, we perform snowpack simulations in a network of 295 daily HS observations stations. 217 stations are located in the Alps, and 78 in the Pyrenees (of which 7 are in Andorra). This network is an aggregate of several data sources. Most of the observations (144 stations) come from ski resorts, where HS is manually observed every morning during the commercial season (mid-December to April in general). The second source is a network of climatological observations (77 stations) in which several meteorological parameters and HS are observed on a daily basis for the whole year. These stations are generally located around populated areas or in ski resorts. A few sites (19 stations) come from various automated measurements in ski resorts. Two networks of automated HS sensors were also used: Météo-France's Nivôses (27 stations) and Électricité de France (EDF) EDFNIVO stations (28 stations), the latter only from the winter season 2016-2017 on. These networks are located in remote areas and at generally higher altitudes than the rest of the observations.

The density of HS observations within each SAFRAN massif (Fig. 1, see Sec. 2.2.2 for more details on SAFRAN) is very variable, from less than 0.5 daily observations per hundred km^2 in the Extremely Southern Alps and Western Pyrenees to more than ten times higher densities in the Mont-Blanc massif. It is mainly explained by the variable density of ski resorts. Although the density of observations is generally lower than in the Alps, the Pyrenees exhibit two clusters of dense observations, in the Central Western part around Bigorre and in the Central eastern part close to Andorra. In the Alps, the density of observations is especially high from the Northern to the South Central area. The Southern massifs, as well as the lower altitude western massifs generally have fewer observations.

Fig. 2a-c shows the number of observation per month for two representative winters. It increases from 3000 during Fall to 6000 in January-March (when the ski resorts are open), suggesting that the beginning and end of season are less well observed both in terms of number of observations and spatial coverage. Fig. 2b-d shows the histograms of the available daily observations per 300 m-elevation bands for the same years. A notable increase in the observations count above 2100 m for the three

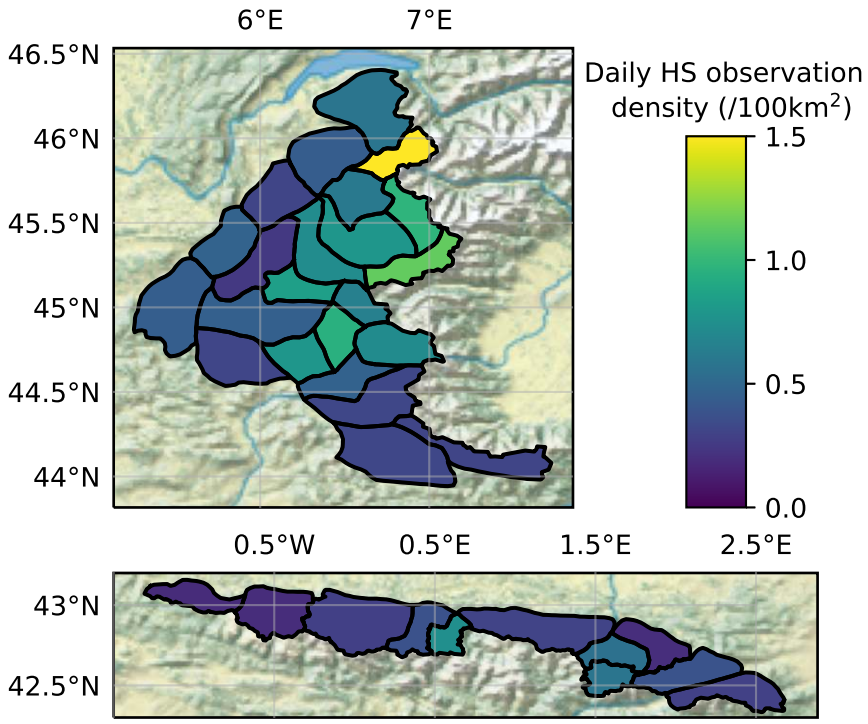

Figure 1. Average daily observation density (per 100 km^2) within each SAFRAN massif, in the French Alps (top panel) and French Pyrenees/Andorra (bottom panel).

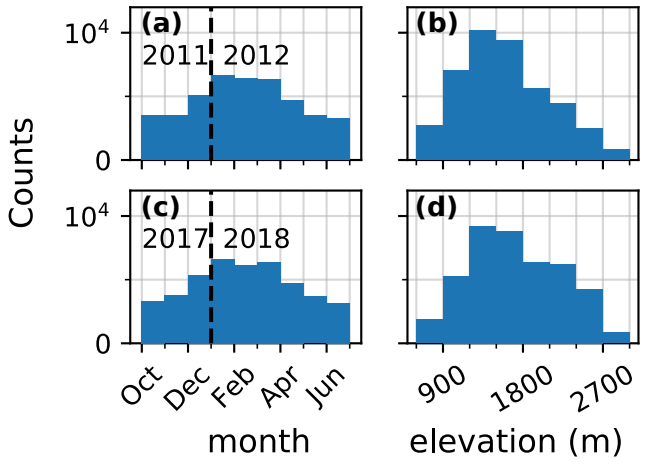

Figure 2. Number of daily observations per month (a-c) and per 300 m elevation bands (b-d) for winters 2011 (239 stations, a-b) and 2017 (250 stations, c-d) over the whole domain.

last years can be explained by the inclusion of the EDFNIVO stations.

2.2 Ensemble data assimilation setup

The ensemble system consists in an ensemble of meteorological forcings generated by stochastic perturbations, forcing a multiphysics ensemble of snow models as described in Cluzet et al. (2020) and Cluzet et al. (2021). The total number of ensemble members (also named particles in the PF context) was set to 160. An open-loop run (i.e. without assimilation) was performed to serve as reference. Only a few changes were performed in the ensemble setup, which are described in Secs. 2.2.1 and 2.2.2.

2.2.1 Ensemble of snowpack models

The simulation setup is based on a multiphysics framework representing the uncertainties of the main physical parameterisations of Crocus (Lafaysse et al., 2017; Cluzet et al., 2020). However, in this paper, the advanced radiative transfer scheme TARTES (Libois et al., 2013, 2015) was not used contrary to previous studies (Cluzet et al., 2020, 2021) because it requires Light Absorbing Particles (LAP) fluxes from chemistry transport models such as MOCAGE, ALADIN or GFDL_AR4 (Josse et al., 2004; Nabat et al., 2015; Horowitz et al., 2020). To date, such products are not interpolated within SAFRAN geometry and would require a specific treatment and validation, going much beyond the scope of this study. Instead, we opted for a single parameterization of the snowpack radiative transfer, the 'B60' option from Brun et al. (1992) presented in Lafaysse et al. (2017), whereby the snow albedo of a layer is a function of its age.

2.2.2 Ensemble of meteorological forcings

Meteorological forcings are taken from SAFRAN (Système D'Analyse Fournissant des Renseignements Adaptés à la Neige, Durand et al. (1993)) reanalysis over the Alps and Pyrenees. SAFRAN is a surface meteorological analysis system adjusting backgrounds from NWP model ARPEGE (Courtier et al., 1991) with local meteorological observations (air temperature, pressure, precipitation, humidity) within so-called massifs of about 1000 km^2 (see Fig. 1) and further downscaled to the stations of our study. Over the considered period of time, 438 observation sites provided precipitation observations to SAFRAN between November and April. These stations are mostly located at lower elevations (below 1500 m) as presented in Fig.4 of Vernay et al. (in review). Among them, 164 of these sites correspond to locations with snow depth observations included in the present study. SAFRAN analysis is issued separately for each massif in a semi-distributed geometry, i.e within 300 m elevation bands, aspect and slopes, the main topographic parameters controlling the snow cover evolution. This analysis is subsequently downscaled into the specific topographic conditions (i.e. elevation, slope, aspect and local topographic mask) of the simulated station (Vionnet et al., 2016). This means that a same analysis is applied to all the points within a same massif, and interpolated consistently with their topographic parameters, while analyses for neighbouring stations located in distinct massifs will be

different.

An ensemble of forcings was generated by applying stochastic perturbations in the same spirit as Charrois et al. (2016) but with slight corrections in the implementation of the perturbations compared with Cluzet et al. (2020, 2021) as described in Deschamps-Berger et al. (in review). For each member, perturbations are auto-correlated in time following an auto-regressive process and are spatially homogeneous. The perturbation parameters were taken from Charrois et al. (2016). Precipitation parameters were adjusted (i.e. multiplicative noise with auto correlation time $\tau = 1500h$, and dispersion $\sigma = 0.5$) in order to obtain a spread-skill close to 1 for the open-loop run (see Sec. 4.1). We used these perturbed analyses as input for the snowpack simulations at the stations.

2.2.3 The Particle Filter in CrocO

The Particle Filter used in this work is based on the version described in Cluzet et al. (2021). Only a brief description of the procedure is given here. The ensemble is updated sequentially with the PF on each assimilation date and propagated forward until the following assimilation date. The PF is localised: each point receives a different analysis. Based on the comparison of neighbouring simulations of HS with their corresponding HS observations, the PF selects a sample of the best ensemble members. The idea is that if a particle is performing well against nearby observations, it should also be efficient locally (Farchi and Bocquet, 2018). Different localisation radius are tested in this study ranging from 17 km to 300 km. Note that when a particle is selected by the PF, the full local state vector is copied: the local physical consistency of the variables is preserved. Particle Filter degeneracy (see Sec. 1) may arise even with a reduced local domain size, and approaches to increase the PF tolerance may be required to overcome it. The localisation is complemented here by two different strategies described in Cluzet et al. (2021), inflation and k-localisation, leading to the 'rlocal' and 'klocal' algorithms, respectively. If the initial analysis is degenerated (i.e. the effective sample size N_{eff} is inferior to a target N^*_{eff}), the rlocal and klocal iteratively modify the assimilation settings to make it more tolerant, so that the PF analysis reaches a sample size of N^*_{eff}. The rlocal algorithm performs an inflation of observation errors inspired by Larue et al. (2018). The klocal algorithm discards observations coming from locations exhibiting the lower ensemble correlations with the considered location. It is important to note that inside a localisation radius, the rlocal method assimilates all available observation stations whereas the klocal method only selects a subset of observations from locations where the ensemble members are sufficiently correlated with the simulation members of the considered point.

2.2.4 Example

This section presents an illustrative example for the propagation of information with the localised PF. On December 3$^{\mathrm{rd}}$, 2009, we perform an analysis at an unobserved point p_{loc} (2135 $\mathrm{m.a.s.l}$) using an observation from a nearby point p_{obs} (2293 $\mathrm{m.a.s.l}$, 7 km away). The top panel of Fig. 3 shows the HS simulated by the 160 ensemble members at the two locations until the

considered assimilation date. The observed HS at p_{obs} is 0.87 m, above the ensemble median at this location (about 0.5 m). The PF will likely select the particles that have above average HS at p_{obs}. The bottom panel of Fig. 3 shows the particles' HS values at p_{obs} as a function of their value at p_{loc}. A correlation can be noted: the particles predicting the highest HS at p_{loc} usually also predict higher than average HS at p_{obs}. It means that the ensemble that we constructed (see Sec. 2.2) considers that the modelling errors are linked: if there is an underestimated snowfall in early December at p_{obs}, it's likely that this is also the case at p_{loc}.

The localised PF performs an analysis for p_{loc} by comparing the values modelled at p_{obs} with the available observation, thereby selecting the 'best' particles at p_{obs}, (bottom panel, in green). The marginal distribution of the ensemble at p_{obs} (right of the bottom panel, in green) is significantly sharpened compared to the background, and is much closer to the observation. At p_{loc}, the distribution of the HS values of these particles is also sharper, and exhibits higher HS than before the analysis.

This example shows how the localised PF has used the non-local observation at p_{obs} to infer information about the local unobserved point p_{loc}. This example can be generalized to the situation where multiple observations are assimilated simultaneously as done in this study. It also highlights the implicit importance of ensemble correlations with distant locations: in the absence of correlation, no information can be transferred. In such a situation, the klocal algorithm would discard the observations from the least areas, while the rlocal would keep them. Finally, note that if the ensemble correlation is dramatically wrong, (i.e. positive correlation instead of negative correlation), the analysis will degrade the ensemble performance.

3 Evaluation strategy

This work aims at assessing the potential transfer of information between points in an HS observation network by means of localized data assimilation, and more specifically to address the questions presented in the end of Sec. 1. To demonstrate that, the data assimilation system must over-perform its ensemble counterpart with the assimilation switched off (open-loop) and the state-of-the-art operational deterministic snow cover modelling system from Météo-France (oper), which consists in a default Crocus version forced by the unperturbed SAFRAN meteorological forcings (Vernay et al., in review).

3.1 Setup

Assessing the ability of data assimilation to propagate information requires use independent data for validation. We opted for a leave-one-out setup in which local observations are removed from the set of observations used in the local PF analysis. Only weekly observations were assimilated, while all available observations between October 1st and June 30th were kept for evaluation.

There are two key design parameters for the data assimilation system: the value of the localisation radius (large or small) and the choice of the PF algorithm (rlocal or klocal). Both exert a direct or indirect control on the number of observations simultaneously assimilated by the PF, and therefore, on its potential degeneracy and its ability to transfer information between locations. Experiments respectively combining the rlocal and klocal algorithm with 4 different localisation radius were conducted: rang-

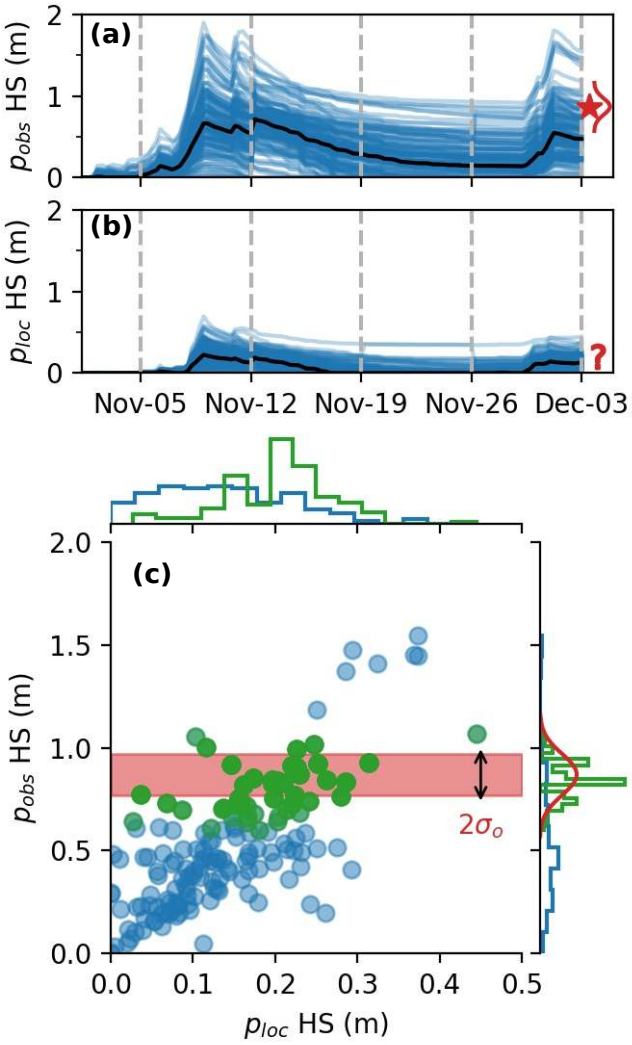

Figure 3. Ensemble HS simulation at the observed location p_{obs} (a) and the unobserved point where we want to perform the local PF, p_{loc} (b). The median (black), assimilation dates (dashed grey lines) and the available observation on December 3rd (red star, and probability density function (PDF) in red) are also represented. Panel (c) is a scatter plot of the ensemble members at the two locations, for the background (blue) and analysis (green, superimposed on the blue). Marginal distributions at the individual locations are added at the top and right side of the plot. The observation PDF is shown on the right side, with a red band showing the $\pm 1\sigma$ range around the observation.

ing from 17 km, (the radius of an idealised circular SAFRAN massif of 1000 km^2) to 300 km (the maximal distance between two observations inside the Pyrenees and the Alps) with two intermediate radius of 35 km and 50 km. The standard deviation of observation errors was set to 0.1 m, as a way to accommodate for measurement and representativeness errors.

Because the klocal approach does not use inflation (except in the case of degeneracy with only one observation), it is quite

sensitive to the initial value of observation error. In case of degeneracy, the smaller the observation error, the fewer observations will be selected by the klocal algorithm. For this reason, the klocal algorithm was run with a multiplication factor of 5 on observation error variance (hence a fixed error standard deviation of $0.22\ \mathrm{m}$) , allowing more observations to be assimilated simultaneously.

3.2 Evaluation Scores

Several metrics are used in this work to assess the performance of the oper, open-loop and assimilation runs with respect to HS observations. From the ensemble $E_{m,p,t}$ of N_e members m at station p and time t, the mean can be computed using Eq. 1:

$$\overline{E}_{p,t} = \frac{1}{N_e} \sum_{m=1}^{N_e} E_{m,p,t} \tag{1}$$

The mean is a convenient way of synthesizing ensemble properties for evaluation, however, some artifacts can be observed with bounded variables such as HS. On a decaying snow cover for example, the mean will not reach zero until every member has melted. For this reason, the ensemble median $\tilde{E}_{p,t}$ will be preferred in the following. From $\tilde{E}_{p,t}$, we can compute the Absolute Error of the ensemble median compared with the observations $o_{p,t}$ (AE):

$$AE_{p,t} = |\tilde{E}_{p,t} - o_{p,t}| \quad \forall (p,t) \in [1, N_{pts}] \times [1, N_t] \tag{2}$$

Where N_t is the number of evaluation time steps.

The ensemble bias is defined as the average difference between the ensemble median and the observations (Eq. 3):

$$\text{bias} = \frac{1}{N_t} \frac{1}{N_{pts}} \sum_{t=1}^{N_t} \sum_{p=1}^{N_{pts}} \tilde{E}_{p,t} - o_{p,t} \tag{3}$$

The Root Mean Squared Error of the median (RMSE) is computed from the AE, following (Eq. 4):

$$\text{RMSE} = \sqrt{\frac{1}{N_t} \frac{1}{N_{pts}} \sum_{t=1}^{N_t} \sum_{p=1}^{N_{pts}} AE_{p,t}^2} \tag{4}$$

Bias and RMSE can be computed for the oper run (treating it as a single-member ensemble) in order to evaluate the median performance, and can be taken over time and/or space by dropping the time/spatial mean in Eqs.3 and 4. These scores are not sufficient because they reduce an ensemble to its median. The ensemble spread (or dispersion) σ (Eq. 5), defined as the average variance, is a first metric to assess an ensemble reliability:

$$\sigma = \sqrt{\frac{1}{N_t} \frac{1}{N_{pts}} \frac{1}{N_e} \sum_{t=1}^{N_t} \sum_{p=1}^{N_{pts}} \sum_{m=1}^{N_e} (E_{m,p,t} - \overline{E}_{p,t})^2} \tag{5}$$

Reliability is a desirable property for an ensemble, it means that all events are forecast with the right probability regardless of the probability value. The pdf of a reliable ensemble matches the actual pdf of observations over a large enough sample. We

introduce the Spread-Skill (SS) as:

$$SS = \frac{\sigma}{\text{RMSE}} \tag{6}$$

Where sigma must be computed only in the dates and locations where the RMSE is computed. For a reliable ensemble, we have $\sigma \sim$ RMSE (Fortin et al., 2015), i.e a spread-skill close to unity (necessary but not sufficient condition). This means that the spread is on average a good estimate of the modeling error, which is useful to make decisions. Rank diagrams (Hamill, 2001) are the histogram of the position of the observation within the ensemble and enable to verify the reliability of an ensemble more closely (e.g. Bellier et al., 2017). Their flatness is a stronger condition for an ensemble's reliability than the SS=1.

The Continuous Ranked Probability Score (CRPS, (Eq. 7) Matheson and Winkler, 1976) is an aggregate, ensemble score evaluating the reliability and resolution of an ensemble based on a verification dataset. An ensemble has a good resolution when it is able to issue different forecasts on different events (contrary to the climatology) (Atger, 1999).
If we denote $F_{p,t}$ the Cumulative Distribution Function (CDF) and $O_{p,t}$ the corresponding observation CDF (Heaviside function centered on the truth value), the CRPS is computed at (p,t) following:

$$\text{CRPS}_{p,t} = \int_{\mathbb{R}} (F_{p,t}(x) - O_{p,t}(x))^2 dx \quad \forall (p,t) \in [1, N_{pts}] \times [1, N_t] \tag{7}$$

The CRPS skill score (CRPSS) is commonly used to compare the performance of an ensemble E to a reference R. Although CRPS can be computed from a deterministic run, R should be preferably an ensemble because comparing CRPS of deterministic and ensemble runs mainly illustrates the obvious fact that an imperfect deterministic run is a poor representation of a probability distribution. The following equation is frequently used:

$$\text{CRPSS*}(E,R) = 1 - \frac{\text{CRPS}(E)}{\text{CRPS}(R)} \tag{8}$$

In this formulation, if E is more skillful than R, CRPSS*(E, R) will be positive, with a perfect score of 1., while less skillful scores range between $-\infty$ and 0, resulting in an asymmetry between positive and negative scores (i.e. $\text{CRPSS*}(E,R) = \frac{\text{CRPSS*}(R,E)}{\text{CRPSS*}(R,E)-1}$). We introduce the new formulation:

$$\begin{cases} \text{CRPSS}(E,R) = 1 - \frac{\text{CRPS}(E)}{\text{CRPS}(R)} & if\ \text{CRPS}(E) < \text{CRPS}(R) \\ \text{CRPSS}(E,R) = \frac{\text{CRPS}(R)}{\text{CRPS}(E)} - 1 & otherwise \end{cases} \tag{9}$$

With such formulation, CRPS(E,R) $\in [-1, 1]$ and CRPS(E,R) = - CRPS(R,E). These properties are important to visually compare and average improvements (positive CRPSS) and degradations (negative CRPSS) of the CRPS.

	oper mean (m)	oper RMSE (m)	oper bias (m)	open-loop RMSE (m)	open-loop sigma (m)	open-loop bias (m)	openloop SS
2009	0.28	0.27	−0.02	0.28	0.28	−0.04	1.02
2010	0.16	0.22	−0.01	0.21	0.18	−0.03	0.85
2011	0.26	0.26	−0.05	0.28	0.26	−0.10	0.92
2012	0.44	0.37	−0.03	0.39	0.38	−0.11	0.98
2013	0.32	0.31	0.01	0.32	0.29	−0.06	0.92
2014	0.23	0.26	0.01	0.26	0.23	−0.03	0.89
2015	0.24	0.27	0.01	0.27	0.25	−0.01	0.92
2016	0.20	0.27	−0.02	0.27	0.19	−0.07	0.70
2017	0.41	0.41	−0.09	0.45	0.31	−0.16	0.70
2018	0.23	0.31	−0.07	0.33	0.19	−0.12	0.56

Table 1. Yearly performance of the reference runs, in terms of RMSE, bias, spread (sigma), and spread-skill (SS).

4 Results

4.1 Performance of the reference runs

The operational deterministic run from Météo-France suffers from significant errors (Lafaysse et al., 2013), which we try to reduce by means of assimilation. The open-loop run is a first step to represent modelling uncertainty using an ensemble. Tab. 1 summarizes the yearly performance of both simulations over the 10 years and the 295 stations. Oper and open-loop simulations exhibit almost identical RMSE scores across all years, with an average error of about 0.2-0.3 m. Their RMSE significantly varies (from 0.21 m in 2010 to 0.45 m in 2017 for the open-loop) in proportion with the yearly average snow depth. Oper and open-loop are slightly negatively biased, especially for the open-loop.

Regarding ensemble metrics, the open-loop exhibits Spread-Skills (SS) around 0.9-1 (SS is obtained by dividing the σ column by the RMSE column in Tab. 1). SS ranges from a good balance between spread and RMSE in 2009 (SS=1.) to under-dispersive values (e.g. SS=0.55 in 2018) in the three last years. In Fig. 4, yearly rank diagrams exhibit higher frequencies in their right part, meaning that observations lie preferentially in the upper half of the ensemble, consistently with the negative biases exhibited in Tab. 1.

A map of the open-loop bias for each station is shown in Fig. 5. The bias is significantly negative in most locations, and its spatial variability is high, with neighbouring stations exhibiting strong biases of opposite signs, e.g. in the Central Alps. Around Andorra and in the Southern Alps the bias is mostly negative. Some stations exhibit positive biases in the Central Alps, more rarely in the Pyrenees.

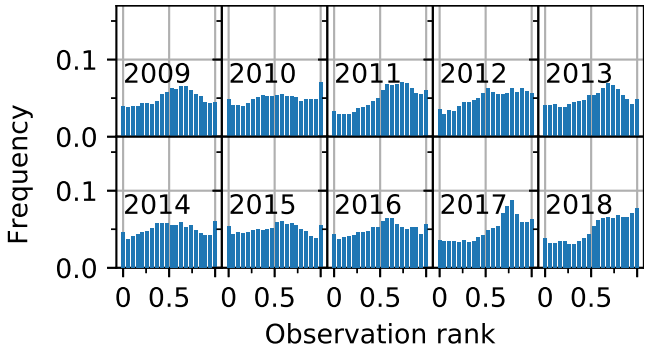

Figure 4. Yearly rank diagrams of the open-loop, binned into 20 bins (i.e. for a reliable ensemble, all bars should be on the 0.05 line). Values on the x-axis correspond to the proportion of ensemble members under the observation.

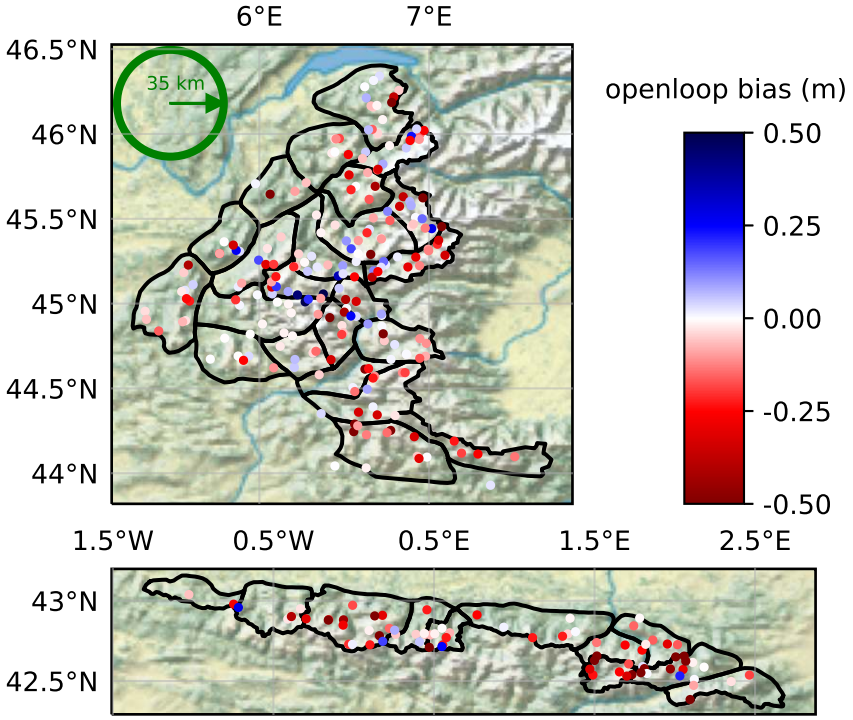

Figure 5. Map of the open-loop bias (m) on each station over the ten considered years (same layout as Fig. 1). SAFRAN massifs are outlined in black. The green circle has a radius of approximately 35 km.

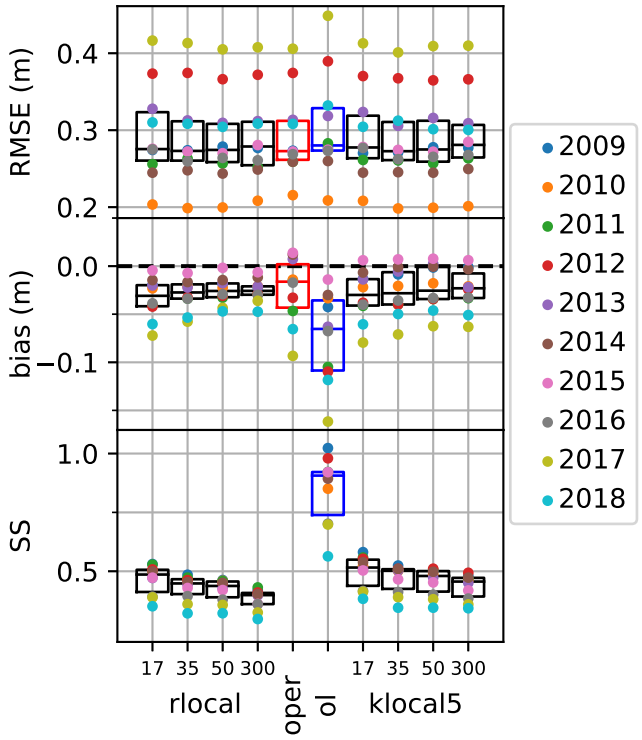

Figure 6. Yearly scores of RMSE (top panel), bias (middle) and Spread-Skill (SS, bottom), for the assimilation experiments compared with the oper and open-loop (ol) scores from Tab. 1. On the background are displayed the corresponding boxplots and medians (black bars).

4.2 Overall results of the assimilation experiments

In this work, we want to compare the performance of the rlocal and klocal algorithm, with different localisation radii (ranging from 17 km to 300 km) with the oper and open-loop runs. Fig. 6 shows the yearly values of RMSE, bias and SS for all these runs. Results show no significant RMSE improvements for the assimilation runs compared with the references. RMSE varies more from one year to another than between assimilation configurations (algorithm and localisation radii). The median RMSE is slightly lower for the intermediate localisation radii of 35 km and 50 km. Compared with the open-loop, assimilation runs significantly reduce the bias both in terms of median value from around -0.06 to about -0.03 and inter-annual variability. Compared with the oper run, the absolute bias of the assimilation runs is higher on average, but in some years, the bias is significantly reduced (e.g. 2015, 2017, 2018).

In terms of SS, the assimilation runs exhibit values almost twice as small as the open-loop run which has a median value around 0.85. The SS significantly decreases with an increasing localisation radii both for the rlocal and klocal algorithm. The assimilation strategy without localisation (radii of 300 km) appears as most efficient in reducing biases (lower absolute

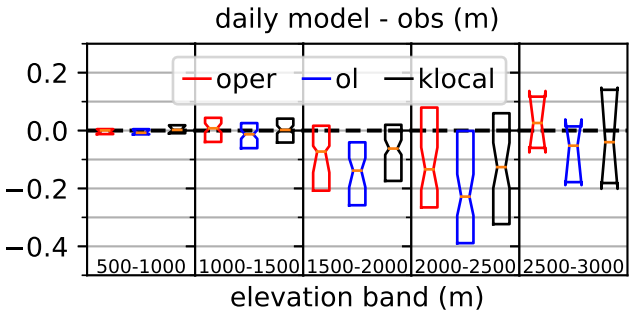

Figure 7. Notched boxplots of the daily difference between modelled and observed values (over the 10 years) of the oper (red), open-loop median (blue) and klocal:35km median (black), by 500 m-wide elevation bands. Occurrences when the three differences are equal to zero are excluded.

median, lower inter-annual variability) but yields the lowest spread-skills and highest RMSE of all the assimilation runs suggesting that this approach is not the most desirable. The most selective localisation strategies (radii of 17 km) achieve the highest SS, but their inter-annual performance variability is higher than for the other localisation radii.

4.3 Factors of variability of the assimilation skill

In the following, we will investigate the different factors influencing the skill variability of the assimilation runs. As described in the previous Sec. 4.2, there are only small skill differences between the localised radii of 17-50 km, and between the rlocal and klocal algorithm. For the sake of illustration, we decided to focus on the assimilation configuration yielding the lowest median RMSE. This configuration, the klocal with a 35 km localisation radii, is further referred to as 'klocal' configuration.

4.3.1 Spatial variability

Fig. 7 shows boxplots of the daily deviation values (difference between the model median $\tilde{E}_{p,t}$ and the observation $o_{p,t}$) for the klocal and the reference runs grouped per 500 m elevation classes. The bias of the oper varies from slightly positive values between 1000-1500 m to negative values in the range 1500-2500 m to finally a positive bias at the highest elevations. The open-loop exhibits a similar pattern, with a negative shift. The klocal algorithm seems to temper these elevation biases, with lower biases (in absolute value) than the oper both at higher and intermediate elevations.

Fig. 8 shows the CRPSS of the klocal (using the open-loop as reference) at each station, over the ten years. Overall performance is only slightly positive (blue), but with a non negligible minority of station showing negative CRPSS (red color) denoting a degradation of performance. Some "clusters" of good performance also appear, as in the Central-Eastern part of the

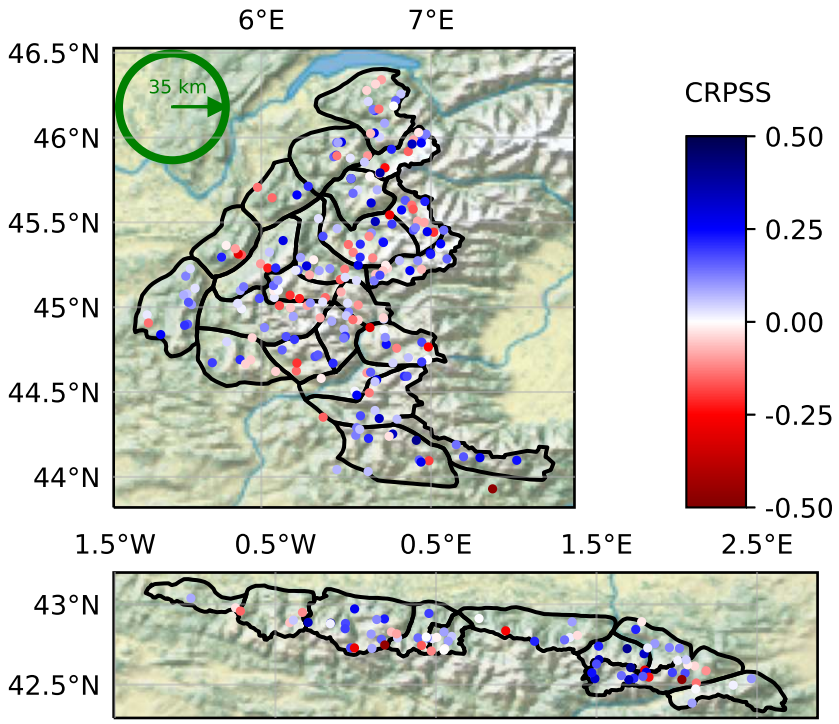

Figure 8. Same as Fig. 5, showing the CRPSS of the klocal against the open-loop over the ten years.

Pyrenees (Andorra and Haute Ariège) or the Southern Alps, while the performance in the Central Alps and Central Western Pyrenees seems poor.

Fig. 9a represents the CRPSS as a function of the station elevation. On average, the analysis exhibits positive CRPSS (between 0. and 0.15) showing that it is more skilful than the open-loop. CRPSS values exhibit a significant spread (of about 0.2) which results in a number of stations with a degradation of skill by the analysis (negative CRPSS). The average CRPSS varies with the altitude, increasing from a very low skill (0.-0.03) in the range 1000-1500 m to a significant skill (0.1-0.15) between 1600-2000 m, and finally decreasing to about 0.05 above 2000 m.

Given the strong link between the bias of the open-loop reference and the elevation, the CRPSS was also plotted against the bias of the open-loop in Fig. 9b. The CRPSS exhibits significant averaged positive values (0.13-0.2) for strong negative biases, under -0.1. The CRPSS varies from null performance around null bias to significant negative performance for positive biases (-0.12).

The density of available observations was identified as an important factor for the success of the assimilation of in-situ measurements (Winstral et al., 2019; Largeron et al., 2020). We define the observation density as the average number of ob-

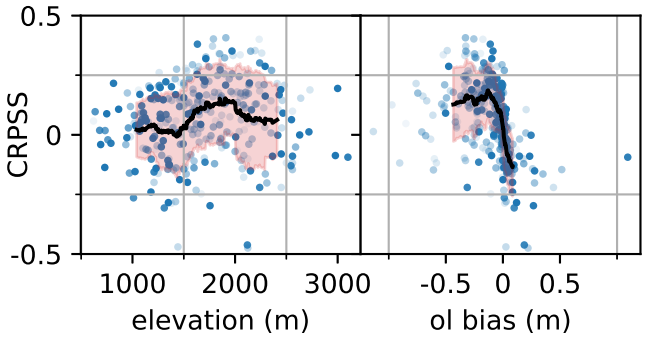

Figure 9. Scatter plot of the CRPSS of the klocal run compared with the open-loop for each station over the 10 years, as a function of the station elevation (left panel) and the open-loop bias at each station (right panel). The transparency of the points is related to the proportion of available observations over the validation period. The black line denotes a 51-stations-wide CRPSS rolling average, with an orange shading $\pm 1\sigma$. This average is weighted proportionally to each station transparency.

servations available on each analysis date, divided by the area of the localisation disk. Fig. 10a shows the values of CRPSS as a function of the observation density. CRPSS values are rather spread, and do not seem to vary much with the observation density. On Fig.10 (bottom panel), the open-loop bias is also plotted against the observation density, showing that the highest biases are obtained for the lowest observation densities, although there cannot be any causal relationship as HS observations are not assimilated in the open-loop.

4.3.2 Temporal variability

Timeseries of ensemble bias can also provide information on their nature and origin. Fig. 11 shows the timeseries of domain wide ensemble median $\tilde{E}$ against the bias and SS of the several runs in 2009. This year is representative of the different runs behaviours over the 10 years. The bias of the oper run is negative except in April during the melting season. During this year, the bias of the klocal run is centered on zero from mid-January to the end of April. The open-loop is negatively biased for the whole season. Consistently, the ensemble median is the highest for the klocal run. The most interesting feature here, is that the biases of all the simulations are increasing (in absolute value) on several drops, coinciding with increases in $\tilde{E}$ during solid precipitation events (e.g. early December, first week of February, late March). The bias difference between the klocal and the open-loop (in mauve) shows the ability of the former to reduce this bias. This reduction is stepwise, with the strongest reductions occurring on analyses (dashed vertical lines) during the accumulation period (e.g. early December, and the two first analyses of January). Between the analyses, and during the melting season, the time evolution of the klocal bias follows the time evolution of the open-loop bias, and the bias difference remains more or less constant.

The SS is an estimate of the ability of ensemble systems to assess their errors (see Sec. 3). Here, consistently with Sec. 4.2 and Fig. 6, we note that throughout the season, the SS of the klocal is less than to 1 and significantly lower compared to the

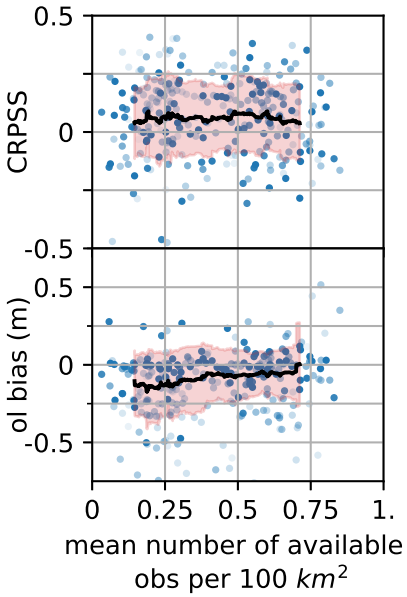

Figure 10. CRPSS of the klocal PF as a function of the average density of available observations (top), and open-loop bias as a function of the average density of observations (per $100km^2$) (bottom)

open-loop. While the SS is similar in both simulations in the early season, klocal analyses seem to coincide with reductions of SS, suggesting that the ensemble spread is more reduced than its error (RMSE) by the PF. In line with the assessment of the reliability, Fig. 12 shows the rank diagrams of the klocal over the 10 years. Compared with the results of the open-loop on Fig. 4, these rank diagrams exhibit a U-shape, consistent with the significant under-dispersion of the klocal. Indeed, by summing the left and right bin frequencies, we observe that the observations lie about 20% of the time in the extremal bins of the rank diagram (twice as much as for a reliable ensemble), and preferentially above, which is consistent with the residual negative bias of the klocal simulation.

5 Discussion

In the following, we analyse the strengths and weaknesses of the operational and open-loop simulations and comment on the performance of the data assimilation algorithms in comparison to them.

5.1 On the performance of the reference simulations

The performance of the operational simulation has been regularly assessed until recently (Durand et al., 2009a; Vernay et al., in review). Overall, it is an accurate modelling system whose potential has been demonstrated in several recent climate studies and projections (e.g. López-Moreno et al., 2020; Verfaillie et al., 2018). However, it exhibits a contrasted regional performance

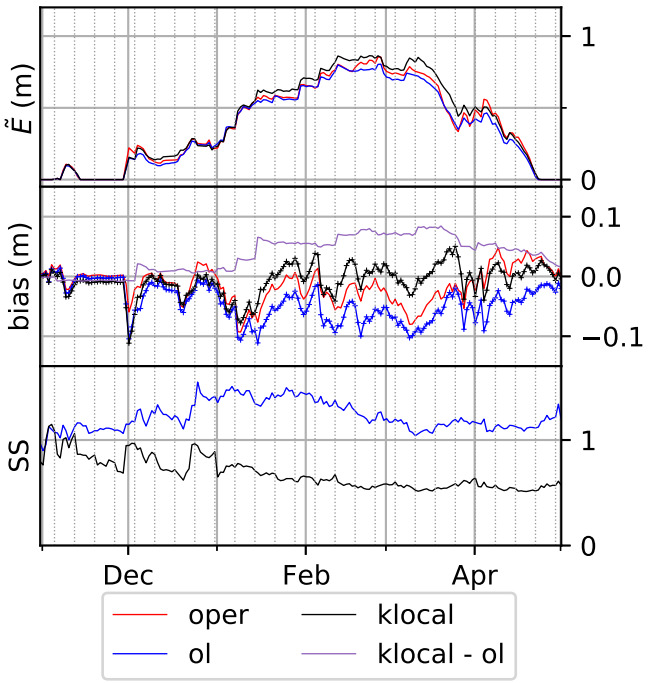

Figure 11. Time series of domain averaged ensemble median ($\tilde{E}$) (top), bias (center) and Spread-Skill (SS, bottom) for the winter season 2009-2010, for the oper (red), open-loop (blue) and klocal (black). The bias difference between the klocal and the oper is also plotted in mauve in the middle panel. Vertical dashed lines correspond to the assimilation dates. The onset (October) and late season (June-July) are not plotted for the sake of clarity.

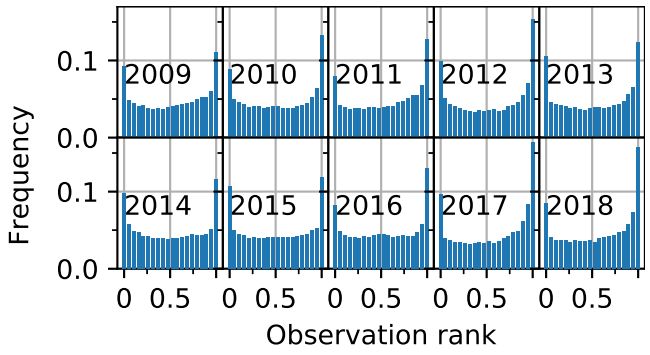

Figure 12. same as Fig. 4 for the klocal.

(Vernay et al., in review, Fig. 13), and its errors are badly known at high altitude, due to the lack of observations (Fig. 12 of Vernay et al. (in review)). This is a common issue in mountainous areas (Frei and Schär, 1998) and is detrimental for the use of the operational chain for all applications (e.g. avalanche hazard forecasting, hydrology etc.).

Results from Tab. 1 shows that the operational version of the system, and its ensemble version, the open-loop, have comparable

RMSE. The open-loop run is reliably accounting for its modelling uncertainties and errors, since its SS is slightly below unity over the ten years. This means that on average, the ensemble spread is almost a reliable estimate of the modelling error. This feature could be valuable for forecasters (Buizza, 2008).

Tab. 1, and Figs. 6 and 11 show that the open-loop is negatively biased compared to the oper. This could be due to the centered stochastic perturbations (Charrois et al., 2016; Deschamps-Berger et al., in review), or a bias in the ESCROC multiphysics model configurations (Lafaysse et al., 2017). However, the oper model configuration is not expected to be perfectly centered in the open-loop, as several configurations, such as the parametrization of surface heat fluxes, ground heat capacity or fresh snow density strongly influence the resulting modelled snow depth. Strong increases in the oper and open-loop biases match with precipitation events, and they are only partly compensated by the following snow settling period (see Sec. 4.3.2), suggesting that it is likely that error compensations take place in the oper chain, between solid precipitation amounts, fresh snow density, snow compaction, and ablation processes as suggested by results from Quéno et al. (2016). Evaluation with co-located SWE and HS data would help disentangle this situation (e.g. Smyth et al., 2019).

Biases of the oper and open-loop strongly depend on the altitude (Fig. 7) in a pattern that matches the evaluation from Vernay et al. (in review), though on a smaller number of stations and considered years. They are unambiguously negative in the range 1500-2500 m, and more variable above, probably due to a higher snow cover variability, and depending on the considered region. In the range 1500-2500 m, this bias may be explained by higher wind speeds than at lower elevations, causing an underestimation of solid precipitation amounts in gauges (Kochendorfer et al., 2017), and consequently in SAFRAN, as evidenced by (Quéno et al., 2016) during strong precipitation events.

5.2 On the PF strategies

In general one of the primary motivations of the domain localisation is to prevent the PF from degenerating (Farchi and Bocquet, 2018). In our case, as evidenced by the reasonable performance of the rlocal with a 300 km localisation radii (e.g. therefore simultaneously assimilating up to 217 observations in the Alps), domain localisation is not required against PF degeneracy thanks to the mitigations (i.e. inflation or k-localisation) developed in Cluzet et al. (2021). Here, localisation is rather used to adapt to the structures of errors of the reference run. From Fig. 5, it seems that open-loop bias is systematic and widespread. Then a large localisation radii, averaging a significant number of observations, seems a good option. However, we also see regional structures in this bias, probably inherited from the oper (Vernay et al., in review). They are likely due to the fact that SAFRAN analyses are performed at the scale of the massif. To address this type of error, reducing the localisation radii is probably a better option. Finally, errors structures can depend on other parameters such as the elevation, and vary in time. In this situation, the klocal approach might be more adapted, since it adjusts the observation selection on the model background correlation patterns. However, these background correlation patterns could sometimes be unrealistic, and therefore, misleading for the algorithm.

The klocal algorithm, by construction, selects observations from locations that are correlated in the model's point of view. However, because we apply spatially homogeneous perturbations to the meteorological forcings, strong large scale background correlation patterns are present in the open-loop, even between the Alps and Pyrenees (not shown). These strong, potentially artificial, large scale correlation patterns could hamper the performance of the klocal PF, leading it to assimilate very distant observation with no actual link with the considered location. Conversely, a completely random field of perturbations would prevent the algorithm from propagating any information between locations (Magnusson et al., 2014; Cantet et al., 2019). Using physically-based meteorological ensemble, such as PEARP (Descamps et al., 2015), used in Vernay et al. (2015) or AROME-EPS (Bouttier et al., 2016), or spatially correlated perturbation fields (Magnusson et al., 2014), could lead to more realistic correlation fields, but this goes much beyond the scope of this study, as actually, domain localisation prevents the klocal from assimilating too distant observations.

5.3 Overall performance of the assimilation compared with the references

Here, we discuss the ability of the proposed assimilation approaches (with several localisation radii) to succeed in reducing the modelling errors from the oper and open-loop shown in Sec. 5.1. Aggregated results from Fig. 6 show that none of the proposed assimilation configurations enable us to significantly reduce overall modelling errors compared to the operational run. However, they overcome the significant negative bias of the open-loop they originate from, but at the expense of a strongly under-dispersive spread-skill. The bias reduction seems more efficient and stable (i.e. less variable from year to year) with the rlocal than with the klocal, and with a larger localisation radii, which makes sense as the open-loop bias is widespread (e.g. Fig. 11) and both tend towards assimilating more observations at the same time. However, the RMSE is slightly larger for the largest localisation radii, and the spread-skill is strongly reduced too.

There are two reasons why the assimilation could not outperform the operational run in terms of RMSE. First, its error may be of a same magnitude than the natural variability of point scale observations and in that case, no added value can be extracted even from nearby observations, or similarly, there are too few observations to efficiently constrain modelling errors. Increasing the observation density could be an option to overcome this issue. However, our results do not show a strong relationship between assimilation skill and density (Fig. 10, see Sec. 5.5 later on). Another explanation could be that there still remain systematic errors to correct, namely biases (as suggested by Fig. 7) but it is difficult to propagate information between locations. In an idealised case, (Cluzet et al., 2021) showed that the potential to propagate information from HS observations across elevations is limited. Here, modelling errors are not systematic and strongly vary with the altitude (Fig. 7). If the ensemble does not account for this specific bias structure, an observation at an elevation affected by a positive bias could never help choose the best member configuration for an elevation affected by a negative bias.

5.4 On the difficulties faced by assimilation algorithms

In this part, we comment the performance of the klocal with a localisation radii of 35 km assimilation configuration against the open-loop. Although it does not outperform other configurations significantly, the klocal seems best suited to solve the bias-elevation relation in the references and an intermediate localisation radii enables to adapt to local error structures (see Sec. 5.2).

The CRPS improvement is the highest for intermediate elevations coinciding with the highest open-loop negative bias (Fig. 9, the latter being consistent with Cluzet et al. (2021) who showed that the largest improvements were obtained in the presence of systematic biases.

However, the klocal is strongly underdispersive, contrary to the open-loop which achieves a SS around 1, and therefore is significantly less reliable as evidenced by the U-shaped rank diagrams in Fig. 12. As the CRPS is a measure of both accuracy and reliability, it seems surprising to see that the klocal is more skilful than the open-loop in terms of CRPS, with average positive CRPSS around 0.06 (Fig. 9).

This under-dispersion is not satisfactory because it implies that the assimilation run is too confident about its simulated distributions. This is a general issue for all the presented assimilation strategies (Fig. 6). In additional experiments (not shown), the assimilation frequency was reduced to 14 days, in order to let the ensemble spread increase between assimilation dates. It seems a reasonable value according to e.g. Smyth et al. (2020) and Viallon-Galinier et al. (2020), and resulted in an increased spread, but was detrimental to the RMSE. We did not consider increasing the target efficient sample size, N^*_{eff}, which is set to 100. This value, is much higher than previous studies (Larue et al., 2018; Cluzet et al., 2021) and was chosen as preliminary experiments (not shown) with values of 25 and 50 which gave an even lower SS. Finally, the spread of the stochastic perturbations on the forcings could be increased, or statistically calibrated distributions of the main forcing variables (e.g. Taillardat and Mestre, 2020) could be used.

Nevertheless, obtaining a perfect spread-skill may be a challenging goal for our assimilation system. Under dispersion is a common issue in the NWP (e.g. Bellier et al., 2017) and snow cover modelling communities (Lafaysse et al., 2017; Nousu et al., 2019). The spatial scale of our ensemble modelling framework cannot account for two important processes affecting the observations at the stations: the variability of the meteorological conditions inside SAFRAN massifs, and the snow redistribution by wind (Mott et al., 2018). On the one hand, the variability of the meteorological conditions inside SAFRAN massifs is limited to topographic parameters (including local masks) so that two distant stations with the same topography will receive the exact same forcing (especially precipitation), and the snow redistribution by wind is not represented (Vionnet et al., 2018). On the other hand, the spatial representativeness of observations is limited by plot-scale variability.

Data assimilation is known to partly compensate for such scale mismatches via error compensation. Error compensations are also possible between physical processes (Klinker and Sardeshmukh, 1992; Rodwell and Palmer, 2007; Wong et al., 2020). For example, an ablation event in one observation can be compensated in the Particle Filter by selecting some members with a lower precipitation factor or a compaction scheme with a higher settling (Deschamps-Berger et al., in review). This compensation

immediately results in lower errors, but implicitly, the model does a wrong assumption, which results in being over confident, thus with a lower spread. The only way to mitigate for this over confidence is to account for any relevant physical phenomenon, which is a desirable goal, but a real challenge when it comes to snowdrift by wind, local meteorology and plot-scale variability. This goal is to date out of reach at the temporal and spatial scale of this study.

Despite these limitations, the assimilation shows some ability to correct weaknesses of the reference runs. The first one is the significant bias above 1500 m in the reference run (Fig. 7). This bias probably originates from a lack of meteorological observations in SAFRAN analysis at those altitudes (see Sec. 5.1 and Fig. 4 of (Vernay et al., in review)). In the range 1500-2000 m, the klocal has a significantly lower bias than the open-loop. There is a lower benefit at higher elevations, above 2000 m. (Fig. 9), maybe owing to the fact that snow cover variability is higher, in particular due to stronger winds. There are also less observations available, and a less clear bias at this altitude (there seems to be a transition from a negative bias to a positive bias), reducing the odds of a successful assimilation. Unfortunately, such elevations are key for avalanche activity (Eckert et al., 2013; Lavigne et al., 2015). Another good feature of the assimilation is to improve the accuracy in areas where the references are less accurate due to a lack of meteorological observations, namely Andorra and Haute-Ariège in the Pyrenees, and Ubaye, Haut Verdon and Mercantour in the southern Alps (Fig. 8). Both features underline the complementarity between HS observations and the meteorological observations already assimilated in SAFRAN.

5.5 Performance in relation to the density of observations

The density of in-situ observations has been pointed out as a critical parameter for the success of data assimilation (Largeron et al., 2020). Winstral et al. (2019) managed to strongly reduce modelling errors with a high observation density, (about 1 observation site every 100 km^2). Because of natural variability, they considered detection of systematic errors may be more difficult with a lower density. Our study case explores a wide range of observation density (Fig. 10), from about 0.1 to 0.8 observations every 100 km^2 (accounting for the availability of observations). Yet, as mentioned in Secs. 4.2 and 5.1, the assimilation performance relative to the open-loop does not decrease with a lower observation density. It may be due to the fact that the assimilation is efficient only for strong open-loop negative biases (Fig. 9b), which seems the highest where the station density is the lowest (Fig. 10b). In other words: the assimilation can not outperform the open-loop in the most densely observed areas (e.g. in the Northern Alps, where the observation density is similar to the studies of Magnusson et al. (2014) and Winstral et al. (2019)) because the open-loop performance is already high there. This behaviour is explained by the fact that the HS observation density is correlated with the density of precipitation observations used by SAFRAN to analyse the meteorological forcings (see Fig. 13 and Sec. 2.2.2)). Both (at the exception of the Nivôse and EDF nivo stations for the HS observations) are actually related to human implantation in the valleys and the presence of ski resorts. A higher weather station density for SAFRAN is likely to result in more accurate meteorological forcings, thus reducing the bias of the reference runs, which finally leaves less room for improvement by the assimilation.

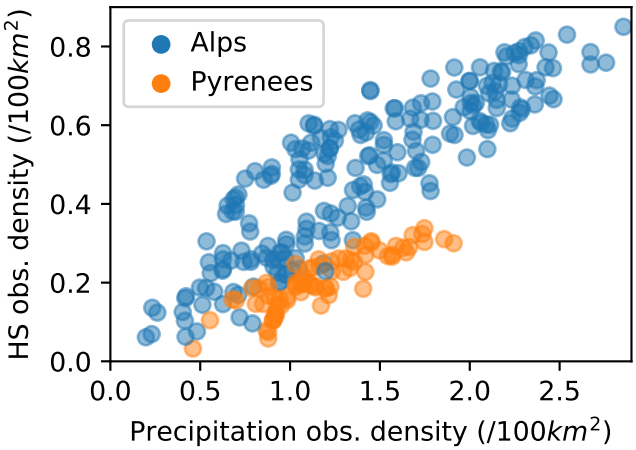

Figure 13. same as Fig. 4 for the klocal.

This assumption may guide the strategies of definition of snow cover networks, not only in terms of observation density but also in terms of localisation. Our study suggests that snowpack observations do not yield significant improvements in areas where a sufficient amount of meteorological observations is already assimilated in the snowpack modelling chain (here, in SAFRAN). The assimilation of snow depth observations rather gives significant improvements at higher altitudes, and in areas where model errors are larger, generally corresponding to areas where less meteorological observations are assimilated. This result could be verified in future work, in either semi distributed or distributed frameworks, validated by e.g. satellite retrievals of the snow cover fraction (Magnusson et al., 2014).

5.6 Towards the assimilation in a semi-distributed geometry?

The aim of this study was to assess the potential of the assimilation of in-situ HS observations to correct nearby simulations, in view of applying it in a semi-distributed or distributed framework (Cluzet et al., 2021), in a similar strategy as Magnusson et al. (2014) and Griessinger et al. (2019). We used CrocO (Cluzet et al., 2021), an ensemble system accounting for meteorological and snowpack modelling uncertainties, using a Particle Filter to assimilate spatialised snowpack observations.

The results are mitigated: an added value is observed only when initial modelling errors are large (Fig. 9b), similarly to results obtained by Winstral et al. (2019). In the Northern Alps, Western Pyrenees and under 1500 m, the added value is null on average, and seems too insufficient to be of a real use. Over these areas, it seems that there is no room for improvement with data assimilation of point scale HS only. There, simulation accuracy may be more limited by snow related processes such as wind drift and uncertain physical processes resulting in snow cover variability, than by meteorological errors. The use of spatialised satellite retrievals (Margulis et al., 2019; Cluzet et al., 2020) to better constrain snow cover variability, or a finer correction of meteorological forcings using radar precipitation data (e.g. Birman et al., 2017; Le Bastard et al., 2019) in combination with

higher resolution NWP models and their ensemble counterparts, might be a solution.

6 Conclusions

This study investigates the potential for localised versions of the Particle Filter to spatially propagate information from in-situ observations of the height of snow (HS) in an ensemble of snowpack simulations. Compared with state-of-the-art deterministic and ensemble open-loop approaches, over ten years, we demonstrate that substantial improvements are only obtained in locations and elevation ranges where the reference errors are the highest. These areas correspond to locations where the density of meteorological observations, which are crucial for the correction of the meteorological forcings within SAFRAN analysis scheme, is the lowest. This demonstrates a good complementarity with the meteorological observation analysed by SAFRAN to reduce the current errors of the operational chain.

Previous studies already demonstrated the added value of in-situ HS observations in a similar setting with a dense observation coverage (Magnusson et al., 2014; Winstral et al., 2019). It was suspected that lower observation densities would reduce the potential for assimilation. Here, we exploit data with a wide range of densities, generally lower than these studies, and find no sensitivity of the assimilation performance to the observation density. This finding may be specific to the error structures of the reference simulations, which are correlated with the observation density.

Results also show that intermediate localisation strategies between 35-50 km of radii yielded slightly lower errors than a strategy addressing large scale errors only (300 km), while lower radii (17 km) may be too small to capture the snow cover variability where the density of observations is too small.

Our results finally show a good complementarity between the HS observations and meteorological observations already assimilated in the modelling chain, in particular in the most remote areas. This result is encouraging in the way of reducing the weaknesses of the current operational modelling chain, and shows that even scarce in-situ snowpack observations could be beneficial for snow cover modelling over large areas.

Code availability. The Crocus snowpack model (including all physical options of the ESCROC system) and the Particle Filter algorithm are developed inside the opensource SURFEX project. The source files of SURFEX code are provided at 10.5281/zenodo.5111449 to guarantee the permanent reproducibility of results. However, we recommend potential future users and developers to access to the code from its git repository (git.umr-cnrm.fr/git/Surfex_Git2.git, tag CrocO_v1.1). Experiments were pre/post-processed using CrocO_toolbox package. It is available on Github (https://github.com/bertrandcz/CrocO_toolbox, release v1.1) along with a documentation.

However, this software could not be applied outside Météo-France HPC environment, CrocO python software offers the possibility to run CrocO simulations locally. This functionality was not used here due to the high numerical cost of our simulations, which required the use of Météo-France HPC environment.

Data availability. SAFRAN reanalyses, corresponding to the unperturbed forcings, are available at: http://dx.doi.org/10.25326/37#v2019 (need to select the *postes* domain). Additional input data necessary to reproduce the manuscript simulations and figures are provided at 10.5281/zenodo.5115557 . This archive includes : namelists, configuration files, spinup files and pre/post-processing scripts. Simulation outputs represent a considerable amount of data (300+Go) and are archived in Météo-France archiving system and can be accessed upon reasonable request to Matthieu Lafaysse (matthieu.lafaysse@meteo.fr).

Author contributions. BC, MD and ML conceived the study, BC performed the simulations, treated the observations and wrote the manuscript, ML downloaded the observations, CDB updated the routines to generate the forcings and helped with the interpretation of CRPS, MV performed the oper runs. All authors contributed to the analysis of results.

Competing interests. The authors have no competing interests to declare.

Acknowledgements. The authors would like to thank the reviewers for their helpful comments which helped improve the manuscript, Emmanuel Cosme from the Institut de Géosciences de l'Environnement in France and Tobias Jonas from the WSL-Institut für Schnee- und Lawinenforschung SLF for helpful discussions and comments and Vincent Vionnet, from Environment and Climate Change Canada for suggestions on how to improve the quality of our figures. Marie Dumont was partially funded by ANR JCJC EBONI. Marie Dumont has received funding from the European Research Council (ERC) under the European Union's Horizon 2020 research and innovation programme (grant agreement no. 949516, IVORI). CNRM/CEN is part of Labex OSUG@2020.

References

Andreadis, K. M. and Lettenmaier, D. P.: Assimilating remotely sensed snow observations into a macroscale hydrology model, Advances in water resources, 29, 872–886, https://doi.org/10.1016/j.advwatres.2005.08.004, 2006.

Atger, F.: The skill of ensemble prediction systems, Monthly Weather Review, 127, 1941–1953, https://doi.org/10.1175/1520-0493(1999)127<1941:TSOEPS>2.0.CO;2, 1999.

Bellier, J., Zin, I., and Bontron, G.: Sample stratification in verification of ensemble forecasts of continuous scalar variables: Potential benefits and pitfalls, Monthly Weather Review, 145, 3529–3544, https://doi.org/10.1175/MWR-D-16-0487.1, 2017.

Bengtsson, T., Bickel, P., and Li, B.: Curse-of-dimensionality revisited: Collapse of the particle filter in very large scale systems, in: Probability and Statistics: Essays in Honor of David A. Freedman, edited by Nolan, D. and Speed, T., vol. Volume 2 of *Collections*, pp. 316–334, Institute of Mathematical Statistics, Beachwood, Ohio, USA, https://doi.org/10.1214/193940307000000518, 2008.

Birman, C., Karbou, F., Mahfouf, J.-F., Lafaysse, M., Durand, Y., Giraud, G., Mérindol, L., and Hermozo, L.: Precipitation analysis over the French Alps using a variational approach and study of potential added value of ground-based radar observations, Journal of Hydrometeorology, 18, 1425–1451, https://doi.org/10.1175/JHM-D-16-0144.1, 2017.

Bouttier, F., Raynaud, L., Nuissier, O., and Ménétrier, B.: Sensitivity of the AROME ensemble to initial and surface perturbations during HyMeX, Quarterly Journal of the Royal Meteorological Society, 142, 390–403, https://doi.org/10.1002/qj.2622, 2016.

Brun, E., David, P., Sudul, M., and Brunot, G.: A numerical model to simulate snow-cover stratigraphy for operational avalanche forecasting, J. Glaciol., 38, 13 – 22, https://doi.org/10.3189/S0022143000009552, 1992.

Buizza, R.: The value of probabilistic prediction, Atmospheric Science Letters, 9, 36–42, https://doi.org/10.1002/asl.170, 2008.

Cantet, P., Boucher, M., Lachance-Coutier, S., Turcotte, R., and Fortin, V.: Using a particle filter to estimate the spatial distribution of the snowpack water equivalent, Journal of Hydrometeorology, 20, 577–594, https://doi.org/10.1175/JHM-D-18-0140.1, 2019.

Charrois, L., Cosme, E., Dumont, M., Lafaysse, M., Morin, S., Libois, Q., and Picard, G.: On the assimilation of optical reflectances and snow depth observations into a detailed snowpack model, The Cryosphere, 10, 1021–1038, https://doi.org/10.5194/tc-10-1021-2016, 2016.

Cluzet, B., Revuelto, J., Lafaysse, M., Tuzet, F., Cosme, E., Picard, G., Arnaud, L., and Dumont, M.: Towards the assimilation of satellite reflectance into semi-distributed ensemble snowpack simulations, Cold Regions Science and Technology, 170, 102 918, https://doi.org/https://doi.org/10.1016/j.coldregions.2019.102918, 2020.

Cluzet, B., Lafaysse, M., Cosme, E., Albergel, C., Meunier, L.-F., and Dumont, M.: CrocO_v1. 0: a particle filter to assimilate snowpack observations in a spatialised framework, Geoscientific Model Development, 14, 1595–1614, https://doi.org/10.5194/gmd-14-1595-2021, 2021.

Courtier, P., Freydier, C., Geleyn, J.-F., Rabier, F., and Rochas, M.: The ARPEGE project at Météo-France, in: Proceedings of the 1991 ECMWF Seminar, pp. 193–231, ECMWF, Reading, U.-K., 1991.

De Lannoy, G. J. M., Reichle, R. H., Arsenault, K. R., Houser, P. R., Kumar, S., Verhoest, N. E. C., and Pauwels, V. R. N.: Multiscale assimilation of Advanced Microwave Scanning Radiometer–EOS snow water equivalent and Moderate Resolution Imaging Spectroradiometer snow cover fraction observations in northern Colorado, Water Resources Research, 48, https://doi.org/https://doi.org/10.1029/2011WR010588, 2012.

Descamps, L., Labadie, C., Joly, A., Bazile, E., Arbogast, P., and Cébron, P.: PEARP, the Météo-France short-range ensemble prediction system, Quarterly Journal of the Royal Meteorological Society, 141, 1671–1685, https://doi.org/10.1002/qj.2469, 2015.

Deschamps-Berger, C., Cluzet, B., Dumont, M., Lafaysse, M., Berthier, E., Fanise, P., and Gascoin, S.: Assimilation of snow depth maps from spaceborne photogrammetry in a detaled snowpack model, in review.

Dumont, M., Tuzet, F., Gascoin, S., Picard, G., Kutuzov, S., Lafaysse, M., Cluzet, B., Nheili, R., and Painter, T.: Accelerated snow melt in the Russian Caucasus mountains after the Saharan dust outbreak in March 2018, Journal of Geophysical Research: Earth Surface, p. e2020JF005641, 2020.

Durand, Y., Brun, E., Mérindol, L., Guyomarc'h, G., Lesaffre, B., and Martin, E.: A meteorological estimation of relevant parameters for snow models, Ann. Glaciol., 18, 65–71, https://doi.org/10.3189/S0260305500011277, 1993.

Durand, Y., Giraud, G., Brun, E., Mérindol, L., and Martin, E.: A computer-based system simulating snowpack structures as a tool for regional avalanche forecasting, J. Glaciol., 45, 469–484, https://doi.org/10.3189/S0022143000001337, 1999.

Durand, Y., Giraud, G., Laternser, M., Etchevers, P., Mérindol, L., and Lesaffre, B.: Reanalysis of 47 Years of Climate in the French Alps (1958–2005): Climatology and Trends for Snow Cover, J. Appl. Meteor. Climat., 48, 2487–2512, https://doi.org/10.1175/2009JAMC1810.1, 2009a.

Durand, Y., Giraud, G., Laternser, M., Etchevers, P., Mérindol, L., and Lesaffre, B.: Reanalysis of 44 Yr of Climate in the French Alps (1958–2002): Methodology, Model Validation, Climatology, and Trends for Air Temperature and Precipitation., J. Appl. Meteor. Climat., 48, 429–449, https://doi.org/10.1175/2008JAMC1808.1, 2009b.

Durand, Y., Giraud, G., Goetz, D., Maris, M., and Payen, V.: Modeled snow cover in Pyrenees mountains and cross-comparisons between remote-sensed and land-based observation data, in: Proceedings of the International Snow Science Workshop, Anchorage, Alaska, vol. 25, p. 9981004, https://arc.lib.montana.edu/snow-science/objects/issw-2012-998-1004.pdf, 2012.

Eckert, N., Keylock, C., Castebrunet, H., Lavigne, A., and Naaim, M.: Temporal trends in avalanche activity in the French Alps and subregions: from occurrences and runout altitudes to unsteady return periods, Journal of Glaciology, 59, 93–114, https://doi.org/10.3189/2013JoG12J091, 2013.

Essery, R., Morin, S., Lejeune, Y., and Bauduin-Ménard, C.: A comparison of 1701 snow models using observations from an alpine site, Adv. Water Res., 55, 131–148, https://doi.org/10.1016/j.advwatres.2012.07.013, 2013.

Evensen, G.: Sequential data assimilation with a nonlinear quasi-geostrophic model using Monte Carlo methods to forecast error statistics, Journal of Geophysical Research: Oceans, 99, 10 143–10 162, 1994.

Farchi, A. and Bocquet, M.: Comparison of local particle filters and new implementations, Nonlinear Processes in Geophysics, 25, 765–807, https://doi.org/10.5194/npg-25-765-2018, 2018.

Fortin, V., Abaza, M., Anctil, F., and Turcotte, R.: Why should ensemble spread match the RMSE of the ensemble mean? (vol 15, pg 1708, 2014), J. Hydrometeorol., 16, 484, https://doi.org/10.1175/JHM-D-14-0161.1, 2015.

Frei, C. and Schär, C.: A precipitation climatology of the Alps from high-resolution rain-gauge observations, International Journal of Climatology: A Journal of the Royal Meteorological Society, 18, 873–900, https://doi.org/10.1002/(SICI)1097-0088(19980630)18:8<873::AID-JOC255>3.0.CO;2-9, 1998.

Gascoin, S., Hagolle, O., Huc, M., Jarlan, L., Dejoux, J.-F., Szczypta, C., Marti, R., and Sánchez, R.: A snow cover climatology for the Pyrenees from MODIS snow products, Hydrol. Earth Syst. Sci, 19, 2337–2351, https://doi.org/10.5194/hess-19-2337-2015, 2015.

Gichamo, T. Z. and Tarboton, D. G.: Ensemble Streamflow Forecasting using an Energy Balance Snowmelt Model Coupled to a Distributed Hydrologic Model with Assimilation of Snow and Streamflow Observations, Water Resources Research, 55, 10 813–10 838, https://doi.org/10.1029/2019WR025472, 2019.

Griessinger, N., Schirmer, M., Helbig, N., Winstral, A., Michel, A., and Jonas, T.: Implications of observation-enhanced energy-balance snowmelt simulations for runoff modeling of Alpine catchments, Advances in Water Resources, 133, 103 410, https://doi.org/10.1016/j.advwatres.2019.103410, 2019.

Grünewald, T. and Lehning, M.: Are flat-field snow depth measurements representative? A comparison of selected index sites with areal snow depth measurements at the small catchment scale, Hydrological Processes, 29, 1717–1728, https://doi.org/10.1002/hyp.10295, 2015.

Hamill, T.: Interpretation of rank histograms for verifying ensemble forecasts, Mon. Weather Rev., 129, 550–560, https://doi.org/10.1175/1520-0493(2001)129<0550:IORHFV>2.0.CO;2, 2001.

Horowitz, L. W., Naik, V., Paulot, F., Ginoux, P. A., Dunne, J. P., Mao, J., Schnell, J., Chen, X., He, J., John, J. G., et al.: The GFDL Global Atmospheric Chemistry-Climate Model AM4. 1: Model Description and Simulation Characteristics, Journal of Advances in Modeling Earth Systems, p. e2019MS002032, https://doi.org/10.1029/2019MS002032, 2020.

Houtekamer, P. L. and Mitchell, H. L.: A sequential ensemble Kalman filter for atmospheric data assimilation, Monthly Weather Review, 129, 123–137, 2001.

Isotta, F. A., Frei, C., Weilguni, V., Perčec Tadić, M., Lassegues, P., Rudolf, B., Pavan, V., Cacciamani, C., Antolini, G., Ratto, S. M., et al.: The climate of daily precipitation in the Alps: development and analysis of a high-resolution grid dataset from pan-Alpine rain-gauge data, International Journal of Climatology, 34, 1657–1675, https://doi.org/10.1002/joc.3794, 2014.

Jonas, T., Marty, C., and Magnusson, J.: Estimating the snow water equivalent from snow depth measurements in the Swiss Alps, J. Hydrol., 378, 161–167, https://doi.org/10.1016/j.jhydrol.2009.09.021, 2009.

Josse, B., Simon, P., and Peuch, V.-H.: Radon global simulations with the multiscale chemistry and transport model MOCAGE, Tellus B: Chemical and Physical Meteorology, 56, 339–356, https://doi.org/10.3402/tellusb.v56i4.16448, 2004.

Klinker, E. and Sardeshmukh, P. D.: The diagnosis of mechanical dissipation in the atmosphere from large-scale balance requirements, Journal of the atmospheric sciences, 49, 608–627, https://doi.org/10.1175/1520-0469(1992)049<0608:TDOMDI>2.0.CO;2, 1992.

Kochendorfer, J., Rasmussen, R., Wolff, M., Baker, B., Hall, M. E., Meyers, T., Landolt, S., Jachcik, A., Isaksen, K., Brækkan, R., et al.: The quantification and correction of wind-induced precipitation measurement errors, Hydrology and Earth System Sciences, 21, 1973, https://doi.org/10.5194/hess-21-1973-2017, 2017.

Krinner, G., Derksen, C., Essery, R., Flanner, M., Hagemann, S., Clark, M., Hall, A., Rott, H., Brutel-Vuilmet, C., Kim, H., et al.: ESM-SnowMIP: assessing snow models and quantifying snow-related climate feedbacks, Geoscientific Model Development, 11, 5027–5049, https://doi.org/10.5194/gmd-11-5027-2018, 2018.

Lafaysse, M., Morin, S., Coléou, C., Vernay, M., Serça, D., Besson, F., Willemet, J.-M., Giraud, G., and Durand, Y.: Toward a new chain of models for avalanche hazard forecasting in French mountain ranges, including low altitude mountains, in: Proceedings of the International Snow Science Workshop - Grenoble and Chamonix, pp. 162–166, https://arc.lib.montana.edu/snow-science/objects/ISSW13_paper_O1-02.pdf, 2013.

Lafaysse, M., Cluzet, B., Dumont, M., Lejeune, Y., Vionnet, V., and Morin, S.: A multiphysical ensemble system of numerical snow modelling, The Cryosphere, 11, 1173–1198, https://doi.org/10.5194/tc-11-1173-2017, 2017.

Largeron, C., Dumont, M., Morin, S., Boone, A., Lafaysse, M., Metref, S., Cosme, E., Jonas, T., Winstral, A., and Margulis, S. A.: Toward Snow Cover Estimation in Mountainous Areas Using Modern Data Assimilation Methods: A Review, Frontiers in Earth Science, 8, 325, https://doi.org/10.3389/feart.2020.00325, 2020.

Larue, F., Royer, A., Sève, D. D., Roy, A., and Cosme, E.: Assimilation of passive microwave AMSR-2 satellite observations in a snowpack evolution model over northeastern Canada, Hydrology and Earth System Sciences, 22, 5711–5734, https://doi.org/10.5194/hess-22-5711-2018, 2018.

Lavigne, A., Eckert, N., Bel, L., and Parent, E.: Adding expert contributions to the spatiotemporal modelling of avalanche activity under different climatic influences, Journal of the Royal Statistical Society: Series C: Applied Statistics, pp. 651–671, https://doi.org/10.1111/rssc.12095, 2015.

Le Bastard, T., Caumont, O., Gaussiat, N., and Karbou, F.: Combined use of volume radar observations and high-resolution numerical weather predictions to estimate precipitation at the ground: methodology and proof of concept, Atmospheric Measurement Techniques, 12, 5669–5684, https://doi.org/10.5194/amt-12-5669-2019, 2019.

Lejeune, Y., Dumont, M., Panel, J.-M., Lafaysse, M., Lapalus, P., Le Gac, E., Lesaffre, B., and Morin, S.: 57 years (1960–2017) of snow and meteorological observations from a mid-altitude mountain site (Col de Porte, France, 1325 m of altitude), Earth System Science Data, 11, 71, https://doi.org/10.5194/essd-11-71-2019, 2019.

Lettenmaier, D. P., Alsdorf, D., Dozier, J., Huffman, G. J., Pan, M., and Wood, E. F.: Inroads of remote sensing into hydrologic science during the WRR era, Water Resources Research, 51, 7309–7342, https://doi.org/10.1002/2015WR017616, 2015.

Libois, Q., Picard, G., France, J., Arnaud, L., Dumont, M., Carmagnola, C. M., and King, M.: Influence of grain shape on light penetration in snow, The Cryosphere, 7, 1803–1818, https://doi.org/10.5194/tc-7-1803-2013, 2013.

Libois, Q., Picard, G., Arnaud, L., Dumont, M., Lafaysse, M., Morin, S., and Lefebvre, E.: Summertime evolution of snow specific surface area close to the surface on the Antarctic Plateau, The Cryosphere, 9, 2383–2398, https://doi.org/10.5194/tc-9-2383-2015, 2015.

Liston, G. E. and Hiemstra, C. A.: A Simple Data Assimilation System for Complex Snow Distributions (SnowAssim), Journal of Hydrometeorology, 9, 989 – 1004, https://doi.org/10.1175/2008JHM871.1, 2008.

López-Moreno, J., Soubeyroux, J. M., Gascoin, S., Alonso-Gonzalez, E., Durán-Gómez, N., Lafaysse, M., Vernay, M., Carmagnola, C., and Morin, S.: Long-term trends (1958–2017) in snow cover duration and depth in the Pyrenees, International Journal of Climatology, https://doi.org/10.1002/joc.6571, 2020.

Magnusson, J., Gustafsson, D., Hüsler, F., and Jonas, T.: Assimilation of point SWE data into a distributed snow cover model comparing two contrasting methods, Water resources research, 50, 7816–7835, https://doi.org/10.1002/2014WR015302, 2014.

Magnusson, J., Winstral, A., Stordal, A. S., Essery, R., and Jonas, T.: Improving physically based snow simulations by assimilating snow depths using the particle filter, Water Resources Research, 53, 1125–1143, https://doi.org/10.1002/2016WR019092, 2017.

Malle, J., Rutter, N., Mazzotti, G., and Jonas, T.: Shading by trees and fractional snow cover control the subcanopy radiation budget, Journal of Geophysical Research: Atmospheres, 124, 3195–3207, https://doi.org/10.1029/2018JD029908, 2019.

Margulis, S. A., Fang, Y., Li, D., Lettenmaier, D. P., and Andreadis, K.: The Utility of Infrequent Snow Depth Images for Deriving Continuous Space-Time Estimates of Seasonal Snow Water Equivalent, Geophysical Research Letters, 46, 5331–5340, https://doi.org/10.1029/2019GL082507, 2019.

Matheson, J. E. and Winkler, R. L.: Scoring rules for continuous probability distributions, Management science, 22, 1087–1096, https://doi.org/10.1287/mnsc.22.10.1087, 1976.

Morin, S., Horton, S., Techel, F., Bavay, M., Coléou, C., Fierz, C., Gobiet, A., Hagenmuller, P., Lafaysse, M., Ližar, M., Mitterer, C., Monti, F., Müller, K., Olefs, M., Snook, J. S., van Herwijnen, A., and Vionnet, V.: Application of physical snowpack models in support of operational avalanche hazard forecasting: A status report on current implementations and prospects for the future, Cold Regions Science and Technology, 170, 102 910, https://doi.org/https://doi.org/10.1016/j.coldregions.2019.102910, 2020.

Mott, R., Vionnet, V., and Grünewald, T.: The seasonal snow cover dynamics: review on wind-driven coupling processes, Frontiers in Earth Science, 6, 197, https://doi.org/10.3389/feart.2018.00197, 2018.

Nabat, P., Somot, S., Mallet, M., Michou, M., Sevault, F., Driouech, F., Meloni, D., di Sarra, A., Di Biagio, C., Formenti, P., et al.: Dust aerosol radiative effects during summer 2012 simulated with a coupled regional aerosol–atmosphere–ocean model over the Mediterranean, Atmospheric Chemistry and physics, 15, 3303–3326, https://doi.org/10.5194/acp-15-3303-2015, 2015.

Nousu, J.-P., Lafaysse, M., Vernay, M., Bellier, J., Evin, G., and Joly, B.: Statistical post-processing of ensemble forecasts of the height of new snow, Nonlinear Processes in Geophysics, 26, 339–357, https://doi.org/10.5194/npg-26-339-2019, 2019.

Oliphant, A., Spronken-Smith, R., Sturman, A., and Owens, I.: Spatial variability of surface radiation fluxes in mountainous terrain, Journal of Applied Meteorology, 42, 113–128, https://doi.org/10.1175/1520-0450(2003)042<0113:svosrf>2.0.co;2, 2003.

Penny, S. G. and Miyoshi, T.: A local particle filter for high-dimensional geophysical systems, Nonlinear Processes in Geophysics, 23, 391, https://doi.org/10.5194/npg-23-391-2016, 2016.

Piazzi, G., Thirel, G., Campo, L., and Gabellani, S.: A particle filter scheme for multivariate data assimilation into a point-scale snowpack model in an Alpine environment, The Cryosphere, 12, 2287–2306, https://doi.org/10.5194/tc-12-2287-2018, 2018.

Poterjoy, J.: A localized particle filter for high-dimensional nonlinear systems, Monthly Weather Review, 144, 59–76, https://doi.org/10.1175/MWR-D-15-0163.1, 2016.

Poterjoy, J. and Anderson, J. L.: Efficient assimilation of simulated observations in a high-dimensional geophysical system using a localized particle filter, Monthly Weather Review, 144, 2007–2020, https://doi.org/10.1175/mwr-d-15-0322.1, 2016.

Potthast, R., Walter, A., and Rhodin, A.: A Localized Adaptive Particle Filter within an Operational NWP Framework, Monthly Weather Review, 147, 345–362, https://doi.org/10.1175/MWR-D-18-0028.1, 2019.

Qu, X. and Hall, A.: On the persistent spread in snow-albedo feedback, Climate dynamics, 42, 69–81, https://doi.org/10.1007/s00382-013-1774-0, 2014.

Quéno, L., Vionnet, V., Dombrowski-Etchevers, I., Lafaysse, M., Dumont, M., and Karbou, F.: Snowpack modelling in the Pyrenees driven by kilometric-resolution meteorological forecasts, The Cryosphere, 10, 1571–1589, https://doi.org/10.5194/tc-10-1571-2016, 2016.

Raleigh, M. S., Lundquist, J. D., and Clark, M. P.: Exploring the impact of forcing error characteristics on physically based snow simulations within a global sensitivity analysis framework, Hydrol. Earth Syst. Sci., 19, 3153–3179, https://doi.org/10.5194/hess-19-3153-2015, 2015.

Rodwell, M. and Palmer, T.: Using numerical weather prediction to assess climate models, Quarterly Journal of the Royal Meteorological Society: A journal of the atmospheric sciences, applied meteorology and physical oceanography, 133, 129–146, https://doi.org/10.1002/qj.23, 2007.

Serreze, M. C., Clark, M. P., Armstrong, R. L., McGinnis, D. A., and Pulwarty, R. S.: Characteristics of the western United States snowpack from snowpack telemetry (SNOTEL) data, Water Resources Research, 35, 2145–2160, https://doi.org/10.1029/1999wr900090, 1999.

Slater, A. G. and Clark, M. P.: Snow data assimilation via an ensemble Kalman filter, Journal of Hydrometeorology, 7, 478–493, https://doi.org/10.1175/jhm505.1, 2006.

Smyth, E. J., Raleigh, M. S., and Small, E. E.: Particle Filter Data Assimilation of Monthly Snow Depth Observations Improves Estimation of Snow Density and SWE, Water Resources Research, 55, 1296–1311, https://doi.org/10.1029/2018wr023400, 2019.

Smyth, E. J., Raleigh, M. S., and Small, E. E.: Improving SWE Estimation with Data Assimilation: The Influence of Snow Depth Observation Timing and Uncertainty, Water Resources Research, 56, e2019WR026 853, https://doi.org/10.1029/2019wr026853, 2020.

Sturm, M., Holmgren, J., McFadden, J. P., Liston, G. E., Chapin III, F. S., and Racine, C. H.: Snow–shrub interactions in Arctic tundra: a hypothesis with climatic implications, Journal of Climate, 14, 336–344, https://doi.org/10.1175/1520-0442(2001)014<0336:ssiiat>2.0.co;2, 2001.

Taillardat, M. and Mestre, O.: From research to applications–examples of operational ensemble post-processing in France using machine learning, Nonlinear Processes in Geophysics, 27, 329–347, https://doi.org/10.5194/npg-27-329-2020, 2020.

Van Leeuwen, P. J.: Particle filtering in geophysical systems, Monthly Weather Review, 137, 4089–4114, https://doi.org/10.1175/2009mwr2835.1, 2009.

Verfaillie, D., Lafaysse, M., Déqué, M., Eckert, N., Lejeune, Y., and Morin, S.: Multi-component ensembles of future meteorological and natural snow conditions for 1500 m altitude in the Chartreuse mountain range, Northern French Alps, The Cryosphere, 12, 1249–1271, https://doi.org/10.5194/tc-12-1249-2018, 2018.

Vernay, M., Lafaysse, M., Merindol, L., Giraud, G., and Morin, S.: Ensemble Forecasting of snowpack conditions and avalanche hazard, Cold. Reg. Sci. Technol., 120, 251–262, https://doi.org/10.1016/j.coldregions.2015.04.010, 2015.

Vernay, M., Lafaysse, M., Monteiro, D., Hagenmuller, P., Nheili, R., Samacoïts, R., Verfaillie, D., and Morin, S.: The S2M meteorological and snow cover reanalysis over the French mountainous areas, description and evaluation (1958–2020), Earth System Science Data Discussions, 2021, 1–36, https://doi.org/10.5194/essd-2021-249, in review.

Viallon-Galinier, L., Hagenmuller, P., and Lafaysse, M.: Forcing and evaluating detailed snow cover models with stratigraphy observations, Cold Regions Science and Technology, p. 103163, https://doi.org/10.1016/j.coldregions.2020.103163, 2020.

Vionnet, V., Brun, E., Morin, S., Boone, A., Martin, E., Faroux, S., Le-Moigne, P., and Willemet, J.-M.: The detailed snowpack scheme Crocus and its implementation in SURFEX v7.2, Geosci. Model. Dev., 5, 773–791, https://doi.org/10.5194/gmd-5-773-2012, 2012.

Vionnet, V., Guyomarc'h, G., Lafaysse, M., Naaim-Bouvet, F., Giraud, G., and Deliot, Y.: Operational implementation and evaluation of a blowing snow scheme for avalanche hazard forecasting, Cold Regions Science and Technology, 147, 1–10, https://doi.org/10.1016/j.coldregions.2017.12.006, 2018.

Vionnet, V., Dombrowski-Etchevers, I., Lafaysse, M., Quéno, L., Seity, Y., and Bazile, E.: Numerical weather forecasts at kilometer scale in the French Alps : evaluation and applications for snowpack modelling, J. Hydrometeor., https://doi.org/http://dx.doi.org/10.1175/JHM-D-15-0241.1, 2016.

Winstral, A., Magnusson, J., Schirmer, M., and Jonas, T.: The Bias-Detecting Ensemble: A New and Efficient Technique for Dynamically Incorporating Observations Into Physics-Based, Multilayer Snow Models, Water Resources Research, 55, 613–631, https://doi.org/10.1029/2018wr024521, 2019.

Wong, M., Romine, G., and Snyder, C.: Model improvement via systematic investigation of physics tendencies, Monthly Weather Review, 148, 671–688, https://doi.org/10.1175/mwr-d-19-0255.1, 2020.

Chapter 5

Conclusions and outlook

Contents

5.1 General conclusion

In this manuscript, we assessed the potential for data assimilation of space-borne snowpack shortwave reflectances and in-situ HS to improve the modelled snowpack variability. We also investigated the problem of the spatial propagation of information from snowpack observations in a rugged terrain. This work answers the three main scientific questions shaping this manuscript:

Can we use observations of snowpack reflectance from satellites to better constrain snowpack modelling over mountainous areas?

Previous work had already assessed the potential for assimilation of space-borne shortwave snow reflectances (Mary et al., 2013; Charrois et al., 2016), but remained partly inconclusive on the ability of such data to constrain snowpack models over large areas. We considered that unrealistic representation of the LAP stratigraphy and imperfect representation of modelling error might explain these limitations. We went one step further, by benefiting from a realistic modelling of the LAP stratigraphy in snow (Tuzet et al., 2017), and a more comprehensive method to account for modelling errors (Lafaysse et al., 2017). The ensemble modelling system we built was the first to account for both meteorological and modelling uncertainty. It seemed successful in representing the modelling error for the reflectance when compared with in-situ observations. Aggregating reflectances retrieved from MODIS observations into the modelling semi-distributed geometry seemed to reduce their noise. However, these observations appeared to be biased. This bias may be caused by an imperfect retrieval of the reflectance in a rugged terrain. This bias is difficult to evaluate, and prevents from assimilating such data directly. We showed that ratios of reflectance were not biased. Assimilation experiments with reflectance ratios were conducted in an idealised framework. Results showed only slight improvements of the modelled SWE. Band ratios seem to convey less information than the raw reflectances.
A good agreement between the time-variations of the ensemble and the observations in a large diversity of topographic conditions was shown, at the exclusion of shadows, steep slopes, mixed terrain and forested areas, where retrievals are not reliable. We concluded that reflectance products had potential for a spatialised data assimilation, provided that their bias would one day be reduced (Lamare et al., 2020). In any case, limitations in their spatial coverage may last, leading to our second scientific question.

Can we propagate information on the snowpack state from observed areas to unobserved areas with data assimilation?

One of the major limitations of satellite and in-situ products is the presence of spatio-temporal gaps. Because of the high spatial variability of snowpack conditions, it is not straightforward that information can be propagated from observed to unobserved areas. We investigated the potential for data assimilation to achieve such a goal in an idealised setting. The semi-distributed framework accounts for the major sources of snowpack variability, at the exception of wind drift, vegetation, gravitational redistribution and local meteorological conditions. Synthetic observations of HS and reflectance were extracted from different quantiles of SWE of an openloop run (i.e. without assimilation), and over 4 years, in order to assess the performance of the assimilation under contrasted snow conditions. In order to emulate the spatial coverage of realistic reflectance observations, observations were assimilated only above the treeline, in flat and South facing gentle slopes only. Only a $1/6^{\text{th}}$ of the semi-distributed domain was observed.

Following Charrois et al. (2016), we used the Particle Filter, a sequential assimilation algorithm well adapted to Crocus, because this model has a variable number of layers (Magnusson et al., 2017). However, we had to find a solution to tackle PF degeneracy, an issue arising when a large number of observations is assimilated simultaneously, or when the prescribed observation errors are too low (Bengtsson et al., 2008). A common practice with the PF is to mitigate PF degeneracy by reducing the number of observations simultaneously assimilated. Domain localisation performs separate analyses at each location, considering only neighbouring observations (Farchi and Bocquet, 2018). The implicit hypothesis of domain localisation is that the similarity between locations decreases with the distance. We tested this hypothesis by computing background correlation patterns over the semi-distributed domain. Strong correlations between locations with distant topographic conditions, and conversely decorrelation of neighbouring locations, were evidenced. Moreover, these correlation patterns vary with the date and the considered variable, with e.g. the rain-snow line or a different metamorphism between shaded and sunny slopes. The underlining hypothesis of domain localisation is not valid for snowpack modelling at these modelling scales.

Therefore, we decided to use ensemble background correlation as a metric of similarity between locations thereby introducing the k-localisation. K-localisation is an original idea inspired on covariance localisation strategies from the EnKF. This approach mitigates degeneracy by ensuring that a minimal sample population is produced by the PF analysis. Iteratively, it rejects the observations coming from locations exhibiting the lowest ensemble background correlation with the current location, until the sample population is large enough. Similar locations may receive similar PF samples, but individual analysed members may exhibit some discontinuities, which might be impractical (Van Leeuwen, 2009).

For this reason, we also considered finding a global analysis assimilating all the observations at the same time. To mitigate PF degeneracy in such a situation, we adapted the inflation of observation errors proposed by Larue et al. (2018), in the spirit of accommodating the observation errors until the PF sample population is large enough.

K-localisation and inflation were used to assimilate the synthetic observations of HS and reflectance. We evaluated the different runs against the SWE of the synthetic members. Results showed that the proposed assimilation strategies successfully mitigated the PF degeneracy. HS assimilation yielded strong CRPS improvements in a large majority of observed and non-observed areas, showing that information could be propagated across different conditions of slopes and aspects. The propagation of information was present, but more limited, across elevations. Our results also evidenced that propagation of information on SWE through reflectances was possible. Reflectance assimilation indeed exhibited similar patterns of improvement than HS assimilation, but with a lower amplitude.
These results were obtained in an idealised setting, whereby synthetic observations probably followed the ensemble background correlations, since they were extracted from the openloop run. A global optimum was therefore likely to exist and could be found by the inflation algorithm. Similarly, the klocal was likely to choose the observations from the appropriate locations, while in reality, background correlations might be misleading. Experiments with real data were therefore necessary.

To what extent can we use in-situ observations of HS to improve snowpack simulations in their neighbourhood?

In-situ observations of HS were a good candidate to constrain the modelled snowpack variability by means of data assimilation. These observations are frequent, accurate, and cover large mountainous areas but lack representativeness. Several studies demonstrated their potential to detect and correct systematic errors in the meteorological forcings, thereby improving neighbouring snowpack simulations (Magnusson et al., 2014; Winstral et al., 2019). However, such approaches did not account for snowpack model and observation uncertainties, and relied on a dense network of HS observations, or were applied in a smooth topography (Cantet et al., 2019). Whether looser observation network could yield significant improvements in a mountainous terrain, remained an open question. We applied the inflation and k-localisation approaches in an HS observation network covering the French Alps, Pyrenees and Andorra, over ten years. The density of observation ranged from ten times lower to similar densities than the previous studies in rugged terrain.
This time, we combined inflation and k-localisation with a classical domain localisation

with four different radius ranging from 17 km to 300 km. The possibility to detect systematic errors of various spatial scales was thereby left open. Assimilation experiments were conducted in a Leave-One-Out setup in which the local observation is excluded from the analysis but kept for the evaluation. Results were mitigated, with an average CRPS improvement of about 10% with respect to the openloop. The high spatial variability of performance resulted in negative skill appearing for about a third of the stations. Assimilation performance relative to the openloop was mostly linked to the openloop bias. The best improvements were obtained for the highest negative biases of the openloop simulation. The bias-elevation relationship present in the references was also successfully mitigated by the assimilation.

Results also showed that observation density was not a dominant factor of the assimilation performance compared to the openloop, in apparent contradiction with speculations from Largeron et al. (2020). We suggested that our result is an artefact linked to the fact that the performance of the reference run strongly decreased with the density of HS observations (because this density is closely related to the density of meteorological observations already assimilated in the openloop). This situation leaves more room for improvement to the assimilation in the lowest density areas. Nevertheless, this experiments showed that HS observations were a good complement of meteorological observations in the most remote areas.

While no significant skill difference between the inflation and k-localisation could be evidenced by these experiments, it seemed that the strategies with intermediate localisation radius of 35 and 50 km yielded the best results. These scales may be a bit larger than the spatial scales at which the meteorological analysis is operated by SAFRAN within the modelling chain. Finally, the assimilation experiments exhibited strongly under-dispersive Spread-Skills. A likely cause for that is wind drift, which may have impacted some of the observation whereas it wasn't taken into account in the snowpack modelling system.

5.2 Perspectives

5.2.1 On the observations

Regardless of their bias, the reflectances retrieved from MODIS observations at 250 m resolution showed significant levels of noise, owing to intra-pixel variability and retrieval errors. These noises would make it difficult to assimilate in a distributed model. The aggregation into topographic classes we performed seemed a good way to overcome this noise. However, the elected topographic aggregation may encompass a significant amount of natural variability, an information which may be lost in the aggregation process. We

could not estimate the relative part of retrieval errors and natural variability inside the topographic classes. Recent progress in retrieval of reflectances (Lamare et al., 2020), could make it possible to retrieve reflectance with a higher accuracy. Such methods could be applied to higher resolution sensors such as Sentinel-2. This higher resolution could make it possible to reduce retrieval errors by aggregation to 250 m, thereby preserving most of the snowpack spatial variability while enabling to estimate observation errors (e.g. Deschamps-Berger et al., 2020).
With our method, an accurate specification of observation errors may not seem crucial. Indeed, the proposed PF variants can partly accommodate for badly specified observation errors, thanks to their iterative process. However, when assimilating several observations simultaneously, the influence of each observation on the PF analysis is determined by its relative error. Misspecified observation errors make the PF very sensitive to noisy outliers. Moreover, assuming that observations are independent (i.e. R is diagonal), as we did, results in sharper analyses than when error covariances are acknowledged, a likely cause for PF degeneracy. Methods providing full estimates of R, thereby acknowledging for discrepancies in the quality of the retrieval, and possible correlated observation errors, would therefore be useful. Lastly, reflectance and HS are bounded variables, and specifying Gaussian observations likelihoods (Eq. 1.9 in Sec. 1.4.3) may be suboptimal in such a situation (e.g. Bocquet et al., 2010).

We proposed a way to solve reflectance biases by computing band ratios. The information content from band ratios seemed unclear. Efforts should be made to understand their physical meaning in order to assess if they are worth further investigation. Another solution would be to use the PF to estimate the reflectance biases, inspiring on other assimilation algorithms (e.g. Dee, 2005; Eyre, 2016).
Another possibility would be to assimilate Top Of Atmosphere (TOA) radiances rather than Bottom Of Atmosphere (BOA) reflectances. In other words, bringing the model to the observations, rather than the opposite. Modelled BOA reflectances would be converted into TOA radiances using an inverse model of MODImLab, following (Lamare et al., 2020) and many other studies in the microwave spectrum (e.g. Durand et al., 2009). This option would have the major theoretical and practical advantage of treating the observation operator (here, MODImLab's inverse) as is: an uncertain model used to convert the modelled variables into observed ones. It might be then possible to determine and mitigate the origin of the bias between observed and modelled variables within this observation operator. Furthermore, this would be in line with the strategies of international weather prediction centres such as ECMWF which aim at a "all-sky, all-reflectance" strategy.

5.2.2 On the propagation of information with the PF variants

Our work demonstrated that information from HS and reflectance can be propagated across topographic classes, in an idealised framework. This opens a way to solve the issue of snow observation scarceness in a rugged terrain. In the snow community, this method could be applied to other bulk or surface snow observations affected by similar gaps. For example, space-borne or airborne stereoscopic HS observations which are limited by clouds, or radar retrievals of SWE or liquid water content, suffering from geometric distortions in a rugged terrain (Veyssière et al., 2019; Marin et al., 2020). Local studies working with ground based LIDAR or drone stereo-photometry, generally suffering from topographic masks, may benefit from such approaches too. Beyond the snow modelling community, such perspectives apply to any scientific field using spatialised observations in a rugged or complex terrain (e.g. glaciology (e.g. Dumont et al., 2012; Davaze et al., 2018) , mountain ecology (e.g. Dedieu et al., 2016) and permafrost (e.g. Zwieback et al., 2019)).

Our work proposed two novel and efficient approaches to tackle PF degeneracy: inflation and k-localisation. Inflation replaces a parameter, the observation error (only used as an initial value), by another: the target effective sample size, so-called N^*_{eff}. This transformation could be convenient for many fields in the geosciences in which the spatial and temporal variations of observations errors (including representativeness) are poorly known. Inflation can be applied at the point scale, on a local or whole domain, however its underlying assumption is that all the observations in the considered domain are meaningful for the analysis. K-localisation is suited to problems in which the definition of localisation domains is not trivial, because correlations are driven by other factors, e.g. topographic parameters. It might show its usefulness to a wide range of problems in a mountainous terrain.

K-localisation has some limitations, however. Like any other PF localisation algorithm –localised inflation algorithm included– it produces discontinuous analyses (e.g. Fig. 3 of Farchi and Bocquet, 2018). The posterior particles are made of the juxtaposition of potentially very different prior members. This behavior had no consequences in our setup since points are independent, but future work implementing snow mass transport by wind between locations might have to account for that. However, we expect the k-localisation to produce similar analyses (i.e. PF samples) for similar locations (because they are expected to assimilate a similar set of observations), thereby reducing the odds for discontinuities to arise. Several solutions exist to reduce the discontinuities, e.g. using optimal transport theory or a state-block-domain localisation (Farchi and Bocquet, 2018).

K-localisation is also sensitive to the initial value prescribed for observation error: the lower the value, the lower the number of observations it will keep for the analysis. Hybridization

with the inflation algorithm might be a convenient way to solve for this problem, by e.g. first selecting the relevant observations, and then applying inflation on it. Because K-localisation requires the computation of background covariances (a novelty for the PF, which could be seen as a breach into the PF non-gaussianity), one could argue that an imperfect representation of the background correlations in the PF would result in badly selected observation locations, and therefore, poor analyses. That is true, but indeed, poor representations of background correlations (equivalently, modelling error) actually affect every other ensemble or deterministic assimilation algorithms, the standard PF included (e.g. Sec. 1.4.3).

5.2.3 Representation and reduction of modelling errors

Several perspectives exist in the way of improving the representation of modelling error. Compared with our stochastic perturbations, using physically-based meteorological ensembles such as PEARP (Descamps et al., 2015), EFS (Molteni et al., 1996), or the higher resolution PEAROME (Bouttier et al., 2016) would improve the physical consistency between the forcing variables, and introduce a dynamic modulation of these uncertainties. More importantly, it would elegantly introduce a realistic representation of spatial correlation of meteorological error, though ways also exist with stochastic perturbations (e.g. Magnusson et al., 2014; Cantet et al., 2019). However, they seem to date to suffer from under-dispersion in mountainous area (Nousu et al., 2019), which could be detrimental for assimilation with the PF. Spread adjustment through statistical post-processing techniques may be a convenient avenue (e.g. Taillardat and Mestre, 2020).
The representation of several snowpack processes could also be improved. In particular, the use of spatially distributed LAP fluxes is encouraging in the way of a finer representation of the snowpack shortwave radiative budget and the associated errors (Réveillet et al., in prep). Significant efforts should be conducted to improve the parameterization of several uncertain physical processes (e.g. turbulent fluxes – essential to the mass and energy budget –, compaction, wet metamorphism, liquid water percolation, soil-vegetation-snow-canopy coupling, etc.). Since such improvements are limited by a lack of sufficient observations (Menard et al., 2020), data assimilation will have to cope with such errors for many years.
However, important phenomenon were ignored in our framework and hamper the representation of modelling error. Accounting for wind drift may come first, and probably requires to make the leap from the semi-distributed to a higher resolution. Such a progress would also allow for a better representation of the incoming and outgoing radiative fluxes, accounting for e.g. terrain shading and re-illumination effects. It would furthermore improve the model representativeness.

Other limitations are inherent to the semi-distributed geometry which framed our work. Meteorological forcings do not account for intra-massif variability, and are discontinuous at the massifs borders. This discontinuities are unrealistic, and partially prevent from the propagation of information across them. In the view of jointly assimilating meteorological and snowpack observations, and given the important information content that in situ snowpack observations handle on meteorological variables (e.g. Magnusson et al., 2014; Winstral et al., 2019) breaking such barriers would probably be also a good step forward.

5.2.4 Assimilation strategies

While recent progresses in atmospheric and land surface modelling have been been substantially driven by data assimilation (Rabier, 2005), data scarcity and intrinsic high variability stems for the progress of meteorological and snowpack operational modelling in the mountains. One day, ground-breaking observations such as airborne or satellite HS observations (e.g. Painter et al., 2016; Deschamps-Berger et al., 2020), or reliable spatialised reflectance observations (Lamare et al., 2020), may be available operationally over whole mountain ranges, and would certainly yield significant advances in modelling capability (e.g. Margulis et al., 2019; Deschamps-Berger et al., in review). Recent work (Li et al., 2017), also showed that coarse passive microwave products could be used to reliably constrain distributed snow models in a rugged terrain which could represent a significant advance. In the meantime, any already available piece of information should be taken advantage of, and snowpack modelling chains must be prepared to assimilate spatialised information. Both objectives require to make the leap into a higher resolution, explicitly spatialised modelling system, assimilating in-situ and spatialised snow and meteorological observations.

Indeed, the distributed geometry is probably the best suited to benefit from radar-derived precipitation fields (Birman et al., 2017), and satellite-derived SW and LW incoming radiation fluxes (Quéno et al., 2020b). In a spatialised geometry, these observations could be directly used to analyse the forcings fields. Of course, subsequent downscaling meteorological models into a resolution relevant to snowpack modelling, will be a challenge (e.g. Vionnet et al., 2019).

Meanwhile, in-situ snow observations often handle precious information on the past meteorological conditions and snowpack modelling errors in remote areas, but are to date too rarely exploited. A way must be found to spatially exploit it somehow, in the spirit of Winstral et al. (2019) (i.e. with severe assumptions on the snow physics), or with the method we proposed in Chap. 4 which may be prone to error compensation (e.g. Smyth et al., 2019), but lets it possible to reduce both meteorological and snow modelling errors. Grasping information from SCF information in a distributed modelling framework is also

definitely an achievable task with the PF (Baba et al., 2018) and would surely benefit to the simulations. Information from ground-based webcams (Portenier et al., 2020) could be assimilated as well in a distributed framework. As we see, there are exciting opportunities at reach.

To conclude, even though the available observations on meteorological and snowpack variability may seem scarce, data assimilation should be able to improve snowpack models by comprehensively ingesting it. Considering all available snow observations just as they are –pure and beautiful– may reveal some of snow's secrets in a near future. Hopefully not all.

Conclusion et perspectives en français

Conclusion générale

Dans ce manuscrit, nous avons évalué la capacité de l'assimilation d'observations de réflectance satellitaires ainsi que de hauteurs de neige (HS) à améliorer la modélisation de la variabilité du manteau neigeux en montagne. Du fait de la parcellarité des observations disponibles, cette question nous a amenés à nous intéresser à la propagations spatiale de l'information sur le manteau neigeux en terrain complexe. Notre travail a répondu aux trois questions scientifiques présentées en introduction :

- **Les observations de réflectances satellites de la neige permettent-elles de mieux contraindre la modélisation du manteau neigeux en montagne ?**

Plusieurs études avaient déjà étudié le potentiel pour l'assimilation de réflectances satellitaires dans le visible-proche infra-rouge (shortwave, SW), mais des zones d'ombres demeuraient sur la capacité de telles observations à être assimilées sur de grandes étendues (Mary et al., 2013; Charrois et al., 2016). Nous avons considéré qu'il était nécessaire de mieux représenter l'influence des impuretés optiquement actives (LAP) et les incertitudes de modélisation. Nous avons mis en œuvre de telles avancées, en bénéficiant de la récente modélisation explicite de la présence de LAP au sein du manteau neigeux (Tuzet et al., 2017), ainsi que d'une méthode permettant de caractériser les erreurs de modélisation du manteau neigeux de manière plus complète (Lafaysse et al., 2017). Nous avons ainsi bâti le premier système de modélisation ensembliste tenant compte des incertitudes liées aux forçages météorologiques et au modèle de manteau neigeux dans un contexte spatialisé. Une comparaison avec des observations in-situ de réflectances nous a permis de considérer que ce système représentait de manière réaliste les erreurs de modélisation pour cette variable. Nous avons agrégé des réflectances calculées à partir d'observations MODIS dans la géométrie du modèle, permettant de réduire leur bruit, mais au détriment d'informations fines sur la variabilité naturelle de cette observation. Un biais de ces réflectances agrégées vis à vis de l'ensemble et des observations in-situ a été mis en valeur. Ce biais est très probablement lié à l'algorithme d'inversion MODImLab qui permet de déduire les réflectances de surface à partir des radiances satellitaires, de la topographie et d'un modèle

de transfert radiatif atmosphérique. C'est un biais difficile à évaluer, et qui empêche l'assimilation directe des données MODIS. Nonobstant, nous avons montré que certain ratios de bandes spectrales MODIS n'étaient pas biaisés, et pourraient donc être assimilés. Nous avons donc conduit des expériences d'assimilations de ratios de réflectance dans un cadre idéalisé (observations synthétiques), n'obtenant qu'une amélioration très modérée de l'équivalent en eau (SWE) modélisé. Les ratios de réflectances semblent contenir moins d'information que les réflectances brutes.
Nous avons cependant montré un bon accord entre les variations des séries temporelles MODIS et de l'ensemble, et ce dans une grande variété de conditions topographiques, à l'exception des ombres, pentes raides, et forêts où les observations étaient peu fiables. Nous en avons conclu que les observations de réflectance avaient du potentiel pour une assimilation spatialisée, à condition que leur biais systématique soit réduit (Lamare et al., 2020). Dans tout les cas, leur couverture spatiale restera limitée, ce qui nous amène à notre deuxième question.

- **Peut-on propager de l'information sur l'état du manteau neigeux depuis des zones observées vers des zones non-observées ?**

Une des principales limitation des observations télédétectées et in-situ est la présence de "trous" dans leur couverture spatio-temporelle. Du fait de la grande variabilité spatio-temporelle des conditions d'enneigement, il n'est pas du tout évident qu'il soit possible de propager de l'information depuis de zones observées vers des zones non observées. Nous avons évalué la capacité de l'assimilation de données à permettre une telle propagation de l'information sur le manteau neigeux en nous plaçant dans un contexte idéalisé. La géométrie semi-distribuée permet de représenter les principales sources de variabilité du manteau neigeux, à l'exception du transport de neige par le vent, de la redistribution gravitaire et de l'hétérogénéité spatiale des conditions météorologiques, notamment. Des observations synthétiques de HS et de réflectance ont été extraites de différents quantiles d'une simulation open-loop (i.e. sans assimilation) sur quatre années, afin d'évaluer la performance de l'assimilation dans des conditions variées. Dans le but de simuler la couverture spatiale d'observations de réflectance, les observations n'ont été assimilées qu'au dessus de la limite des forêts, à plat ou dans les pentes sud peu raides d'un large secteur sud. Ainsi, seulement un sixième du domaine semi-distribué disposait d'observations.

Dans la suite de Charrois et al. (2016), nous avons utilisé le filtre particulaire (PF), un algorithme d'assimilation séquentielle bien adapté à Crocus, modèle ayant un nombre de coches numériques variable (Magnusson et al., 2017). Cependant, il était nécessaire

d'affronter la dégénérescence du PF, un problème apparaissant lorsqu'un nombre important d'observations est assimilé simultanément, ou en cas d'erreurs d'observations trop faibles (Bengtsson et al., 2008). La solution la plus couramment employée est de réduire le nombre d'observations assimilées à la fois. La localisation par domaine réalise une analyse séparée en chaque point, en ne considérant que les observations voisines (Farchi and Bocquet, 2018). L'hypothèse implicite de cette approche est que la similarité entre deux localisations décroit avec leur distance. Nous avons testé cette hypothèse en calculant les corrélations d'ébauche sur le domaine semi-distribué, mettant en valeur de fortes corrélations à travers le domaine, y compris dans des conditions topographiques très différentes, tandis que des localisations proches pouvaient être décorrélées. En outre, nous avons noté que ces motifs de corrélation variaient selon la date et la variable considérée, par exemple avec la limite pluie-neige ou un métamorphisme différent entre des pentes au soleil et à l'ombre. L'hypothèse sous-tendant la localisation par domaine n'était pas valide pour la modélisation du manteau neigeux à cette résolution.
Par conséquent, nous avons décidé d'utiliser les corrélations d'ébauche comme une mesure de la similarité entre deux endroits en introduisant la k-localisation du PF. Cette approche s'inspire de la localisation par covariance couramment utilisée pour l'EnKF. Il s'agit d'éviter la dégénérescence en s'assurant qu'un nombre minimal de membres a été choisi par l'analyse du PF. De manière itérative, la k-localisation rejette les observations qui viennent de localisations exhibant les plus faibles corrélations d'ébauche avec l'endroit considéré, jusqu'à ce que la population de l'échantillon d'analyse soit suffisante. Ainsi, des localisations similaires recevront probablement des analyses proches, mais des discontinuités peuvent apparaître au sein de chaque membre, avec des conséquences potentiellement négatives (Van Leeuwen, 2009).
Pour cette raison, nous avons aussi essayé de construire une analyse globale qui assimile toutes les observations à la fois. Afin d'empêcher le PF de dégénérer, une éventualité très probable dans cette situation, nous avons adapté l'approche de Larue et al. (2018) consistant à augmenter les erreurs d'observation jusqu'à ce que la population de l'analyse du PF soit suffisante.

Nous avons ensuite utilisé la k-localisation et l'inflation afin d'assimiler les observations de HS et de réflectance précédemment décrites. La performance des différentes simulations a été évaluée par comparaison avec les valeurs de SWE des observations synthétiques. Les résultats ont montré que ces deux stratégies d'assimilation permettaient d'éviter la dégénérescence du PF. L'assimilation de HS apportait une très forte amélioration de CRPS quasiment partout, tant dans les zones observées que dans les endroits dépourvus d'observations. La propagation d'information semblait cependant un peu plus limitée à

travers des conditions d'altitude sensiblement différentes. Nous avons aussi montré que la propagation spatiale d'information sur le SWE portée par les réflectances était possible. En efet, l'assimilation de réflectance montrait des structures d'amélioration du CRPS similaire que pour HS, avec une amplitude certes plus faible.
Ces résultats ont été obtenus dans un cadre idéalisé, dans lequel les observation synthétiques, provenant de l'open-loop, avaient de grandes chances de respecter les structures de corrélation spatiales de l'ensemble assimilé. L'existence d'un optimum global était donc possible, et trouvable par l'algorithme d'inflation. De la même manière, la k-localisation avait de bonnes chances de choisir les observations provenant de localisations appropriées, alors qu'en réalité, cet algorithme pourrait être trompé par de mauvais motifs de corrélation. Il était donc nécessaire de vérifier le comportement de cet algorithme avec des observations réelles.

- **Dans quelle mesure peut-on utiliser les observations in-situ de HN pour améliorer les simulations du manteau neigeux dans leur voisinage ?**

Les observations in-situ de HS sont bien adaptées pour contraindre la représentation de la variabilité spatiale dans les modèles, car elles sont répandues à travers de nombreux massifs montagneux, et précises. En revanche, leur représentativité spatiale est limitée. Plusieurs études ont démontré leur potentiel pour détecter et corriger des erreurs systématiques dans les forçages météorologiques, améliorant par conséquent les simulations du manteau neigeux dans leur voisinage (Magnusson et al., 2014; Winstral et al., 2019). Cependant, ces approches ne prenaient pas en compte les incertitudes des modèles de neige et des observations, et s'appuyaient sur un réseau d'observations in-situ particulièrement dense, ou bien étaient appliquées sur des étendues peu accidentées (Cantet et al., 2019). Il n'était pas certain que l'assimilation donne d'aussi bons résultats dans des régions moins densément observées. Nous avons appliqué l'inflation et la k-localisation à un réseau d'observations de HS couvrant les Alpes et les Pyrénées françaises, ainsi que sur l'Andorre, sur une période de dix ans. En comparaison des précédentes études en terrain montagneux, la densité variait de équivalente à dix fois plus faible, environ.
Cette fois-ci, nous avons combiné l'inflation et la k-localisation avec une approche de localisation par domaine classique, en testant quatre rayons de localisation entre 17 km et 300 km. Ceci laissait la possibilité aux différents algorithmes de détecter des erreurs systématiques de plus ou moins grande échelle. Afin d'assurer une évaluation indépendante, les expériences ont été conduites dans un cadre "Leave-One-Out", où l'observation locale est exclue de l'analyse mais est conservée pour l'évaluation. Nous avons obtenu des résultats mitigés, avec une amélioration de CRPS de l'ordre de 10% par rapport à l'open-loop. La grande variabilité

spatiale de la performance s'est traduite par une dégradation de performance dans environ un tiers des postes considérés. Il se trouve que la performance de l'assimilation par rapport à l'open-loop était très liée au biais de celui-ci, les meilleurs améliorations étant obtenues pour les biais open-loop les plus importants. Une relation entre le biais des références (open-loop et run opérationnel) a aussi été montrée. Celle-ci était relativement bien corrigée par l'assimilation.

Les résultats ont aussi montré que la performance de l'assimilation n'était pas liée à la densité d'observations, contrairement aux attentes de Largeron et al. (2020). Nous pensons qu'il s'agit d'un artefact causé par le fait que la performance de l'open-loop décroissait sensiblement avec la densité d'observations de HS (parce que celle-ci est très liée à la densité d'observations météorologiques déjà assimilées dans l'open-loop). Cette situations laisse plus de potentiel d'amélioration dans les zones les moins densément observées. Nonobstant, ces expériences ont montré que les observations de HS complétaient bien les observations météo dans les zones les plus reculées.

Alors qu'aucune différence significative de performance ne pouvait être mise en évidence entre l'inflation et la k-localisation, les rayons de localisations intermédiaires (35 et 50 km) donnaient les meilleurs résultats. Ces échelles spatiales sont un peu plus grandes que l'échelle à laquelle sont conduites les analyses météorologiques dans SAFRAN. Pour finir, les expériences d'assimilation étaient significativement sous-dispersives. Ce comportement s'explique probablement par la non prise en compte du transport de neige par le vent dans le modèle alors qu'il impacte sûrement certaines observations.

Perspectives

Les observations

Indépendamment de leur biais d'inversion, les réflectances issues d'observations MODIS à 250 m de résolution sont affectées par d'importants bruits, dûs à la variabilité intra-pixel et à des erreurs d'inversion. Ces bruits rendraient très incertaine l'assimilation dans un modèle distribué de résolution équivalente. L'agrégation par classes topographiques que nous avons mis en place semblait une bonne solution pour réduire ce bruit. Cependant, la résolution topographique choisie est trop frustre pour représenter toute la variabilité naturelle, ainsi une part de l'information information se perd probablement au cours du processus d'agrégation. Nous n'avons pas pu estimer la part relative des erreurs d'inversion et de la variabilité naturelle au sein des classes topographiques. Les avancées récentes dans l'inversion des réflectances (Lamare et al., 2020) pourraient permettre de réduire significativement ces erreurs. Ces avancées pourraient être appliquées à des capteurs de plus haute résolution, comme Sentinel-2 (10-20 m) . De telles résolutions pourraient permettre

d'agréger les pixels à 250 m, de sorte à réduire les erreurs d'inversion tout en conservant une part de la variabilité naturelle, voire même en offrant la possibilité d'estimer les erreurs d'observation (e.g. Deschamps-Berger et al., 2020).
Avec notre méthode, il peut sembler secondaire d'accorder un grand soin à la spécification des erreurs d'observations. En effet, les variantes du PF que nous proposons peuvent en partie compenser des erreurs d'observation mal spécifiées, grâce à leur approche itérative. Cependant, lorsque plusieurs observations sont assimilées simultanément, l'influence de chaque observation sur l'analyse est en partie déterminée par l'importance de son erreur, comparativement à celle des autres observations. Une mauvaise spécification des erreurs d'observation rend le PF très sensible à des observations aberrantes. En outre, le fait de supposer que les observations sont indépendantes comme nous l'avons fait (i.e. matrice de covariance d'erreur d'observation R diagonale), se traduit généralement par des analyses plus fortes que lorsqu'on tient compte des covariances d'erreur. Une méthode permettant d'estimer complètement R, c'est a dire des corrélations croisées comme de l'inégale qualité des observations, serait par conséquent très utile. Enfin, la réflectance et la hauteur de neige sont des variable bornées, et supposer des erreurs gaussiennes dans un tel cas est sous-optimal (e.g. Bocquet et al., 2010).

Nous avons proposé de résoudre le biais des réflectances en calculant des ratios de bandes spectrales. Cependant, l'information contenue dans ces ratios de bandes semble incertaine. Des efforts supplémentaires sont nécessaires pour comprendre leur sens physique afin d'évaluer si cette piste est pertinente. Une autre solution serait d'utiliser le PF pour estimer directement le biais des réflectances, en s'inspirant d'autres algorithmes (Dee, 2005; Eyre, 2016).

Propagation d'information avec les différentes variantes du PF

Dans un cadre idéalisé, notre travail a montré que l'information issue d'observations de HS et de réflectances pouvait être propagée à travers différentes conditions topographiques. Ce résultat peut permettre de résoudre le problème de la couverture spatiale partielle dont les observations souffrent en terrain complexe. Dans la communauté neige, cette méthode pourrait être employée pour assimiler d'autres observations intégrées ou surfaciques souffrant des mêmes manques. Par exemple, les observations stéréoscopiques de HS, provenant de satellites ou de campagnes aéroportées sont limitées par la couverture nuageuse, tandis que le signal radar, permettant de remonter au SWE ou à la présence d'eau liquide, souffre de distorsions géométriques en montagne (Veyssière et al., 2019; Marin et al., 2020). Des études plus localisées, utilisant des lidar au sol ou de la stéréo-photogrammétrie par drone, qui

souffrent également de masques topographiques, pourraient bénéficier de telles approches également. Au delà de cette communauté, ces méthodes ouvrent des perspectives dans tout domaine des géosciences utilisant des observations spatialisées en terrain complexe (e.g. glaciologie (e.g. Dumont et al., 2012; Davaze et al., 2018) , écologie de montagne (e.g. Dedieu et al., 2016) et permafrost (e.g. Zwieback et al., 2019)).

Nos travaux ont proposé deux nouvelles approches résolvant efficacement le problème de dégénérescence: l'inflation, et la k-localisation. L'inflation remplace un paramètre, l'erreur d'observation (seulement utilisée comme valeur initiale) par un autre : la taille d'échantillon cible, ou N^*_{eff}. Cette transformation peut s'avérer pertinente pour les disciplines dans lesquelles le variations spatiales et temporelles des erreurs d'observation (représentativité comprise) sont mal maîtrisées. L'inflation peut être appliqué à l'échelle locale comme sur un domaine localisé ou sur tout le domaine, cependant elle suppose que toutes les observations considérées sont pertinentes pour l'analyse. La k-localisation est elle adaptée aux problèmes dans lesquels la définition du domaine de localisation n'est pas triviale car les corrélations sont liées à d'autres facteurs tels que des paramètres topographiques. Elle pourrait ainsi s'avérer très pertinente pour toutes sortes de problèmes en terrain montagneux.
Cependant, la k-localisation a plusieurs limitations. Comme toutes les approches localisées du PF, –inflation localisée comprise– elle produit des analyses discontinues (e.g. Fig. 3 de Farchi and Bocquet, 2018). Les particules analysées sont constituées d'une juxtaposition de plusieurs membres d'ébauche potentiellement très différents. Ce comportement était sans conséquence sur notre système car aucun couplage n'est modélisé entre les points de simulation, mais cela sera probablement à prendre en compte dans des systèmes simulant le transport de neige par le vent. On s'attend cependant à ce que la k-localisation produise des analyses similaires (i.e. des échantillons du PF) pour des localisation similaires (car celles-ci sont censées assimiler un jeu d'observations similaires), réduisant de la sorte les chances de voir des discontinuités apparaître. En outre, plusieurs solutions existent pour réduire ces discontinuités, en s'appuyant sur le transport optimal ou la localisation "state-block-domain" (Farchi and Bocquet, 2018).
La k-localisation est également sensible à la valeur initiale prescrite pour les erreurs d'observations. Plus celle-ci est basse, moins il gardera d'observations différentes pour son analyse. Hybrider cette approche avec l'inflation pourrait résoudre cette difficulté, par exemple en sélectionnant tout d'abord les observations pertinent avec la k-localisation, plus en appliquant l'inflation dessus (si nécessaire). On pourrait également objecter que l'analyse de la k-localisation est sensible à une mauvaise représentation des erreurs d'ébauche par la matrice de corrélation, puisque celle-ci l'utilise pour opérer sa sélection d'observations. Une mauvaise matrice de corrélation résulterait ainsi en une analyse dégradée. C'est vrai, mais

de fait, ce problème affecte de manière explicite ou implicite n'importe quel autre algorithme d'assimilation, qu'il soit déterministe ou ensembliste, y compris le PF "standard" (voir e.g. Sec. 1.4.3).

Mieux représenter et réduire les erreurs de modélisation

Il existe plusieurs pistes pour améliorer la représentation de l'erreur de modélisation. L'utilisation d'ensembles à base physique, comme PEARP (Descamps et al., 2015), EFS (Molteni et al., 1996), ou même l'ensemble à haute résolution PEAROME (Bouttier et al., 2016) serait plus juste physiquement que les perturbations stochastiques que nous avons utilisées, et introduirait une estimation dynamique des erreurs de forçage. De plus, cela permettrait une représentation réaliste des corrélation spatiales d'erreur météorologiques, bien que des solutions existent également pour en introduire avec les méthodes stochastiques (e.g. Magnusson et al., 2014; Cantet et al., 2019). Cependant, ces ensembles souffrent toujours à l'heure actuelle de biais et de sous-dispersion en montagne (Nousu et al., 2019), avec des conséquences rédhibitoires sur l'assimilation avec le PF. Un ajustement de la dispersion de certaines variables pourrait être mis en place à l'aide de techniques de post-traitement statistiques (Taillardat and Mestre, 2020).

La représentation de plusieurs processus physiques du manteau neigeux pourrait également être améliorée. En particulier, l'utilisation de flux spatialisés d'impuretés absorbantes permettrait une meilleure représentation spatiale du transfert radiatif dans le manteau neigeux et des erreurs associées (Réveillet et al., in prep). D'important efforts devraient également être menés afin d'affiner la paramétrisation de certains processus physiques particulièrement incertains (e.g. les flux turbulents –très importants pour les bilans de masse et d'énergie–, le tassement, le métamorphisme de neige humide, la percolation de l'eau liquide, les interactions sol-végétation-neige- canopée, etc.). De tels progrès sont malheureusement limités par un manque d'observations à même de mieux contraindre ces processus (Menard et al., 2020), et l'assimilation devra composer avec de telles erreurs pour encore de nombreuses années.

Cependant, certains phénomènes importants ont été ignorés dans notre cadre de simulation et obèrent sa capacité à représenter correctement ses erreurs. La prise en compte du transport de neige par le vent vient bien sûr en premier, et requiert probablement de franchir le pas vers une géométrie explicite, distribuée. Une telle avancée permettrait de plus de mieux représenter les flux radiatifs entrants et sortants, en tenant compte des ombrages et réilluminations. Cela permettrait en outre d'améliorer la représentativité du modèle.

D'autres limitations sont inhérentes à la géométrie semi-distribuée dans laquelle nous avons travaillé. Les forçages météorologiques ne tiennent pas compte de la variabilité intra-massif,

et sont discontinus entre les différents massifs. Ces discontinuités sont artificielles, et la propagation d'information a travers elle est plus incertaine. Dans la perspective d'assimiler conjointement des observations météo et neige, et étant donné l'important contenu en informations météorologiques porté par les observations in-situ de neige (e.g. Magnusson et al., 2014), s'affranchir de telles barrières serait probablement bénéfique.

Stratégies d'assimilation

Tandis que la prévision numérique du temps et la modélisation des surfaces continentales ont progressé sous l'impulsion de l'assimilation de données (Rabier, 2005), un manque criant d'observations, et la grande variabilité intrinsèque du milieu montagneux ont grandement limité les avancées de la prévision nivo-météorologique en montagne. Un jour, nous disposerons d' observations révolutionnaires, comme les observations satellites ou aéroportées de hauteur de neige (e.g. Painter et al., 2016; Deschamps-Berger et al., 2020), ou de fiables observations de réflectance de surface (Lamare et al., 2020), de manière opérationnelle sur des montagnes entières. Celles-ci amélioreront de manière certaine les capacités des systèmes de modélisation (e.g. Margulis et al., 2019; Deschamps-Berger et al., in review). En attendant, la moindre information disponible doit être exploitée, et les chaines de modélisation du manteau neigeux doivent se préparer à l'assimilation d'informations spatialisées. Ces deux objectifs impliquent un passage vers une modélisation à plus haute résolution, explicite, et capable d'assimiler des observations in-situ comme spatialisées.

La géométrie distribuée est probablement la plus adaptée pour tirer parti d'observations de champs de précipitations radar (Birman et al., 2017) ou de flux SW et LW déduits d'observations satellites (Quéno et al., 2020b). Dans une géométrie spatialisée, ces observations pourraient en effet être directement utilisées pour analyser les champs de forçages météorologiques. Il faut cependant noter que la descente d'échelle des forçages météorologiques à une résolution pertinente pour la modélisation du manteau neigeux est un défi (Vionnet et al., 2019).

En parallèle, les observations d'enneigement in-situ contiennent de précieuses informations sur les conditions météorologiques passées ainsi que sur les erreurs de modélisation dans les zones reculées, mais sont à ce jour trop peu exploitées. Il faut trouver une solution pour les exploiter en domaine spatialisé, suivant l'approche de (Winstral et al., 2019) (i.e. avec des hypothèses fortes sur la physique de la neige) ou bien avec la méthode que nous avons proposé en Chap 4 qui peut être soumise à des compensations d'erreurs (e.g. Smyth et al., 2019), mais laisse la possibilité de corriger également des erreurs de modélisation du manteau neigeux. Tirer profit des informations de SCF dans un contexte distribué semble

tout à fait réalisable avec le PF (Baba et al., 2018). Enfin les informations provenant des nombreuses "webcams" de montagne (Portenier et al., 2020) pourraient également être assimilées dans un tel contexte. Nous le voyons, des pistes d'améliorations sont à notre portée.

Pour conclure, bien que les observations nivo-météorologiques en montagne semblent pauvres, l'assimilation de données pourrait permettre d'améliorer les modèles de manteau neigeux, si elle parvenait à toutes les intégrer. La neige pourrait alors nous révéler une partie de ses secrets. En espérant qu'elle en garde quelques uns...

Bibliography

Aalstad, K., Westermann, S., Schuler, T. V., Boike, J., and Bertino, L.: Ensemble-based assimilation of fractional snow-covered area satellite retrievals to estimate the snow distribution at Arctic sites, The Cryosphere, 12, 10.5194/tc-12-247-2018], 2018.

Abe, O.: Shear strength and angle of repose of snow layers including graupel, Annals of Glaciology, 38, 305–308, 10.3189/172756404781815149], 2004.

Ajami, H., Khan, U., Tuteja, N. K., and Sharma, A.: Development of a computationally efficient semi-distributed hydrologic modeling application for soil moisture, lateral flow and runoff simulation, Environmental Modelling & Software, 85, 319–331, 10.1016/j.envsoft.2016.09.002], 2016.

Albrecht, G., Sartore, G.-M., Connor, L., Higginbotham, N., Freeman, S., Kelly, B., Stain, H., Tonna, A., and Pollard, G.: Solastalgia: the distress caused by environmental change, Australasian psychiatry, 15, S95–S98, 10.1080/10398560701701288], 2007.

Alonso-Gónzalez, E., Gutmann, E., Aalstad, K., Fayad, A., and Gascoin, S.: Snowpack dynamics in the Lebanese mountains from quasi-dynamically downscaled ERA5 reanalysis updated by assimilating remotely-sensed fractional snow-covered area, Hydrology and Earth System Sciences Discussions, pp. 1–31, 10.5194/hess-2020-335], 2020.

Anderson, E. A.: A point energy and mass balance model of a snow cover, Tech. rep., Office of Hydrology - National Weather Service, 1976.

Andreadis, K. M. and Lettenmaier, D. P.: Assimilating remotely sensed snow observations into a macroscale hydrology model, Advances in water resources, 29, 872–886, 10.1016/j.advwatres.2005.08.004], 2006.

Arduini, G., Balsamo, G., Dutra, E., Day, J. J., Sandu, I., Boussetta, S., and Haiden, T.: Impact of a Multi-Layer Snow Scheme on Near-Surface Weather Forecasts, Journal of Advances in Modeling Earth Systems, 11, 4687–4710, 2019.

Arnell, N. and Reynard, N.: The effects of climate change due to global warming on river flows in Great Britain, Journal of hydrology, 183, 397–424, 1996.

Arulampalam, M. S., Maskell, S., Gordon, N., and Clapp, T.: A tutorial on particle filters for online nonlinear/non-Gaussian Bayesian tracking, IEEE Transactions on signal processing, 50, 174–188, 2002.

Atger, F.: The skill of ensemble prediction systems, Monthly Weather Review, 127, 1941–1953, 10.1175/1520-0493(1999)127<1941:TSOEPS>2.0.CO;2], 1999.

Baba, M., Gascoin, S., and Hanich, L.: Assimilation of Sentinel-2 Data into a Snowpack Model in the High Atlas of Morocco, Remote Sensing, 10, 1982, 10.3390/rs10121982], 2018.

Baba, M. W., Gascoin, S., Kinnard, C., Marchane, A., and Hanich, L.: Effect of Digital Elevation Model Resolution on the Simulation of the Snow Cover Evolution in the High Atlas, Water Resources Research, 55, 5360–5378, 10.1029/2018wr023789], 2019.

Bannister, R.: A review of operational methods of variational and ensemble-variational data assimilation, Quarterly Journal of the Royal Meteorological Society, 143, 607–633, 2017.

Barnett, T. P., Adam, J. C., and Lettenmaier, D. P.: Potential impacts of a warming climate on water availability in snow-dominated regions, Nature, 438(7066), 303–309, 10.1038/nature04141], 2005.

Bebi, P., Kulakowski, D., and Rixen, C.: Snow avalanche disturbances in forest ecosystems—State of research and implications for management, Forest ecology and Management, 257, 1883–1892, 2009.

Bellaire, S. and Schweizer, J.: Measuring spatial variations of weak layer and slab properties with regard to snow slope stability, Cold regions science and technology, 65, 234–241, 2011.

Bellier, J., Zin, I., and Bontron, G.: Sample stratification in verification of ensemble forecasts of continuous scalar variables: Potential benefits and pitfalls, Monthly Weather Review, 145, 3529–3544, 10.1175/MWR-D-16-0487.1], 2017.

Bengtsson, L.: Evaporation from a snow cover: Review and discussion of measurements, Hydrology Research, 11, 221–234, 1980.

Bengtsson, T., Bickel, P., and Li, B.: Curse-of-dimensionality revisited: Collapse of the particle filter in very large scale systems, in: Probability and Statistics: Essays in Honor of David A. Freedman, edited by Nolan, D. and Speed, T., vol. Volume 2 of *Collections*, pp. 316–334, Institute of Mathematical Statistics, Beachwood, Ohio, USA, 10.1214/193940307000000518], 2008.

Beven, K. J. and Kirkby, M. J.: A physically based, variable contributing area model of basin hydrology/Un modèle à base physique de zone d'appel variable de l'hydrologie du bassin versant, Hydrological Sciences Journal, 24, 43–69, 1979.

Birman, C., Karbou, F., Mahfouf, J.-F., Lafaysse, M., Durand, Y., Giraud, G., Mérindol, L., and Hermozo, L.: Precipitation analysis over the French Alps using a variational approach and study of potential added value of ground-based radar observations, Journal of Hydrometeorology, 18, 1425–1451, 10.1175/JHM-D-16-0144.1], 2017.

Blayo, É., Bocquet, M., Cosme, E., and Cugliandolo, L. F.: Advanced Data Assimilation for Geosciences: Lecture Notes of the Les Houches School of Physics: Special Issue, June 2012, Oxford University Press, USA, 2014.

Blöschl, G.: Scaling issues in snow hydrology, Hydrological processes, 13, 2149–2175, 1999.

Bocquet, M., Pires, C. A., and Wu, L.: Beyond Gaussian statistical modeling in geophysical data assimilation, Monthly Weather Review, 138, 2997–3023, 2010.

Bonavita, M., Isaksen, L., and Hólm, E.: On the use of EDA background error variances in the ECMWF 4D-Var, Quarterly journal of the royal meteorological society, 138, 1540–1559, 2012.

Bouttier, F., Raynaud, L., Nuissier, O., and Ménétrier, B.: Sensitivity of the AROME ensemble to initial and surface perturbations during HyMeX, Quarterly Journal of the Royal Meteorological Society, 142, 390–403, 10.1002/qj.2622], 2016.

Brasnett, B.: A global analysis of snow depth for numerical weather prediction, Journal of Applied Meteorology, 38, 726–740, 1999.

Brun, E., Martin, E., Simon, V., Gendre, C., and Coléou, C.: An energy and mass model of snow cover suitable for operational avalanche forecasting, J. Glaciol., 35, 333 – 342, 1989.

Brun, E., David, P., Sudul, M., and Brunot, G.: A numerical model to simulate snow-cover stratigraphy for operational avalanche forecasting, J. Glaciol., 38, 13 – 22, 10.3189/S0022143000009552], 1992.

Brun, E., Six, D., Picard, G., Vionnet, V., Arnaud, L., Bazile, E., Boone, A., Bouchard, A., Genthon, C., Guidard, V., Moigne, P. L., Rabier, F., and Seity, Y.: Snow/atmosphere coupled simulation at Dome C, Antarctica, J. Glaciol., 52, 721 – 736, 10.3189/002214311797409794], 2011.

Bühler, Y., Marty, M., Egli, L., Veitinger, J., Jonas, T., Thee, P., and Ginzler, C.: Snow depth mapping in high-alpine catchments using digital photogrammetry., Cryosphere, 9, 2015.

Buizza, R., Milleer, M., and Palmer, T. N.: Stochastic representation of model uncertainties in the ECMWF ensemble prediction system, Quarterly Journal of the Royal Meteorological Society, 125, 2887–2908, 1999.

Cantet, P., Boucher, M., Lachance-Coutier, S., Turcotte, R., and Fortin, V.: Using a particle filter to estimate the spatial distribution of the snowpack water equivalent, Journal of Hydrometeorology, 20, 577–594, 10.1175/JHM-D-18-0140.1], 2019.

Carrassi, A., Bocquet, M., Bertino, L., and Evensen, G.: Data assimilation in the geosciences: An overview of methods, issues, and perspectives, Wiley Interdisciplinary Reviews: Climate Change, 9, e535, 2018.

Charrois, L.: Assimilation de réflectances satellitaires du domaine visible et proche infrarouge dans un modèle détaillé de manteau neigeux, Ph.D. thesis, Grenoble Alpes, 2017.

Charrois, L., Cosme, E., Dumont, M., Lafaysse, M., Morin, S., Libois, Q., and Picard, G.: On the assimilation of optical reflectances and snow depth observations into a detailed snowpack model, The Cryosphere, 10, 1021–1038, 10.5194/tc-10-1021-2016], 2016.

Choquette, Y., Lavigne, P., Nadeau, M., Ducharme, P., Martin, J., Houdayer, A., and Rogoza, J.: GMON, a new sensor for snow water equivalent via gamma monitoring, in: Proceedings Whistler 2008 International Snow Science Workshop September 21-27, 2008, p. 802, 2008.

Clark, M. P. and Hay, L. E.: Use of medium-range numerical weather prediction model output to produce forecasts of streamflow, Journal of Hydrometeorology, 5, 15–32, 2004.

Clark, M. P., Slater, A. G., Rupp, D. E., Woods, R. A., Vrugt, J. A., Gupta, H. V., Wagener, T., and Hay, L. E.: Framework for Understanding Structural Errors (FUSE): A modular framework to diagnose differences between hydrological models, Water Resources Research, 44, 2008.

Clark, M. P., Hendrikx, J., Slater, A. G., Kavetski, D., Anderson, B., Cullen, N. J., Kerr, T., Örn Hreinsson, E., and Woods, R. A.: Representing spatial variability of snow water equivalent in hydrologic and land-surface models: A review, Water Resources Research, 47, 2011.

Clayton, A. M., Lorenc, A. C., and Barker, D. M.: Operational implementation of a hybrid ensemble/4D-Var global data assimilation system at the Met Office, Quarterly Journal of the Royal Meteorological Society, 139, 1445–1461, 2013.

Cloke, H. and Pappenberger, F.: Ensemble flood forecasting: A review, Journal of hydrology, 375, 613–626, 2009.

Cluzet, B., Revuelto, J., Lafaysse, M., Tuzet, F., Cosme, E., Picard, G., Arnaud, L., and Dumont, M.: Towards the assimilation of satellite reflectance into semi-distributed ensemble snowpack simulations, Cold Regions Science and Technology, 170, 102 918, https://doi.org/10.1016/j.coldregions.2019.102918], 2020.

Cluzet, B., Lafaysse, M., Cosme, E., Albergel, C., Meunier, L.-F., and Dumont, M.: CrocO_v1. 0: a particle filter to assimilate snowpack observations in a spatialised framework, Geoscientific Model Development, 14, 1595–1614, 10.5194/gmd-14-1595-2021], 2021.

Colbeck, S. C.: An overview of seasonal snow metamorphism, Reviews of Geophysics and Space Physics, 20, 45–61, 1982.

Cosme, E., Verron, J., Brasseur, P., Blum, J., and Auroux, D.: Smoothing problems in a Bayesian framework and their linear Gaussian solutions, Monthly Weather Review, 140, 683–695, 2012.

Cressman, G. P.: An operational objective analysis system, Mon. Wea. Rev, 87, 367–374, 1959.

Davaze, L., Rabatel, A., Arnaud, Y., Sirguey, P., Six, D., Letreguilly, A., and Dumont, M.: Monitoring glacier albedo as a proxy to derive summer and annual surface mass balances from optical remote-sensing data, The Cryosphere, 12, 271–286, 10.5194/tc-12-271-2018], 2018.

De Lannoy, G. J. M., Reichle, R. H., Arsenault, K. R., Houser, P. R., Kumar, S., Verhoest, N. E. C., and Pauwels, V. R. N.: Multiscale assimilation of Advanced Microwave Scanning Radiometer–EOS snow water equivalent and Moderate Resolution Imaging Spectroradiometer snow cover fraction observations in northern Colorado, Water Resources Research, 48, https://doi.org/10.1029/2011WR010588], 2012.

Decharme, B., Brun, E., Boone, A., Delire, C., Le Moigne, P., and Morin, S.: Impacts of snow and organic soils parameterization on northern Eurasian soil temperature profiles simulated by the ISBA land surface model, The Cryosphere, 10, 853–877, 10.5194/tc-10-853-2016], 2016.

Dedieu, J.-P., Carlson, B. Z., Bigot, S., Sirguey, P., Vionnet, V., and Choler, P.: On the importance of high-resolution time series of optical imagery for quantifying the effects of snow cover duration on alpine plant habitat, Remote Sensing, 8, 481, 2016.

Dee, D. P.: Bias and data assimilation, Quarterly Journal of the Royal Meteorological Society: A journal of the atmospheric sciences, applied meteorology and physical oceanography, 131, 3323–3343, 2005.

Descamps, L., Labadie, C., Joly, A., Bazile, E., Arbogast, P., and Cébron, P.: PEARP, the Météo-France short-range ensemble prediction system, Quarterly Journal of the Royal Meteorological Society, 141, 1671–1685, 10.1002/qj.2469], 2015.

Deschamps-Berger, C., Gascoin, S., Berthier, E., Deems, J., Gutmann, E., Dehecq, A., Shean, D., and Dumont, M.: Snow depth mapping from stereo satellite imagery in mountainous terrain: evaluation using airborne laser-scanning data, The Cryosphere, 14, 2925–2940, 10.5194/tc-14-2925-2020], 2020.

Deschamps-Berger, C., Cluzet, B., Dumont, M., Lafaysse, M., Berthier, E., Fanise, P., and Gascoin, S.: Assimilation of snow depth maps from spaceborne photogrammetry in a detaled snowpack model, in review.

Desroziers, G., Berre, L., Chapnik, B., and Poli, P.: Diagnosis of observation, background and analysis-error statistics in observation space, Quarterly Journal of the Royal Meteorological Society: A journal of the atmospheric sciences, applied meteorology and physical oceanography, 131, 3385–3396, 2005.

Di Mauro, B., Fava, F., Ferrero, L., Garzonio, R., Baccolo, G., Delmonte, B., and Colombo, R.: Mineral dust impact on snow radiative properties in the European Alps combining ground, UAV, and satellite observations, Journal of Geophysical Research: Atmospheres, 120, 6080–6097, 2015.

Di Mauro, B., Garzonio, R., Rossini, M., Filippa, G., Pogliotti, P., Galvagno, M., Morra di Cella, U., Migliavacca, M., Baccolo, G., Clemenza, M., et al.: Saharan dust events in the European Alps: role in snowmelt and geochemical characterization, The Cryosphere, 13, 1147–1165, 2019.

Domine, F., Salvatori, R., Legagneux, L., Salzano, R., Fily, M., and Casacchia, R.: Correlation between the specific surface area and the short wave infrared (SWIR) reflectance of snow: preliminary investigation., Cold Reg. Sci. Technol., 46, 60–68, 10.1016/j.coldregions.2006.06.002], 2006a.

Domine, F., Taillandier, A., Houdier, S., Parrenin, F., Simpson, W. R., and Douglas, T. A.: Interactions between snow metamorphism and climate: Physical and chemical aspects, SPECIAL PUBLICATION-ROYAL SOCIETY OF CHEMISTRY, 311, 27, 2006b.

Domine, F., Gauthier, G., Vionnet, V., Fauteux, D., Dumont, M., and Barrere, M.: Snow physical properties may be a significant determinant of lemming population dynamics in the high Arctic, Arctic Science, 4, 813–826, 2018.

Doucet, A.: On sequential simulation-based methods for Bayesian filtering, Tech. rep., 1998.

Dozier, J., Green, R. O., Nolin, A. W., and Painter, T. H.: Interpretation of snow properties from imaging spectrometry, Remote Sensing of Environment, 113, S25–S37, 2009.

Dozier, J., Bair, E. H., and Davis, R. E.: Estimating the spatial distribution of snow water equivalent in the world's mountains, Wiley Interdisciplinary Reviews: Water, 3, 461–474, 2016.

Dumont, M., Brissaud, O., Picard, G., Schmitt, B., Gallet, J.-C., and Arnaud, Y.: High-accuracy measurements of snow Bidirectional Reflectance Distribution Function at visible and NIR wavelengths – comparison with modelling results, Atmos. Chem. Phys., 10, 2507–2520, 2010.

Dumont, M., Durand, Y., Arnaud, Y., and Six, D.: Variational assimilation of albedo in a snowpack model and reconstruction of the spatial mass-balance distribution of an alpine glacier, J. Glaciol., 58(207), 151 – 164, 10.3189/2012JoG11J163], 2012.

Dumont, M., Arnaud, L., Picard, G., Libois, Q., Lejeune, Y., Nabat, P., Voisin, D., and Morin, S.: In situ continuous visible and near-infrared spectroscopy of an alpine snowpack, The Cryosphere, 11, 1091–1110, 2017.

Dumont, M., Tuzet, F., Gascoin, S., Picard, G., Kutuzov, S., Lafaysse, M., Cluzet, B., Nheili, R., and Painter, T. H.: Accelerated Snow Melt in the Russian Caucasus Mountains After the Saharan Dust Outbreak in March 2018, Journal of Geophysical Research: Earth Surface, 125, e2020JF005 641, https://doi.org/10.1029/2020JF005641], e2020JF005641 10.1029/2020JF005641, 2020.

Durand, M. and Margulis, S. A.: Feasibility test of multifrequency radiometric data assimilation to estimate snow water equivalent, Journal of Hydrometeorology, 7, 443–457, 2006.

Durand, M. and Margulis, S. A.: Correcting first-order errors in snow water equivalent estimates using a multifrequency, multiscale radiometric data assimilation scheme, Journal of Geophysical Research: Atmospheres, 112, https://doi.org/10.1029/2006JD008067], 2007.

Durand, M. and Margulis, S. A.: Effects of uncertainty magnitude and accuracy on assimilation of multiscale measurements for snowpack characterization, Journal of Geophysical Research: Atmospheres, 113, 2008.

Durand, M., Molotch, N. P., and Margulis, S. A.: A Bayesian approach to snow water equivalent reconstruction, Journal of Geophysical Research: Atmospheres, 113, 2008.

Durand, M., Kim, E. J., and Margulis, S. A.: Radiance assimilation shows promise for snowpack characterization, Geophysical Research Letters, 36, 2009.

Durand, Y., Brun, E., Mérindol, L., Guyomarc'h, G., Lesaffre, B., and Martin, E.: A meteorological estimation of relevant parameters for snow models, Ann. Glaciol., 18, 65–71, 10.3189/S0260305500011277], 1993.

Durand, Y., Giraud, G., Brun, E., Mérindol, L., and Martin, E.: A computer-based system simulating snowpack structures as a tool for regional avalanche forecasting, J. Glaciol., 45, 469–484, 10.3189/S0022143000001337], 1999.

Dutra, E., Viterbo, P., Miranda, P. M., and Balsamo, G.: Complexity of snow schemes in a climate model and its impact on surface energy and hydrology, Journal of Hydrometeorology, 13, 521–538, 2012.

Eberhard, L. A., Sirguey, P., Miller, A., Marty, M., Schindler, K., Stoffel, A., and Bühler, Y.: Intercomparison of photogrammetric platforms for spatially continuous snow depth mapping, The Cryosphere Discussions, pp. 1–40, 2020.

Elder, K., Rosenthal, W., and Davis, R. E.: Estimating the spatial distribution of snow water equivalence in a montane watershed, Hydrological Processes, 12, 1793–1808, 1998.

Essery, R.: A factorial snowpack model (FSM 1.0), Geosci. Model Dev., 8, 3867–3876, 10.5194/gmd-8-3867-2015], 2015.

Essery, R., Morin, S., Lejeune, Y., and Bauduin-Ménard, C.: A comparison of 1701 snow models using observations from an alpine site, Adv. Water Res., 55, 131–148, 10.1016/j.advwatres.2012.07.013], 2013.

Essery, R., Kontu, A., Lemmetyinen, J., Dumont, M., and Ménard, C. B.: A 7-year dataset for driving and evaluating snow models at an arctic site (Sodankylä, Finland), Geosci. Instrum. Method. Data Syst., 5, 219–227, 2016.

Evensen, G.: Sequential data assimilation with a nonlinear quasi-geostrophic model using Monte Carlo methods to forecast error statistics, Journal of Geophysical Research: Oceans, 99, 10 143–10 162, 1994.

Evensen, G.: The ensemble Kalman filter: Theoretical formulation and practical implementation, Ocean dynamics, 53, 343–367, 2003.

Evensen, G. and Van Leeuwen, P. J.: An ensemble Kalman smoother for nonlinear dynamics, Monthly Weather Review, 128, 1852–1867, 2000.

Eyre, J.: Observation bias correction schemes in data assimilation systems: A theoretical study of some of their properties, Quarterly Journal of the Royal Meteorological Society, 142, 2284–2291, 2016.

Farchi, A. and Bocquet, M.: Comparison of local particle filters and new implementations, Nonlinear Processes in Geophysics, 25, 765–807, 10.5194/npg-25-765-2018], 2018.

Fiddes, J. and Gruber, S.: TopoSUB: a tool for efficient large area numerical modelling in complex topography at sub-grid scales, Geoscientific Model Development, 5, 1245–1257, 10.5194/gmd-5-1245-2012], 2012.

Fiddes, J., Aalstad, K., and Westermann, S.: Hyper-resolution ensemble-based snow reanalysis in mountain regions using clustering, Hydrology and Earth System Sciences, 23, 4717–4736, 2019.

Fierz, C., Armstrong, R. L., Durand, Y., Etchevers, P., Greene, E., McClung, D. M., Nishimura, K., Satyawali, P. K., and Sokratov, S. A.: The international classification for seasonal snow on the ground, IHP-VII Technical Documents in Hydrology n 83, IACS Contribution n 1, 2009.

Fily, M., Dedieu, J.-P., and Durand, Y.: Comparison between the results of a snow metamorphism model and remote sensing derived snow parameters in the Alps, Remote Sens. Environ., 68 (3), 254–263, 10.1016/S0034-4257(98)00116-3], 1999.

Flanner, M. G., Zender, C. S., Randerson, J. T., and Rasch, P. J.: Present-day climate forcing and response from black carbon in snow, Journal of Geophysical Research: Atmospheres, 112, 2007.

Fortin, V., Abaza, M., Anctil, F., and Turcotte, R.: Why should ensemble spread match the RMSE of the ensemble mean? (vol 15, pg 1708, 2014), J. Hydrometeorol., 16, 484, 10.1175/JHM-D-14-0008.1], 2015.

Francon, L., Corona, C., Till-Bottraud, I., Choler, P., Carlson, B., Charrier, G., Améglio, T., Morin, S., Eckert, N., Roussel, E., et al.: Assessing the effects of earlier snow melt-out on alpine shrub growth: The sooner the better?, Ecological Indicators, 115, 106 455, 2020.

Frappier, J.: Les trois ballades du temps jadis dans le Testament de François Villon, Bulletins de l'Académie Royale de Belgique, 57, 316–341, 1971.

Fuhrer, J., Smith, P., and Gobiet, A.: Implications of climate change scenarios for agriculture in alpine regions—A case study in the Swiss Rhone catchment, Science of the Total Environment, 493, 1232–1241, 2014.

Gagné, K., Rasmussen, M. B., and Orlove, B.: Glaciers and society: Attributions, perceptions, and valuations, Wiley Interdisciplinary Reviews: Climate Change, 5, 793–808, 2014.

Gascoin, S., Hagolle, O., Huc, M., Jarlan, L., Dejoux, J.-F., Szczypta, C., Marti, R., and Sánchez, R.: A snow cover climatology for the Pyrenees from MODIS snow products, Hydrol. Earth Syst. Sci, 19, 2337–2351, 10.5194/hess-19-2337-2015], 2015.

Gascoin, S., Grizonnet, M., Bouchet, M., Salgues, G., and Hagolle, O.: Theia Snow collection: high-resolution operational snow cover maps from Sentinel-2 and Landsat-8 data, Earth System Science Data, 11, 493–514, 2019.

Gaudard, L., Romerio, F., Dalla Valle, F., Gorret, R., Maran, S., Ravazzani, G., Stoffel, M., and Volonterio, M.: Climate change impacts on hydropower in the Swiss and Italian Alps, Science of the Total Environment, 493, 1211–1221, 2014.

Geer, A. J. and Bauer, P.: Observation errors in all-sky data assimilation, Quarterly Journal of the Royal Meteorological Society, 137, 2024–2037, 2011.

Ghil, M., Cohn, S., Tavantzis, J., Bube, K., and Isaacson, E.: Applications of estimation theory to numerical weather prediction, in: Dynamic meteorology: Data assimilation methods, pp. 139–224, Springer, 1981.

Gichamo, T. Z. and Tarboton, D. G.: Ensemble Streamflow Forecasting using an Energy Balance Snowmelt Model Coupled to a Distributed Hydrologic Model with Assimilation of Snow and Streamflow Observations, Water Resources Research, 55, 10 813–10 838, 10.1029/2019WR025472], 2019.

Gordon, N. J., Salmond, D. J., and Smith, A. F.: Novel approach to nonlinear/non-Gaussian Bayesian state estimation, in: IEE Proceedings F (Radar and Signal Processing), vol. 140, pp. 107–113, IET, 1993.

Gottardi, F., Paquet, E., Carrier, P., Laval, M.-T., Gailhard, J., and Garçon, R.: A decade of snow water equivalent monitoring in the French Mountain ranges, in: Proceedings of the International Snow Science Workshop Grenoble - Chamonix Mont-Blanc - 2013, 7-11 October, Grenoble, France, pp. 926–930, 2013.

Grünewald, T. and Lehning, M.: Are flat-field snow depth measurements representative? A comparison of selected index sites with areal snow depth measurements at the small catchment scale, Hydrological Processes, 29, 1717–1728, 10.1002/hyp.10295], 2015.

Günther, D., Marke, T., Essery, R., and Strasser, U.: Uncertainties in Snowpack Simulations—Assessing the Impact of Model Structure, Parameter Choice, and Forcing Data Error on Point-Scale Energy Balance Snow Model Performance, Water Resources Research, 55, 2779–2800, 2019.

Hachikubo, A. and Akitaya, E.: Effect of wind on surface hoar growth on snow, Journal of Geophysical Research: Atmospheres, 102, 4367–4373, 1997.

Haeberli, W. and Whiteman, C.: Snow and ice-related hazards, risks, and disasters: a general framework, in: Snow and Ice-Related Hazards, Risks and Disasters, pp. 1–34, Elsevier, 2015.

Hagolle, O., Huc, M., Descardins, C., Auer, S., and Richter, R.: MAJA Algorithm Theoretical Baseline Document, Tech. rep., https://doi.org/10.5281/zenodo.1209633], 2017.

Hamill, T. M., Whitaker, J. S., and Snyder, C.: Distance-dependent filtering of background error covariance estimates in an ensemble Kalman filter, Monthly Weather Review, 129, 2776–2790, 2001.

Hanzer, F., Helfricht, K., Marke, T., and Strasser, U.: Multilevel spatiotemporal validation of snow/ice mass balance and runoff modeling in glacierized catchments, The Cryosphere, 10, 1859–1881, 2016.

Harder, P., Pomeroy, J. W., and Helgason, W. D.: Improving sub-canopy snow depth mapping with unmanned aerial vehicles: lidar versus structure-from-motion techniques, The Cryosphere, 14, 1919–1935, 2020.

Helbig, N., Bühler, Y., Eberhard, L., Deschamps-Berger, C., Gascoin, S., Dumont, M., Revuelto, J., Deems, J. S., and Jonas, T.: Fractional snow-covered area: Scale-independent peak of winter parameterization, The Cryosphere Discussions, pp. 1–28, 2020.

Helmert, J., Şensoy Şorman, A., Alvarado Montero, R., De Michele, C., de Rosnay, P., Dumont, M., Finger, D., Lange, M., Picard, G., Potopová, V., et al.: Review of Snow Data Assimilation Methods for Hydrological, Land Surface, Meteorological and Climate Models: Results from a COST HarmoSnow Survey, Geosciences, 8, 489, 2018.

Henderson, C. R.: Best linear unbiased estimation and prediction under a selection model, Biometrics, pp. 423–447, 1975.

Hersbach, H.: Decomposition of the continuous ranked probability score for ensemble prediction systems, Weather and Forecasting, 15, 559–570, 2000.

Hersbach, H., Bell, B., Berrisford, P., Hirahara, S., Horányi, A., Muñoz-Sabater, J., Nicolas, J., Peubey, C., Radu, R., Schepers, D., et al.: The ERA5 global reanalysis, Quarterly Journal of the Royal Meteorological Society, 146, 1999–2049, 2020.

Hock, R., Rasul, G., Adler, C., Caceres, B., Gruber, S., Hirabayashi, Y., Jackson, M., Kääb, A., Kang, S., Kutuzov, S., et al.: High Mountain Areas: In: IPCC Special Report on the Ocean and Cryosphere in a Changing Climate, 2019.

Hori, M., Aoki, T., Tanikawa, T., Motoyoshi, H., Hachikubo, A., Sugiura, K., Yasunari, T. J., Eide, H., Storvold, R., Nakajima, Y., et al.: In-situ measured spectral directional emissivity of snow and ice in the 8–14 μm atmospheric window, Remote Sensing of Environment, 100, 486–502, 2006.

Horowitz, L. W., Naik, V., Paulot, F., Ginoux, P. A., Dunne, J. P., Mao, J., Schnell, J., Chen, X., He, J., John, J. G., Lin, M., Lin, P., Malyshev, S., Paynter, D., Shevliakova, E., and Zhao, M.: The GFDL Global Atmospheric Chemistry-Climate Model AM4.1: Model Description and Simulation Characteristics, Journal of Advances in Modeling Earth Systems, 12, e2019MS002 032, https://doi.org/10.1029/2019MS002032], e2019MS002032 2019MS002032, 2020.

Houtekamer, P. L. and Mitchell, H. L.: A sequential ensemble Kalman filter for atmospheric data assimilation, Monthly Weather Review, 129, 123–137, 2001.

Jonas, T., Rixen, C., Sturm, M., and Stoeckli, V.: How alpine plant growth is linked to snow cover and climate variability, Journal of Geophysical Research: Biogeosciences, 113, 2008.

Josse, B., Simon, P., and Peuch, V.-H.: Radon global simulations with the multiscale chemistry and transport model MOCAGE, Tellus B: Chemical and Physical Meteorology, 56, 339–356, 10.3402/tellusb.v56i4.16448], 2004.

Jurt, C., Burga, M. D., Vicuña, L., Huggel, C., and Orlove, B.: Local perceptions in climate change debates: insights from case studies in the Alps and the Andes, Climatic Change, 133, 511–523, 2015.

Kalnay, E.: Atmospheric modeling, data assimilation and predictability, Cambridge university press, 2003.

Kantas, N., Doucet, A., Singh, S. S., Maciejowski, J., Chopin, N., et al.: On particle methods for parameter estimation in state-space models, Statistical science, 30, 328–351, 2015.

Kim, R. S., Durand, M., Li, D., Baldo, E., Margulis, S. A., Dumont, M., and Morin, S.: Estimating alpine snow depth by combining multifrequency passive radiance observations with ensemble snowpack modeling, Remote Sensing of Environment, 226, 1–15, 2019.

Kitagawa, G.: Monte Carlo filter and smoother for non-Gaussian nonlinear state space models, Journal of computational and graphical statistics, 5, 1–25, 1996.

Klinker, E. and Sardeshmukh, P. D.: The diagnosis of mechanical dissipation in the atmosphere from large-scale balance requirements, Journal of the atmospheric sciences, 49, 608–627, 10.1175/1520-0469(1992)049<0608:TDOMDI>2.0.CO;2], 1992.

Kochanski, K., Anderson, R. S., and Tucker, G. E.: The evolution of snow bedforms in the Colorado Front Range and the processes that shape them, The Cryosphere (Online), 13, 2019.

Körner, C., Paulsen, J., and Spehn, E. M.: A definition of mountains and their bioclimatic belts for global comparisons of biodiversity data, Alpine Botany, 121, 73, 2011.

Krinner, G., Derksen, C., Essery, R., Flanner, M., Hagemann, S., Clark, M., Hall, A., Rott, H., Brutel-Vuilmet, C., Kim, H., et al.: ESM-SnowMIP: assessing snow models and quantifying snow-related climate feedbacks, Geoscientific Model Development, 11, 5027–5049, 10.5194/gmd-11-5027-2018], 2018.

Lafaysse, M., Hingray, B., Mezghani, A., Gailhard, J., and Terray, L.: Internal variability and model uncertainty components in future hydrometeorological projections: The Alpine Durance basin, Water resources research, 50, 3317–3341, 2014.

Lafaysse, M., Cluzet, B., Dumont, M., Lejeune, Y., Vionnet, V., and Morin, S.: A multiphysical ensemble system of numerical snow modelling, The Cryosphere, 11, 1173–1198, 10.5194/tc-11-1173-2017], 2017.

Lafaysse, M., Hingray, B., Etchevers, P., Martin, E., and Obled, C.: Influence of spatial discretization, underground water storage and glacier melt on a physically-based hydrological model of the Upper Durance River basin, J. Hydrol., 403, 116–129, 10.1016/j.jhydrol.2011.03.046], 2011.

Lahoz, B. K. W. and Menard, R.: Data assimilation, Springer, Berlin, Heidelberg, https://doi.org/10.1007/978-3-540-74703-1], 2010.

Lamare, M., Dumont, M., Picard, G., Larue, F., Tuzet, F., Delcourt, C., and Arnaud, L.: Simulating Optical Top-Of-Atmosphere Radiance Satellite Images over Snow-Covered Rugged Terrain, The Cryosphere Discussions, pp. 1–46, 2020.

Largeron, C., Dumont, M., Morin, S., Boone, A., Lafaysse, M., Metref, S., Cosme, E., Jonas, T., Winstral, A., and Margulis, S. A.: Toward Snow Cover Estimation in Mountainous Areas Using Modern Data Assimilation Methods: A Review, Frontiers in Earth Science, 8, 10.3389/feart.2020.00325], 2020.

Larue, F., Royer, A., Sève, D. D., Roy, A., and Cosme, E.: Assimilation of passive microwave AMSR-2 satellite observations in a snowpack evolution model over northeastern Canada, Hydrology and Earth System Sciences, 22, 5711–5734, 10.5194/hess-22-5711-2018], 2018.

Larue, F., Picard, G., Arnaud, L., Ollivier, I., Delcourt, C., Lamare, M., Tuzet, F., Revuelto, J., and Dumont, M.: Snow albedo sensitivity to macroscopic surface roughness using a new ray-tracing model, The Cryosphere, 14, 1651–1672, 2020.

Le Moigne, P., Besson, F., Martin, E., Boé, J., Boone, A., Decharme, B., Etchevers, P., Faroux, S., Habets, F., Lafaysse, M., Leroux, D., and Rousset-Regimbeau, F.: The latest improvements with SURFEX v8.0 of the Safran–Isba–Modcou hydrometeorological model for France, Geoscientific Model Development, 13, 3925–3946, 10.5194/gmd-13-3925-2020], 2020.

Lehning, M., Bartelt, P., Brown, B., Russi, T., Stöckli, U., and Zimmerli, M.: SNOWPACK model calculations for avalanche warning based upon a new network of weather and snow stations, Cold Regions Science and Technology, 30, 145–157, 1999.

Lehning, M., Völksch, I., Gustafsson, D., Nguyen, T. A., Stähli, M., and Zappa, M.: ALPINE3D: a detailed model of mountain surface processes and its application to snow hydrology, Hydrol. Process., 20, 2111–2128, 10.1002/hyp.6204], 2006.

Lehning, M., Löwe, H., Ryser, M., and Raderschall, N.: Inhomogeneous precipitation distribution and snow transport in steep terrain, Water Resources Research, 44, 2008.

Leisenring, M. and Moradkhani, H.: Snow water equivalent prediction using Bayesian data assimilation methods, Stochastic Environmental Research and Risk Assessment, 25, 253–270, 2011.

Lejeune, Y., Dumont, M., Panel, J.-M., Lafaysse, M., Lapalus, P., Le Gac, E., Lesaffre, B., and Morin, S.: 57 years (1960–2017) of snow and meteorological observations from a mid-altitude mountain site (Col de Porte, France, 1325 m of altitude), Earth System Science Data, 11, 71, 10.5194/essd-11-71-2019], 2019.

Leutbecher, M., Lock, S.-J., Ollinaho, P., Lang, S. T., Balsamo, G., Bechtold, P., Bonavita, M., Christensen, H. M., Diamantakis, M., Dutra, E., et al.: Stochastic representations of

model uncertainties at ECMWF: State of the art and future vision, Quarterly Journal of the Royal Meteorological Society, 143, 2315–2339, 2017.

Li, D., Durand, M., and Margulis, S. A.: Estimating snow water equivalent in a Sierra Nevada watershed via spaceborne radiance data assimilation, Water Resources Research, 53, 647–671, 2017.

Libbrecht, K. G.: The physics of snow crystals, Rep. Prog. Phys., 68, 855–895, doi:10.1088/0034-4885/68/4/R03], 2005.

Libois, Q.: Evolution des propriétés physiques de la neige de surface sur le Plateau Antarctique. Observations et modélisation du transfert radiatif et du métamorphisme, Ph.D. thesis, Université de Grenoble, 2014.

Libois, Q., Picard, G., France, J., Arnaud, L., Dumont, M., Carmagnola, C. M., and King, M.: Influence of grain shape on light penetration in snow, The Cryosphere, 7, 1803–1818, 10.5194/tc-7-1803-2013], 2013.

Lievens, H., Demuzere, M., Marshall, H.-P., Reichle, R. H., Brucker, L., Brangers, I., de Rosnay, P., Dumont, M., Girotto, M., Immerzeel, W. W., et al.: Snow depth variability in the Northern Hemisphere mountains observed from space, Nature communications, 10, 1–12, 2019.

Liston, G. E., Haehnel, R. B., Sturm, M., Hiemstra, C. A., Berezovskaya, S., and Tabler, R. D.: Simulating complex snow distributions in windy environments using SnowTran-3D, Journal of Glaciology, 53, 241–256, 2007.

López-Moreno, J. I., Fassnacht, S., Heath, J., Musselman, K., Revuelto, J., Latron, J., Morán-Tejeda, E., and Jonas, T.: Small scale spatial variability of snow density and depth over complex alpine terrain: Implications for estimating snow water equivalent, Advances in water resources, 55, 40–52, 2013.

Lorenz, E. N. and Haman, K.: The essence of chaos, Pure and Applied Geophysics, 147, 598–599, 1996.

Lyapustin, A., Tedesco, M., Wang, Y., Aoki, T., Hori, M., and Kokhanovsky, A.: Retrieval of snow grain size over Greenland from MODIS, Remote Sens. Environ., 113, 1976 – 1987, 10.1016/j.rse.2009.05.008], 2009.

Magand, C., Ducharne, A., Le Moine, N., and Gascoin, S.: Introducing hysteresis in snow depletion curves to improve the water budget of a land surface model in an Alpine catchment, Journal of hydrometeorology, 15, 631–649, 2014.

Magnusson, J., Gustafsson, D., Hüsler, F., and Jonas, T.: Assimilation of point SWE data into a distributed snow cover model comparing two contrasting methods, Water resources research, 50, 7816–7835, 10.1002/2014WR015302], 2014.

Magnusson, J., Winstral, A., Stordal, A. S., Essery, R., and Jonas, T.: Improving physically based snow simulations by assimilating snow depths using the particle filter, Water Resources Research, 53, 1125–1143, 10.1002/2016WR019092], 2017.

Malardel, S.: Fondamentaux de météorologie, Cépadues Editions, 2009.

Margulis, S. A., Girotto, M., Cortés, G., and Durand, M.: A particle batch smoother approach to snow water equivalent estimation, Journal of Hydrometeorology, 16, 1752–1772, 2015.

Margulis, S. A., Fang, Y., Li, D., Lettenmaier, D. P., and Andreadis, K.: The Utility of Infrequent Snow Depth Images for Deriving Continuous Space-Time Estimates of Seasonal Snow Water Equivalent, Geophysical Research Letters, 46, 5331–5340, 10.1029/2019GL082507], 2019.

Marin, C., Bertoldi, G., Premier, V., Callegari, M., Brida, C., Hürkamp, K., Tschiersch, J., Zebisch, M., and Notarnicola, C.: Use of Sentinel-1 radar observations to evaluate snowmelt dynamics in alpine regions., The Cryosphere, 14, 935–935, 2020.

Marsh, C. B., Pomeroy, J. W., and Wheater, H. S.: The Canadian Hydrological Model (CHM) v1. 0: a multi-scale, multi-extent, variable-complexity hydrological model-design and overview., Geoscientific Model Development, 13, 225–225, 2020.

Marti, R., Gascoin, S., Berthier, E., Pinel, M. d., Houet, T., and Laffly, D.: Mapping snow depth in open alpine terrain from stereo satellite imagery, The Cryosphere, 10, 1361–1380, 2016.

Martin, E. and Lejeune, Y.: Turbulent fluxes above the snow surface, Ann. Glaciol., 26, 179–183, 1998.

Mary, A., Dumont, M., Dedieu, J.-P., Durand, Y., Sirguey, P., Milhem, H., Mestre, O., Negi, H. S., Kokhanovsky, A. A., Lafaysse, M., and Morin, S.: Intercomparison of retrieval algorithms for the specific surface area of snow from near-infrared satellite data in mountainous terrain, and comparison with the output of a semi-distributed snowpack model, The Cryosphere, 7, 741–761, 10.5194/tc-7-741-2013], 2013.

Masson, T., Dumont, M., Mura, M. D., Sirguey, P., Gascoin, S., Dedieu, J.-P., and Chanussot, J.: An Assessment of Existing Methodologies to Retrieve Snow Cover Fraction from MODIS Data, Remote Sensing, 10, 10.3390/rs10040619], 2018.

Masson, V., Le Moigne, P., Martin, E., Faroux, S., Alias, A., Alkama, R., Belamari, S., Barbu, A., Boone, A., Bouyssel, F., Brousseau, P., Brun, E., Calvet, J.-C., Carrer, D., Decharme, B., Delire, C., Donier, S., Essaouini, K., Gibelin, A.-L., Giordani, H., Habets, F., Jidane, M., Kerdraon, G., Kourzeneva, E., Lafaysse, M., Lafont, S., Lebeaupin Brossier, C., Lemonsu, A., Mahfouf, J.-F., Marguinaud, P., Mokhtari, M., Morin, S., Pigeon, G., Salgado, R., Seity, Y., Taillefer, F., Tanguy, G., Tulet, P., Vincendon, B., Vionnet, V., and Voldoire, A.: The SURFEXv7.2 land and ocean surface platform for coupled or offline simulation of Earth surface variables and fluxes, Geoscientific Model Development, 6, 929–960, 10.5194/gmd-6-929-2013], 2013.

McNeeley, S. M.: Sustainable climate change adaptation in Indian country, Weather, Climate, and Society, 9, 393–404, 2017.

Ménard, C. B., Essery, R., Barr, A., Bartlett, P., Derry, J., Dumont, M., Fierz, C., Kim, H., Kontu, A., Lejeune, Y., et al.: Meteorological and evaluation datasets for snow modelling at 10 reference sites: description of in situ and bias-corrected reanalysis data, Earth System Science Data, 11, 865–880, 2019.

Menard, C. B., Essery, R., Krinner, G., Arduini, G., Bartlett, P., Boone, A., Brutel-Vuilmet, C., Burke, E., Cuntz, M., Dai, Y., et al.: Scientific and human errors in a snow model intercomparison, Bulletin of the American Meteorological Society, pp. 1–46, 2020.

Minzner, R.: The 1976 standard atmosphere and its relationship to earlier standards, Reviews of geophysics, 15, 375–384, 1977.

Molotch, N. P. and Bales, R. C.: SNOTEL representativeness in the Rio Grande headwaters on the basis of physiographics and remotely sensed snow cover persistence, Hydrological Processes: An International Journal, 20, 723–739, 2006.

Molteni, F., Buizza, R., Palmer, T. N., and Petroliagis, T.: The ECMWF ensemble prediction system: Methodology and validation, Quarterly journal of the royal meteorological society, 122, 73–119, 1996.

Morin, S., Lejeune, Y., Lesaffre, B., Panel, J.-M., Poncet, D., David, P., and Sudul, M.: A 18-years long (1993 - 2011) snow and meteorological dataset from a mid-altitude mountain site (Col de Porte, France, 1325 m alt.) for driving and evaluating snowpack models, Earth Syst. Sci. Data, 4, 13–21, 10.5194/essd-4-13-2012], 2012.

Morin, S., Horton, S., Techel, F., Bavay, M., Coléou, C., Fierz, C., Gobiet, A., Hagenmuller, P., Lafaysse, M., Ližar, M., Mitterer, C., Monti, F., Müller, K., Olefs, M., Snook, J. S., van Herwijnen, A., and Vionnet, V.: Application of physical snowpack models in

support of operational avalanche hazard forecasting: A status report on current implementations and prospects for the future, Cold Regions Science and Technology, 170, 102 910, https://doi.org/10.1016/j.coldregions.2019.102910], 2020.

Mott, R., Vionnet, V., and Grünewald, T.: The Seasonal Snow Cover Dynamics: Review on Wind-Driven Coupling Processes, Frontiers in Earth Science, 6, 10.3389/feart.2018.00197], 2018.

Mutke, J. and Barthlott, W.: Patterns of vascular plant diversity at continental to global scales, Biologiske skrifter, 55, 521–531, 2005.

Nabat, P., Somot, S., Mallet, M., Michou, M., Sevault, F., Driouech, F., Meloni, D., di Sarra, A., Di Biagio, C., Formenti, P., et al.: Dust aerosol radiative effects during summer 2012 simulated with a coupled regional aerosol–atmosphere–ocean model over the Mediterranean, Atmospheric Chemistry and physics, 15, 3303–3326, 10.5194/acp-15-3303-2015], 2015.

Niwano, M., Aoki, T., Hashimoto, A., Matoba, S., Yamaguchi, S., Tanikawa, T., Fujita, K., Tsushima, A., Iizuka, Y., Shimada, R., et al.: NHM–SMAP: spatially and temporally high-resolution nonhydrostatic atmospheric model coupled with detailed snow process model for Greenland Ice Sheet, The Cryosphere, 12, 635, 10.5194/tc-12-635-2018], 2018.

Noilhan, J. and Planton, S.: A simple parameterization of land surface processes for meteorological models, Mon. Weather Rev., 117, 536–549, 10.1175/1520-0493(1989)117<0536:ASPOLS>2.0.CO;2], 1989.

Nousu, J.-P., Lafaysse, M., Vernay, M., Bellier, J., Evin, G., and Joly, B.: Statistical post-processing of ensemble forecasts of the height of new snow, Nonlinear Processes in Geophysics, 26, 339–357, 10.5194/npg-26-339-2019], 2019.

Nüsser, M. and Schmidt, S.: Nanga Parbat revisited: Evolution and dynamics of sociohydrological interactions in the Northwestern Himalaya, Annals of the American Association of Geographers, 107, 403–415, 10.4324/9781315158914-15], 2017.

Ollinaho, P., Lock, S.-J., Leutbecher, M., Bechtold, P., Beljaars, A., Bozzo, A., Forbes, R. M., Haiden, T., Hogan, R. J., and Sandu, I.: Towards process-level representation of model uncertainties: stochastically perturbed parametrizations in the ECMWF ensemble, Quarterly Journal of the Royal Meteorological Society, 143, 408–422, 2017.

Painter, T. H., Rittger, K., McKenzie, C., Slaughter, P., Davis, R. E., and Dozier, J.: Retrieval of subpixel snow covered area, grain size, and albedo from MODIS, Remote Sens. Environ., 113, 868 – 879, 10.1016/j.rse.2009.01.001], 2009.

Painter, T. H., Berisford, D. F., Boardman, J. W., Bormann, K. J., Deems, J. S., Gehrke, F., Hedrick, A., Joyce, M., Laidlaw, R., Marks, D., et al.: The Airborne Snow Observatory: Fusion of scanning lidar, imaging spectrometer, and physically-based modeling for mapping snow water equivalent and snow albedo, Remote Sensing of Environment, 184, 139–152, 10.1016/j.rse.2016.06.018], 2016.

Palchetti, L., Barucci, M., Belotti, C., Bianchini, G., Cluzet, B., D'Amato, F., Del Bianco, S., Di Natale, G., Gai, M., Khordakova, D., Montori, A., Oetjen, H., Rettinger, M., Rolf, C., Schuettemeyer, D., Sussmann, R., Viciani, S., Vogelmann, H., and Wienhold, F. G.: Observations of the downwelling far-infrared atmospheric emission at the Zugspitze observatory, Earth System Science Data, 13, 4303–4312, 10.5194/essd-13-4303-2021], 2021.

Palmer, T., Buizza, R., Doblas-Reyes, F., Jung, T., Leutbecher, M., Shutts, G., M., S., and Weisheimer, A.: Stochastic Parametrization and Model Uncertainty, Technical Memorandum 598, ECMWF, URL http://www.ecmwf.int/sites/default/files/elibrary/2009/11577-stochastic-parametrization-and-model-uncertainty.pdf, 2009.

Palmer, T. N.: Extended-range atmospheric prediction and the Lorenz model, Bulletin of the American Meteorological Society, 74, 49–66, 10.1175/1520-0477(1993)074<0049:erapat>2.0.co;2], 1993.

Paquet, E. and Laval, M.-T.: Operation feedback and prospects of EDF Cosmic-Ray Snow Sensors, La Houille Blanche, 2, 113 – 119, 10.1051/lhb:200602015], 2006.

Penny, S. G. and Miyoshi, T.: A local particle filter for high-dimensional geophysical systems, Nonlinear Processes in Geophysics, 23, 391, 10.5194/npg-23-391-2016], 2016.

Piazzi, G., Thirel, G., Campo, L., and Gabellani, S.: A particle filter scheme for multivariate data assimilation into a point-scale snowpack model in an Alpine environment, The Cryosphere, 12, 2287–2306, 10.5194/tc-12-2287-2018], 2018.

Piazzi, G., Campo, L., Gabellani, S., Castelli, F., Cremonese, E., di Cella, U. M., Stevenin, H., and Ratto, S. M.: An EnKF-based scheme for snow multivariable data assimilation at an Alpine site, Journal of Hydrology and Hydromechanics, 67, 4–19, 2019.

Picard, G., Dumont, M., Lamare, M., Tuzet, F., Larue, F., Pirazzini, R., and Arnaud, L.: Spectral albedo measurements over snow-covered slopes: theory and slope effect corrections, The Cryosphere, 14, 1497–1517, 10.5194/tc-14-1497-2020], 2020.

Pielke, R., Liston, G., Chapman, W., and Robinson, D.: Actual and insolation-weighted Northern Hemisphere snow cover and sea-ice between 1973–2002, Climate Dynamics, 22, 591–595, 10.1007/s00382-004-0401-5], 2004.

Pomeroy, J. W., Fang, X., and Marks, D. G.: The cold rain-on-snow event of June 2013 in the Canadian Rockies—Characteristics and diagnosis, Hydrological Processes, 30, 2899–2914, 10.1002/hyp.10905], 2016.

Portenier, C., Hüsler, F., Härer, S., and Wunderle, S.: Towards a webcam-based snow cover monitoring network: methodology and evaluation, The Cryosphere, 14, 1409–1423, 10.5194/tc-14-1409-2020], 2020.

Poterjoy, J.: A localized particle filter for high-dimensional nonlinear systems, Monthly Weather Review, 144, 59–76, 10.1175/MWR-D-15-0163.1], 2016.

Pritchard, D. M., Forsythe, N., O'Donnell, G., Fowler, H. J., and Rutter, N.: Multi-physics ensemble snow modelling in the western Himalaya, The Cryosphere, 14, 1225–1244, 10.5194/tc-14-1225-2020], 2020.

Prokop, A.: Assessing the applicability of terrestrial laser scanning for spatial snow depth measurements, Cold Reg. Sci. Technol., 54, 155–163, 10.1016/j.coldregions.2008.07.002], 2008.

Pulliainen, J., Aurela, M., Laurila, T., Aalto, T., Takala, M., Salminen, M., Kulmala, M., Barr, A., Heimann, M., Lindroth, A., et al.: Early snowmelt significantly enhances boreal springtime carbon uptake, Proceedings of the National Academy of Sciences, 114, 11 081–11 086, 10.1073/pnas.1707889114], 2017.

Quéno, L., Fierz, C., van Herwijnen, A., Longridge, D., and Wever, N.: Ice layer formation in the snowpack due to preferential water flow: case study at an alpine site, The Cryosphere Discussions, pp. 1–23, 10.5194/tc-2020-24], 2020a.

Quéno, L., Karbou, F., Vionnet, V., and Dombrowski-Etchevers, I.: Satellite-derived products of solar and longwave irradiances used for snowpack modelling in mountainous terrain., Hydrology & Earth System Sciences, 24, 10.5194/hess-24-2083-2020], 2020b.

Quéno, L., Vionnet, V., Dombrowski-Etchevers, I., Lafaysse, M., Dumont, M., and Karbou, F.: Snowpack modelling in the Pyrenees driven by kilometric-resolution meteorological forecasts, The Cryosphere, 10, 1571–1589, 10.5194/tc-10-1571-2016], 2016.

Rabier, F.: Overview of global data assimilation developments in numerical weather-prediction centres, Quarterly Journal of the Royal Meteorological Society: A journal of the atmospheric sciences, applied meteorology and physical oceanography, 131, 3215–3233, 10.1256/qj.05.129], 2005.

Raleigh, M. S., Lundquist, J. D., and Clark, M. P.: Exploring the impact of forcing error characteristics on physically based snow simulations within a global sensitivity analysis framework, Hydrol. Earth Syst. Sci., 19, 3153–3179, 10.5194/hess-19-3153-2015], 2015.

Reichle, R. H.: Data assimilation methods in the Earth sciences, Advances in water resources, 31, 1411–1418, 10.1016/j.advwatres.2008.01.001], 2008.

Reichle, R. H. and Koster, R. D.: Assessing the impact of horizontal error correlations in background fields on soil moisture estimation, Journal of Hydrometeorology, 4, 1229–1242, 10.1175/1525-7541(2003)004<1229:atiohe>2.0.co;2], 2003.

Reinking, R. F.: Formation of graupel, Journal of Applied Meteorology, 14, 745–754, 10.1175/1520-0450(1975)014<0745:fog>2.0.co;2], 1975.

Revuelto, J., Cluzet, B., Duran, N., Fructus, M., Lafaysse, M., Cosme, E., and Dumont, M.: Assimilation of surface reflectance in snow simulations: Impact on bulk snow variables, Journal of Hydrology, 603, 126 966, https://doi.org/10.1016/j.jhydrol.2021.126966], 2021.

Richner, H. and Hächler, P.: Understanding and forecasting Alpine foehn, in: Mountain Weather Research and Forecasting, pp. 219–260, Springer, 2013.

Rodwell, M. and Palmer, T.: Using numerical weather prediction to assess climate models, Quarterly Journal of the Royal Meteorological Society: A journal of the atmospheric sciences, applied meteorology and physical oceanography, 133, 129–146, 10.1002/qj.23], 2007.

Rolls, R. J., Leigh, C., and Sheldon, F.: Mechanistic effects of low-flow hydrology on riverine ecosystems: ecological principles and consequences of alteration, Freshwater Science, 31, 1163–1186, 10.1899/12-002.1], 2012.

Ruiz, J. J., Pulido, M., and Miyoshi, T.: Estimating model parameters with ensemble-based data assimilation: A review, Journal of the Meteorological Society of Japan. Ser. II, 91, 79–99, 10.2151/jmsj.2013-201], 2013.

Rutter, N., Essery, R., Pomeroy, J., Altimir, N., Andreadis, K., Baker, I., Barr, A., Bartlett, P., Boone, A., Deng, H., et al.: Evaluation of forest snow processes models (SnowMIP2), J. Geophys. Res., 114, D06 111, 10.1029/2008jd011063], 2009.

Réveillet, M., Dumont, M., Gascoin, S., Lafaysse, M., Nabat, P., Ribes, A., Nheili, R., Tuzet, F., Menegoz, M., and Ginoux, P.: Light absorbing impurities change the dynamics and impacts of the snow cover under climate change, in prep.

Sandells, M., Essery, R., Rutter, N., Wake, L., Leppänen, L., and Lemmetyinen, J.: Microstructure representation of snow in coupled snowpack and microwave emission models, The Cryosphere, 11, 229–246, 10.5194/tc-11-229-2017], 2017.

Schaake, J. C., Hamill, T. M., Buizza, R., and Clark, M.: HEPEX: the hydrological ensemble prediction experiment, Bulletin of the American Meteorological Society, 88, 1541–1548, 10.1175/bams-88-10-1541], 2007.

Schweizer, J., Bruce Jamieson, J., and Schneebeli, M.: Snow avalanche formation, Reviews of Geophysics, 41, 1016, 10.1029/2002rg000123], 2003.

Serreze, M. C., Clark, M. P., Armstrong, R. L., McGinnis, D. A., and Pulwarty, R. S.: Characteristics of the western United States snowpack from snowpack telemetry (SNOTEL) data, Water Resources Research, 35, 2145–2160, 10.1029/1999wr900090], 1999.

Sirguey, P.: Simple correction of multiple reflection effects in rugged terrain, Int. J. Remote Sens., 30, 1075–1081, 10.1080/01431160802348101], 2009.

Sirguey, P., Mathieu, R., and Arnaud, Y.: Subpixel monitoring of the seasonal snow cover with MODIS at 250m spatial resolution in the Southern Alps of New Zealand: methodology and accuracy assessment, Remote Sens. Environ., 113, 160–181, 10.1016/j.rse.2008.09.008], 2009.

Sirguey, P. J. B.: Monitoring snow cover and modelling catchment discharge with remote sensing in the Upper Waitaki Basin, New Zealand, Ph.D. thesis, University of Otago, 2010.

Skiles, S. M. and Painter, T. H.: Toward Understanding Direct Absorption and Grain Size Feedbacks by Dust Radiative Forcing in Snow With Coupled Snow Physical and Radiative Transfer Modeling, Water Resources Research, 55, 7362–7378, 10.1029/2018wr024573], 2019.

Skiles, S. M., Flanner, M., Cook, J. M., Dumont, M., and Painter, T. H.: Radiative forcing by light-absorbing particles in snow, Nature Climate Change, p. 1, 10.1038/s41558-018-0296-5], 2018.

Slater, A. et al.: The representation of snow in land surface schemes: results from PILPS 2(d), J. Hydrometeorol., 2, 7–25, 10.1175/1525-7541(2001)002<0007:trosil>2.0.co;2], 2001.

Slater, A. G. and Clark, M. P.: Snow data assimilation via an ensemble Kalman filter, Journal of Hydrometeorology, 7, 478–493, 10.1175/jhm505.1], 2006.

Smyth, E. J., Raleigh, M. S., and Small, E. E.: Particle Filter Data Assimilation of Monthly Snow Depth Observations Improves Estimation of Snow Density and SWE, Water Resources Research, 55, 1296–1311, 10.1029/2018wr023400], 2019.

Snyder, C., Bengtsson, T., Bickel, P., and Anderson, J.: Obstacles to high-dimensional particle filtering, Monthly Weather Review, 136, 4629–4640, 10.1175/2008mwr2529.1], 2008.

Snyder, C., Bengtsson, T., and Morzfeld, M.: Performance bounds for particle filters using the optimal proposal, Monthly Weather Review, 143, 4750–4761, 10.1175/mwr-d-15-0144.1], 2015.

Solomon, S., Qin, D., Manning, M., Chen, Z., Marquis, M., Averyt, K., Tignor, M., and Miller, H.: IPCC fourth assessment report (AR4), Climate change, 2007.

Spandre, P., François, H., Verfaillie, D., Pons, M., Vernay, M., Lafaysse, M., George, E., and Morin, S.: Winter tourism under climate change in the Pyrenees and the French Alps: relevance of snowmaking as a technical adaptation, Cryosphere, 13, 1325–1347, 10.5194/tc-13-1325-2019], 2019.

Stigter, E. E., Wanders, N., Saloranta, T. M., Shea, J. M., Bierkens, M. F., and Immerzeel, W. W.: Assimilation of snow cover and snow depth into a snow model to estimate snow water equivalent and snowmelt runoff in a Himalayan catchment, The Cryosphere, 11, 1647–1664, 10.5194/tc-11-1647-2017], 2017.

Storch, I.: Patterns and strategies of winter habitat selection in alpine capercaillie, Ecography, 16, 351–359, 10.1111/j.1600-0587.1993.tb00224.x], 1993.

Strasser, U., Bernhardt, M., Weber, M., Liston, G., and Mauser, W.: Is snow sublimation important in the alpine water balance?, The Cryosphere, 2, 53–66, 10.5194/tc-2-53-2008], 2008a.

Strasser, U., Corripio, J., Brock, B., Pellicciotti, F., and Burlando, P.: Distributed modeling of snow processes in The Berchtesgaden National Park, in: Alpine Snow Workshop, Berchtesgaden Natl. Park Munich, Germany, 2008b.

Sturm, M., Holmgren, J., McFadden, J. P., Liston, G. E., Chapin III, F. S., and Racine, C. H.: Snow–shrub interactions in Arctic tundra: a hypothesis with climatic implications, Journal of Climate, 14, 336–344, 10.1175/1520-0442(2001)014<0336:ssiiat>2.0.co;2], 2001.

Taillardat, M. and Mestre, O.: From research to applications–examples of operational ensemble post-processing in France using machine learning, Nonlinear Processes in Geophysics, 27, 329–347, 10.5194/npg-27-329-2020], 2020.

Talagrand, O. and Courtier, P.: Variational assimilation of meteorological observations with the adjoint vorticity equation. I: Theory, Quarterly Journal of the Royal Meteorological Society, 113, 1311–1328, 10.1002/qj.49711347812], 1987.

Thirel, G., Salamon, P., Burek, P., and Kalas, M.: Assimilation of MODIS snow cover area data in a distributed hydrological model using the particle filter, Remote Sensing, 5, 5825–5850, 10.3390/rs5115825], 2013.

Tracton, M. S. and Kalnay, E.: Operational ensemble prediction at the National Meteorological Center: Practical aspects, Weather and Forecasting, 8, 379–398, 10.1175/1520-0434(1993)008<0379:oepatn>2.0.co;2], 1993.

Tuzet, F.: Dépôt, devenir et impact radiatif des impuretés dans le manteau neigeux: analyse des processus, simulations numériques et implications, Ph.D. thesis, Université Toulouse III - Paul sabatier, 2019.

Tuzet, F., Dumont, M., Lafaysse, M., Picard, G., Laurent, A., Voisin, D., Lejeune, Y., Charrois, L., Nabat, P., and Morin, S.: A multilayer physically based snowpack model simulating direct and indirect radiative impacts of light-absorbing impurities in snow, The Cryosphere, 11, 2633, 10.5194/tc-11-2633-2017], 2017.

Tuzet, F., Dumont, M., Arnaud, L., Voisin, D., Lamare, M., Larue, F., Revuelto, J., and Picard, G.: Influence of light-absorbing particles on snow spectral irradiance profiles, The Cryosphere, 13, 2169–2187, 10.5194/tc-13-2169-2019], 2019.

Tuzet, F., Dumont, M., Picard, G., Lamare, M., Voisin, D., Nabat, P., Lafaysse, M., Larue, F., Revuelto, J., and Arnaud, L.: Quantification of the radiative impact of light-absorbing particles during two contrasted snow seasons at Col du Lautaret (2058 m a.s.l., French Alps), The Cryosphere Discussions, 2020, 1–38, 10.5194/tc-2019-287], 2020.

Udina, M., Bech, J., Gonzalez, S., Soler, M. R., Paci, A., Miró, J. R., Trapero, L., Donier, J. M., Douffet, T., Codina, B., et al.: Multi-sensor observations of an elevated rotor during a mountain wave event in the Eastern Pyrenees, Atmospheric Research, 234, 104 698, 10.1016/j.atmosres.2019.104698], 2020.

Van Leeuwen, P. J.: Particle filtering in geophysical systems, Monthly Weather Review, 137, 4089–4114, 10.1175/2009mwr2835.1], 2009.

van Leeuwen, P. J.: Nonlinear data assimilation in geosciences: an extremely efficient particle filter, Quarterly Journal of the Royal Meteorological Society, 136, 1991–1999, 10.1002/qj.699], 2010.

Van Leeuwen, P. J., Künsch, H. R., Nerger, L., Potthast, R., and Reich, S.: Particle filters for high-dimensional geoscience applications: A review, Quarterly Journal of the Royal Meteorological Society, 145, 2335–2365, 10.1002/qj.3551], 2019.

Velázquez, J., Anctil, F., Ramos, M., and Perrin, C.: Can a multi-model approach improve hydrological ensemble forecasting? A study on 29 French catchments using 16 hydrological model structures, Advances in Geosciences, 29, 33, 10.5194/adgeo-29-33-2011], 2011.

Vernay, M., Lafaysse, M., Merindol, L., Giraud, G., and Morin, S.: Ensemble Forecasting of snowpack conditions and avalanche hazard, Cold. Reg. Sci. Technol., 120, 251–262, 10.1016/j.coldregions.2015.04.010], 2015.

Veyssière, G., Karbou, F., Morin, S., Lafaysse, M., and Vionnet, V.: Evaluation of Sub-Kilometric Numerical Simulations of C-Band Radar Backscatter over the French Alps against Sentinel-1 Observations, Remote Sensing, 11, 10.3390/rs11010008], 2019.

Vincendon, B., Ducrocq, V., Saulnier, G.-M., Bouilloud, L., Chancibault, K., Habets, F., and Noilhan, J.: Benefit of coupling the ISBA land surface model with a TOPMODEL hydrological model version dedicated to Mediterranean flash-floods, J. Hydrol., 394, 256–266, 10.1016/j.jhydrol.2010.04.012], 2010.

Vionnet, V., Brun, E., Morin, S., Boone, A., Martin, E., Faroux, S., Le-Moigne, P., and Willemet, J.-M.: The detailed snowpack scheme Crocus and its implementation in SURFEX v7.2, Geosci. Model. Dev., 5, 773–791, 10.5194/gmd-5-773-2012], 2012.

Vionnet, V., Martin, E., Masson, V., Guyomarc'h, G., Naaim-Bouvet, F., Prokop, A., Durand, Y., and Lac, C.: Simulation of wind-induced snow transport and sublimation in alpine terrain using a fully coupled snowpack/atmosphere model, The Cryosphere, 8, 395–415, 10.5194/tc-8-395-2014], 2014.

Vionnet, V., Martin, E., Masson, V., Lac, C., Bouvet, F. N., and Guyomarc'h, G.: High-resolution large eddy simulation of snow accumulation in alpine terrain, Journal of Geophysical Research: Atmospheres, 122, 11–005, 10.1002/2017jd026947], 2017.

Vionnet, V., Six, D., Auger, L., Dumont, M., Lafaysse, M., Quéno, L., Réveillet, M., Dombrowski Etchevers, I., Thibert, E., and Vincent, C.: Sub-kilometer precipitation datasets for snowpack and glacier modeling in alpine terrain, Frontiers in Earth Science, 7, 182, 10.3389/feart.2019.00182], 2019.

Vionnet, V., Marsh, C. B., Menounos, B., Gascoin, S., Wayand, N. E., Shea, J., Mukherjee, K., and Pomeroy, J. W.: Multi-scale snowdrift-permitting modelling of mountain snowpack, The Cryosphere Discussions, pp. 1–43, 10.5194/tc-15-743-2021], 2020.

Warren, S.: Optical properties of snow, Rev. Geophys., 20, 67–89, 10.1029/RG020i001p00067], 1982.

Warren, S. G.: Can black carbon in snow be detected by remote sensing?, J. Geophys. Res., 118, 779–786, 10.1029/2012JD018476], 2013.

Wever, N., Würzer, S., Fierz, C., and Lehning, M.: Simulating ice layer formation under the presence of preferential flow in layered snowpacks, Cryosphere, 10, 2731–2744, 10.5194/tc-10-2731-2016], 2016.

Wever, N., Schmid, L., Heilig, A., Eisen, O., Fierz, C., and Lehning, M.: Verification of the multi-layer SNOWPACK model with different water transport schemes, The Cryosphere, 9, 2271–2293, 10.5194/tc-9-2271-2015], 2015.

Winstral, A., Marks, D., and Gurney, R.: Assessing the sensitivities of a distributed snow model to forcing data resolution, Journal of Hydrometeorology, 15, 1366–1383, 10.1175/jhm-d-13-0169.1], 2014.

Winstral, A., Magnusson, J., Schirmer, M., and Jonas, T.: The Bias-Detecting Ensemble: A New and Efficient Technique for Dynamically Incorporating Observations Into Physics-Based, Multilayer Snow Models, Water Resources Research, 55, 613–631, 10.1029/2018wr024521], 2019.

Wiscombe, W. J. and Warren, S. G.: A model for the spectral albedo of snow. I: Pure snow, J. Atmos. Sci., 37(12), 2712 – 2733, 10.1175/1520-0469(1980)037<2712:amftsa>2.0.co;2], 1980.

Wong, M., Romine, G., and Snyder, C.: Model improvement via systematic investigation of physics tendencies, Monthly Weather Review, 148, 671–688, 10.1175/mwr-d-19-0255.1], 2020.

Wright, P., Bergin, M., Dibb, J., Lefer, B., Domine, F., Carman, T., Carmagnola, C., Dumont, M., Courville, Z., Schaaf, C., and Wang, Z.: Comparing MODIS daily snow albedo to spectral albedo field measurements in Central Greenland, Remote Sensing of Environment, 140, 118–129, https://doi.org/10.1016/j.rse.2013.08.044], 2014.

Xiao, C.-D., Wang, S.-J., and Qin, D.-H.: A preliminary study of cryosphere service function and value evaluation, Advances in Climate Change Research, 6, 181–187, 10.1016/j.accre.2015.11.004], 2015.

Xie, H., Longuevergne, L., Ringler, C., and Scanlon, B.: Calibration and evaluation of a semi-distributed watershed model of Sub-Saharan Africa using GRACE data, 10.5194/hess-16-3083-2012], 2012.

Yen, Y.-C.: Review of the thermal properties of snow, ice and sea ice, Tech. Rep. 81-10, Cold Regions Research and Engineering Laboratory, Hanover, NH, 1981.

Zimova, M., Hackländer, K., Good, J. M., Melo-Ferreira, J., Alves, P. C., and Mills, L. S.: Function and underlying mechanisms of seasonal colour moulting in mammals and birds: what keeps them changing in a warming world?, Biological Reviews, 93, 1478–1498, 10.1111/brv.12405], 2018.

Zwieback, S., Westermann, S., Langer, M., Boike, J., Marsh, P., and Berg, A.: Improving permafrost modeling by assimilating remotely sensed soil moisture, Water Resources Research, 55, 1814–1832, 10.1029/2018wr023247], 2019.

List of Figures

Appendix A

List of publications

List of publications

My work on data assimilation and ensemble modelling on the snowpack, as well as my involvement in field campaigns from fellow PhD and post-docs were an opportunity to collaborate in several publications.

Peer-reviewed publications

1. Lafaysse, M., **Cluzet, B.**, Dumont, M., Lejeune, Y., Vionnet, V., and Morin, S. : A multiphysical ensemble system of numerical snow modelling, The Cryosphere, 11, 1173-1198, https://doi.org/10.5194/tc-11-1173-2017, 2017.

   Contribution:
   This publication corresponds to a gap-year reasearch internship I did at CEN under the supervision of Matthieu Lafaysse in 2015. Design and implementation of the multiphysics options in Crocus. Embedding the ensemble simulations and its post-processing in an High Performance Computing environment. Performing simulations at a field Site (Col de Porte). Conception of the analysis and evaluation data treatment. Contribution to the redaction of the article.

2. **B. Cluzet**, J. Revuelto, M. Lafaysse, F. Tuzet, E. Cosme, G. Picard, L. Arnaud and M. Dumont Towards the assimilation of satellite reflectance into semi-distributed ensemble snowpack simulations, Cold Regions Science and Technology„ 170, 2020, https://doi.org/10.1016/j.coldregions.2019.102918.

Contribution:
This article is included in Chap 2 of the manuscript.

3. Dumont, M., Tuzet, F., Gascoin, S., Picard, G., Kutuzov, S., Lafaysse, M., **Cluzet, B.**, Nheili, R., and Painter, T. H. (2020). Accelerated snow melt in the Russian Caucasus mountains after the Saharan dust outbreak in March 2018. Journal of Geophysical Research: Earth Surface, https://doi.org/10.1029/2020JF005641.

   Contribution:
   Participation to the conception of the ESCROC multiphysics ensemble used in the study and code development to include developments of (Tuzet et al., 2017) into Crocus main code branch.

4. J. Revuelto, P. Billecocq, F. Larue, M. Lamare, F. Tuzet, **B. Cluzet** and M. Dumont, Random forests as a tool to understand the snow depth distribution and its evolution in mountain areas, Hydrological Processes, 34, 24, 5384-5401, https://onlinelibrary.wiley.com/doi/abs/10.1002/hyp.13951, 2020.

   Contribution:
   Contribution to the field work campaign during the acquisition of Terrestrial Laser Scans at Col du Lautaret.

5. **Cluzet, B.**, Lafaysse, M., Cosme, E., Albergel, C., Meunier, L.F., and Dumont, M. (2021). CrocO_v1.0: a Particle Filter to assimilate snowpack observations in a spatialised framework. Geoscientific Model Development, 14, 1595-1614, https://doi.org/10.5194/gmd-14-1595-2021, 2021

   Contribution:
   This article is included in Chap 3 of the manuscript.

6. J. Revuelto, **B. Cluzet**, N. Duran, M. Fructus, M. Lafaysse, E. Cosme, and M. Dumont. Assimilation of surface reflectance in snow simulations: Impact on bulk snow variables, Journal of Hydrology, 603, 126 966, https://doi.org/10.1016/j.jhydrol.2021.126966, 2021 **Contribution:**
   Conception and implementation of the data assimilation system. Help with the launching of the simulations on an HPC environment. Contribution to the design of the study, the analysis of results, the post-processing of data and the writing of the

paper.

7. Palchetti, L., Barucci, M., Belotti, C., Bianchini, G., **Cluzet, B.**, D'Amato, F., Del Bianco, S., Di Natale, G., Gai, M., Khordakova, D., Montori, A., Oetjen, H., Rettinger, M., Rolf, C., Schuettemeyer, D., Sussmann, R., Viciani, S., Vogelmann, H. and Wienhold, F. G., Observations of the downwelling far-infrared atmospheric emission at the Zugspitze observatory, Earth System Science Data, 13, 4303–4312, 10.5194/essd-13-4303-2021, 2021.

   Contribution:
   Performed a 3 day field campaign on Zugspitze (Austria/Germany, 2962m). Collected 10 snow samples, measured their SSA and density, and monitored the emissivity measurements.

Discussion articles

1. (in review) Deschamps-Berger, C., **Cluzet, B.**, Dumont, M., Lafaysse, M., Berthier, E., Fanise, P., and Gascoin, S., Assimilation of snow depth maps from spaceborne photogrammetry in a detailed snowpack model.

   Contribution:
   Conception and implementation of the Data assimilation system. Help with the launching of the simulations on an HPC environment. Contribution to the design of the study, and the interpretation of results. Help with the pre/post-processing of the data.

2. (in review) **B. Cluzet**, M. Lafaysse, C. Deschamps-Berger, M. Vernay and M. Dumont, Propagating information from snow observations with CrocO ensemble data assimilation system: a 10-years case study over a snow depth observation network.

   Contribution:
   This article is included in Chap 4 of the manuscript.

Oral and poster presentations

1. (oral) **B. Cluzet**, N.J. Rodriguez - Fernandez, A. Mialon, A. Al Bitar, Y. H. Kerr, A. Al Yaari, J. P Wigneron, Evaluation of 14 years of SMOS and SMOS-like soil moisture against the ESA CCI dataset, CCI Soil Moisture User Workshop, Vienna.
2. (oral) **Bertrand Cluzet**, Jesus Revuelto, Matthieu Lafaysse, Marie Dumont, François Tuzet, Emmanuel Cosme, and Simon Gascoin, Assimilation of MODIS observations of snowpack surface properties into one year of spatialized ensemble snowpack simulations at a field site in the French Alps ISSW 2018, Innsbruck, Austria
3. (poster) **Bertrand Cluzet**, Jesus Revuelto, Matthieu Lafaysse, François Tuzet, Emmanuel Cosme, Ghsilain Picard, Laurent Arnaud and Marie Dumont, Comparison of MODIS and Sentinel2 Observations of Snow Reflectance and SCF with Ensemble Simulations of the Snowpack Properties, IUGG 2019, Montreal, Canada
4. (oral) **Bertrand Cluzet**, Matthieu Lafaysse, Marie Dumont, Emmanuel Cosme, Jesus Revuelto, A particle filter to spatially assimilate synthetical satellite reflectance observations into a detailed snowpack model, IUGG 2019, Montreal, Canada
5. (oral) **Bertrand Cluzet**, Matthieu Lafaysse, Marie Dumont, Emmanuel Cosme, and Clément Albergel, CRAMPON: A Particle Filter to assimilate sparse snowpack observations into a semi-distributed geometry, EGU General Assembly 2020, Online, 4–8 May 2020, EGU2020-9037, https://doi.org/10.5194/egusphere-egu2020-9037, 2020
6. (invited online seminar) **Bertrand Cluzet**, CRAMPON: A Particle Filter to assimilate sparse snowpack observations into a semi-distributed geometry, University of Oslo, April
7. (invited online seminar) **Bertrand Cluzet**, CrocO: A Particle Filter to assimilate sparse snowpack observations into a semi-distributed geometry, ETH Zurich, July
8. (sollicited talk) **Bertrand Cluzet**, Matthieu Lafaysse, Emmanuel Cosme, Clément Albergel, Louis-François Meunier and Marie Dumont, Can we propagate information from sparse snowpack observations into space using a Particle Filter? AGU Fall Meeting 2020